ISBN: 978-623-7525-15-8

2019 ICOIRS

THE FIFTH INTERNATIONAL CONFERENCE OF INDONESIAN SOCIETY FOR REMOTE SENSING (ICOIRS) AND MAPIN CONGRESS

17-20 September 2019, ITENAS-Bandung, West Java Indonesia

"The Revolution of Earth Observation for a Better Human Life"

PROCEEDINGS

VOLUME 2

penerbit itenas

Proceeding *The Fifth International Conferences of Indonesian Society for Remote Sensing (ICOIRS)* 2019

Themes:
The Revolution of Earth Observation for a Better Human Life

Reviewer Team:
1. Prof. Dr. Ir. Dewayany Sutrisno, M.App.Sc. (Indonesia)
2. Dr. Ir. Bambang Edhi Leksono (Indonesia)
3. Dr. Dewi Kania Sari, M.T. (Indonesia)
4. Prof. Dr. Ketut Wikantika, M.Sc (Indonesia)
5. Dr. Agustan (Indonesia)
6. Prof. Wataru Takeuchi (Japan)
7. Prof. Chao-Hung Lin (Taiwan)
8. Prof. Dr. Mazlan Hashim (Malaysia)
9. Tanakorn Sritarapipat, Ph.D., ME., BE (Thailand)

Editor Team:
1. Dr. Henri Kuncoro, M.T.
2. Dr. Eng. Anjar Dimara Sakti, M.Sc.
3. Dr. Lili Somantri, S.Pd., M.Si.
4. Dr. Lissa Fajri Yayusman
5. Rika Hernawati, S.T., M.T.
6. Gusti Ayu Jessy Kartini, S.T., M.T.
7. Nurul Yuhanafia, S.T., M.T.
8. Thonas Indra Maryanto, S.Kel., M.T.
9. Monica Maharani, S.T., M.Eng.
10. Anggun Tridawati, S.T.

Committee:
General Chair : Dr. Soni Darmawan, M.T.
Secretary : Rika Hernawati, S.T., M.T.
Technical Program : Dr. Henri Kuncoro, M.T.
Web Master : Abhi Adhiguna, S.T.

ISBN : 978-623-7525-15-8
First Print : September 2019
Publisher : Penerbit Itenas

Address:
Jl. P.K.H. Mustapha No. 23, Bandung 40124
Telp: +62 22 7272215,
Fax: +62 22 7202892
Email: penerbit@itenas.ac.id

2019

ICOIRS

THE FIFTH INTERNATIONAL CONFERENCE OF INDONESIAN SOCIETY FOR REMOTE SENSING (ICOIRS) AND MAPIN CONGRESS

"The Revolution of Earth Observation
for a Better Human Life"

17-20 SEPTEMBER 2019
BALE DAYANG SUMBI
INSTITUT TEKNOLOGI NASIONAL BANDUNG
WEST JAVA - INDONESIA

FOREWORD

Assalamualaikum Warahmatullahi Wabarakatuh.

First, I would like to say thanks to all committee, sponsor, our students, and our colleague for supporting The Fifth International Conferences of Indonesian Society for Remote Sensing (ICOIRS) and Indonesian Society for Remote Sensing Congress.

The 5th ICOIRS and MAPIN Congress was organized by collaboration of Indonesian Society for Remote Sensing (ISRS/MAPIN), Institut Teknologi Nasional (ITENAS), Center for Remote Sensing Institut Teknologi Bandung, Universitas Pendidikan Indonesia, Universitas Winaya Mukti and Universitas Pajajaran and supported by Ministry of Researh, Technology and Higher Education (RISTEKDIKTI), Geospatial Information Agency (BIG), Indonesian National Institute of Aeronautics and Space (LAPAN), Agency for the Assessment and Application of Technology (BPPT), The Ministry of Agrarian Affairs and Spatial Planning/National Land Agency (ATR/BPN) and Meteorological, Climatological, and Geophysical Agency (BMKG). This event bring together researchers, policy makers, and practitioners from developed and developing countries to share insights into the challenges and opportunities of remote sensing technology and its application in solving the problems of Indonesia especially and South East Asia countries. It showcase cutting-edge research from around South East Asia, cutting-edge research from around South East Asia, focusing on themes of equity and risk, learning, capacity building, methodology, and possibly investment approaches in remote sensing. It explore practical adaptation policies and approaches, and share strategies for decision making to support global cooperation for conserving the earth and for a better human life.

The four-day conference among others consist of plenary, technical and poster sessions, panel discussions, congress of ISRS/MAPIN, exhibition, talk show, workshop, hands on training and city tour. We invite you to join us full time on The 5th ICOIRS and MAPIN Congress and make a successful conference on the application of Remote Sensing, Photogrammetry, GIS, GPS/GNSS, and other related digital mapping technologies in Indonesia and South East Asia.

Hopefully this technical programme can help and guide all of you to absorb all new things on this conference.

Please enjoy it. Thanks…

Wassalamualaikum warahmatullahi wabarakatuh.

Sincerely
Dr. Soni Darmawan
(General Chair of ICOIRS2019 Organizing Committee)

KEYNOTE SPEAKERS

H. M. Ridwan Kamil, S.T., M.U.D.
Governor of West Java

Prof. Hasanuddin Z. Abidin
Head of Indonesian Geospatial Agency (BIG)

Dr. Orbita Roswintiarti, M.Sc
Deputy of Remote Sensing (LAPAN)

Prof.Dr.Ir. Dewayany Sutrisno, M.AppSc
President of Indonesian Society for
Remote Sensing (ISRS/MAPIN)

Prof. Chao-Hung Lin
National Cheng-Kung University, Taiwan

Prof. Wataru Takeuchi
Institute of Industrial Science, The University of Tokyo, Japan

Prof. Tian-Yuan Shih
National Chiao Tung University, Taiwan

Prof. Josaphat Tetuko Sri Sumantyo, Ph.D.
Chiba University, Japan

Prof. Sr. Dr. Mazlan Hashim FASc
Universiti Teknologi Malaysia (UTM), Malaysia

Dr. Gay Jane Perez
University of The Philippines, Philippines

Li Zhang, Ph.D
Co-chair of the Coastal Zone Working Group of the Digital Silk Road
International Scientific Program (DBAR)
Chinese Academy of Sciences, China

Tanakorn Sritarapipat, Ph.D., ME., BE
Suranaree University of Technology, Thailand

Dr. Firman Hadi
Geoinformatics Centre – AIT, Thailand

INVITED SPEAKERS

Prof. Dr. Ir. Bangun Muljo DEA.DESS
Institut Teknologi Sepuluh Nopember

Prof. Projo Danoedoro
Universitas Gajah Mada

Prof. Dr. Ketut Wikantika
Institut Teknologi Bandung

Prof. Dr.-Ing Fahmi Amhar
Badan Informasi Geospasial (BIG)

Prof. Lilik Prasetyo
Institut Pertanian Bogor

Dr. Agustan
Pusat Teknologi Inventarisasi Sumber Daya Alam (PTISDA), BPPT

Dr. Soni Darmawan
Institut Teknologi Nasional Bandung

MAIN PROGRAMME

	07.30 - 08.30	08.30 - 09.45	09.45 -10.00	10.00 - 12.00	12.00-13.00	13.00-15.00	15.00-16.00	17.00-20.00
Day 1 - Tuesday (17th Sep 2019)	Registration	Opening Ceremony			Lunch	Commercial Session / Poster session	Technical Session	Gala Dinner for Invitation
						Technical Session I	Technical Session I	
						Technical Session II	Technical Session II	
						Technical Session III	Technical Session III	
						Workshop GEE	MAPIN Training	
						Commercial Session	Commercial Session	
Day 2 - Wednesday (18th Sep 2019)		Keynote Speaker	Coffee Break	Keynote speaker	Lunch	Commercial Session / Poster session	Technical Session	
				Technical Session I		Technical Session I	Technical Session I	
				Technical Session II		Technical Session II	Technical Session II	
				Technical Session III		Technical Session III	Technical Session III	
				Geomatics Scientific Meeting		Geomatics Scientific Meeting	Geomatics Scientific Meeting	
				Commercial Session		Commercial Session	Commercial Session	

	07.30 - 08.30	08.30 - 09.45	09.45 -10.00	10.00 - 12.00	12.00-13.00	13.00-15.00	15.00-16.00	17.00-20.00
Day 3 - Thursday (19th Sep 2019)		Keynote Speaker	Coffee Break	Talkshow Technical Session I Technical Session II Technical Session III Technical Session Commercial Session	Lunch	Talkshow Technical Session I Technical Session II Technical Session III MAPIN Congress Commercial Session	Closing Ceremony	Gala Dinner for MAPIN Committee and invitation
Day 4 - Friday (20th Sep 2019)	Preparation	**CITY TOUR**						

Information:

- Main Hall at Bale Dayang Sumbi
- At second floor of Bale Dayang Sumbi
- At second floor of Bale Dayang Sumbi
- At second floor of Bale Dayang Sumbi
- At Audio Visual, Building No. 12
- Demonstration stage at Bale Dayang Sumbi
- At Cafe Cinde

TABLE OF CONTENTS

Economic Evaluation of Carbon Dioxide (CO2) Emissions from Land Use Change in South Sumatra Province Using SPOT Imagery

Riissiyani[1], Grace Tiara[1], Citra Paramita[1], and Wisnu Ali Martono[1]

[1]Center of Regional Resources Development (PTPSW), Agency for The Assessment and Application of Technology (BPPT) Geostech 820 Puspitek District Serpong, Indonesia

e-mail: Riissiyani@bppt.go.id

Abstract. Currently in Indonesia, the Gross Regional Domestic Product (GRDP), does not calculate the non-economic value benefits from natural capital resources such as peat swamp forests. Conservation activities of peat swamp forests with economic growth are not carried out by conserving peat swamp ecosystems. It is necessary for economic studies to find out how much non-economic value is lost due to economic development activities. Peat swamp forests have the largest terrestrial carbon dioxide (CO2) reserves. Based on observations of Landsat Imagery in 2006-2011 there has been a change in land use cover from peat swamp forest to Plantation Forest, Plantation, Settlement, Dry Land Agriculture and Open Land. This will release large amounts of carbon dioxide (CO2) emissions to the atmosphere. In the period 2006-2009 there were CO2 net emissions of 13,378,419 Tons of CO2-eq and the period of 2009-2011 amounted to 3,206,461 Tons of CO2-eq. Suffered losses in CO2 emissions due to changes in land use cover from 2006 amounted to IDR 1,839,000,000 per tons of CO2-eq/ha/year. In 2007, IDR 1,958,000,000 per tons of CO2-eq/ha/year, in 2008 amounted to IDR 2,038,000,000 per tons of CO2-eq/ha/year, in 2009 amounting to IDR 424,000,000 per tons of CO2-eq / Ha / Year, in 2010 amounting to IDR 444,000,000 per tons of CO2-eq/ha/year and in 2011 amounting to IDR 468,000,000 per tons CO2-eq/ha/year.

1. Introduction

In Indonesia, the rate of economic growth is measured by an increase in Gross Regional Domestic Product (GRDP) per year in each region at the district or provincial level and GDP at the national level. This rate of economic growth does not consider the value of non-economic benefits from natural capital such as peat swamp forests which have many tangible and intangible benefits for the life of living things on earth. So that economic development whose aim is to prosper the people will ultimately damage the quality of the environment.

In South Sumatra Province in 2000-2011, the primary land use cover swamp forest and secondary swamp forest where the land use was mostly in the form of peat land experiencing land conversion to plantations, open land, logged over and natural primary forests. Ogan Komering Ilir Regency (OKI) experienced the widest conversion of peat land to other land uses, as the peat moisture decreased rapidly during dry season [1]. The conversion was higher than other districts in South Sumatra Province. That is changing from peat to plantations of 30,584 ha [2]. The conversion of peatlands to other land uses will have an impact on increasing CO2 emissions, because peatlands have certain characteristics of CO2 emissions. This is due to the decomposition process of peatlands by practicing the drainage system on peatlands which will be changed for other uses

Increasing CO2 emissions in the atmosphere, will also increases the concentration of Greenhouse Gases (GHGs) and results in environmental damage. Around 20% of GHGs are caused by the release of CO2 that has been stored for hundreds to thousands of years as aboveground biomass and in peat soils [3]. Therefore, in order to increase economic growth in South Sumatra to not cause a decline in the welfare of the people, then economic development policies must be accompanied by policies to preserve the environment.

2. Material and Methodology

2.1. Material

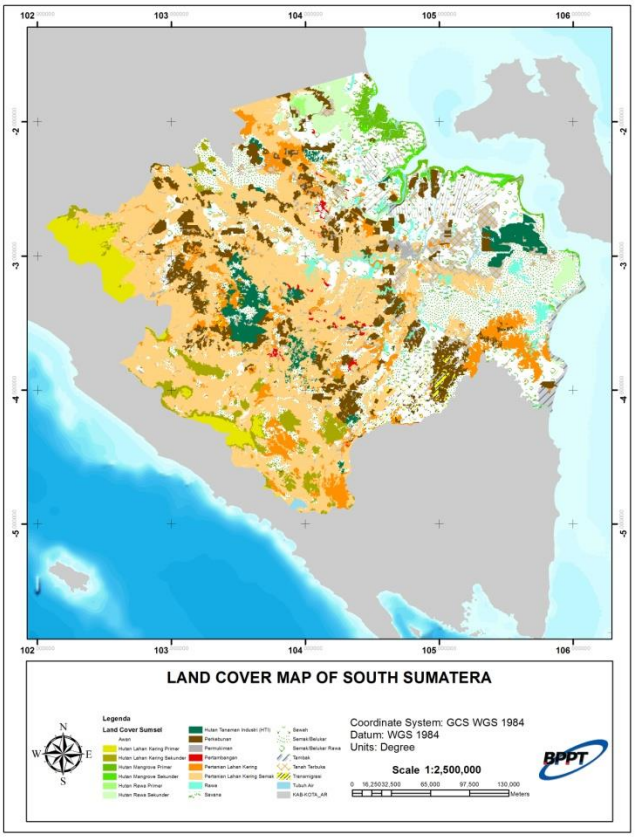

Figure 1. Land Cover Map of South Sumatra Province.

The study was conducted in South Sumatra Province with an area of 91,806.38 Km^2, which is located at 1° - 4° South Latitude and 102° - 106° East Longitude. South Sumatra Province is administratively divided into 13 (thirteen) Regencies and 4 (four) cities, and 217 districts. The boundaries of the South Sumatra Province are as follows:

- Northern side: Bordered by the Province of Jambi
- Southern Side: Bordered by Lampung Province
- West side: Bordered by Bengkulu Province
- East side: It borders the Bangka Belitung Islands Province

This research was conducted for a period of time from 2006-2011.

2.2. Methodology

2.2.1. Land Use Change

Before estimating emissions in the Province of South Sumatra, it is necessary to know the changes in land use that occurred in the past. Land use change analysis is performed using spatial analysis of multi-time land cover maps.

Table 1. Coverage Area of Land Use Changes in South Sumatra in 2006-2011

No	Land Use Change	Land Use in Ha			Land use Change	
		2006 (Ha)	2009 (Ha)	2011 (Ha)	2006-2009 (Ha)	2009-2011 (Ha)
1	Primary dryland forest	303.560	301.412	301.380	(2.148)	(32)
2	Secondary dryland forest	392.956	369.216	365.896	(23.740)	(3.320)
3	Primary swamp forest	40.212	25.588	16.412	(14.624)	(9.176)
4	Secondary swamp forest	466.944	369.980	361.520	(69.964)	(35.460)
5	Primary mangrove forest	110.252	96.572	96.576	(13.680)	4
6	Secondary mangrove forest	58.616	70.668	69.368	12.052	(1.300)
7	Plantation forest	303.840	351.224	380.352	47.384	29.128
8	Plantation	1.225.316	1.296.304	1.327.160	70.988	30.856
9	Shrubs	529.584	525.600	533.912	(3.984)	8.312
10	Swamp shrubs	378.656	374.044	387.272	(4.612)	13.228
11	Savanna	276.940	275.568	250.604	(1.372)	(24.964)
12	Dry land agriculture	542.368	543.176	544.420	808	1.244
13	Dry land agriculture with shrubs	2.870.016	2.883.260	2.844.084	13.244	(39.176)
14	Rice fields	456.800	458.028	457.752	1.228	(276)
15	Fish pond	43.980	44.360	46.072	380	1.712
16	Settlement	175.760	178.672	178.324	2.912	(348)
17	Transmigration	54.648	54.648	54.648	-	-
18	Open field	170.368	156.316	176.392	(14.052)	20.076
19	Mining	26.620	26.620	25.988	-	(632)
20	Irrigation	100.140	100.100	99.928	(40)	(172)
21	Swamp	126.944	126.336	136.628	(608)	10.292
22	Airport	228	184	184	(44)	-

Source: BAPPEDA, South Sumatra

Based on the table above, the largest land use change was used for agriculture of dry land mixed with shrub/farm covering 2,870,016 Ha in 2006 and 2,844,084 Ha in 2011. Then, it was followed by the use of plantations which were 1,225,316 Ha in 2006 and 1,327,160 Ha in 2011. While those that experienced changes in land use change for the period 2006-2009 were secondary swamp forests by experiencing a reduction in land area of 96,964 Ha and plantations experiencing an increase of 70,988 Ha in 2006 - 2009 and 30,856 Ha in the period in 2009-2011.

Peatlands are included in the land uses change such as primary swamp forest, secondary swamp forest, primary mangrove forest, secondary mangrove forest and swamp shrubs. Among the land use closures in which there are peat, experienced a very high reduction in land use cover in 2006-2009 which amounted to 117,828 Ha and 5,704 Ha in 2009-2011. This can be seen in the table 2.

Table 2. Land Use Change of Peatlands to primary swamp forest & secondary swamp forest

No	Land Use Change	2006 (Ha)	2009 (Ha)	2011 (Ha)	2006 - 2009 (Ha)	2009 - 2011 (Ha)
1	Primary swamp forest	40.212	25.588	16.412	(14.624)	(9.176)
2	Secondary swamp forest	466.944	369.980	361.520	(69.964)	(35.460)
3	Primary mangrove forest	110.252	96.572	96.576	(13.680)	4
4	Secondary mangrove forest	58.616	70.668	69.368	12.052	(1.300)
5	Swamp shrubs	378.656	374.044	387.272	(4.612)	13.228

Source: BAPPEDA South Sumatra Data Processed

2.2.2. CO2 Emissions

Based on the results of the processing of land cover maps in time series from 2006 to 2011 and carbon reserve data in each category of land cover can be used to make carbon density maps. Carbon density map shows carbon stocks for a certain period. The calculation of CO2 emissions is done using a carbon stock difference approach (Stock difference). By definition emissions occur due to changes in land use from land uses with high carbon stocks to land uses with lower carbon stocks. Net emissions are values that describe the amount of emissions reduced by carbon sequestration.

Table 3. Total Net Emissions Based on Land Use Change in South Sumatra from 2006-2011

No	Land Use Change on Peatland	Total Net Emissions (Ton CO2-eq)	
		2006 - 2009	2009 - 2011
1	Primary swamp forest to Secondary swamp forest	-	758.418
2	Primary swamp forest to Plantation	795.672	-
3	Primary swamp forest to Settlement	635.834	-
4	Primary swamp forest to Open field	-	758.418
5	Secondary swamp forest to Shrubs	1.182.084	-
6	Secondary swamp forest to Swamp shrubs	1.149.211	-
7	Secondary swamp forest to Plantation	852.945	-
8	Secondary swamp forest to Savanna	-	-
9	Secondary swamp forest to Rice fields	-	-
10	Secondary swamp forest to Dryland Agriculture	-	523.710
11	Secondary swamp forest to Open field	-	1.165.915
12	Primary mangrove forest to Secondary mangrove forest	8.186.297	-
13	Primary mangrove forest to Swamp shrubs	576.376	-
	Total Emisi	**13.378.419**	**3.206.461**

Based on the table above, the total net emissions caused by the change in land cover from peat to non-peat in South Sumatra in the period 2006-2009 amounted to 13,378,419 Tons of CO2-eq. But in the period 2009-2011 it decreased which became 3,206,461 tons of CO2-eq. The largest net emission occurred in land cover changes from primary mangrove forests to secondary mangrove forests amounting to 8,186,297 Tons of CO2-eq in the period 2006-2009. Whereas in the period 2009-2011 the largest emissions occurred in the change from secondary swamp forest to open land amounting to 1,165,915 tons of CO2-eq.

2.2.3. Gross Regional Domestic Product (GRDP) of South Sumatra Province

For GRDP obtained from the publication of the Central Statistics Agency (BPS) of South Sumatra from 2009-2011 in a time series.

Table 4. South Sumatra Province GRDP According to Business Fields Based on Constant Prices (million rupiah) in 2006-2011

No	Lapangan Usaha	PDRB Menurut Lapangan Usaha Atas Dasar Harga Konstan (juta rupiah)					
		2006	2007	2008	2009	2010	2011
1	Pertanian	10.437.334	11.113.699	11.567.788	11.927.064	12.482.952	13.141.056
2	Pertambangan	13.377.903	13.411.653	13.616.652	13.836.934	14.223.391	14.592.393
3	Industri Pengolahan	9.273.621	9.801.805	10.136.764	10.353.290	10.826.416	11.454.879
	a. Industri Migas	2.119.979	2.087.757	2.114.175	2.133.649	2.138.687	2.147.123
	b. Industri Tanpa Migas	7.153.642	7.714.048	8.022.589	8.219.641	8.687.729	9.307.756
4	Listrik, Gas & Air Bersih	248.673	267.073	281.069	295.377	314.021	339.337
5	Bangunan	3.845.876	4.157.657	4.412.936	4.737.050	5.151.465	5.814.656
6	Perdagangan, Hotel & Restoran	6.939.621	7.567.159	8.086.906	8.340.138	8.918.122	9.627.768
7	Pengangkutan dan Komunikasi	2.216.756	2.534.185	2.886.983	3.284.286	3.701.700	4.165.509
	Pengangkutan	1.492.152	1.596.752	1.703.748	1.832.771	1.979.601	2.138.836
	Komunikasi	724.604	937.433	1.183.235	1.451.515	1.722.099	2.026.673
8	Keuangan, Persewaan & Jasa Perusahaan	2.013.374	2.197.304	2.386.939	2.550.333	2.738.700	2.965.951
9	Jasa-jasa	3.861.690	4.211.579	4.689.418	5.128.472	5.502.373	5.906.947
	a.Pemerintahan Umum	2.249.280	2.461.461	2.761.434	2.978.488	3.182.514	3.397.394
	b. Swasta	1.612.410	1.750.118	1.927.984	2.149.984	2.319.859	2.509.553
10	PDRB DENGAN MIGAS	52.214.848	55.262.114	58.065.455	60.452.944	63.859.140	68.008.496
11	PDRB TANPA MIGAS	38.971.024	42.106.149	44.763.105	47.029.273	50.315.032	54.386.209

Source: BPS of South Sumatra Province

Based on data from the Gross Regional Domestic Product (GRDP) of South Sumatra Province according to the business field on the basis of constant prices from 2006-2011, it has increased from year to year. The mining sector is the biggest contributor to South Sumatra's GRDP followed by the Agriculture Sector, which includes a food crops, plantation, livestock, forestry and fisheries subsector. GRDP is the amount of gross domestic product received by the South Sumatra Provincial Government within one year, in its calculation the GRDP has not considered the value of environmental externalities as a result of activities to obtain these domestic products.

2.2.4. Economic Valuation of CO2 Emissions

Calculation of economic valuation on carbon dioxide (CO2) emissions due to land use changes can be calculated from the multiplication between the total amount of CO2 emissions due to land use changes with the percentage of Social Cost of Carbon from Interagency Working Group (IWG) study in United States of America which equal to 2% of the GRDP of South Sumatra Province in 2009-2011. In this paper the CO2 emissions used are limited to land use changes originating from peatlands which are part of the agricultural sector business in the GRDP. The economic valuation value of CO2 emissions used by 2% of the Agricultural Sector of the South Sumatra Province GRDP in 2009-2011.

3. Results & Discussion

3.1. Results and Discussion

3.1.1. CO2 emissions

Based on an analysis of land use changes in 2006-2011 in South Sumatra Province, land cover such as primary swamp forest, secondary swamp forest, primary mangrove forest and secondary mangrove forest which is peat land that has been replaced by land such as plantations, settlements, open land, shrubs, and dry land agriculture where peat is lost. This phenomenon of land conversion from peat to non-peat land will result in a CO2 net emission of 13,378,419 tons of CO2-eq with changes in the use of 117,828 hectares of land cover in 2006-2009. Whereas in 2009-2011 this land use change resulted in CO2 net emission of 3,206,461 Tons of CO2-eq with an area in land use change of 5,704 Ha.

CO2 emissions each year are:

- CO2 emissions in 2006-2009 due to Land use change = 13,378,419 Tons of CO2 -eq / 3 = 4,459,473 Tons of CO2-eq.
- CO2 emissions in 2009-2011 due to Land use change = 3,206,461 tons of CO2-eq / 3 = 1,068,820 tons of CO2-eq.

3.1.2. CO2 emissions per year for each hectare in land use change

Year of 2006-2009

$$= \frac{\text{Total net CO2 emissions in 2006-2009}}{\text{Extensive area of land use change in 2006-2009}}$$

$$= \frac{\text{13,378. 419 Tons of CO2-eq}}{\text{117.828 Ha}}$$

$$= 113.54 \text{ Ton } CO_2\text{-eq / Ha.}$$

Due to land use change, especially peatland in 2006-2009, 1 Ha of land will result in CO2 emissions – eq of 113.54 tons of CO2-eq for 3 years, or of 37.85 tons of CO2-eq / Ha per year.

Year of 2009-2011

$$= \frac{\text{Total net CO2 emissions in 2009-2011}}{\text{Extent of land use change in 2009-2011}}$$

$$= \frac{\text{3,206,461 Tons of CO2-eq}}{\text{5,704 Ha}}$$

$$= 562.14 \text{ Tons of CO2-eq / Ha.}$$

Due to land use change, especially land cover with peat in 2009-2011 in 1 Ha of land will cause CO2 emissions - eq of 562.14 tons CO2-eq for 3 years, or as much as 187.38 tons of CO2-eq / Ha per year.

3.1.3. Economic valuation of CO2 carbon emissions resulting from land use change

Economic valuation of CO2 carbon emissions calculated based on the results of a study from the Inter Agency Working Group (IWG) in United with Social Cost of Carbon (SCC) of emission CO2 equivalent to 2% of the amount of Gross Domestic Product (GDP) or GRDP from the agriculture sector in 2006-2011 and divided to the amount of CO2 emissions in each hectare of land use change per year. Therefore, the magnitude of the economic valuation of losses due to CO2 emissions in land use change is seen in the Table 5.

Table 5. Economic Valuation Losses Due to CO2 Emissions Release in Land Use Change

No	Lapangan Usaha	PDRB Menurut Lapangan Usaha Atas Dasar Harga Konstan (juta rupiah)					
		2006	2007	2008	2009	2010	2011
1	Pertanian	10.437.334	11.113.699	11.567.788	11.927.064	12.482.952	13.141.056
2	Pertambangan	13.377.903	13.411.653	13.616.652	13.836.934	14.223.391	14.592.393
3	Industri Pengolahan	9.273.621	9.801.805	10.136.764	10.353.290	10.826.416	11.454.879
	a. Industri Migas	2.119.979	2.087.757	2.114.175	2.133.649	2.138.687	2.147.123
	b. Industri Tanpa Migas	7.153.642	7.714.048	8.022.589	8.219.641	8.687.729	9.307.756
4	Listrik, Gas & Air Bersih	248.673	267.073	281.069	295.377	314.021	339.337
5	Bangunan	3.845.876	4.157.657	4.412.936	4.737.050	5.151.465	5.814.656
6	Perdagangan, Hotel & Restoran	6.939.621	7.567.159	8.086.906	8.340.138	8.918.122	9.627.768
7	Pengangkutan dan Komunikasi	2.216.756	2.534.185	2.886.983	3.284.286	3.701.700	4.165.509
	Pengangkutan	1.492.152	1.596.752	1.703.748	1.832.771	1.979.601	2.138.836
	Komunikasi	724.604	937.433	1.183.235	1.451.515	1.722.099	2.026.673
8	Keuangan, Persewaan & Jasa Perusahaan	2.013.374	2.197.304	2.386.939	2.550.333	2.738.700	2.965.951
9	Jasa-jasa	3.861.690	4.211.579	4.689.418	5.128.472	5.502.373	5.906.947
	a.Pemerintahan Umum	2.249.280	2.461.461	2.761.434	2.978.488	3.182.514	3.397.394
	b. Swasta	1.612.410	1.750.118	1.927.984	2.149.984	2.319.859	2.509.553
10	PDRB DENGAN MIGAS	52.214.848	55.262.114	58.065.455	60.452.944	63.859.140	68.008.496
11	PDRB TANPA MIGAS	38.971.024	42.106.149	44.763.105	47.029.273	50.315.032	54.386.209
	SCC Emisi Carbon CO2= 2% dari PDRB Sektor Pertanian	208.747	222.274	231.356	238.541	249.659	262.821

Based on the table above, the economic valuation of CO2 carbon emission losses due to land use change in 2006 was IDR 208,746.68, in 2007 IDR 222,273.98; 2008 in the amount of IDR 231,355.76; 2009 in the amount of IDR 238.541,28; in 2010 amounting to IDR 249.659.04 and in 2011 amounting to IDR 262.821,12

The economic valuation of losses due to changes in land cover use in 2006-2001 for each hectare of land use changes is as follows:

$$\frac{\text{2\% x PDRB from Agriculture Sector Year (n)}}{\text{Emission per ha year (n)}}$$

Year of 2006 = $\frac{\text{IDR 208,746,680.000}}{\text{113, 54 Tons of CO2-eq / Ha}}$
= IDR 1,839,000,000 / Ton CO2-eq / Ha / Year
Year of 2007 = $\frac{\text{IDR 222,273980,000}}{\text{113, 54 Tons of CO2-eq / Ha}}$
= IDR 1,958 ,000,000 / Ton CO2-eq / Ha / Year
Year of 2008 = $\frac{\text{IDR 231,355,760,000}}{\text{113, 54 Tons of CO2-eq / Ha}}$
= IDR 2,038,000,000 / Ton CO2-eq / Ha / Year
Year of 2009 = $\frac{\text{IDR 238,541,280,000}}{\text{562.14 Tons of CO2-eq / Ha}}$
= IDR 424,000,000 Tons of CO2-eq / Ha / Year

Year of 2010 = $\frac{\text{IDR 249,659,040,000}}{\text{562.14 Tons of CO2-eq / Ha}}$
= IDR 444,000,000 / Ton CO2-eq / Ha / Year
Year of 2011 = $\frac{\text{IDR 262,821,120,000}}{\text{562.14 Tons of CO2-eq / Ha}}$
= IDR 468,000,000 / Ton CO2-eq / Ha / Year.

4. Conclusions

Based on the results of the discussion above, total CO2 emissions resulting from land use change on peatland in the period 2009-2011 decreased compared to total CO2 emissions in 2006-2009. This is due the extent of changes in land cover use in the period 2009-2011 also declined. The amount of economic valuation due to CO2 emissions caused by changes in land cover use for each hectare (Ha) and per year for the 2009-2011 period is less than the amount of economic valuation due to CO2 emissions caused by changes in land cover use for each hectare (Ha) and per year for the period 2006-2009. The highest value for economic valuation due to loss of CO2 carbon emissions from changes in land cover use per hectare (Ha) during the study period occurred in 2008, amounting to IDR 2,038,000,000 /Ton CO2-eq /Ha/Year.

5. References

1. Marpaung, F., D. Fernando, and S. Putiamini. *Tropical Peat Moisture Profiles for Early Information of Drought in Indonesia*. in *2018 IEEE Asia-Pacific Conference on Geoscience, Electronics and Remote Sensing Technology (AGERS)*. 2018. IEEE.
2. Selatan, P.P.S., *Rencana Aksi Daerah (RAD) Penurunan Emisi Gas Rumah Kaca (GRK) Provinsi Sumatera Selatan Tahun 2010-2030*, ed. W.A. Centre. 2017, Sumatera Selatan: Pemerintah Provinsi Sumatera Selatan.
3. Marpaung, F. and T. Hirano, *Environmental dependence and seasonal variation of diffuse solar radiation in tropical peatland.* Journal of Agricultural Meteorology, 2014. **70**(4): p. 223-232.

Simulating the Overland Flow in Prospectively Cleared Tropical Forest for Expressway Using Airborne LIDAR & High-Resolution Optical Images

Abd. Ramlizauyahhudin Mahli[1]*, Mohd. Rizaludin Mahmud[2], Mohd. Nadzri Mohd. Reba[2]

[1]Faculty of Built Environment & Surveying, Universiti Teknologi Malaysia, 81310, Johor Bharu, Malaysia
[2]Geoscience & Digital Earth Centre (InsTeG), Research Institute for Sustainable Environment, Universiti Teknologi Malaysia, 81310, Johor Bharu, Malaysia

e-mail: ramli.mahli@gmail.com

Abstract. This study simulates the overland flow using the forest structural parameters and high-resolution terrain information attained from the airborne LIDAR, the high resolution (HiRes) optical imagery and rainfall data in the potentially cleared tropical forest due to road development. Significant overland flow would affect the driving convenience in the prospective road. Measuring the overland flow using field measurement was constrained by small site coverage, enduring harsh tropical forest environment, complex computation with various input variables and time-ineffective. A substitute or support methodology is required in order to measure the throughfall for large areas in economic time frame. Prior to that, an experiment was conducted in Limbang, one of the prospective Pan-Borneo routes located in the state of Sarawak in Borneo Island. The overland flow is simulated for two conditions, (i) present situation (natural condition), and (ii) prospective future situation (cleared forest condition and terrain changes). Canopy throughfall is derived from the three-dimensional tree canopy structure using the LIDAR information and HiRes optical images. The simulation of the future overland flow after the road development is carried out by quantifying the amount of run-off with the areas involve with the actual road alignment is removed. Subsequently, the overland flow value before and after the prospective road development is compared. The output of this study would be useful to understand the aftermath effect of tropical forest removal to driving convenience; one of the critical aspects that influenced the sustainable transportation and environmental safety in the humid tropics.

1. Introduction

Drastic forest clearing for road development in humid tropical landscape would result significant hydrological changes that affect the road and driving safety. Tropical forest is known for having high canopy interception. Its removal has significant implication on the increase of throughfall that will create an inconvenience driving environment including limited visibility. Adaptation to these changes require accurate and fine scale information regarding the types of the impacts and its severity, prone locations, and period of occurrence. Using field-based measurement require an expensive, time consuming, and laborious works; therefore, opting for an aerial survey with precise laser scanners would be a useful substitute. Such investigation in the humid tropical landscape are scarcely found especially at the high precision engineering scale, reaching 1 meter. Anticipating this gap by formulating an appropriate operational methodology with minimum field variables would enable effective assessment of the hydrological impacts to road driving at precise working scale.

LIDAR was proven to be useful tool in forestry especially in height characterization of the tree structure and also the forest landscapes ([1]; [2]; and [3]). Together with the integration of digital optical camera, the horizontal canopy crown information is effectively captured. Scientific studies showed that various efforts had been done in studying the crown morphology using these two variables (e.g., [4] and [5]). In estimating rainfall interception, indirect method was theoretically possible using both the vertical and

horizontal canopy morphology information together with auxiliary information. Tree height information would enable estimation of canopy vertical thickness. Meanwhile, the crown canopy optical photo can provide rough estimation on the canopy closure which associated to the throughfall (amount of rainwater penetrated the canopy and reach the ground). However, reliable computation is rarely found.

As for overland flow estimation, the role of the LiDaR is primarily in providing high resolution 3D information of the terrain. Upon the development, the properties of slope and topographic changes that occur would affect the movement of the water. Many present hydrological simulations had embedded digital terrain model in their modelling for accurate representation of hydraulic properties [6]. If high resolution digital elevation model is used, then it is possible to modelled the overland flow for the current and post development at high resolution engineering scale simulation. Hence, tropical rainforest of Borneo received substantial amount of annual rainfall (> 2000mm) and intense storm (~25mm/d), therefore slight forest canopy losses might cause significant hydrological effects. While the theory is scientifically sound, evidences are hard to find and require thorough study.

Prior to the aforementioned circumstance, this study has taken initiative to formulate an appropriate LIDAR and spatial methodology to assess the future overflow prior to the road development in humid tropics. The chosen experimental site would be the specific Limbang interchange road network to Brunei, which is approximately 5km of length. The current interception & expected overland flow for the potential future highway will be computed on quadrat basis and its spatial variation will be mapped. There are two major significant contribution of this study, first is the operational methodological development using LIDAR and ancillary data to perform efficient large-scale interception and second to obtain knowledge on the possible amount of throughfall impact upon the highway development. The output of this study is useful for preventive, mitigation and adaptation action to reduce the risk of driving safety in humid tropics.

2. Materials & Method

2.1. Method

This method is separated into two sections, (A) the three-dimensional (3D) canopy interception estimation, (B) overland flow simulation. In section A, there are three main steps in computing the volumetric canopy infiltration in this study; (1) compute the horizontal (2D) canopy relative openness using UAV orthophoto images, (2) compute the vertical canopy thickness using LIDAR data, and (3) compute the 3D volumetric canopy infiltration. Instead of computing the canopy infiltration for individual crown which a common approach in forestry sciences and ecology, we chose to compute it at 10 meter grid, as for two reasons; first is delineating individual tree crown in tropical forest is extremely challenging where many studies are not reaching reliable independent results and second is the remote sensing measurement are based on the average reflective signals of electromagnetic wave at specific field of view rather than individual canopy.

In section B, two steps are involved, first is the estimation of post road development rainfall at various intensity, and second is the computation of the present and post development of overland flow. The resolution of the overland flow is 0.5 meters.

2.1.1. Horizontal (2D) canopy openness estimation using UAV orthophoto images (HCO)

Due to limited available technique to indirectly estimate the canopy openness using high resolution of remotely sensed image or aerial photo without using too many support variables which are limited in the study area, the fundamental technique applied in computing canopy closure using hemispheric photo is adapted.

The fundamental approach is by computing the ratio between the numbers of bright pixel (non-leaf area) over the dark pixel (canopy leaf). High number of ratios mean large canopy openness. By using that principle on greyscale digital aerial photograph, one can also estimate the canopy openness. Bright pixel represents areas that covered by the canopy leaf, and dark pixel represent the uncovered canopy areas.

For default to 8-bit photo, the threshold brightness value for the dark pixel will be defined as below than 10, meanwhile the rest are considered bright pixel. The equation below expressed the mathematical concept.

$$\text{Horizontal Canopy openness, HCO , per grid (\%)} = \left(1 - \frac{\text{No. of pixelwith BV<10}}{\text{No. of pixel with BV>10}}\right) * 100\% \quad (1)$$

where BV is brightness value.

2.1.2. Vertical canopy infiltration (VCI) estimation using LIDAR data

The estimation of the vertical canopy thickness is done by subtracting the maximum tree height with the average tree height found in each of the 10m grid. The tree height in the meantime were obtained by subtracting the surface model height (2nd pulse LIDAR return) with the terrain model height (1st pulse LIDAR return). In realizing the throughfall phenomena, we assumed that high thickness canopy would have higher interception of rainfall and vice versa, therefore the calculation of vertical canopy infiltration (VCI) is acquired by subtracting the percentage of vertical canopy thickness (against average tree height) with 1 (perfect interception). Figure below illustrated the two processes.

$$\text{VCI, per grid (\%)} = \left(1 - \frac{CT}{Th}\right) * 100\% \quad (2)$$

where Th is average tree height (m), CT is canopy thickness (m).

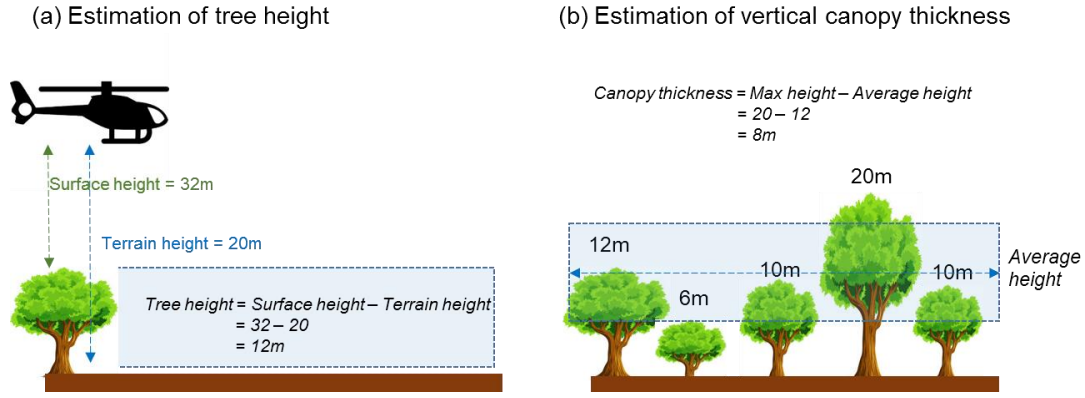

Figure 1. Schematic diagram of the tree height and vertical canopy thickness estimation.

2.1.3. 3D volumetric canopy throughfall (VCT)

The average volumetric canopy throughfall (VCT) is obtained by computing the average of vertical and horizontal canopy thickness. The amount of canopy throughfall (mm/hr) is computed by multiplying it with the actual rainfall intensity (mm/hr) for each quadrat. Based on the literature review and observation dataset in the humid tropics, we adapted the theory that throughfall is proportional with canopy openness either horizontal or vertical. Because throughfall is also depending on the intensity of rainfall, we also take into consideration the effects of canopy saturated condition. Evidences had showed that throughfall is 100% when the rainfall intensity exceeding 40mm/hr (CITA). The corresponding VCT computation is expressed in the equation below.

$$\text{VCT, per grid (mm)} = \left(\frac{\text{VCI} + \text{HCO}}{2}\right) * R \quad (3)$$

where VCT is the volumetric canopy throughfall (mm/hr), VCI is vertical crown thickness, HCO is canopy openness, and R is rainfall in mm/hr. For R <5mm/hr, the VCT value is set to zero as all the rainfall is intercepted by the canopy, R>35mm/hr, the VCT value is set to 100% as all the rainfall will penetrate the canopy.

2.1.4. Overland flow simulation

In simulating the overland flow, we used the rational method. To represent the overland flow after road development, the surface run-off coefficient is change to parking land use from forest (Table 1). Slope value is obtained and computed from the digital surface model of the study area. Equation (4) expressed the computation process while table 1 showed the run-off co-efficient.

$$\text{Overland flow, per grid } (m^3/s) = (C * i * A) \ * cf \quad (4)$$

where C is the is run-off coefficient, i is the net rainfall (Precipitation-Interception), and A is pixel area (in hectares), cf is the conversion factor to S.I. units, 0.0028.

Table 1. Surface run-off coefficient for various land use types and slope effects.

Land use / Slope	Soil group A			Soil group B			Soil group C			Soil group D		
	<2%	2-6%	>6%	<2%	2-6%	>6%	<2%	2-6%	>6%	<2%	2-6%	>6%
Forest	0.08	0.11	0.14	0.10	0.14	0.18	0.12	0.16	0.20	0.15	0.20	0.25
Meadow	0.14	0.22	0.30	0.20	0.28	0.37	0.26	0.35	0.44	0.30	0.40	0.50
Pasture	0.15	0.25	0.37	0.23	0.34	0.45	0.30	0.42	0.52	0.37	0.50	0.62
Farmland	0.14	0.18	0.22	0.16	0.21	0.28	0.20	0.25	0.34	0.24	0.29	0.41
Res. 1 acre (100%)	0.22	0.26	0.29	0.24	0.28	0.34	0.28	0.32	0.4	0.31	0.35	0.46
Res. 0.5 acre (50%)	0.25	0.29	0.32	0.28	0.32	0.36	0.31	0.35	0.42	0.34	0.38	0.46
Res. 0.3 acre (30%)	0.28	0.32	0.35	0.3	0.35	0.39	0.33	0.38	0.45	0.36	0.4	0.5
Res. 0.25 acre (25%)	0.30	0.34	0.37	0.33	0.37	0.43	0.36	0.4	0.47	0.38	0.42	0.52
Res. 0.13 acre (13%)	0.33	0.37	0.40	0.35	0.39	0.44	0.38	0.42	0.49	0.41	0.45	0.54
Industrial	0.85	0.85	0.86	0.85	0.86	0.86	0.86	0.86	0.87	0.86	0.86	0.88
Commercial	0.88	0.88	0.89	0.89	0.89	0.89	0.89	0.89	0.9	0.89	0.89	0.9
Streets	0.76	0.77	0.79	0.8	0.82	0.84	0.84	0.85	0.89	0.89	0.91	0.95
Parking	0.95	0.96	0.97	0.95	0.96	0.97	0.95	0.96	0.97	0.95	0.96	0.97
Disturbed area	0.65	0.67	0.69	0.66	0.68	0.7	0.68	0.7	0.72	0.69	0.72	0.75

2.2. Rainfall data

To provide the information on the daily rainfall, the satellite data from the Global Precipitation Mission satellite be used. The average daily rainfall was obtained from the half-hourly rain rate estimates. The size of this data is re-gridded from 0.1° resolution to 0.01° using inverse distance weight interpolation scheme. However, because our experimental site in this preliminary study is relatively very small, we assumed constant rainfall were occurred for all the respective grids.

2.3. Terrain and tree height from LIDAR data

The high precision terrain height and tree height information were obtained through a LIDAR scanning. The measurement was done at 4 discrete returns per pulse - 1st, 2nd, 3rd, and last. The aerial scanning was done by following the proposed highway path with 100-meter buffer. The measurement of up to 4 intensity readings per pulse, with 12-bit dynamic range. To ensure extensive coverage and sufficient instantaneous field of view of the scanning, a minimum sidelap of 20% between swathes and half-scan angle of 20% was chosen. The scanning was done using narrow beam divergence with footprint of under 0.4m. The digital terrain model was produced by processing the last return signals. Meanwhile, the digital surface model was generated using the information from the first return. Other information about flying and scanning details were provided in the table below.

Table 2. LiDaR scanning specification

Specification	Description
Flying height	~ 800-1100 meter above the terrain
Point spacing	1.4m along track; 0.8 across-track
Frequency	50-500Hz
Scan density	1-4 points per meter square
Pulse recording	4 discrete returns per pulse
Pulse rate	100 000Hz

2.4. Aerial orthophoto

In order to provide tree canopy information of the study area, aerial orthophoto will be used. This data was obtained simultaneously during the LiDaR scanning process. 16 mega pixels with 12-bit radiometric digital based frame camera is used. This colored orthophoto was mosaicked prior to the rectification geo-tagged imageries with 15-60cm ground sample distance (GSD).

2.5. Pan Borneo Highway support documents

There are several informations that are required in this study which includes; (1) the proposed road network, (2) the proposed road design. The proposed road network comprises the path of the highway; primarily consisting its location and length. Because our study area relatively covered a small portion of the whole PBE route, specific proposed road network for Limbang section is obtained from the Lebuhraya Borneo Utara Sdn. Bhd. Meanwhile, the proposed road design containing information about the width, types of lanes, reserve road areas, and targeted elevation of the road. This information is crucial in mapping the risk areas for the throughfall and run-off at pre and post highway development. The proposed road design is shown in figure below.

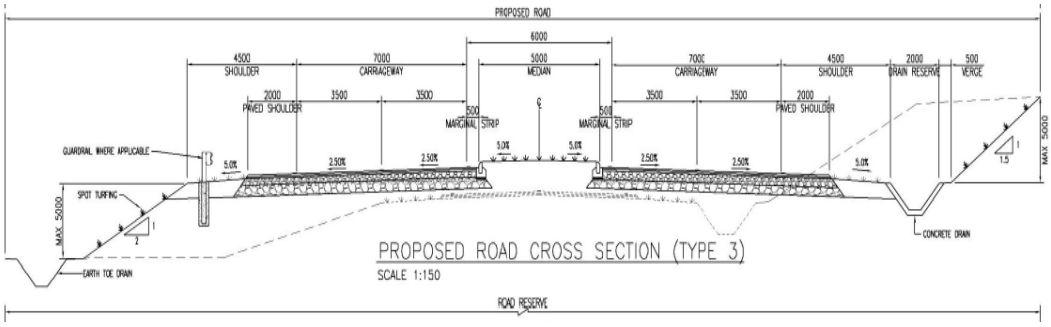

Figure 2. Proposed road design in Limbang section [7].

2.6. Study Area Description

Limbang was a district located at Sarawak which situated at the border between Sabah and Brunei Darussalam. The total length of the Pan Borneo Highway of Limbang section is 48.15 km which includes construction of 15.91km of new highway. There is a newly proposed route also known as Limbang conceptual alignment (blue route in Figure 1) which deviated from the existing alignment at about 3km south of Limbang town; a specific linkage route to Brunei. Like any other region in Sarawak, Limbang received significant large amount of rainfall; maximum occurred from October to December (>300mm/month). The climate is strongly influenced by the monsoon and the surge cold Borneo flux [8] which resulted extreme anomalies including strong prevailing wind. For this study we chose a small experimental site inside the proposed road alignment in order to test the reliability of our method. The main reason for this selection is to reduce the complexity of abundance pixel during processing and also to assist our understanding since the sample were relatively small.

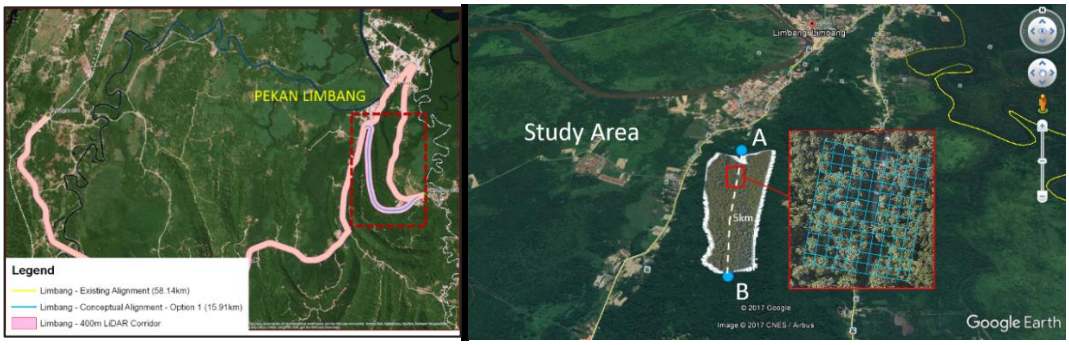

Figure 3. Study area.

3. Results & Discussion

3.1. Simulated volumetric canopy throughfall changes: Pre and post expressway development

Table 3. Average Estimated and Simulated Volumetric Canopy Throughfall for Pre and Post Expressway Development at Different Rainfall Intensity

Rainfall intensity	Rainfall intensity (mm/hr)	Volumetric throughfall (*mm/hr*)	
		Pre-expressway development	Post-expressway development
Light	<2	0.013	2
Moderate	5	1.6	5
Heavy	20	6.66	20

Our result showed that the simulated throughfall prior to the expressway development had increased drastically (>100%) with an increasing rainfall from light (<2mm/hr) to moderate (5mm/hr) (Table 3). During the light rainfall, the amount of throughfall is almost none; indicating that the thick and closed canopy coverage of the study area potentially intercept all the rainfall. From the throughfall map (fig. 4), the amount of volumetric canopy throughfall (VCT) had increased as the rainfall intensity increased from light to moderate(2-5mm/hr). Despite the increasing VCT value with increasing rainfall intensity, the spatial pattern of the VCT exhibited during the moderate and heavy rainfall is almost similar.

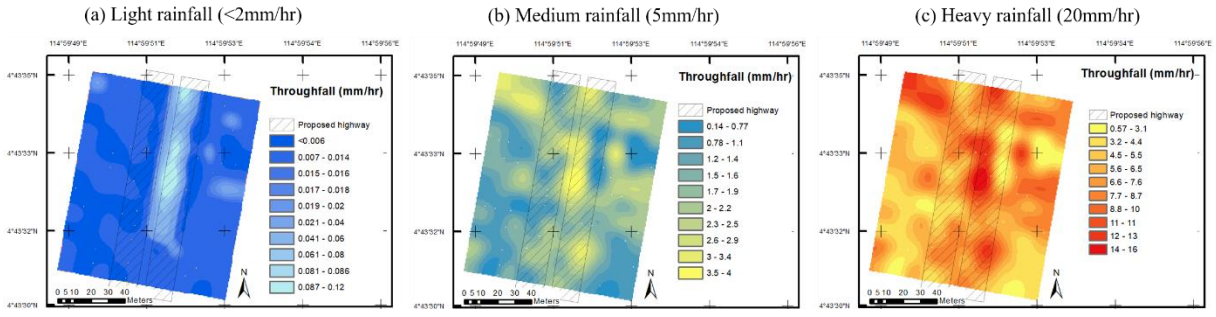

Figure 4. Volumetric canopy throughfall, for light, medium (moderate) and heavy rainfall condition.

3.2. Simulated overland flow changes: Pre and post expressway development

The post expressway development resulted significant increment of overland flow (>100%). The largest increment occurred during the light rainfall (2mm/hr) because most of the rainfall initially is completely intercepted by the canopy. The maps showed that the development of the expressway has completely changed the overland flow pattern and increased its volume; linearly with increasing rainfall. The range

of overland flow for light to heavy rainfall has drastically changed from 0.014 - 0.696 cubic mm/s to 0.638 – 6.381 cubic mm/s.

Table 4. Simulated Overland Flow During Pre and Post Expressway Development at Different Rainfall Intensity

Rainfall intensity	Rainfall intensity (mm/hr)	Average overland flow (mm³/s)	
		Pre-expressway development	Post-expressway development
Light	2	0.014	0.638
Moderate	5	0.174	1.595
Heavy	20	0.696	6.381

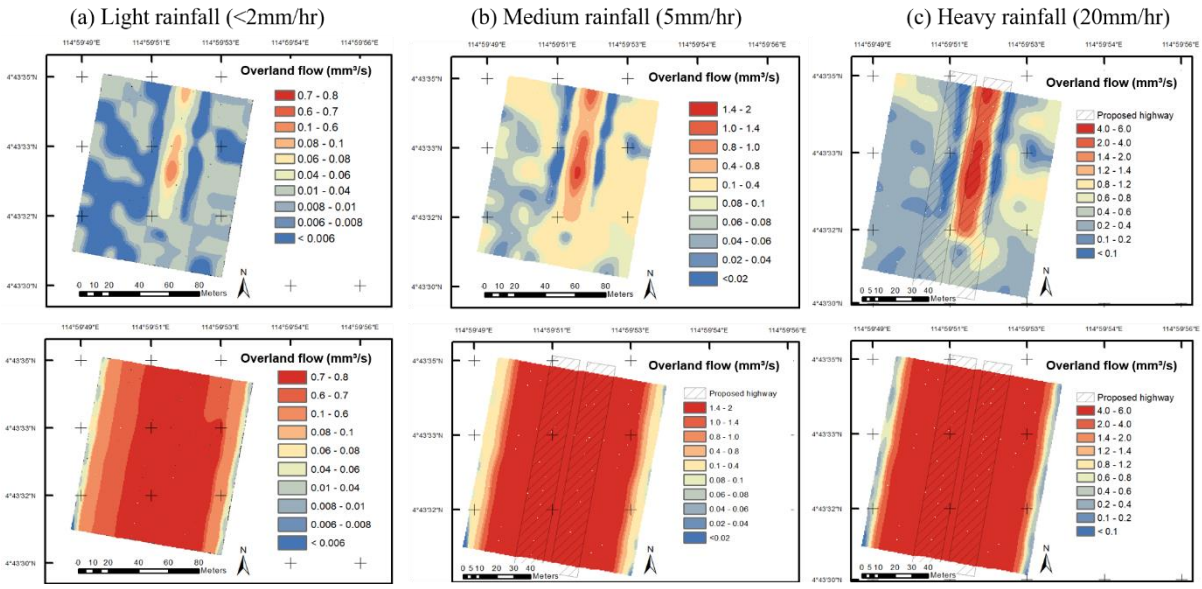

Figure 5. Maps of simulated overland flow during pre and post expressway development at different rainfall intensity.

4. Conclusion & Future works

This study has demonstrated the utility of airborne LiDAR and high-resolution optical images to simulate the impact of expressway development towards hydrological variables that affect driving safety and convenience namely throughfall and overland flow. Major findings are the removal of the forest canopy would result drastic increment of throughfall and overland flow (>100%) and also changed the heterogeneous spatial pattern to completely homogenous despite relatively small area of forest removal compared to logging activities. Future works would involve field verification since in-situ validation is absent in this research paper. It would potentially cover the verification of the canopy thickness with in-situ measurement (LAI, hemispheric photo, etc.) and also throughfall via separate on and off canopy gauge measurement.

5. Acknowledgments

Authors wish to thank Sarawak Forestry Department, collaboration by respective industries, and colleagues who assists the technical stuffs.

6. References

1. Goodwin, N.R., N.C. Coops, and D.S. Culvenor, *Assessment of forest structure with airborne LiDAR and the effects of platform altitude.* Remote Sensing of Environment, 2006. **103**(2): p. 140-152.
2. Lovell, J., et al., *Using airborne and ground-based ranging lidar to measure canopy structure in Australian forests.* Canadian Journal of Remote Sensing, 2003. **29**(5): p. 607-622.
3. Kelly, M. and S. Di Tommaso, *Mapping forests with Lidar provides flexible, accurate data with many uses.* California Agriculture, 2015. **69**(1): p. 14-20.
4. Shamsoddini, A., R. Turner, and J. Trinder, *Improving lidar-based forest structure mapping with crown-level pit removal.* Journal of Spatial Science, 2013. **58**(1): p. 29-51.
5. Jing, L., et al. *Automated individual tree crown delineation from LIDAR data using morphological techniques*. in *IOP Conference Series: Earth and Environmental Science*. 2014. IOP Publishing.
6. Barber, C.P. and A. Shortridge, *Lidar elevation data for surface hydrologic modeling: Resolution and representation issues.* Cartography and Geographic Information Science, 2005. **32**(4): p. 401-410.

Determination of Window Image Matching Size for Geometric Accuracy Test of Very High Resolution Images

Sukentyas E.S.[1*], Mulia Inda R[1], Randy Prima B[1], Fadila Muchsin[1], Yudhi Prabowo[1], Kurnia Ulfa[1], Marendra Eko B[1], Destri Yanti H[1], Choirun Nisaa[1], Ratih Dewanti[1]

Remote Sensing Technology and Data Center, LAPAN
Jl.LAPAN No.70, Pekayon, Pasar Rebo, Jakarta Timur, 13710

e-mail: *sukentyas.estuti@lapan.go.id*

Abstract. The very high resolution data owned by LAPAN are Pléiades 1A and 1B, with incidence angles ranging from 0º to 30º. Pléiades 1A-1B imagery has been systematically geometric corrected at LAPAN Parepare Ground Station, but still do not know how much the horizontal accuracy of the image is against the coordinates of the GPS (Global Positioning System). Mapping using remote sensing data requires well-corrected data requirements, so a study is needed to examine the geometric quality of Pléiades 1A-1B data. One method of testing accuracy is matching images. In the process of matching images, the RMSE value generated depends on the size of the GCP window chip used. This study uses the window size of the GCP chip with a radius of 50, 100, 150 and 200 pixels, and the incidence angles of the image used is ≤ 20º. The purpose of this study is to determine the best window size of GCP chips to produce the smallest RMSE value.

1. Introduction

Pléiades 1A and 1B data has been recorded and received from 2017 until now at LAPAN Parepare Ground Station. The Pléiades twins are very high-resolution satellites delivering 50-cm as a standard. The Pléiades 1A spacecraft was launched on December 16, 2011 on a Soyuz ST from Europe's spaceport in Kourou, French Guiana. It will be followed by Pléiades 1B in late 2012. Offering an ideal combination of coverage, resolution and speed, Pléiades products are especially useful for applications in defense, civil protection, hazard management, urban mapping, precision agriculture, and network and infrastructure management [1].

Image registration can be interpreted as a process of transformation from one image to another so that each object that has been recorded has the same coordinate pair with the reference image. So for the process we need to do geometric corrections. There are various methods for making geometric corrections, one of which is ortho-rectification. Where ortho-rectification considers the displacement of pixel positions caused by the curvature of the Earth and gives real ground coordinates (values of x, y and z) for all pixels. The ortho images produced have good accuracy depending on the input and reference sources used, such as the use of digital elevation models (DEM) and ground control points (GCP). Appropriate GCP collection presents a significant problem, because existing GCP sources may not be available to the public. However, DEM can be easily available and can be obtained from commercial suppliers (eg Airbus Defense and Space), for example WorldDEM ™ products (resolution 12 m) or available as public products for example SRTM (resolution 30 m or 90 m) [2].

Image registration is a fundamental task in image processing to overlay two or more images used. Registration methods can be loosely divided into the following classes: algorithms that use image pixel values directly, e.g., correlation methods [3][4]; algorithms that use the frequency domain, e.g., fast Fourier transform-based (FFTbased) methods [5][6]; ; and algorithms that use high-level features such as identified (parts of) objects, or relations between features, e.g., object detection methods [7].

Measurement of geometry quality of an image is very necessary to provide information about geometric differences between images, especially ortho-rectification images.

Objective of the research are to search the optimal GCP Chip window size to produce the smallest RMSE and to calculate the value of Pleiades imagery shifts using GPS points from field measurements.

2. Metodology

2.1. Satellite image data

LAPAN's Pléiades 1A-1B imagery are available in two different processing levels: Primary and Ortho Standard. The Primary product is the processing level closest to the natural image acquired by the sensor. Where the sensor is placed in square geometry without coordinates (X, Y) and the image is clear of all radiometric distortion. For own orthorectification or 3D modeling, the Primary product completed with Rational Polynomial Coefficients (RPCs) and the sensor model. The Ortho Standard product is a georeferenced image in Earth geometry, corrected from acquisition and terrain offnadir effects. All processing is fully automatic on Ground Stasion. Ortho Standard products offer the bundle product is in Panchromatic channel (product resolution: 0.5 m) or the Multispectral channels (4 bands, product resolution: 2 m) already registered and possibly merged (Pan-sharpened). For the specification can be seen in Table 1.

Table 1. Specification of Pléiades 1A-1B imagery

Mode Imaging	Panchromatic	Multispectral
Spatial resolution	0.5 m GSD at the nadir	0.2 m GSD at the nadir
Spectral range	480 – 830 nm	Blue (430 –550 nm) Green (490 –610 nm) Red (600 – 720nm) Near Infrared (750 –950 nm)
Swath Width	20 km at nadir	
Off-Nadir imaging	up to 47°	
Radiometric range	12 bit per pixel	
Revisit frequency	2 days for combine Pléiades 1A-1B	
Altitude	694 km	
Orbit	Sun-synchronous, 10:15 A.M	
Image Location Accuracy	▪ Without ground control points: 3m CE90 ▪ With ground control points: 1m	

Source: [1], [3]

The data used in this study was Pleiades 1A-1B Pan-sharpened Ortho Standard and the location can be seen in Figure 1 and Table 2.

Table 2. Specification of Pléiades PMS 1A-1B imagery

Scene ID	square km	Incidence Angle	Sun Azimuth	Sun Elevation
LPN_PHR1A_PMS _201707230253194_ORT	1228.25	19.28	43.43	51.55
LPN_PHR1A_PMS_201807220253354_ORT	2083.63	22.92	42.99	51.27
LPN_PHR1B_PMS_201705240304200_ORT	2279.99	14.08	36.91	54.51

2.2. Ground Control Point (GCP)

In addition, ground control points (GCPs) were acquired with GPS by field surveying, which were used to select the significant feature area on the images. The method used for collecting GCP points in the field is the Rapid Static method. Measurement of GNSS (Global Navigation Satellite System) using Rapid Static method is done to get coordinates from 37 points spread in AOI (Area of Interest). Measurements use a GNSS receiver in the form of a Trimble GeoXT 3000 Series using the Magetan City CORS (Continuous Operating Reference System) base station from . The length of observation carried out is for ± 30 minutes at each point. The observation of GNSS rapid static method is done by post-processing with the GPS Pathfinder Office software in RINEX format.

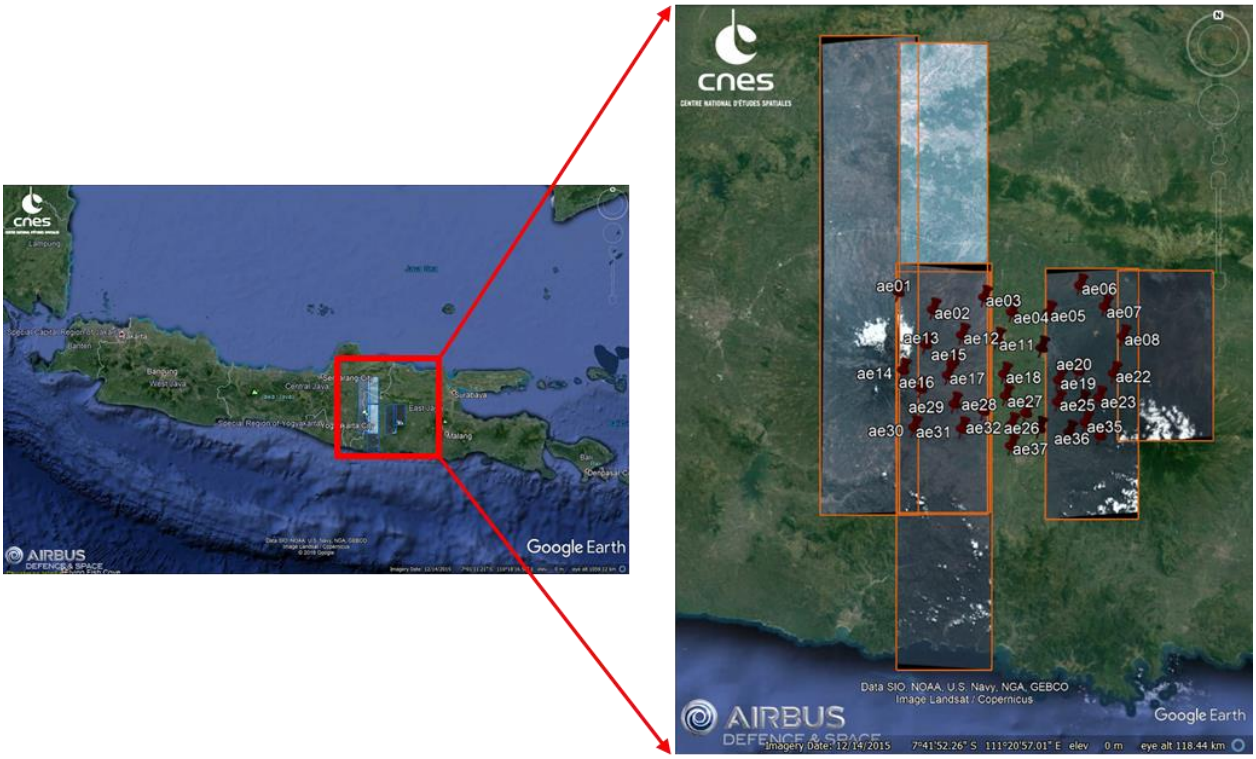

Figure 1. Research location is a cover part of Madiun district, province of East Java (blue box are Pleiades 1A-1B Ortho Standard 50cm year 2017-2018 and pin points are GPS points).

2.3. GCP Chip

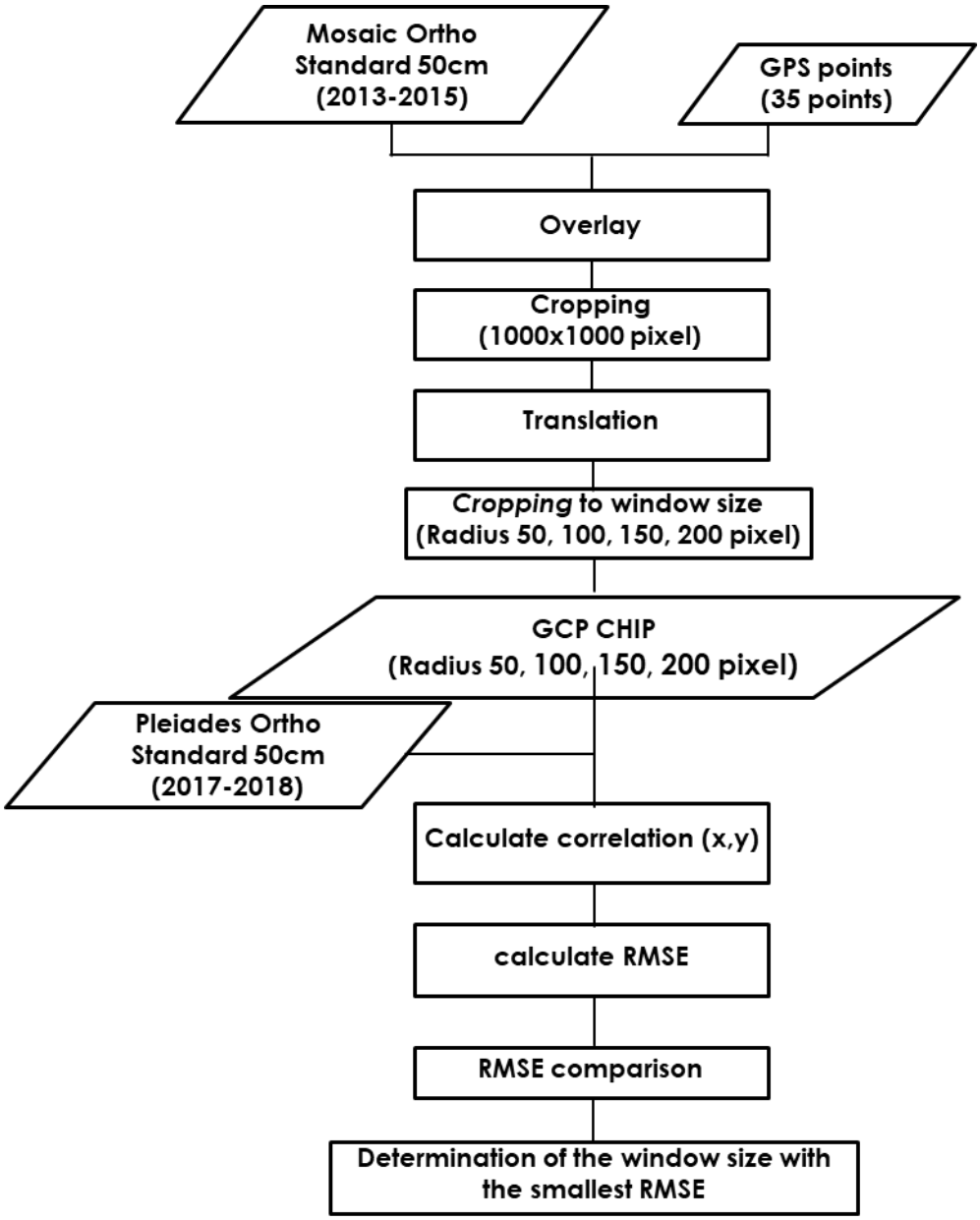

Figure 2. Window size determination flow chart.

3. Result

Penghitungan RMS Error dilakukan terhadap tiga citra Pleiades dengan cakupan area yang sama, dengan ukuran radius window 50, 100, 150, dan 200. Hasil penghitungan RMSE disajikan dalam Tabel 3.1 sampai Tabel 3.3.

Tabel 3. Hasil Penghitungan RMSE citra Pleiades scene id LPN_PHR1A_201707230253194_ORT

Nomor Chip	Radius window 50			Radius window 100			Radius window 150			Radius window 200		
	dx (m)	dy (m)	RMSE	dx (m)	dy (m)	RMSE	dx (m)	dy (m)	RMSE	dx (m)	dy (m)	RMSE
2.00	-0.01	0.13	0.13	0.60	0.01	0.60	0.12	0.12	0.17	-0.02	0.04	0.05
3.00	-0.03	-6.86	6.86	0.02	3.43	3.43	0.02	3.44	3.44	0.00	32.57	32.57
14.00	5.43	-14.99	15.95	0.05	-0.01	0.06	0.07	-2.02	2.02	-0.09	-26.68	26.68
16.00	-0.05	0.49	0.49	4.86	-1.38	5.06	0.16	-2.48	2.48	0.00	-2.53	2.53
29.00	0.15	-1.52	1.53	-0.03	-2.48	2.48	0.01	0.02	0.02	-0.52	-0.04	0.52
30.00	-0.01	-0.10	0.10	0.17	-1.03	1.05	0.86	0.07	0.86	-0.93	0.06	0.93
31.00	1.47	-0.02	1.47	0.79	0.11	0.80	0.51	1.98	2.05	0.02	4.16	4.16
15.00	1.52	-0.03	1.52	0.15	0.01	0.15	0.17	0.07	0.18	-0.09	-0.87	0.87
17.00	10.25	0.06	10.25	-0.03	13.97	13.97	0.52	0.07	0.53	0.05	0.09	0.10
12.00	2.42	-0.07	2.42	1.53	0.12	1.53	0.19	0.17	0.25	0.10	0.88	0.89
28.00	1.95	-1.46	2.43	2.39	-1.47	2.81	2.27	-1.50	2.72	2.21	-1.51	2.68
Total	3.68	5.01	6.22	1.73	4.45	4.78	0.77	1.60	1.78	0.74	12.79	12.81
	CE90 =		9.44	CE90 =		7.25	CE90 =		2.70	CE90 =		19.44

Tabel 4. Hasil Penghitungan RMSE citra Pleiades scene id LPN_PHR1A_201807220253354_ORT

Nomor Chip	Radius window 50			Radius window 100			Radius window 150			Radius window 200		
	dx (m)	dy (m)	RMSE	dx (m)	dy (m)	RMSE	dx (m)	dy (m)	RMSE	dx (m)	dy (m)	RMSE
2.00	0.10	-0.05	0.11	0.14	0.02	0.15	0.17	0.83	0.85	-0.07	0.91	0.91
3.00	-5.46	-0.06	5.46	0.14	3.62	3.62	0.03	3.66	3.66	-0.04	32.48	32.48
14.00	-18.12	14.46	23.18	-0.01	0.12	0.12	0.05	-0.14	0.15	0.01	-54.96	54.96
16.00	-0.01	0.36	0.36	-0.01	-0.87	0.87	0.05	-0.10	0.11	-0.07	-0.93	0.93
29.00	9.03	-0.05	9.03	-0.07	-2.00	2.00	0.04	-0.10	0.11	-0.83	-0.03	0.83
30.00	-0.09	-0.16	0.18	0.02	0.20	0.20	-0.09	0.01	0.10	37.93	-0.41	37.94
31.00	-0.05	-5.54	5.54	-0.03	32.68	32.68	-43.34	-0.07	43.34	-0.02	0.03	0.03
15.00	0.17	0.07	0.18	1.06	1.25	1.64	0.24	-0.05	0.24	0.01	7.54	7.54
17.00	9.02	0.02	9.02	-5.62	-0.01	5.62	37.85	-0.03	37.85	-0.03	1.03	1.03
12.00	19.86	0.05	19.86	-35.84	-0.01	35.84	-53.85	0.07	53.85	0.97	0.08	0.97
28.00	2.62	-0.16	2.62	-0.05	-0.09	0.11	0.02	0.00	0.02	2.65	-0.77	2.76
Total	9.16	4.67	10.28	10.94	9.94	14.79	23.76	1.13	23.79	11.47	19.39	22.53
	CE90 =		15.60	CE90 =		22.44	CE90 =		36.10	CE90 =		34.19

Tabel 5. Hasil Penghitungan RMSE citra Pleiades scene id LPN_PHR1B_201705240304200_ORT

Nomor Chip	Radius window 50			Radius window 100			Radius window 150			Radius window 200		
	dx (m)	dy (m)	RMSE	dx (m)	dy (m)	RMSE	dx (m)	dy (m)	RMSE	dx (m)	dy (m)	RMSE
2.00	0.11	0.05	0.12	25.66	0.04	25.66	0.08	0.94	0.94	-0.13	4.29	4.29
3.00	3.07	0.04	3.07	0.12	2.96	2.96	0.11	3.47	3.47	-0.02	4.03	4.03
14.00	0.60	-0.17	0.62	0.01	-0.05	0.05	-0.04	5.46	5.46	-2.40	-0.07	2.40
16.00	0.16	0.10	0.19	0.07	-2.83	2.83	0.13	-1.47	1.47	-0.08	-1.09	1.09
29.00	-0.01	-2.01	2.01	-0.04	-2.32	2.32	-0.38	-0.06	0.38	-1.13	-0.09	1.13
30.00	-0.01	-0.18	0.19	0.20	0.41	0.46	-0.85	0.00	0.85	0.88	-0.05	0.88
31.00	3.40	0.03	3.40	0.90	-0.05	0.90	0.15	0.44	0.46	-0.06	0.12	0.13
15.00	0.10	-0.01	0.11	15.54	16.05	22.34	0.10	3.48	3.48	-0.87	0.03	0.87
17.00	7.18	0.02	7.18	0.05	10.64	10.64	0.02	50.12	50.12	0.04	-0.91	0.91
12.00	0.04	2.98	2.98	1.95	0.06	1.95	1.05	0.10	1.05	0.23	0.89	0.92
28.00	0.03	-10.39	10.39	0.09	-0.18	0.21	2.05	-0.60	2.14	2.05	-0.28	2.07
Total	2.57	3.32	4.20	9.07	5.98	10.86	0.75	15.28	15.30	1.08	1.85	2.14
	CE90 =		6.37	CE90 =		16.48	CE90 =		23.22	CE90 =		3.25

Pada citra Pleiades scene id LPN_PHR1A_201707230253194_ORT, nilai CE90 terkecil diperoleh dari hasil penghitungan menggunakan GCP Chip dengan ukuran radius window 150 piksel, sedangkan pada citra Pleiades scene id LPN_PHR1A_201807220253354_ORT, nilai CE90 terkecil diperoleh dari hasil penghitungan menggunakan GCP Chip dengan ukuran radius window 50 piksel, dan pada citra Pleiades scene id LPN_PHR1B_201705240304200_ORT, nilai CE90 terkecil diperoleh dari hasil penghitungan menggunakan GCP Chip dengan ukuran radius window 200 piksel.

4. References

[1] Astrium, "Pléiades Imagery User Guide," *GEO-Information Serv.*, no. October, pp. 1–106, 2012.
[2] I. Henrico, L. Combrinck, and C. Eloff, "Accuracy comparison of Pléiades satellite ortho-images using GPS device based GCPs against TerraSAR-X-based GCPs," *South African J. Geomatics*, vol. 5, no. 3, p. 358, 2016.
[3] I. L. Sari, S. E. Siwi, R. P. Brahmantara, H. S. Dyatmika, A. Suprijanto, and K. A. Pradono, "Geometric Accuracy Assessment of Very High-Resolution Optical Data Orthorectified using TerraSAR-X DSM to Support Disaster Management in Indonesia," *Int. J. Adv. Sci. Eng. Inf. Technol.*, vol. 8, no. 6, p. 2450, 2018.
[4] R. P. Brahmantara, Kustiyo, and S. E. Siwi, "Pengujian Metode Korelasi Pearson untuk Image Registration pada Citra SPOT-6 Ortho," *Pros. Semin. Nas. Penginderaan Jauh 201*, vol. 6, no. November, pp. 978–979, 2015.
[5] B. Srinivasa Reddy and B. N. Chatterji, "An FFT-based technique for translation, rotation, and scale-invariant image registration," *IEEE Trans. Image Process.*, vol. 5, no. 8, pp. 1266–1271, 1996.
[6] C. Saint-jean, L. Mascarilla, C. Saint-jean, L. Mascarilla, and C. Fourier-mellin, "Color Fourier-Mellin Descriptors for Image Recognition To cite this version :," 2014.
[7] Z. Q. Zhao, P. Zheng, S. T. Xu, and X. Wu, "Object Detection With Deep Learning: A Review," *IEEE Trans. Neural Networks Learn. Syst.*, pp. 1–21, 2019.

Trial of monitoring the propagation of forest and land fires based on hotspot detection and smoke distribution using Himawari-8 satellite (case study: forest and land fires in Central Kalimantan on October 2015)

Gabriella T Adolong[1], Zadrach L Dupe[1], Hana L Fitriana[2]

[1] Meteorology Study Program, Bandung Institute of Technology 10 Ganesha Street, 40132 Bandung, Indonesia
[2]Remote Sensing Applications Center, Indonesian National Institute of Aeronautics and Space 8 Kalisari Street, 13710 East Jakarta, Indonesia

e-mail: gabrielladolong@gmail.com

Abstract. Land forest fire event in Indonesia every year always happens. These forest fire have an impact on health, transportation, economy, etc. In the prevention of forest and land fires, it is necessary to monitor with good temporal resolution as a mitigation effort. At present, monitoring of forest and land fires used by the Indonesian government is the detection of hotspots issued from MODIS image data. This data has a limitation in temporal resolution that is only acquisition the same area twice a day while in disaster management forest fires are needed at all times. The latest technology that is developing at this time is the existence of satellite imagery that can update the earth with better temporal resolution, known as Himawari-8. The image data has resulted in forest fire detection with a hotspot. For this initial research, trying to validate the data with the hotspot data from Himawari-8 and MODIS to be applied to the area of land forest fire in Indonesia. To supporting the accuracy of hotspots can also be done by detecting patterns of smoke distribution as soon as the wind data parameters are supported by spatial estimation of time. In hotspot validation is used with commission omission errors while distribution immediately uses RGB composite colours. The results obtained state that receiving a hotspot from Himawari-8 with MODIS is 11.125% while the pattern of wind distribution to hotspots needs to be done by other additional methods.

1. Introduction

One of the causes of deforestation in Indonesia is the occurrence of land forest fires. National Disaster Management Authority (BNPB) defines forest and land fires as a condition that forest and land is burned by fire, causing deforestation that also cause economic loss, decreasing of biodiversity (killing wild animal, decreasing plant species), and/or decreasing other environmental values (1, 2). In 2015, huge land forest fires happened in Indonesia, specifically Central Kalimantan, with 122,882.90 Ha burned area (3) and made this area as the widest area of land forest fires in Indonesia. This fire in 2015 contribute to economic loss approximately 221 trillion Rupiah (4). Land forest fires event also create smoke disaster harmful to people's health and disturb of activities.

Land and forest fires mostly relate to existence of hotspot and smoke. One of the tool to monitor of hotspot and smoke distribution by using satellite technology. Some previous researches have used to weather and environment satellites data to monitor hotspot and smoke distribution, using polar orbit satellites such as Terra and Aqua equipped with Moderate Resolution Imaging Spectroradiometer (MODIS) sensor. Polar orbit satellites has well enough spectral and spatial resolution to monitor hotspot and smoke distribution, but not with the temporal resolution. Other research used geostationary orbit satellite such as Multifunctional Transport Satellites (MTSAT) giving horary image (5). These two types of satellites still give high probability of land forest fire being not monitored in real time. Therefore, this research will be use Himawari-8 satellite to monitor land forest fire event having 10 minutes temporal resolution.

On December 21, 2016 Earth Observation Research Center (EORC), Japan Aerospace Exploration Agency (JAXA) released data of wild fire in hotspot form. These hotspot data of Himawari-8 produced by JAXA are Level 2 data and are still in beta version, which is issued for testing in actual conditions so that these hotspot data's accuracy is still unknown in Indonesia. Therefore, before using it in trial of monitoring forest and land fires, validation of hotspot Himawari-8 produced by JAXA is needed in Indonesia, especially Central Kalimantan.

2. Data and Methods

These are the data used in this research.

- Himawari L1 Gridded Data band 3 (0,64 μm), band 4 (0,86 μm), and band 6 (2,3 μm) on October 13, October 20, and October 22, 2015
- Himawari-8 hotspot data in Central Kalimantan on October 2015 produced by JAXA
- MODIS Terra-Aqua and VIIRS SNPP hotspot data by LAPAN
- RGB images data (band 6,5,4) of Landsat-8 satellite, scene path/row 120/62, 119/61, 118/62, and 117/61
- Observed data of mean wind speed and mean wind direction from meteorological stations in Central Kalimantan
- ECMWF reanalysis wind parameter data

The validation of Himawari-8 hotspot produced by JAXA use the single buffer technique to MODIS and VIIRS hotspot in 2 km radius. RGB images data of Landsat-8 satellite are used as the background so that the burned area can be seen clearly. The output of this validation is accuracy value of Himawari-8 hotspot produced by JAXA calculated using Short's Mapping Accuracy equation (6):

$$Accuracy\ (\%) = \frac{correct}{correct + commision + omission}$$

Himawari-8 hotspot can be said as valid/correct if the hotspot is found inside the buffer area of the fire spots and inside the burned area. Commission error is a condition that Himawari-8 hotspot is detected but there is no fire. Omission error is a condition that fire exists but Himawari-8 hotspot is not detected (7). Data of Himawari-8 satellite for smoke distribution is processed using RGB false colour method combined by data of band 3, 4, and 6 of Himawari-8 satellite. The trial of monitoring forest and land fires is done by overlaying the data of Himawari-8 hotspot produced by JAXA to MODIS and VIIRS hotspot as the indicator of fire spots assuming 100% accuracy and to RGB false colour image of Himawari-8 satellite. The selection of sample areas for this monitoring trial is based on Landsat-8 image that showing the presence of fire spots. The pattern of hotspot and smoke distribution as the indicator of fire propagation is analyzed based on wind direction using ECMWF reanalysis data.

3. Results and Discussion

3.1. Validation Result of Himawari-8 Hotspot Produced by JAXA

These are the validation result of Himawari-8 hotspot produced by JAXA that had been done to some Area of Interest (AoI) selected from all images scene of Landsat-8 satellite that being used.

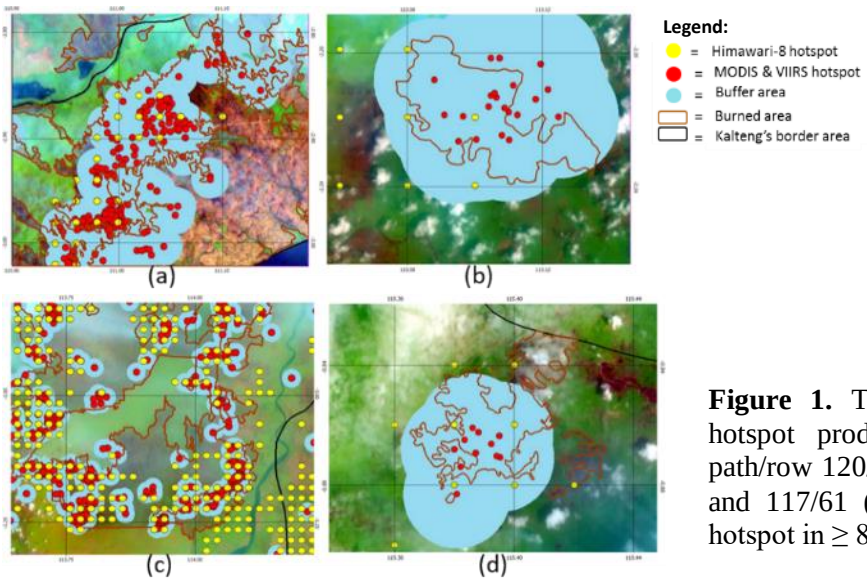

Figure 1. The validation of Himawari-8 hotspot produced by JAXA in AoI of path/row 120/62 (a), 119/61 (b), 118/62 (c), and 117/61 (d) using MODIS and VIIRS hotspot in ≥ 80% level confidence

Table 1. Accuracy result of Himawari-8 hotspot produced by JAXA using MODIS and VIIRS hotspot in ≥ 80% level confidence

Scene Path/Row	Number of Himawari-8 Hotspot in AoI	Number of MODIS and VIIRS Hotspot (≥ 80% level confidence) in AoI	Correct	Commission	Omission
117/61	33	11	12	21	0
118/62	830	399	114	687	274
119/61	45	26	7	35	18
120/62	193	243	40	153	194
Total	**1101**	**679**	**173**	**896**	**486**
Accuracy (%)			**11.125**		
Commission error (%)			**81.38**		
Omission error (%)			**44.14**		

The validation of Himawari-8 hotspot produced by JAXA to MODIS Terra-Aqua and VIIRS SNPP hotspot with ≥ 80% level confidence show high commission error. This concludes that most Himawari-8 hotspot produced by JAXA is detected when forest and land fires occurred in Central Kalimantan on October 2015 (overestimate).

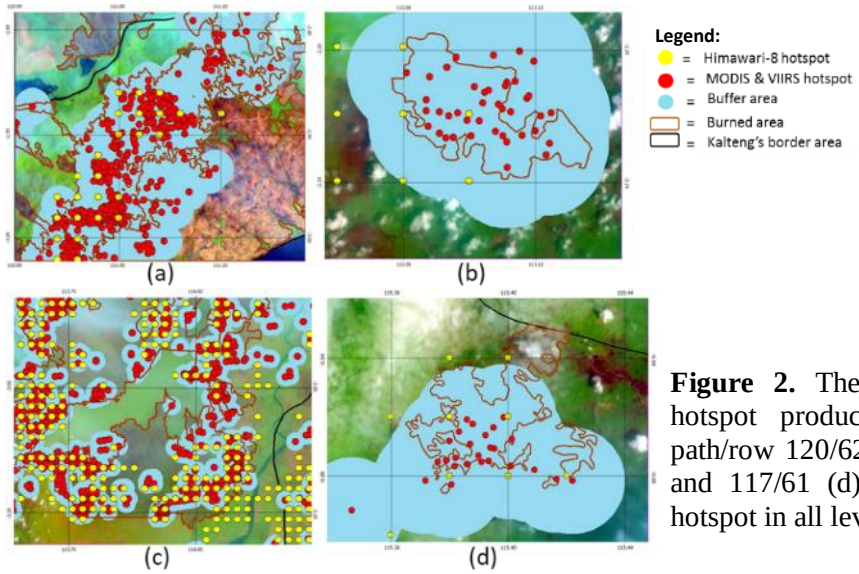

Figure 2. The validation of Himawari-8 hotspot produced by JAXA in AoI of path/row 120/62 (a), 119/61 (b), 118/62 (c), and 117/61 (d) using MODIS and VIIRS hotspot in all level confidence

Table 2. Accuracy result of Himawari-8 hotspot produced by JAXA using MODIS and VIIRS hotspot in all level confidence

Scene Path/Row	Number of Himawari-8 Hotspot in AoI	Number of MODIS and VIIRS Hotspot (all level confidence) in AoI	Correct	Commission	Omission
117/61	33	28	13	20	0
118/62	830	852	179	651	615
119/61	45	40	7	35	31
120/62	193	538	87	106	422
Total	**1101**	**1458**	**286**	**812**	**1076**
Accuracy (%)			**13.155**		
Commission error (%)			**73.75**		
Omission error (%)			**97.73**		

The validation of Himawari-8 hotspot produced by JAXA to MODIS Terra-Aqua and VIIRS SNPP hotspot in all level confidence does not increase accuracy level significantly, but increasing omission error to 97.73%. This concludes that many forest and land fires are not detected by Himawari-8 satellite (underestimate). This is due to the cloud being covered so that it cannot be detected and the limitations of the spatial resolution of Himawari-8. Therefore, the MODIS and VIIRS hotspot chosen as fire point indicator in the trial of monitoring forest and land fires is the hotspot in ≥ 80% level confidence.

3.2. Trial of Monitoring the Propagation of Forest and Land Fires on October 13, 2015

Based on Landsat-8 imagery on scene path/row 119/61, it is seen that on October 13, 2015 there were fire spots proving that forest and land fires occurred on that date. Therefore, in this section the monitoring will focus on the sample area in the red box as shown in Figure 1 which is the area of scene path/row 119/61. Himawari-8 hotspots produced by JAXA was detected in the sample area on 13:00 LT (d), even though there was no MODIS and VIIRS hotspot. This happened because during the study time, the sample area was covered by thick clouds indicated by existence of white objects (8). On 13:00 LT when clouds have disappeared from the sample area, there was no brownish yellow color indicating fires' smoke, but only dim yellow was seen. This condition continued until some times ahead. This indicated forest and land fires happened in the sample area was not too big.

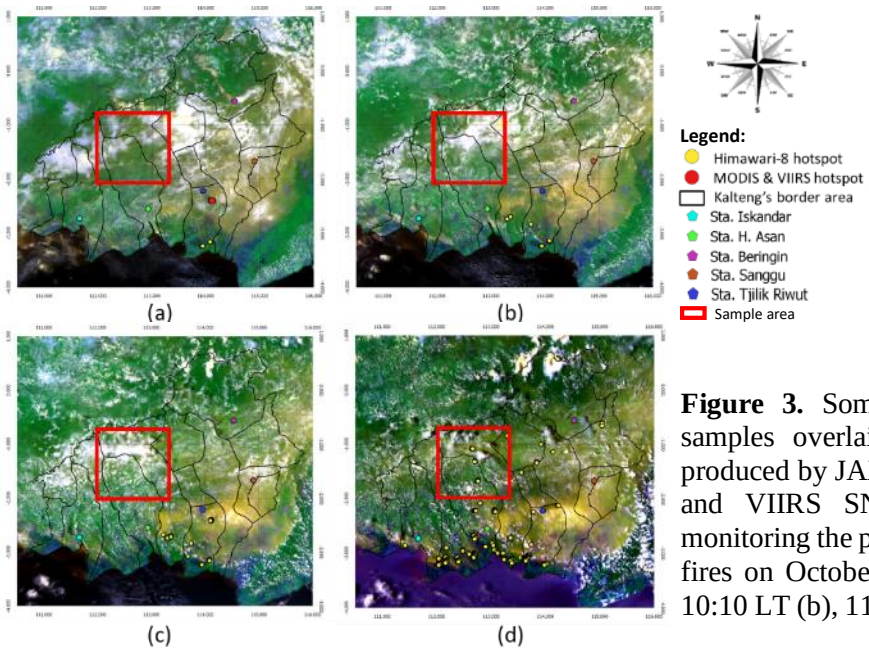

Figure 3. Some RGB false color image samples overlaid to Himawari-8 hotspots produced by JAXA and MODIS Terra-Aqua and VIIRS SNPP hotspots for trial of monitoring the propagation of forest and land fires on October 13, 2015 at 08:40 LT (a), 10:10 LT (b), 11:40 LT (c), and 13:00 LT (d)

3.3. *Trial of Monitoring the Propagation of Forest and Land Fires on October 20, 2015*

Based on Landsat-8 imagery on scene path/row 120/62, it is seen that on October 20, 2015 there were fire spots proving that forest and land fires occurred on that date. Therefore, in this section the monitoring will focus on the sample area in the red box as shown in Figure 2 which is the area of scene path/row 120/62. Himawari-8 hotspots produced by JAXA started to be detected on 09:00 LT (b), but up to study time, MODIS and VIIRS hotspot indicating forest and land fires were not detected in the sample area. As start being detected, Himawari-8 hotspots produced by JAXA start increasing every time as can be seen in the image of 11:10 LT (c) and 13:00 LT (d) in Figure 2. On 13:00 LT (d), Himawari-8 hotspots produced by JAXA seemed spreading and appeared at several new points. Based on RGB false color images, yellow fine lined objects were seen in sample area. These objects indicated fires' smokes because on 11:10 LT (c), the object seemed coming from the hotspots detected in sample area.

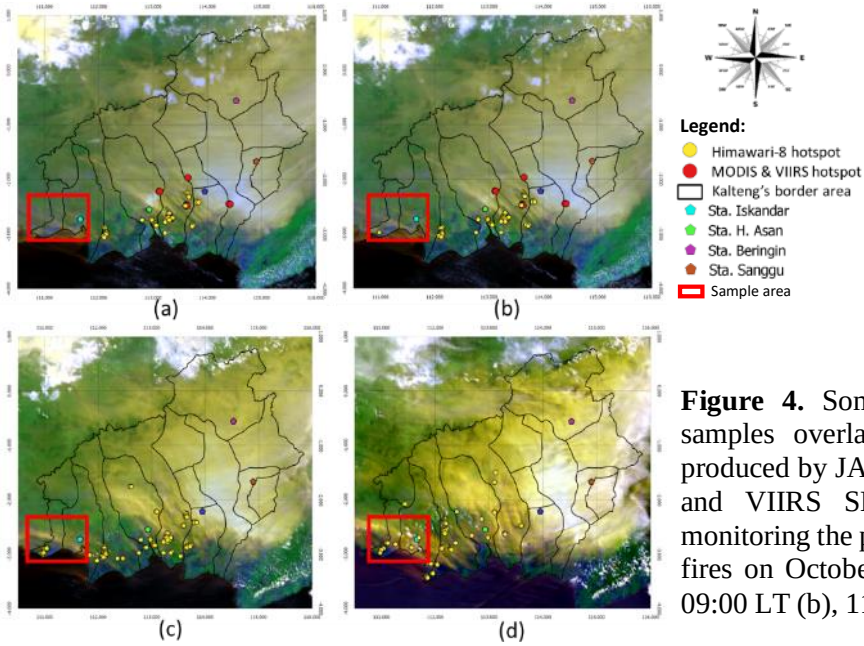

Figure 4. Some RGB false color image samples overlaid to Himawari-8 hotspots produced by JAXA and MODIS Terra-Aqua and VIIRS SNPP hotspots for trial of monitoring the propagation of forest and land fires on October 20, 2015 at 08:40 LT (a), 09:00 LT (b), 11:10 LT (c), and 13:00 LT (d)

MODIS Terra-Aqua and SNPP VIIRS hotspots were detected on 13:42 LT and 13:43 LT, which is 42 to 43 minutes after the study time, on several points similar to Himawari-8 hotspots produced by JAXA on 13:00 LT as shown in Figure 3. This condition indicates that forest and land fires actually did occur at that area on October 20, 2015. This also shows that the use of Himawari-8 hotspot data produced by JAXA is very helpful in monitoring the propagation of forest and land fires because the hotspots have been detected at the same point as the fire spots some time before MODIS and VIIRS hotspots detected.

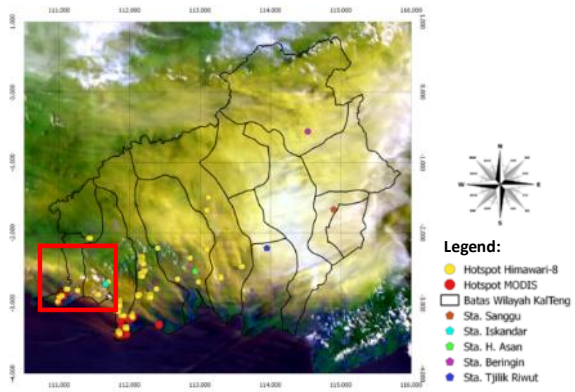

Figure 5. RGB false color image overlaid to Himawari-8 hotspots produced by JAXA on 13:00 LT and MODIS Terra-Aqua and VIIRS SNPP hotspots on 13:42 LT and 13:43 LT

3.4. Trial of Monitoring the Propagation of Forest and Land Fires on October 22, 2015

Based on Landsat-8 imagery on scene path/row 118/62, it is seen that on October 22, 2015 there were fire spots proving that forest and land fires occurred on that date. Therefore, in this section the monitoring will focus on the sample area in the red box as shown in Figure 4 which is the area of scene path/row 118/62. Himawari-8 hotspots produced by JAXA that had been detected were already at the same exact points as MODIS and VIIRS hotspots, but MODIS and VIIRS hotspots were no longer detected after 09:10 LT (b). Even though based on RGB false color images, yellow object got denser time by time indicating big smokes in the sample area. Based on RGB false color images, line shaped smoke objects was seen and came from some points/small areas in sample area. Himawari-8 hotspots produced by JAXA were also detected near points seemed as source of the smokes. This indicated forest and land fires. On 13:00 LT (d), smokes seemed to be denser and spread wider, but less hotspots were detected. This did not mean the fires went out, but could be indicated as ground fire as usually happened in peat areas, as in Central Kalimantan.

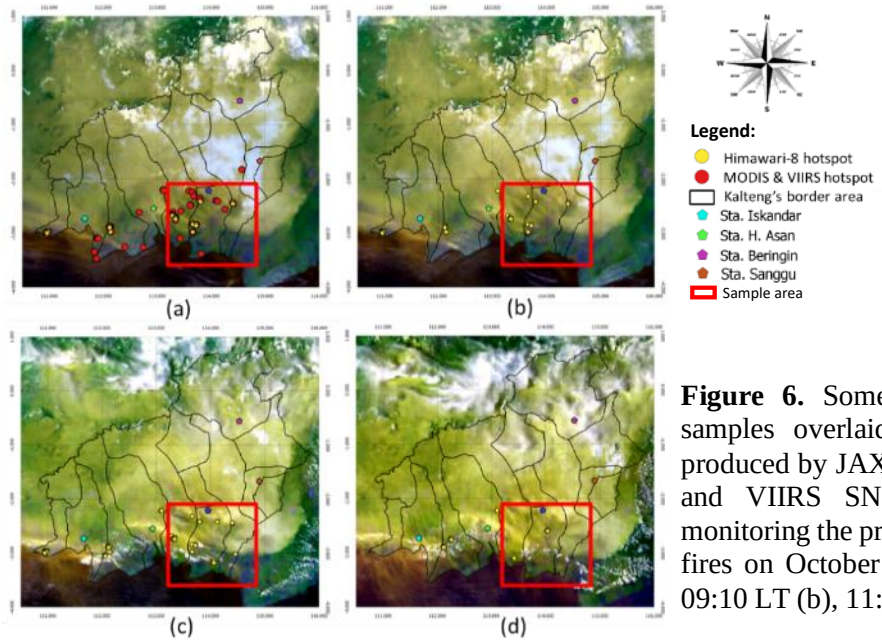

Figure 6. Some RGB false color image samples overlaid to Himawari-8 hotspots produced by JAXA and MODIS Terra-Aqua and VIIRS SNPP hotspots for trial of monitoring the propagation of forest and land fires on October 22, 2015 at 08:40 LT (a), 09:10 LT (b), 11:40 LT (c), and 13:00 LT (d)

3.5. Analysis Result of Propagation of Forest and Land Fires Based on Wind Direction on October 20, 2015

The yellow fine line shaped objects indicating fires' smokes moved from West of North-west to North of North-west. Himawari-8 hotspots produced by JAXA increased time by time and moved to North-west until North as shown in Figure 5 (a) and (b). On the image on 13:00 LT as shown in Figure 5 (d), Himawari-8 hotspots produced by JAXA were less detected and spread more, but the hotspots existence had moved upper than when first detected.

As shown in Figure 6, the wind vector on 07:00 LT (a) in sample area went to West of North-west then on 13:00 LT (b), the wind field had gone to North-west. The spread of hotspots and smokes moved along with the wind direction because their movement are still in the same quadrant as the wind direction. Then the propagation of forest and land fires was also indicated moving as the wind direction.

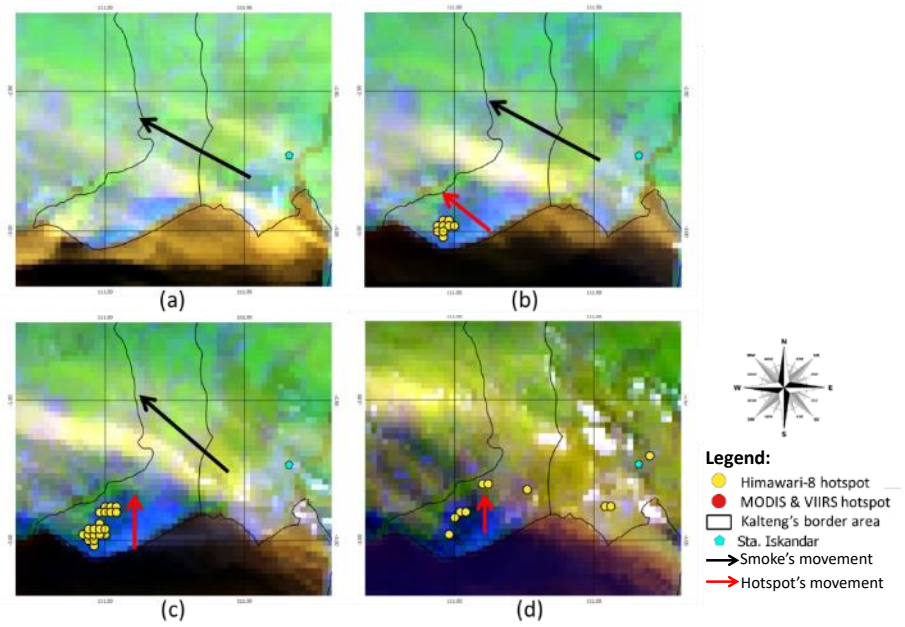

Figure 7. Clip area sample results of Himawari-8 images on October 20, 2015 08:40 LT (a), 10:20 LT (b), 11:40 LT (c), and 13:00 LT (d), adjusted to image of Landsat-8 path/row 120/62

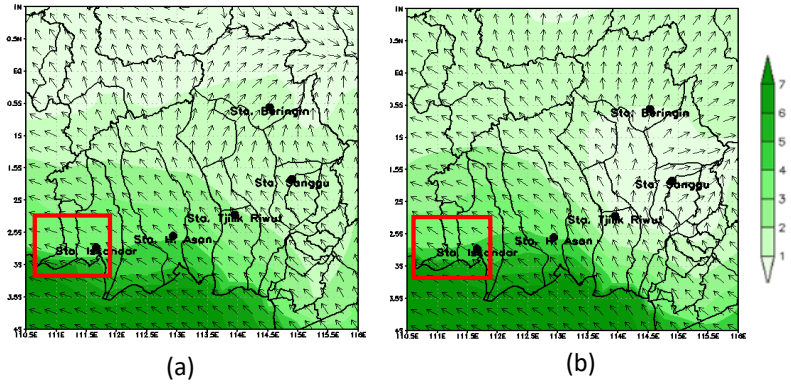

Figure 8. Spatial data plot of ECMWF wind speed and direction in area of Central Kalimantan on October 20, 2015 07:00 LT (a) and 13:00 LT (b)

3.6. Analysis Result of Propagation of Forest and Land Fires Based on Wind Direction on October 22, 2015

At the beginning of study time, fires' smoke seemed to move to North-west until North of North-west, however the movement was very diverse until the end of the study. On this date, most Himawari-8 hotspots produced by JAXA were detected on same points during the study time. This indicated that forest and land fires were still happened around the points (± 2 km) on the duration time. As time flied, the hotspots movement was still found. As shown in Figure 7, on 10:50 LT (b), more Himawari-8 hotspots went to North of North-west and on 11:30 LT (c), more went to West. On 13:00 LT (d), a few Himawari-8 hotspots were detected indicating the propagation of forest and land fires happened under surface (ground fires).

As shown in Figure 8, on 07:00 LT (a), wind vector of ECMWF data in sample area went to West of North-west to North of North-west. On 13:00 LT (b), the wind vectors did look varied, but some wind vector went to North-west, West, and South-west. The spread of hotspots and smokes went along with the wind direction because their movement are still in the same quadrant as the wind direction. Then the propagation of forest and land fires was also indicated moving as the wind direction.\

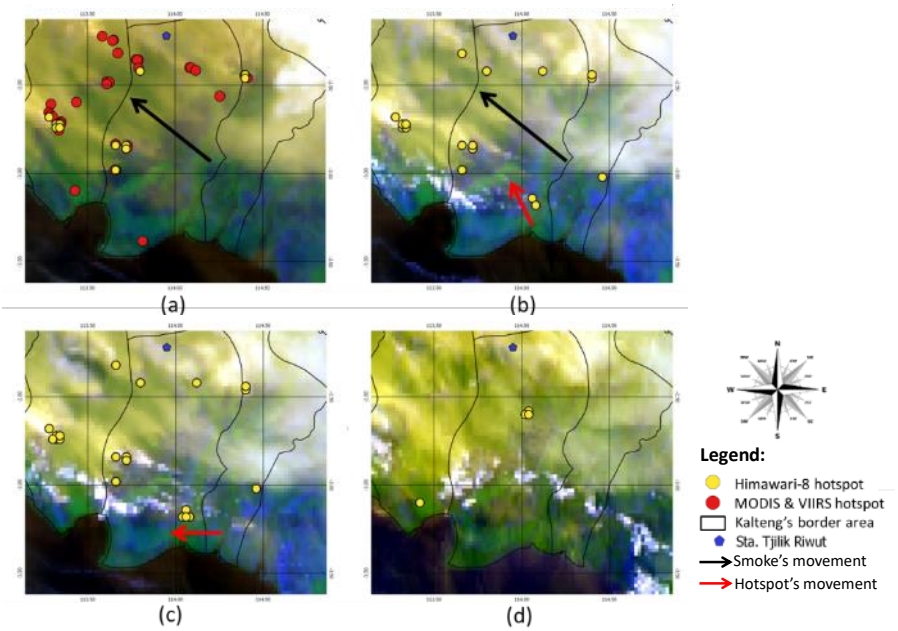

Figure 7. Clip area sample result of Himawari-8 images on October 22, 2015 08:40 LT (a), 10:50 LT (b), 11:30 LT (c), and 13:00 LT (d), adjusted to image of Landsat-8 path/row 118/62

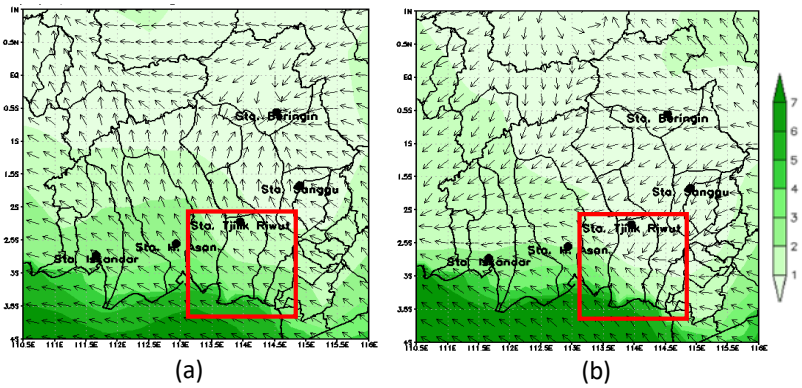

Figure 8. Spatial data plot of ECMWF wind speed and direction in area of Central Kalimantan on October 22, 2015 07.00 LT (a) and 13.00 LT (b)

4. Conclusions

This research concludes that the validation of Himawari-8 hotspot produced by JAXA on some AoI in scene path/row 120/62, 119/61, 118/62, and 117/61 Central Kalimantan during October 2015 results 11.125% accuracy value using MODIS and VIIRS hotspots in ≥ 80% level confidence and increase to 13.155% using MODIS and VIIRS hotspots in all level confidence. Monitoring the propagation of forest and land fires can be done, despite Himawari-8 hotspot produced by JAXA's low accuracy, using Himawari-8 hotspot data produced by JAXA overlaid to RGB false colour images of Himawari-8 satellite band 3, 4, and 6.

5. Acknowledgments

Authors want to say thank you to Weather and Climate Prediction Laboratory (WCPL) ITB and Remote Sensing Applications Center (Pusfatja) LAPAN for providing working place and data used in this research.

6. References

[1] BNPB. Definisi dan Jenis Bencana 2019 [Available from: https://bnpb.go.id/home/definisi.
[2] Phelps J, Hariyanti B, Sinaga A, Dermawan A. Valuasi Lingkungan di Indonesia: Implikasi pada kebijakan di kehutanan, pertanggung-jawaban hukum dan estimasi kerugian negara. Center for International Forestry Research (CIFOR), Bogor, Indonesia; 2014.
[3] System SKM. Rekapitulasi Luas Kebakaran Hutan dan Lahan (Ha) Per Provinsi Di Indonesia Tahun 2014-2019. Kementrian Lingkungan Hidup Dan Kehutanan RI, PKHL D; 2019.
[4] Adriyanto R, Manurung AS, Pujiastuti TT. Rapid Hotspot Detection Using Himawari-8. 2017.
[5] Wati T, Panjaitan A, editors. Forest fires detection in Indonesia using satellite Himawari-8 (case study: Sumatera and Kalimantan on august-october 2015). IOP Conference Series: Earth and Environmental Science; 2017: IOP Publishing.
[6] Short NM. Landsat tutorial workbook. 1982.
[7] Zubaidah A, Vetrita Y, Khomarudin MR. Validasi Hotspot Modis Di Wilayah Sumatera Dan Kalimantan Berdasarkan Data Penginderaan Jauh Spot-4 Tahun 2012 (Modis Hotspot Validation Over Sumatera And Kalimantan Based On Remote Sensing Data Spot-4 In 2012). Jurnal Penginderaan Jauh Dan Pengolahan Data Citra Digital. 2014;11(1).
[8] Sulma S, Fitriana HL, Zubaidah A, Suwarsono, Prasasti I, editors. Spectral Analysis of Smokes from Forest / Land Fires in Sumatera and Kalimantan from Advanced Himawari Imager Data. Seminar Nasional Penginderaan Jauh ke-4 Tahun 2017; 2017: Deputi Bidang Penginderaan Jauh-LAPAN.

Automatic Aura Remote Sensing Satellite Data Acquisition System

Olivia Maftukhaturrizqoh[1], Budhi Gustiandi[1]

[1)]Remote Sensing Technology and Data Center, Indonesia National Institute of Aeronautics and Space (LAPAN)
Jalan LAPAN No. 70, Pekayon, Pasar Rebo, 13710 Jakarta Timur, Indonesia

e-mail: olivia.maftukhaturrizqoh@lapan.go.id

Abstract. Aura is one of National Aeronautics and Space Administration (NASA) Earth Observing System (EOS) satellite series. It measures aerosols, ozone, and other gases from space to gain knowledge about the chemistry of our atmosphere. Although it was launched on 15 July 2004, there is still no system available to acquire its data and products specifically for Indonesian region. Scientists usually download the data through Goddard Earth Science (GES) Data and Information Services Center (DISC) or NASA Langley Atmospheric Sciences Data Center manually if they need them. An automatic data acquisition system was established to obtain Aura satellite data in near real-time. The system includes storage management sub system that mimics the data management system in GES DISC. Selenium package in Python programming language was used to program the automatic acquisition through browser crawling and bash shell scripting was used to build the storage management sub system. Analysis of system time in acquiring the data will be done to ensure that the system fulfill the near real-time criteria. Further, analysis of the data volume will also be taken to calculate how many storage that will be required to store the data. In the end, the system will be integrated into low-resolution remote sensing satellite data processing system that is already available in Remote Sensing Technology and Data Center, National Institute of Aeronautics and Space (LAPAN).

1. Introduction

Aura (Latin for "breeze", formerly EOS CHEM) is one and the last of NASA's core satellites for Earth Observing System (EOS) program. It is dedicated to understand how chemistry composition changes in the Earth's atmosphere, especially in stratosphere and troposphere, by measuring ozone, aerosols, and key gases using innovative space technologies. The satellite was successfully launched from the Vandenberg Western Test Range about 15 years ago, exactly on 15 July 2004, using a Delta II 7920-10L rocket. The platform orbits the Earth at 705 km (438 miles) altitude in sun-synchronous polar orbit with a 98.2o inclination. It crosses the equator in ascending (north-going) mode at 1:45 p.m. (±15 min) and cycles the planet in 98.8 period (sixteen-day repeat cycle with 233 revolutions per cycle) [1].

There are four instruments that fly with the Aura platform, viz. the High Resolution Dynamics Limb Sounder (HIRDLS) [2], the Microwave Limb Sounder (MLS) [3], the Ozone Monitoring Instrument (OMI) [4] and the Tropospheric Emission Spectrometer (TES) [5].The platform and its instruments are shown in Figure 1. The instruments and their configuration were selected because they can make complementary measurements based on previous proven technologies so that they can bring new capabilities in measuring the Earth's atmosphere[6]. Summary of each instrument is listed in Table 1.

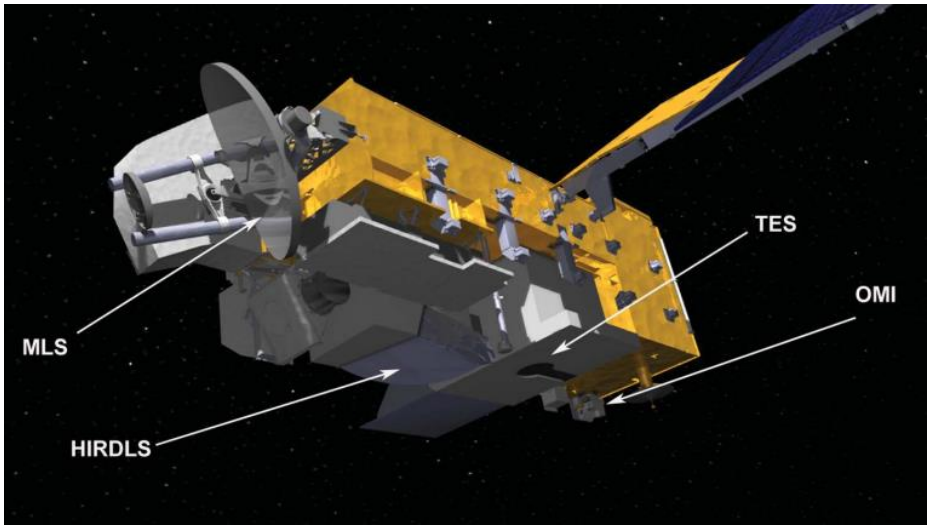

Figure 1. The Aura platform and its four instruments' location in a computer model that was made by Jesse Allen from NASA Earth Observatory[7].

Table 1. Summary of four instruments flying in the Aura satellite.

Instrument Name	Type	Spectral Characteristics	Constituents Measured
High Resolution Dynamic Limb Sounder (HIRDLS)	Limb infrared filter radiometer	6.2 to 17.76 μm	Profiles of temperature, O_3, H_2O, CH_4, N_2O, NO_2, HNO_3, N_2O_5, CF_3Cl, CF_2Cl_2, $ClONO_2$, and aerosols (2)
Microwave Limb Sounder (MLS)	Microwave limb sounder	118 GHz to 2.5 THz	Profiles of temperature, H_2O, O_3, ClO, BrO, HCl, OH, HO_2, HNO_3, HCN, N_2O, CO, and cloud ice (3)
Ozone Monitoring Instrument (OMI)	Hyperspectral nadir imager	270 to 500 nm	Profiles of O_3 and UV-B; Column O_3, SO_2, aerosols, NO_2, BrO, OclO, HCHO, and cloud top pressure [8]
Tropospheric Emission Spectrometer (TES)	Limb and nadir infrared Fourier transform spectrometer	3.2 to 15.4 μm	Profiles of temperature, O_3, NO_2, CO, HNO_3, CH_4, and H_2O (5)

The satellite instruments take data and store them on board until broadcast them to several major downlink facilities that are located in Poker Flat (Alaska), McMurdo Base (Antarctica), and Svalbard (Norway) via a highspeed data link [7]. Then, the data are sent to processing facilities at NASA's Goddard Space Flight Center (GSFC) through optical fiber network. After that, the data are processed into geophysical measurements by the instrument teams. Processed data are sent and store in NASA Data Active Archive Center (DAAC).

Aura data users can access the NASA DAAC through several channels. They can access HIRDLS, MLS, and OMI instruments data via the Goddard Earth Science Data and Information Services Center (DISC) (https://daac.gsfc.nasa.gov/) or the Giovanni system (https://giovanni.gsfc.nasa.gov/giovanni/)[9]. Daily OMI images can also be retrieved from the OMI Sulfur Dioxide Group (https://so2.gsfc.nasa.gov/). The users can access TES data through NASA Langley Atmospheric Sciences Data Center (https://eosweb.larc.nasa.gov/).

However, users has to check the availability of new data provided by the distribution systems manually. The users also has to do some several steps provided by the systems to download required data manually. Some data are updated several times daily and it will take a significant time for a user to check and download the new required data.

In this paper, we propose an automatic system to search for new required data and download them automatically if they are available. It is hoped that the proposed system can help users in their operational activities by efficiently reducing time required to do the search and download processes.

2. Method

Aura satellite was designed to have mission life for five years with operational goal of six years [10]. However, it has operated for almost 15 years. Therefore, the first step in designing an automation system to search and download its data or products is by ensuring which instruments that are still operational nowadays.

2.1. Aura Satellite's Operational Instrument

Soon after the HIRLDS instrument was activated after the satellite launch, something was blocking the optical path of the instrument so that it could only view a small portion of the Earth's atmosphere. Attempts to remove the blocking material were failed. Although the measurements were conducted with 80% blockage, the data or products are only available until 17 March 2008 in the NASA GSFC DISC system.

Similar problem was also found in the TES instrument. Ice was covering its detectors soon after the instrument was activated. Signs of bearing wear were also found after several months of operation. The instrument only works in nadir mode since then. NASA decommissioned the instrument operation on 31 January 2019 [11]. Therefore, the automation system will not focus to search and download the HIRDLS and TES instruments data or products.

On the other hand, there was no problem that has been found since the MLS and OMI instruments were activated. Both instruments are operating flawlessly and their data are currently available in the NASA GSFC DISC system. As a result, the automatic system will focus to data or products that are derived from these instruments.

The next step is to identify types of MLS and OMI data or products that are available in the NASA GSFC DISC system. Some data or products are produced from multiple instruments other than those that are included in the Aura satellite. The automatic system will only focus to data or products that are derived from the MLS and/or the OMI instruments.

2.2. Work of the System

The system was built for Windows environment using Python 3.7 programming language. In general, the automatic system was designed in three main modules of processing. They are search module, download module, and classification module. The modules are shown in Figure 2.

The search module consists of program routines with main purpose to search and list all available data or products from the MLS and/or the OMI instruments that are available in the NASA GSFC DISC system. The module crawls through the web site automatically, check the data availability updates, and list all the required links to be used as inputs to the next module (download module). Furthermore, the search module also limits the search criteria built on the web site to only occupy the Indonesian region. The module was built using Python version 3.7 and selenium web driver package inside it. The block diagram for the search module is illustrated in Figure 3.

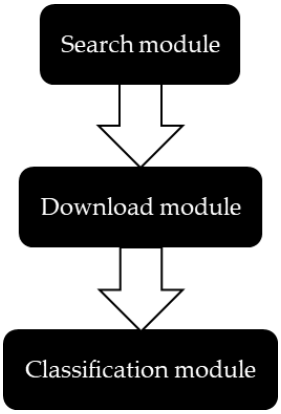

Figure 2. Three main modules that build the automatic system.

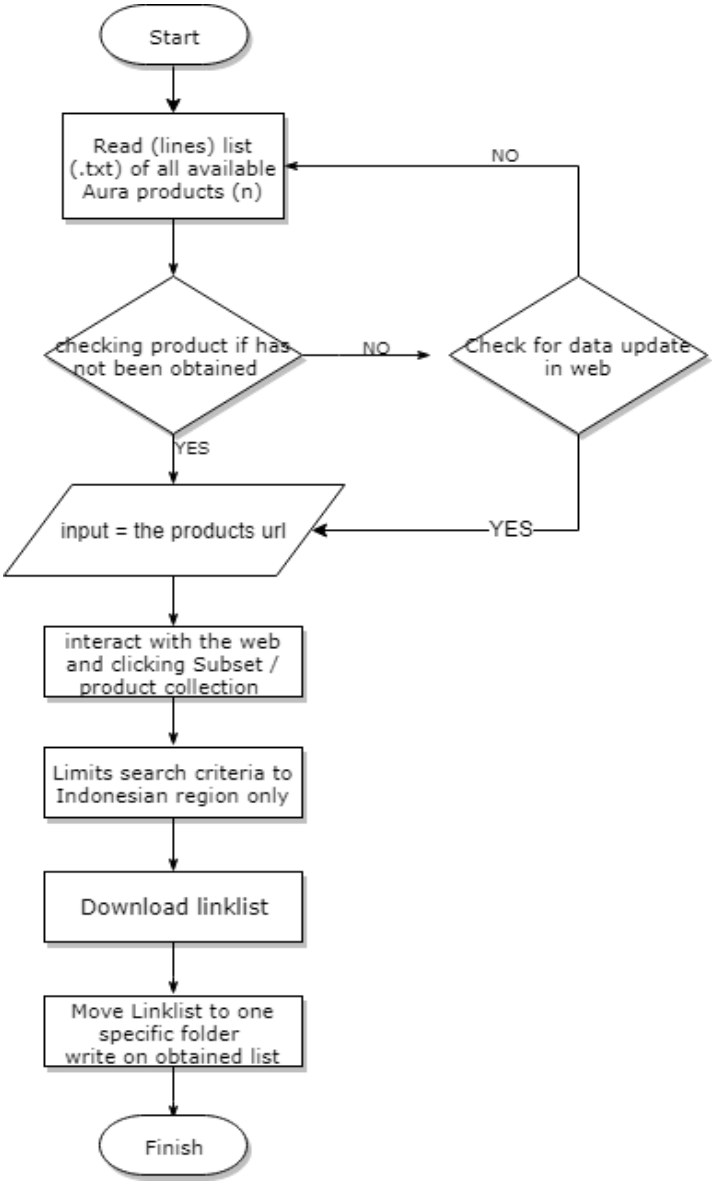

Figure 3. Block diagram of the search module in the automatic system

The download module filters information that is provided by the search module. Lists of data or products provided by the search module will be compared with lists of data or products that have been downloaded by the system. The block diagram for the download module is depicted in Figure 4.

The classification module classifies the downloaded data or products into different directories based on instrument, processing level, and type of product. This is intended to make users easier in searching the downloaded data or products in their storage system. In general, the directory structure that will be produced as the result of the classification module is shown in Figure 5.

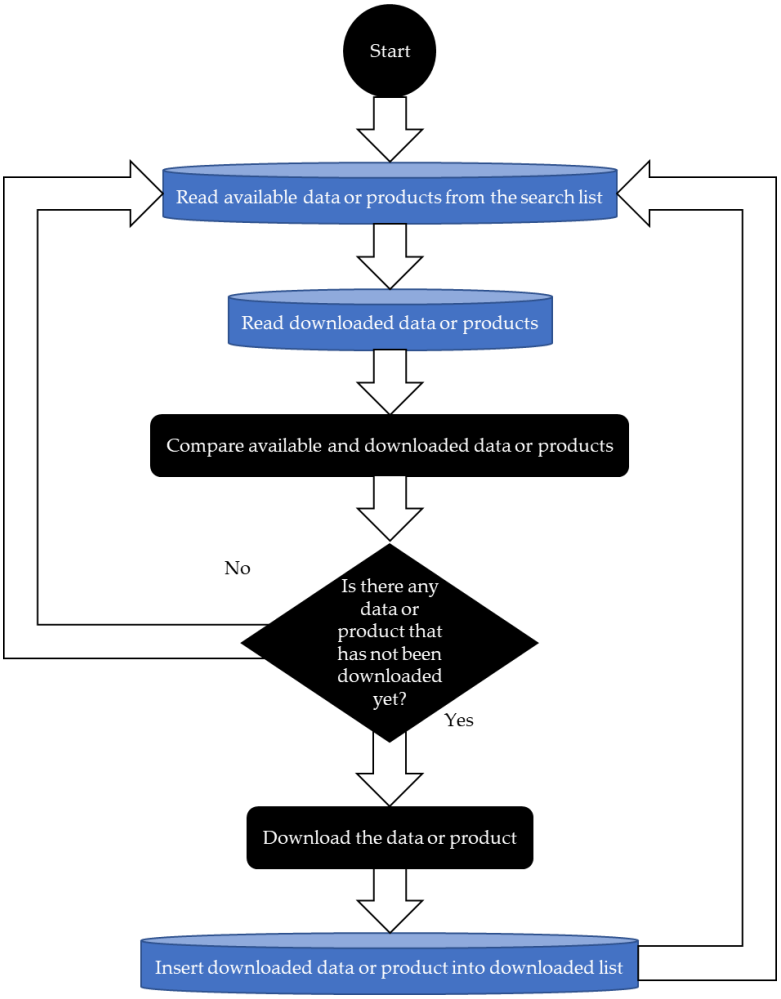

Figure 4. Block diagram of the download module in the automatic system.

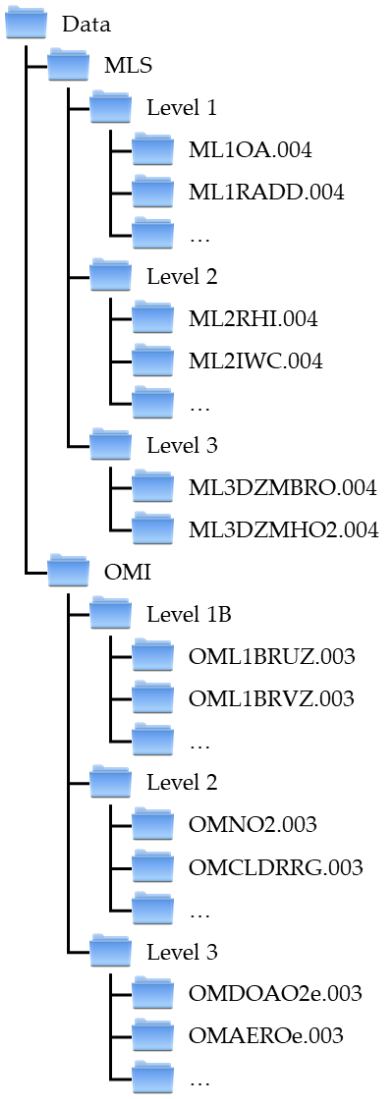

Figure 5. Directory structure as output of the classification module.

3. Results

There are 73 types of MLS data or products that are identified in the NASA GSFC DISC web site and there are 57 types of OMI data or products that are disseminated through the web site. The focus of the automatic system designed is to data or products that are still updated until now. Therefore, we only focus on 34 types of MLS data or products and 43 types of OMI products. A list of the data or the products is shown in Table 2.

Table 2. List of data or products that become the focus of the automatic acquisition system.

	MLS
Level 3	Bromine Monoxide (BrO) Daily 10degrees Lat Zonal Mean; Hydroperoxy (HO2) Daily 10degrees Lat Zonal Mean
Level 2	Relative Humidity With Respect To Ice; Cloud Ice Product; Near-Real-Time Water Vapor (H2O) Mixing Ratio; Diagnostics, Geophysical Parameter Grid; Near-Real-Time Sulfur Dioxide (SO2) Mixing Ratio; Water Vapor (H2O) Mixing Ratio; Near-Real-Time Ozone (O3) Mixing Ratio; Near-Real-Time Nitric Acid (HNO3) Mixing Ratio; Methanol (CH3OH) Mixing Ratio; Geopotential Height; Nitric Acid (HNO3) Mixing Ratio; Near-Real-Time Temperature; Ozone (O3) Mixing Ratio; Hydrogen Chloride (HCl) Mixing Ratio; Hypochlorus Acid (HOCl) Mixing Ratio; Chlorine Monoxide (ClO) Mixing Ratio; Near-Real-Time Carbon Monoxide (CO) Mixing Ratio; Methyl Chloride (CH3CL) Mixing Ratio; Bromine Monoxide (BrO) Mixing Ratio; Temperature; Nitrous Oxide (N2O) Mixing Ratio; Near-Real-Time Nitrous Oxide (N2O) Mixing Ratio; Diagnostics, Miscellaneous Grid; Carbon Monoxide (CO) Mixing Ratio; Hydrogen Cyanide (HCN) Mixing Ratio; Hydroperoxy (HO2) Mixing Ratio; Methyl Cyanide (CH3CN) Mixing Ratio; Sulfur Dioxide (SO2) Mixing Ratio
Level 1	Orbit/Attitude and Tangent Point Geolocation Data; Radiances from Digital Autocorrelators; Radiances from Filter Banks for THz; Radiances from Filter Banks for GHz
OMI	
Level 3	Ozone (O3) DOAS Total Column 1 day 0.25 degree x 0.25 degree; Multi-wavelength Aerosol Optical Depth and Single Scattering Albedo 1 day Best Pixel in 0.25 degree x 0.25 degree; Sulfur Dioxide (SO2) Total Column 1 day Best Pixel in 0.25 degree x 0.25 degree; TOMS-Like Ozone and Radiative Cloud Fraction 1 day 0.25 degree x 0.25 degree; Surface UVB Irradiance and Erythemal Dose Daily Global Gridded 1.0 degree x 1.0 degree; TOMS-Like Ozone, Aerosol Index, Cloud Radiance Fraction 1 day 1 degree x 1 degree; NO2 Cloud-Screened Total and Tropospheric Column Global Gridded 0.25 degree x 0.25 degree; Near UV Aerosol Optical Depth and Single Scattering Albedo 1 day 1.0 degree x 1.0 degree
Level 2	Nitrogen Dioxide (NO2) Total and Tropospheric Column 1-orbit Swath 13x24 km; Effective Cloud Pressure and Fraction (Raman Scattering) Daily Global Gridded 0.25 degree x 0.25 degree; Ozone (O3) Profile 1-Orbit Swath 13x48km; Formaldehyde (HCHO) Total Column Daily Global Gridded 0.25 degree x 0.25 degree; Ozone (O3) Total Column 1-Orbit Swath 13x24 km; Aerosol product Multi-wavelength Algorithm Zoomed 1-Orbit Swath 13x12km; Cloud Pressure and Fraction (Raman Scattering) 200-km swath subset along CloudSat track; Cloud Pressure and Fraction (Raman Scattering) 1-Orbit Swath 13x24 km; Sulphur Dioxide (SO2) Total Column Daily Global Gridded 0.125 degree x 0.125 degree; Cloud Pressure and Fraction (O2-O2 Absorption) Daily Global Gridded 0.25 degree x 0.25 degree; Surface UV Irradiance 1-orbit Swath 13x24 km; Near UV Aerosol Optical Depth and Single Scattering Albedo 1-orbit Swath 13x24 km; NO2 Total and Tropospheric Column Daily Global Gridded 0.25 degree x 0.25 degree; Sulphur Dioxide (SO2) Total Column 1-orbit Swath 13x24 km; Ozone (O3) DOAS Total Column 1-Orbit Swath 13x24 km; Formaldehyde (HCHO) Total Column 1-orbit Swath 13x24 km; Cloud Pressure and Fraction (O2-O2 Absorption) 1-Orbit Swath; Zoom-in Ground Pixel Corners 1-Orbit Swath 13x12km; Global Ground Pixel Corners 1-Orbit Swath 13x24km; Near UV Aerosol Optical Depth and Single Scattering Albedo Daily Global Gridded 0.25 degree x 0.25 degree; Surface UVB Irradiance and Erythemal Dose Daily Global Gridded 0.25 degree x 0.25 degree; Ozone (O3) DOAS Total Column Daily Global Gridded 0.25 degree x 0.25 degree; DOAS Total Column Ozone Zoomed 1-Orbit Swath 13x12km; Cloud Pressure and Fraction (O2-O2 Absorption) Zoomed 1-Orbit Swath 13x12km; Multi-wavelength Aerosol Optical Depth and Single Scattering Albedo 1-orbit Swath 13x24 km; Chlorine Dioxide (OClO) Total Column 1-orbit Swath 13x24 km; Multi-wavelength Aerosol Optical Depth and Single

	Scattering Albedo Daily Global Gridded 0.25 degree x 0.25 degree; Bromine Monoxide (BrO) Total Column 1-orbit Swath 13x24 km; Ozone (O3) Total Column Daily Global Gridded 0.25 degree x 0.25 degree; Near UV Aerosol Index, Optical Depth and Single Scattering Albedo 1-Orbit 13x24km
Level 1B	UV Zoom-in Geolocated Earthshine Radiances 1-orbit L2 Swath 13x12 km; VIS Zoom-in Geolocated Earthshine Radiances 1-orbit L2 Swath 13x12 km; UV Global Geolocated Earthshine Radiances 1-orbit L2 Swath 13x24 km; Solar Irradiances; VIS Global Geolocated Earth Shine Radiances 1-orbit L2 Swath 13x24 km

The automatic acquisition system that was designed successfully crawls all the data or the products listed in the Table 2 above. The data or the products that are successfully downloaded into storage system are classified based on their instrument, processing level, and type. The directories follows the convention that is described in Figure 5 above. Directory names use the code of each data or product as described in the NASA GSFC DISC web site.

4. Discussions

Although the automatic acquisition system runs successfully to search and download all required data or products from the NASA GSFC DISC web site, there were some problems faced during the development of the system. One of the primary problems was update in the web site. Since the search module uses crawl method that searches for certain tag in the web site structure, every change in the structure will affect the behavior of the module. For example, when the web site added an additional pop up menu about tour to the web site feature in its home page, the search module had to be modified to skip the pop up. Another example was when the results from the search box in the web site not only include results for an exact code of required data or products but also any relevant data or products, the module had to be modified again to exclude irrelevant data or products.

An analysis was conducted to know how the automatic system affects time required in obtaining an Aura satellite product compared with a manual process. Table 3 shows the result of this comparison and Figure 6 depicts the chart of the comparison.

Table 3. Comparison of manual and automatic time required to obtain Aura satellite product. Style and spacing

Checking steps run	amount of data	time required	
		manual	automatic
1 data without update	1	00:01:03	00:00:32
3 data without update	3	00:02:27	00:01:00
1 data update and download linklist	1	00:02:17	00:01:07
3 data update and download linklist	3	00:05:12	00:04:17

As shown in the chart below, the automatic system always requires less time than manual processes. Although the analysis process was only conducted using only several data and the time difference was not significant, the automatic process will help users when they have to deal with thousands of products. A manual process will take hours to check all the available data while the automatic system can do the same process in just under 60 minutes.

Additionally, analysis of the data volume also has been conducted to calculate how many storage that required to store the data. According to data volume calculation the total storage volume of Aura for level 1, 2, and 3 products which is acquired by this system is approximately 20 TB. While, data volume

of Aura OMI from 2004 to 2019 required about 16 TB storage. Accordingly, LAPAN has to provide approximately 36 TB to store Aura data from 2004 to 2019.

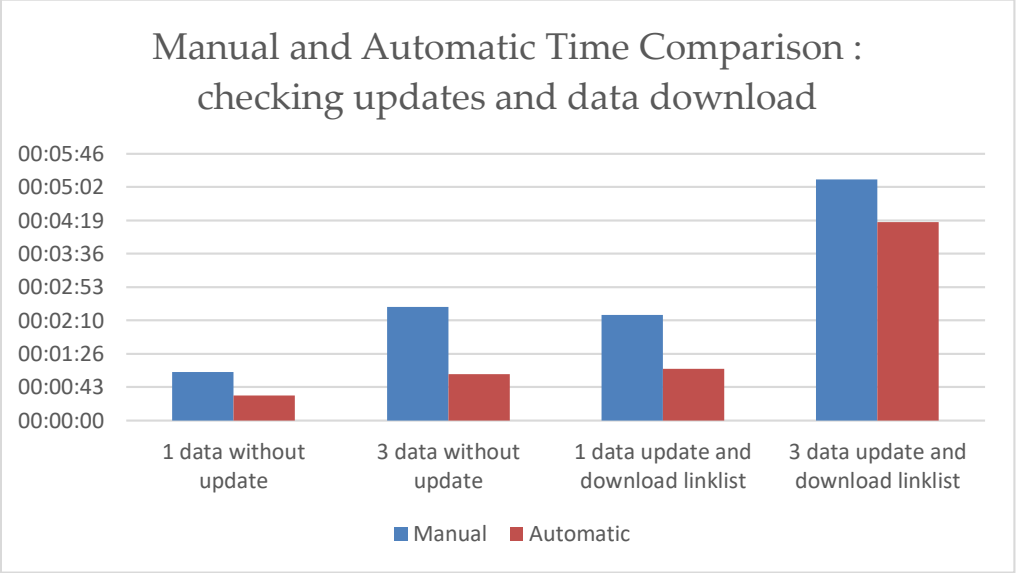

Figure 6. Comparison chart of the automatic system efficiency compared to manual process.

5. Conclusions

An automatic acquisition system was successfully built to obtain Aura remote sensing satellite data or products. The system has capabilities to search for required Aura MLS and OMI data or products from NASA GSFC DISC dissemination system, to download them, and to classify them based on their instrument, processing level, and types of data or products.

Currently, the automatic acquisition system was only designed to be run in a computer with Windows operating system. In the future, the system will be developed further so that it can run in a computer, especially a server, with Linux or Unix operating system. It is hoped that the system can be integrated into the current low resolution remote sensing data processing system that is available in Remote Sensing Technology and Data Center, LAPAN. The system design concept can also be implemented to be used in developing other remote sensing data acquisition systems that require search and download steps from a website-based dissemination system.

6. References

[1] NASA, *Our Changing Atmosphere: Discoveries from EOS Aura.* 2010.
[2] Gille, J., et al., *High Resolution Dynamics Limb Sounder: Experiment overview, recovery, and validation of initial temperature data.* Journal of Geophysical Research: Atmospheres, 2008. **113**(D16).
[3] Waters, J.W., et al., *The earth observing system microwave limb sounder (EOS MLS) on the Aura satellite.* IEEE Transactions on Geoscience and Remote Sensing, 2006. **44**(5): p. 1075-1092.
[4] Levelt, P.F., et al., *The ozone monitoring instrument.* IEEE Transactions on geoscience and remote sensing, 2006. **44**(5): p. 1093-1101.
[5] Beer, R., *TES on the Aura mission: Scientific objectives, measurements, and analysis overview.* IEEE Transactions on Geoscience and remote sensing, 2006. **44**(5): p. 1102-1105.
[6] Beer, R., T.A. Glavich, and D.M. Rider, *Tropospheric emission spectrometer for the Earth Observing System's Aura satellite.* Applied optics, 2001. **40**(15): p. 2356-2367.

[7] Schoeberl, M., et al., *Earth observing system missions benefit atmospheric research.* Eos, Transactions American Geophysical Union, 2004. **85**(18): p. 177-181.
[8] Ahmad, S.P., et al. *Atmospheric products from the ozone monitoring instrument (OMI)*. in *Earth Observing Systems VIII*. 2003. International Society for Optics and Photonics.
[9] NASA. *GES DISC*. 2004.
[10] Schoeberl, M.R., et al., *Overview of the EOS Aura mission.* IEEE Transactions on Geoscience and Remote Sensing, 2006. **44**(5): p. 1066-1074.
[11] Kusterer, J.M. *TES Data and Information* 2019.

Peat depth mapping in Penyabungan area, Ogan Komering Ilir (OKI) Regency using GPR (Ground Penetrating Radar)

Sumirah[1], Lena Sumargana[1], Djoko Nugroho[1], Afifuddin[1]

[1]Agency for the Assessment and Application of Technology (BPPT)
M. H. Thamrin Street, No. 8, Jakarta, 10340, Indonesia

e-mail: sumirah@bppt.go.id

Abstrak. Mapping of peat thickness done in Penyabungan Area, Ogan Komering Ilir (OKI) Regency. The method used is Ultra GPR (Ground Penetrating Radar) and drill data collection. The Ultra GPR method is a geophysical method that uses electromagnetic waves to detect objects under the surface of both metal and non-metals, such as pipes, tunnels, coal. From Ultra GPR data processing, it is shown that the cross section of peat layer thickness then correlated with the drill data. From Ultra GPR radargram clearly shows the depth of the peat bordering minerals below. The results of mapping the peat depth in the Penyabungan area show a value of between 4-5 meters. The Ultra GPR method is an effective method used to determine the boundary of the peat layer.

1. Introduction

Indonesia is the fourth country that has the largest peatlands in the world. Peatlands in Indonesia are around 14.9 million hectares, the most widely found in Sumatra followed by Kalimantan and Papua [1]. The estimated area of peat is based on the results of updating the compilation of land maps from previous mapping, legacy soil data and soil survey results until 2011. In its development, the area of Indonesia's peatlands fluctuated from 13.2 to 26.5 million hectares [2]. Until now there has been no technology that can accurately map the area and thickness of peatlands. Field observation data with directly sampling is still the most accurate and there is no substitute but it costs a lot of money so peat aqcuisition data are very extensive. Data on characteristics, distribution, area and thickness of peatlands always change. Therefore it needs to be updated regularly by adding data and validation in areas that can be reached to get the actual data.

This paper presents the results of the mapping of peatland thickness in the Penyabungan area, OKI regency, South Sumatra province using Ultra GPR data that has been correlated with drill data collection. Even though the area is very small, it is expected to be an example in mapping peat thickness with quite accurate results. This mapping information on peatland thickness is useful for relevant stakeholders in the management and use of peatlands, especially in agriculture, as well as land use change.

2. Material and Methods

2.1. Study Area

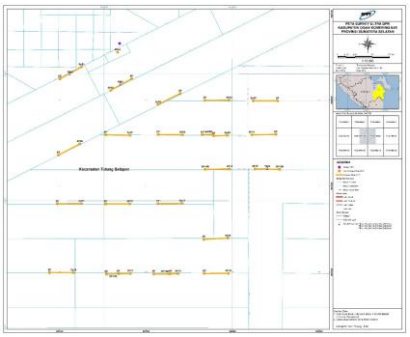

Figure 1. Data retrieval path in Penyabungan area.

The survey was conducted in the Penyabungan area which is the KHG (Peat Hydrological Unit) of the Sugihan River - Lumpur River), OKI (Ogan Komering Ilir) district of South Sumatra province. The survey was conducted in April - May 2018. The survey was carried out by pulling the ultra GPR device along the track. This is very effective and efficient with various terrain conditions. The data from the ultra GPR processing are validated by manually drill data at the point the ultra GPR track passes. By taking drill data per 50 cm depth we can find out the actual thickness of the peat and its level of maturity. The total trajectory taken was 19 trajectories, with variations in the length of the trajectory around 330 - 350 meters and 1 drill point as validation.

(a) (b)

Figure 2. (a) Ultra GPR survey, (b) Hand coring to determine the thickness of peat in real time.

2.2. Methods

The method used for mapping the thickness of peatlands is the ultra-GPR survey which is correlated with drill data collection. Ultra GPRS is a non-destructive geophysical method, using electromagnetic waves to detect the presence of objects or structures below the surface. The Ultra GPR system consists of a signal transmitter, control unit (CPU), and signal receiver. Ultra GPR working system is drawn as follows:

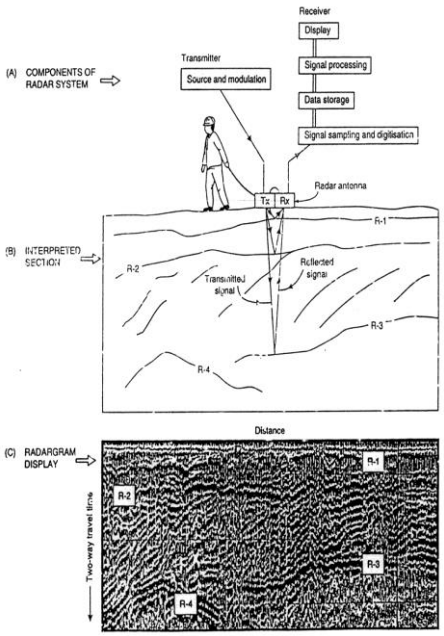

Figure 3. Illustration of Georadar System [3]

The ultra GPR system works similar to the usual GPR, it's just that the ultra GPR captures the full reflected waves in real time. This allows a buildup of 32,000 - 64,000 times during the same period as the GPR in general which can only accumulate 32 times practically [4], this increase in buildup can significantly increase penetration by two or more times.

Ultra GPR dimensions are even more concise. GPR in general weighs more than 20 kg. But the ultra GPR only weighs less than 5 kg, including data loggers. The collinear, or in-line antenna system, uses a resistive dipole load placed in a thin flexible hose as an antenna. Receiver and transmitter antennas are in the tube located along the hose, while the radar control unit and the recording computer are in the backpack. This system uses wireless technology in the form of Bluetooth and WiFi for communication between the receiver and the recording computer. Laptops that are usually used on GPR in general have been changed to android tablets that are resistant to water and of course more simple making it possible to conduct surveys in heavy terrain though.

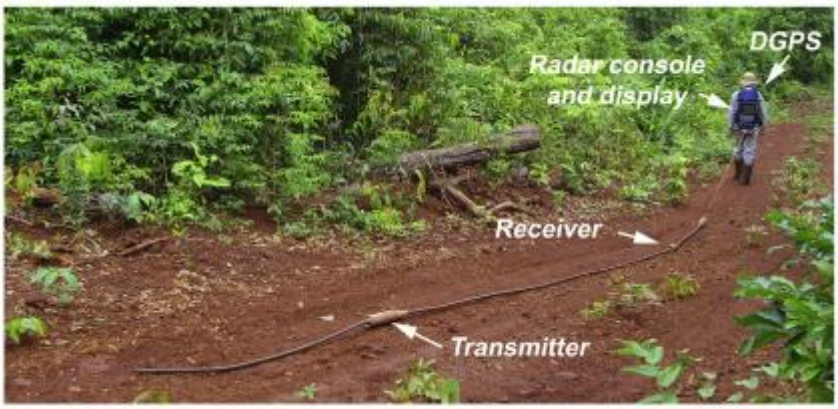

Figure 4. Image of Ultra GPR system with collinear and CPU [5]

3. Results and Discuss

3.1. Result

Based on data from BBSDLP (Center for Agricultural Land Resources Research and Development) that the depth of peat in the KHG of the Sugihan River and the Lumpur river is around 1-2 meters. The process of taking ultra GPR data generates a radargram and is processed with Reflex software and the processing results are as shown at table 1 below:

Table 1. Ultra GPR processing table

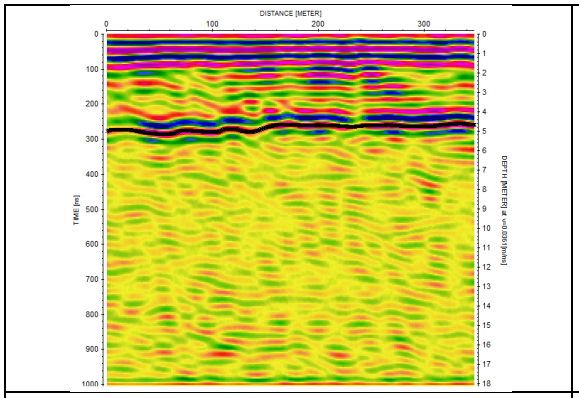	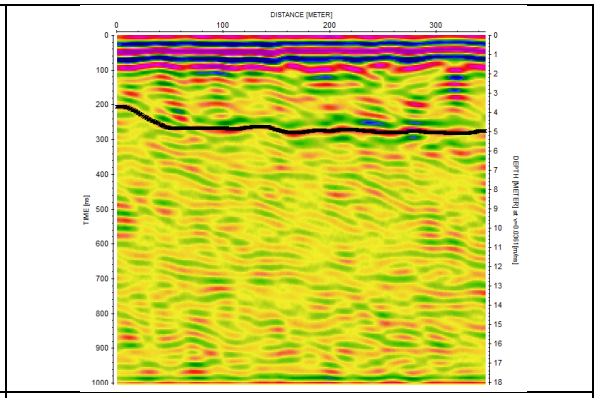
Line SP02	Line SP03
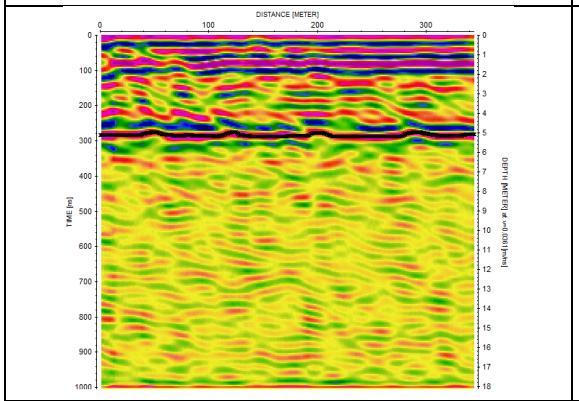	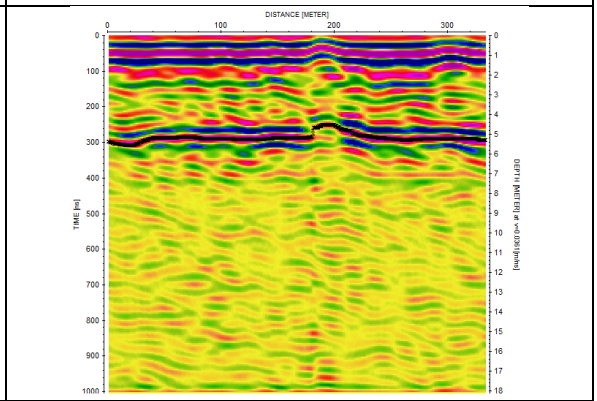
Line SP04	Line SP05
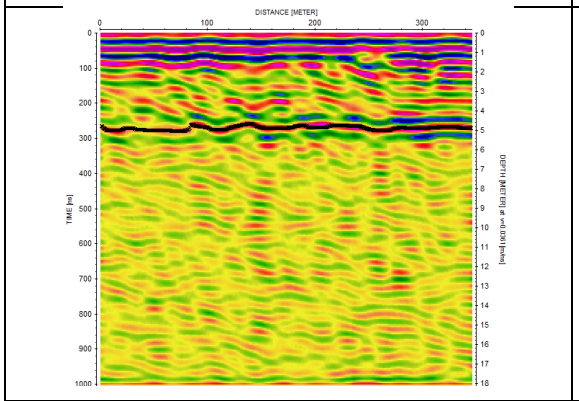	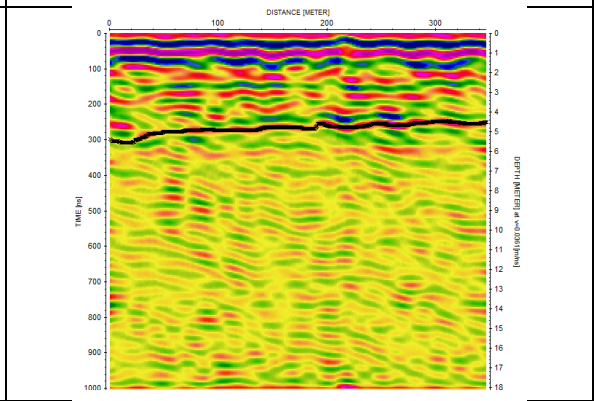
Line SP06	Line SP07

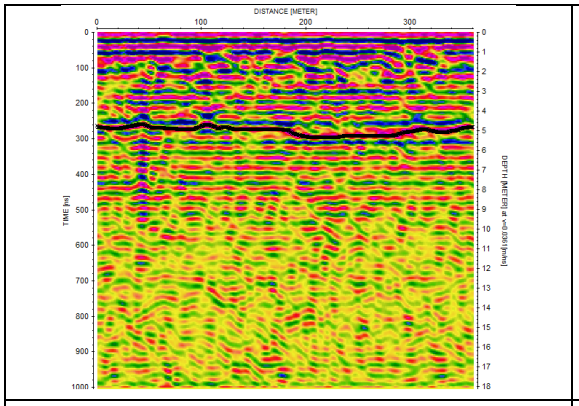

Line SP08

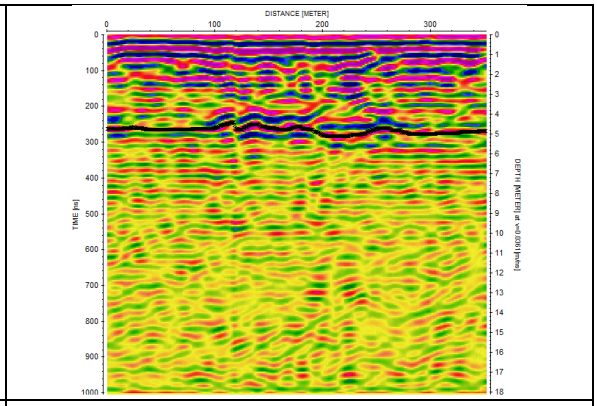

Line SP09

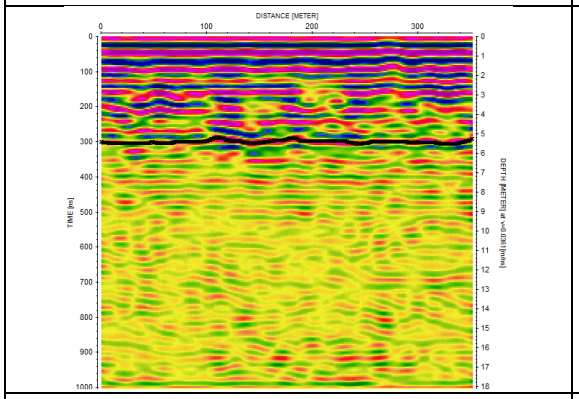

Line SP10

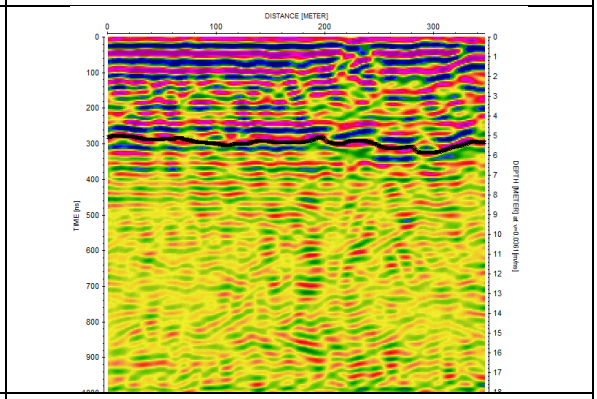

Line SP11

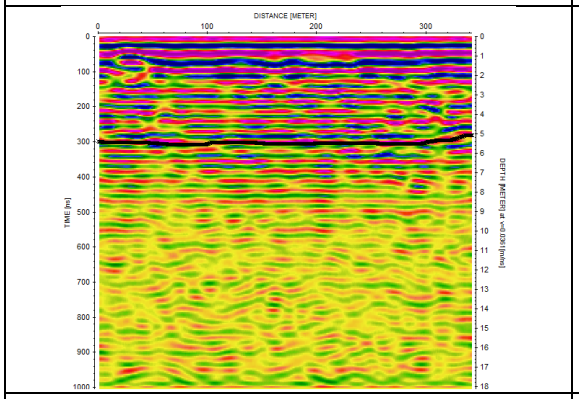

Line SP12

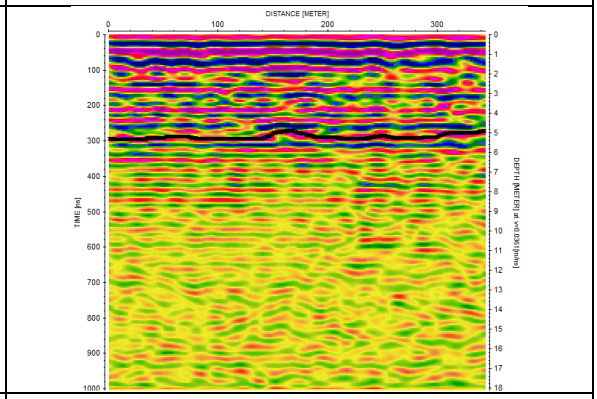

Line SP13

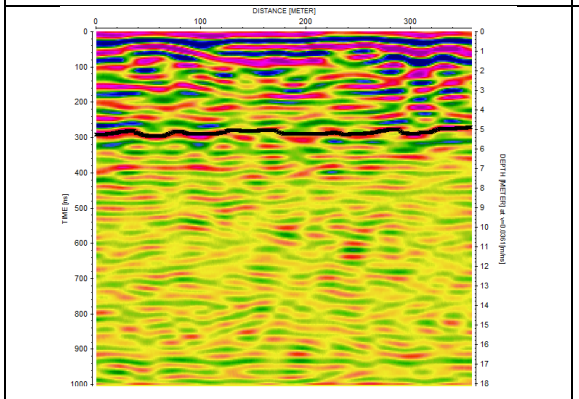

Line SP14

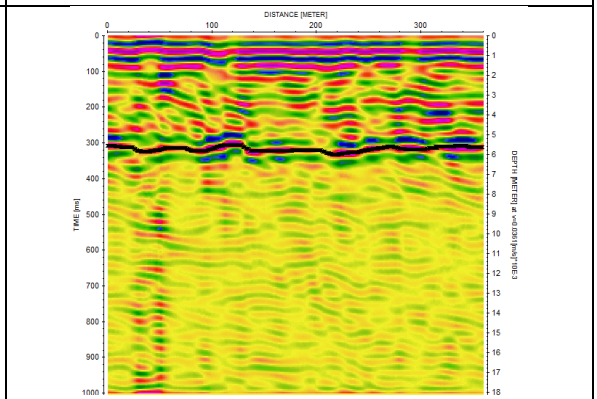

Line SP15

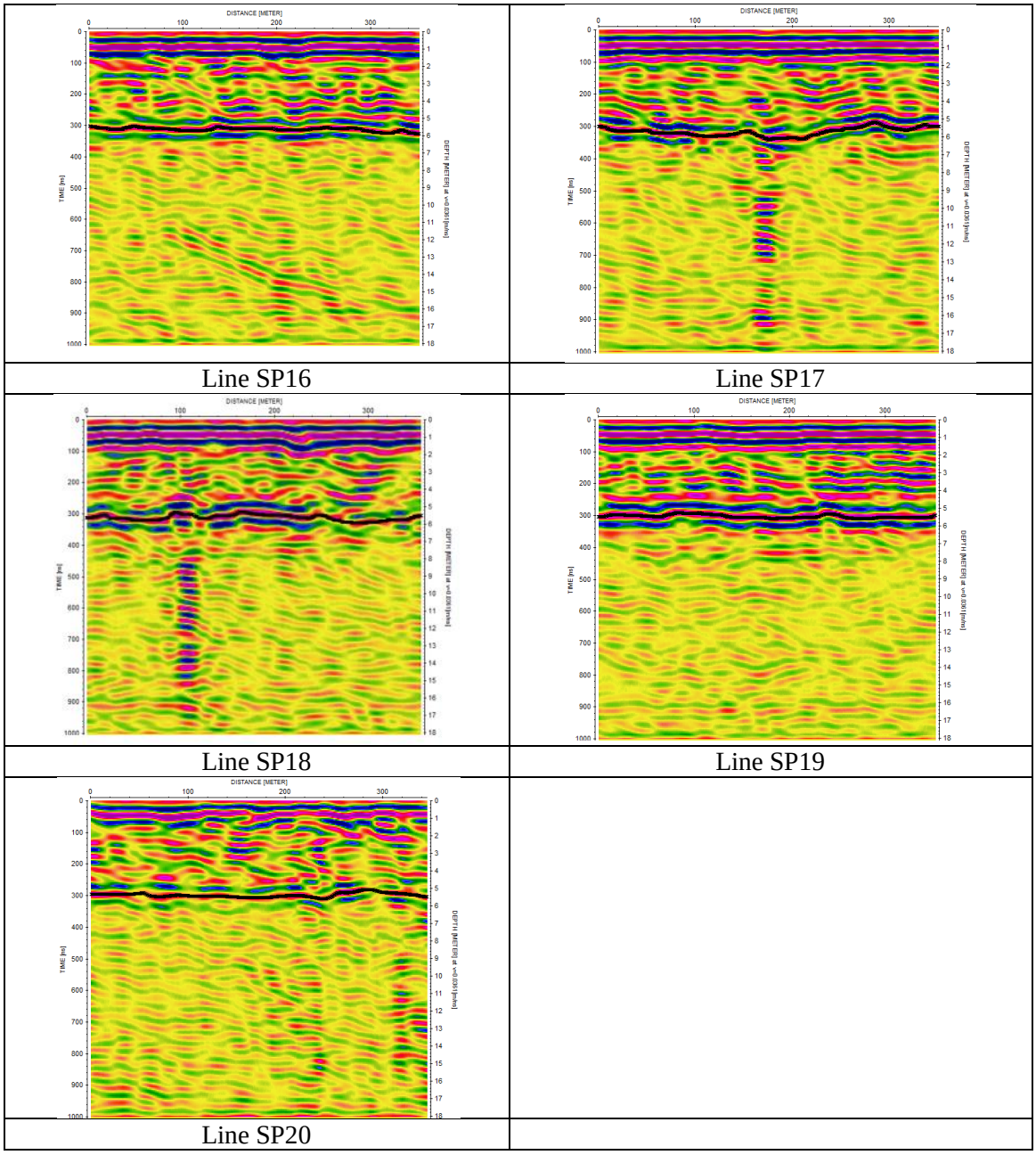

Line SP16	Line SP17
Line SP18	Line SP19
Line SP20	

3.2. Discuss

Coring data is performed on the SP15 track. With correlation of drill data at a depth of 5.02 m on the 177th meter velocity was obtained 0.0359 m/ns. This velocity is then used to be applied in all data processing for all trajectories.

From the picture above clearly seen the boundary between the peat above and the mineral below, thickness between 4-6 meters. From each radargram profile, a boundary layer is formed between the peat above it and the minerals below, then from this profile a contour map is made as shown below. The results show variations in peat depth. In the north the peat is shallower than the south, there is a fairly thick layer in the southwest and southeast of the study area and a thin layer of peat extends from north to south.

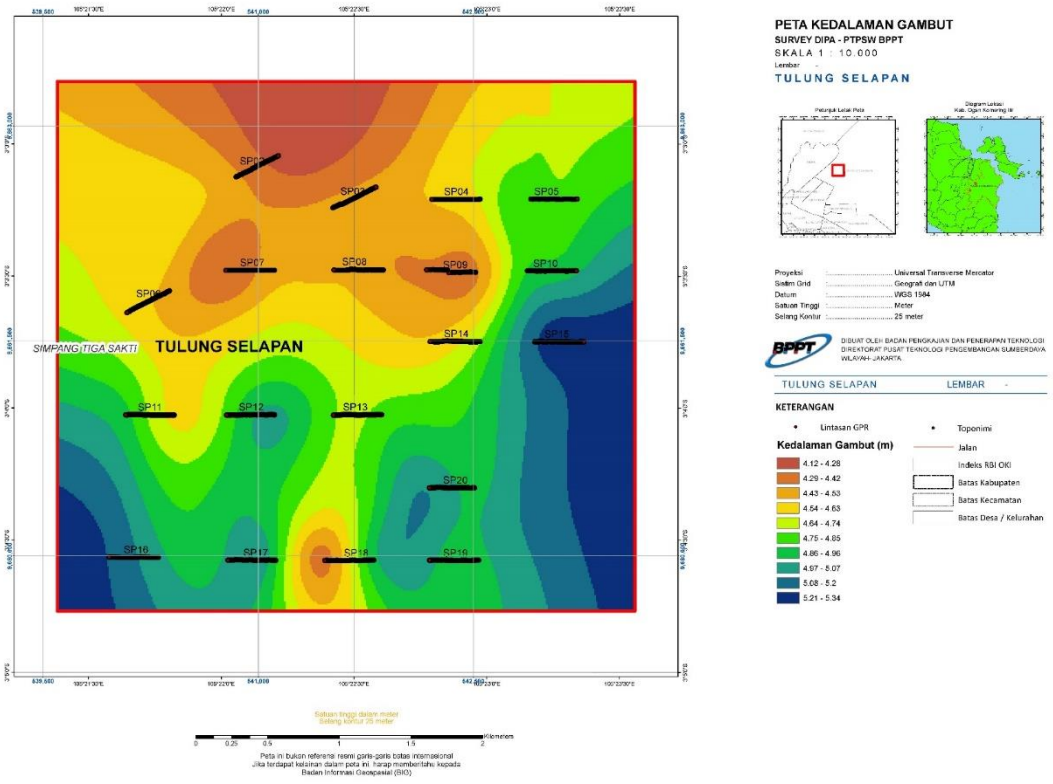

Figure 5. Results of mapping thickness of the Panyabungan area

4. Conclusions

Ultra GPR method can quickly get more data than conventional GPR methods. This method can quickly aqcuire data in a variety of terrain conditions. The ultra-GPR method is able to determine the boundaries of peat layers effectively, efficiently and in more detail. This method is able to map the thickness of peat in a wider area quickly.

5. Acknowledgements

This research was funded by the Agency for the Assessment and Application of Technology (BPPT). The authors would like to thank all colleague of Center For Regional Resources Development Technology (PTPSW), BPPT for field data collection and technical support.

6. References

[1] Ritung, S.W.K.N.S.H.S.C.T., *Peta Lahan Gambut Indonesia Skala 1:250.000 (Indonesian peatland map at the scale 1:250,000).* 2011.
[2] Agus, W.K.N.F., *Perkembangan Pemetaan dan Distribusi lahan gambut di Indonesia.* 2016.
[3] Reynolds, J.M., *An Introduction to Applied and Environmental Geophysics.* 1997.
[4] Sumargana, L., et al. *Identify depth of peat using Ultra GPR in Siak Regency, Riau Province*. in *2018 IEEE Asia-Pacific Conference on Geoscience, Electronics and Remote Sensing Technology (AGERS)*. 2018. IEEE.
[5] Francke, J., *A review of selected ground penetrating radar applications to mineral resource evaluations.* Journal of Applied Geophysics, 2012. **81**: p. 29-37.

Suitability of space utilization of settlement in coastal areas of Abeli and Nambo Sub-District, Kendari City using spatial and non-spatial methods

M. Aris Rauf[1], Hasbullah Syaf[1], and Muslim Tadjuddah[2]

[1]Agricultural Faculty, University of Halu Oleo Kendari, Indonesia
[2]Fisheries and Marine Sciences Faculty, University of Halu Oleo Kendari Indonesia

e-mail: muslim22jan@uho.ac.id

Abstract. Land use for settlements needs to be regulated properly so that it is suitable with the city spatial plan by considering ecological balance aspect so that there is no deterioration in the land quality. Environmental damage can also occur because of the pattern of settlement development that exceeds the carrying capacity of the environment such as density, size and shape of settlements. Abeli and Nambo Sub-Districts, cover an area of 43.85 Km2 or 16.40% of the total area of Kendari city (BPS Kendari 2017), it is a strategic area for urban development because it has a relatively wide location and it is directly facing the Banda Sea. This study aimed to: (1) analyze the level of suitability of land for settlements in the coastal areas of Abeli and Nambo Sub-Sub-Districts; (2) figure out of community perspective in the selecting the location of settlements in Abeli and Nambo Sub-Districts. The study used qualitative and quantitative research methods with descriptive qualitative analysis and spatial analysis. This study consisted of 8 variables namely slope, distance from the coast boundary, distance from river boundary, distance from tsunami prone location, distance from flood location, distance from mangrove ecosystem, sea tide fluctuations, and high ROB flood inundation. The results showed that (1) suitability land in the settlement in Abeli and Nambo Sub-Districts that were included in the very suitable criteria were 2,382.87 Ha or 80.44 %, suitable criteria were 15.56 Ha or 15.56 %, the criteria for Less Suitable was 114.26 or 3.86 %, and Not Suitable criteria was 4.24 hectares or 0.14 %; (2) Respondents' reasons for selecting a settlement location were influenced by consideration of house price (11 %) location or access to workplaces and public facilities (34 %), security against natural disasters (19 %), environmental health (21 %), convenience (11 %,) and others (3 %) while the reasons for respondents choosing the location of settlements based on residential Land Suitability were Very Suitable (40 %), Suitable (37 %), Less Suitable (21 %) and Not Suitable (1 %).

1. Introduction

Abeli and Nambo Sub-Districts located in the east of Kendari City has an area of 43.85 Km2 or 16.40% of the vast area of Kendari City [1], which is a strategic area for urban development because it has a relatively wide location directly with the Banda Sea. This is indicated by the number of activities along the coastal area ranging from residential activities, coastal tourism, to the industrial sector.

Abeli and Nambo Sub-District are relatively undeveloped Sub-Districts compared to other sub-Sub-Districts in Kendari. but both Sub-Districts have many potential resources. The potential of the existing resources is tourism potential in Bungkutoko Sub-District which has a 2 ha mangrove forest which is being developed into a tourist mangrove forest and Nambo Coast and Bungkotoko Island which also has the potential for coastal tourism development. Another activity that can also be developed is mariculture business. Another cultivation business is seaweed, which is quite rapidly developing in Sambuli and Tondonggeu Villages [2].

The development in Abeli and Nambo Sub-Districts, especially in land use for settlements must pay attention to the natural and physical condition of the land. This is intended to make the development of existing settlements does not cause environmental problems in the future. The unsuitability of land use with a natural physical condition can cause environmental problems such as floods, erosion and landslides.

These environmental problems can cause material (property) and non-material (soul) losses. Placement of settlement construction locations needs to be harmonized with Land Suitability in the coastal areas of Abeli and Nambo Sub-Districts. Environmental balance and staying awake from negative impacts that can cause long term losses can be avoided. Based on these problems, this study aimed to (1) analyze the level of suitability of land for settlements in the coastal areas of Abeli Sub-Sub-District and Nambo Sub-Sub-District; (2) figure out of community perspective in the selecting the location of settlements in Abeli and Nambo Sub-Districts.

1. Methodology

1.1. Location and Time

This research was conducted in Abeli and Nambo Sub-Districts located in the east of Kendari city. It started in August - October 2017 using the research variables namely : land slope (%), distance from the coast boundary (m), distance from the river boundary (m), distance from tsunami prone location (m), distance from flood location (m), distance from mangrove ecosystem (m), tidal fluctuation (m), and height of flood inundation (m). The location of the study is shown in Figure 1.

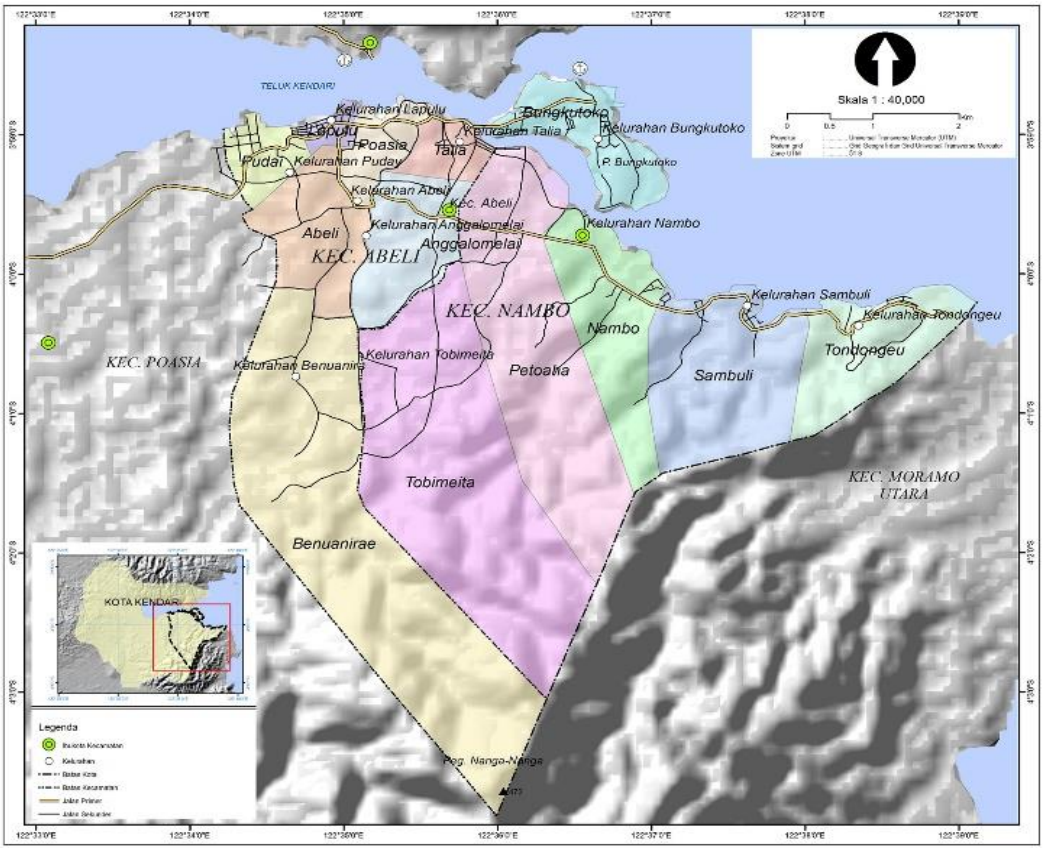

Figure 1. Research location.

1.2. Data Collection

This study used two types of data analysis, namely spatial analysis and non-spatial analysis. Spatial data derived from analysis of satellite images and GPS surveys, satellite imagery used consists of 2 (two) types, namely DEM type image (Digital Elevation Model) S 30 meter 2009 RTM product and SPOT-6 Year Satellite Imagery in 2015. DEM-STRM image is to obtain altitude and slope data and SPOT-6

images to obtain coastline data and land cover. DEM data that has been processed is then corrected using BIG Topography Data with Scale of 1:25.000 in 2013 while coastline data and land cover and the highest tide boundary were observed through field surveys using GPS. DEM-SRTM imagery can be obtained by downloading through the Earth Explorer-USGS website (https://earthexplorer.usgs.gov). Source of non-spatial data from questionnaires containing a list of questions about the conditions and situations faced in the community settlement to find out the perceptions of the people living around the area and the location of suitable settlements.

1.3. Data Collection

Land Suitability for settlement using overlay technique and scoring showed by Figure 2.

.

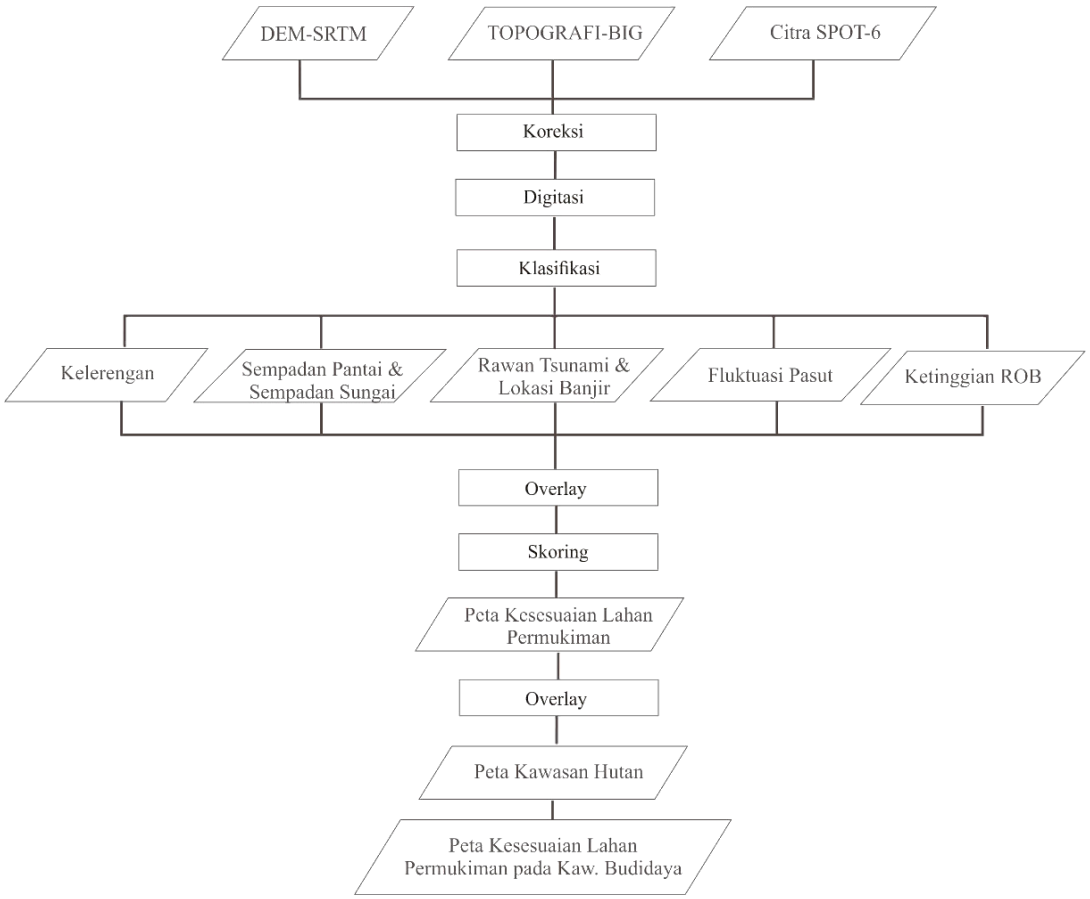

Figure 2. Overlay technique for land suitability for settlement.

Based on the results of land suitability assessment, a map of land suitability is made by using GIS technology. The level is divided by four suitability classes namely S1, S2, S3 and N, namely:

- S1 Class: *Very Suitable* that island that does not have a heavy barrier for certain use in a sustainably or only has a barrier that is less meaningful and does not significantly affect the production of the land and will not add input from the business.
- S2 Class *Suitable*, that is land that has rather heavy restrictions for certain sustainable uses. The Boundary will reduce land productivity and the profits obtained and increase input to cultivate the land.
- S3 Class: *Less Suitable* that is land that has a very heavy Boundary level, but it is still possible to overcome/repair, it means that it can still be improved to be suitable if repair is carried out with a high level of technology introduction or can be done with additional treatment with rational costs.

- N Class: *Not Suitable*, that is land that has very heavy/permanent, so it is impossible to be used as sustainable use. As for the parameter and indicator used can be seen in Settlement land suitability as seen in Table 1.

Table 1. Operational Definition

No.	Variable	Indicator	Suitability Class
1.	Slope (%) [3], [4]	0 – 8	S3 Very Suitable
		8 - 15	S2 Suitable
		15 - 25	S1 Less Suitable
		> 25	N Not Suitable
2.	Distance from Coast Boundary (m) [4]	> 100	S3 Very Suitable
		50 - 100	S2 Suitable
		30 - 50	S1 Less Suitable
		0 – 30	N Not Suitable
3.	Distance from River Boundary (m) [4], [5]	> 10	S3 Very Suitable
		5 - 10	S2 Suitable
		3 - 5	S1 Less Suitable
		0 – 3	N Not Suitable
4.	Distance from Tsunami Prone Point (m) [4]	> 1.000	S3 Very Suitable
		500 - 1.000	S2 Suitable
		0 – 500	N Not Suitable
5.	Distance from Flood location (m) [6]	>100	S3 Very Suitable
		50 – 100	S2 Suitable
		0 - 50	N Not Suitable
6.	Distance from Mangrove ecosystem (m) [5]	> 200	S3 Very Suitable
		100 - 200	S2 Suitable
		0 – 100	N Not Suitable
7.	Seawater Fluctuation (m) [4], [7]	0	S3 Very Suitable
		0,5 – 2	S2 Suitable
		> 2	N Not Suitable
8.	High flood inundation (m.dpl) [8]	0	S3 Very Suitable
		0 – 1	S2 Suitable
		> 1	N Not Suitable

2. Results

2.1. Land Suitability Variable for Settlement

Land suitability process for settlement can be done based on variables that can be boundary of land use. As for the variables are:

2.1.1. Slope

Based on the results of the study, the areas with slopes of 0-8% (Very Suitable) in Abeli Sub-District were 785.96 Ha or 49.33%, while in Nambo Sub-District they were 947.31 Ha or 38.31%, the areas with slopes were 8 - 15% (Suitable) in Abeli Sub-District that covers an area of 272.73 Ha or 15.73% while in Nambo Sub-District an area of 440.60 Ha or 17.88%, an area with a slope of 15-25% (Less Suitable) in Abeli Sub-District with an area of 254.00 Ha or 15.94% while in Nambo Sub-District covering 535.84 Ha or 21.75%, and areas with slopes > 25% (Not Suitable) in Abeli Sub-District covering an area of 310.59 Ha or 19.49% while in Nambo Sub-District covering an area of 540, 05 Ha or 21.92%. The results of slope analysis in Abeli Sub-District and Nambo Sub-District are showed in Table 2.

Table 2. Analysis results of slope in Abeli and Nambo Sub-Sub-District

No	Suitability	Abeli Sub-district		Nambo Sub-district		Total	
		Ha	%	Ha	%	Ha	%
1	Very Suitable	785,96	49,33	947,31	38,45	1.733,27	42,72
2	Suitable	242,73	15,23	440,60	17,88	683,33	16,84
3	Less Suitable	254,00	15,94	535,84	21,75	789,84	19,47
4	Not Suitable	310,59	19,49	540,05	21,92	850,64	20,97
	Total	1.593,29	100,00	2.463,80	100,00	4.057,09	100,00

2.1.2. Distance from Coast Boundary

Based on the results of the study, the condition of the available land in Abeli and Nambo sub-districts, which is more than 100 meters wide, as quite wide, covering an area of 3,857.39 ha or 95.08%. The wide distribution of land in Abeli and Nambo sub-districts was based on the suitability of distance from the coastal Boundary as presented in Table 3.

Table 3. Distribution of Land area in Abeli and Nambo Sub-District from Coast Boundary

No	Suitability	Abeli Sub-District		Nambo Sub-District		Total	
		Ha	%	Ha	%	Ha	%
1	Very Suitable	1.544,80	96,96	2.312,58	93,86	3.857,39	95,08
2	Suitable	21,77	1,37	73,44	2,98	95,21	2,35
3	Less Suitable	10,07	0,63	30,41	1,23	40,48	1,00
4	Not Suitable	16,65	1,04	47,37	1,92	64,02	1,58
	Total	1.593,29	100,00	2.463,80	100,00	4.057,09	100,00

2.1.3. Distance from River Boundary

Based on the overall results of the study, in Abeli and Nambo Subdistricts it was dominated by Very Suitable condition with an area of 3,987.89 Ha or 98.03%, then suitable conditions with an area of 34.65 Ha or 0.85%, and the smallest land suitability was the variable distance from the river border, namely in the Not Suitable category that is 20.69 Ha or 0.51%. It can be seen in Table 4.

Table 4. Distribution of Land Area in Abeli and Nambo Sub-District from River Boundary

No	Suitability	Abeli Sub-District		Nambo Sub-District		Total	
		Ha	%	Ha	%	Ha	%
1	Very Suitable	1.572,99	98,73	2.414,90	98,02	3.987,89	98,30
2	Suitable	10,16	0,64	24,49	0,99	34,65	0,85
3	Less Suitable	4,06	0,25	9,77	0,40	13,83	0,34
4	Not Suitable	6,07	0,38	14,62	0,59	20,69	0,51
	Total	1.593,28	100,00	2.463,78	100,00	4.057,09	100,00

2.1.4. Distance from Tsunami Prone Area

Based on the results of the study, overall in Abeli and Nambo Sub district the distance from tsunami-prone areas was dominated by very suitable conditions with an area of 3,611.99 Ha or 89.03%, then the conditions were Not Suitable with an area of 161.11 Ha or 7.00% and the smallest Land Suitability in the distance variable from Tsunami-prone area that was in the Suitable category as large as 161.11 Ha or 3.97%. It is shown in Table 5.

Table 5. Distribution of Land Area in Abeli and Nambo Sub-District from Tsunami Prone Location

No	Land Suitability	Abeli Sub-District		Nambo Sub-District		Total	
		Ha	%	Ha	%	Ha	%
1	Very Suitable	1.593,28	100,00	2.018,71	81,93	3.611,99	89,03
2	Suitable	-	-	161,11	6,54	161,11	3,97
3	Not Suitable	-	-	283,99	11,53	283,99	7,00
	Total	1.593,28	100,00	2.463,81	100,00	4.057,09	100,00

2.1.5. Distance from Flood Location

Based on the results of the study, the area that was not suitable for the overall settlement in Abeli and Nambo sub-districts was an area of 311.40 ha or 7.68% because it is an that is area very close to the river flow. The data can be seen in Table 6.

Table 6. Distribution of Land Area in Abeli and Nambo Sub-District from Flood Location

No	Land Suitability	Abeli Sub-District		Nambo Sub-District		Total	
		Ha	%	Ha	%	Ha	%
1	Very Suitable	1.247,02	78,27	2.318,59	94,11	3.565,61	87,89
2	Suitable	116,26	7,30	63,84	2,59	180,10	4,44
3	Not Suitable	230,02	14,44	81,38	3,30	311,40	7,68
	Total	1.593,3	100,00	2.463,81	100,00	4.057,09	100,00

2.1.6. Distance from Mangrove Ecosystem

Based on the results of the study, it showed that overall in Abeli and Nambo Sub-districts the distance from the mangrove ecosystem was dominated by very suitable conditions with an area of 3,764.68 Ha or 92.79%, then not suitable condition for settlements with an area of 177.61 Ha or 4.38% and the smallest Land Suitability on the distance variable from the mangrove ecosystem was in the suitable category that was an area of 114.78 Ha or 2.83% as shown in Table 7.

Table 7. Distribution of Land Area in Abeli and Nambo Sub-District from Mangrove Ecosystem

No	Land Suitability	Abeli		Nambo		Total	
		Ha	%	Ha	%	Ha	%
1	Very Suitable	1.546,86	97,09	2.217,82	90,02	3.764,68	92,79
2	Suitable	23,93	1,50	90,85	3,69	114,78	2,83
3	Not Suitable	22,49	1,41	155,12	6,30	177,61	4,38
	Total	1.593,28	100,00	2.463,79	100,00	4.057,09	100,00

2.1.7. Seawater Fluctuation

Based on the results of the study, it was shown that overall in Abeli and Nambo Sub-districts the sea tidal fluctuation was dominated by very suitable conditions with an area of 3,869.59 Ha or 95.38%, then the suitable condition for settlements with an area of 187.49 Ha or 4.62% as shown in Table 8.

Table 8. Distribution of Land Area in Abeli and Nambo Sub-District based on Tide fluctuation

No	Land Suitability	Abeli		Nambo		Total	
		Ha	%	Ha	%	Ha	%
1	Not Suitable	-	-	-	-	-	-
2	Suitable	47,47	2,98	140,02	5,68	187,49	4,62
3	Very Suitable	1.545,80	97,02	2.323,79	94,32	3.869,59	95,38
	Total	1.593,27	100,00	2.463,81	100,00	4.057,08	100,00

2.1.8. High floodwaters ROB

Based on the results of the study, Overall, Domination in the very suitable category was 3,869.59 Ha or 95.38%, the suitable category was 167.64 Ha or 4.13%, whereas in the not suitable category for settlements was 19.86 Ha or 0.49% as shown in Table 9.

Table 9. Distribution of Land based on suitability of high floodwaters ROB in Abeli and Nambo Sub-District

No	Land Suitability	Abeli		Nambo		Total	
		Ha	%	Ha	%	Ha	%
1	Very Suitable	1.545,80	97,02	2.323,79	94,32	3.869,59	95,38
2	Suitable	41,33	2,59	126,31	5,13	167,64	4,13
3	Not Suitable	6,15	0,39	13,71	0,56	19,86	0,49
	Total	1.593,28	100,00	2.463,81	100,00	4.057,09	100,00

2.2. Analysis of Land Suitability for Settlement in Abeli and Nambo Sub-district

Based on the overlay results with forest areas, land suitability in Abeli and Nambo Districts is dominated by the very suitable category with a land area of 2,382.87 Ha or 80.44%. The conditions in the not suitable category were 0.21 Ha or 0.01% in the Lapulu Village, while in the Nambo Sub district it was 4.24 Ha or 0.14%. Land suitability for settlements in the coast area of Abeli and Nambo Sub- District as shown in Figure 3 and Table 10.

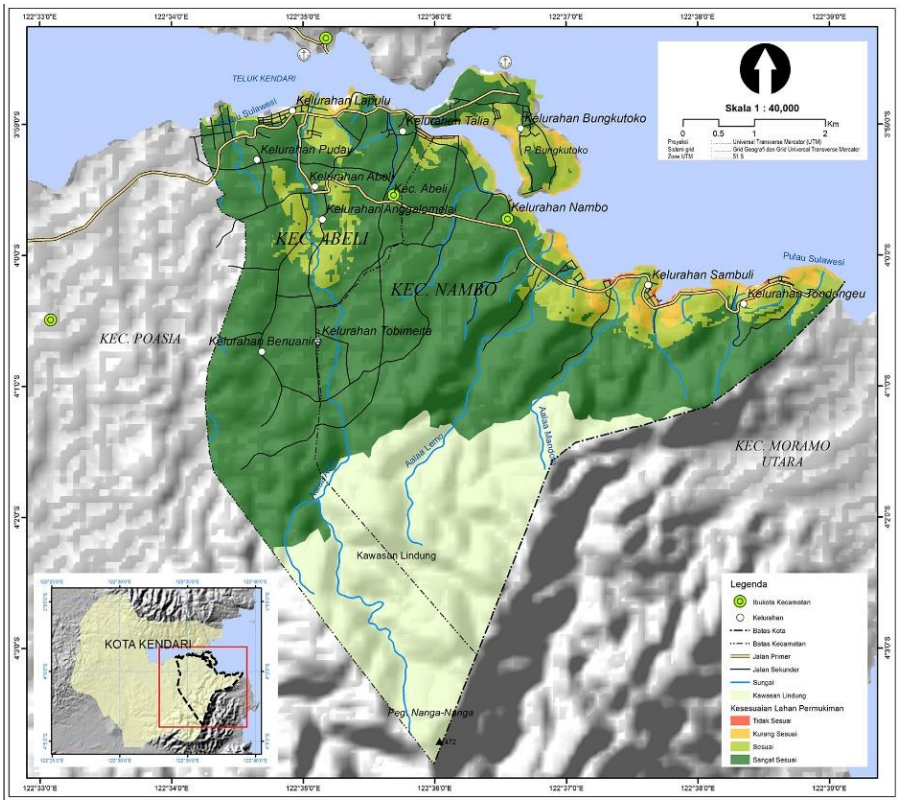

Figure 3. Settlement land suitability map.

Table 10. Land Suitability of Settlement in Abeli and Nambo Sub-Sub-District

No	Land Suitability	Abeli		Nambo		Total	
		Ha	%	Ha	%	Ha	%
1	Very Suitable	978,73	85,09	1.404,14	77,48	2.382,87	80,44
2	Suitable	161,00	14,00	300,01	16,56	461,01	15,56
3	Less Suitable	10,48	0,91	103,78	5,73	114,26	3,86
4	Not Suitable	0,01	0,00	4,23	0,23	4,24	0,14
	Total	1.150,22	100,00	1.812,16	100,00	2.962,38	100,00

2.3. Analysis of People Argumentation at Coast of Abeli and Nambo Sub-Sub-District

The results of the interview illustrated that generally, people who occupy coastal areas were in middle-income groups that prioritize accessibility that is close to the transportation routes, the location of public facilities, and accessibility to markets. In addition, most people chose to live in coastal areas because of environmental safety factors and according to th2e people in the coastal areas they were still quite safe. Reasons to in choosing a place of residence include the price of a house, location or access to a workplace, public facilities, security for natural disasters such as floods, environmental health (clean air), comfort (shady, cool, etc.) then 34% respondents chose their place of residence by reason of access to workplaces and public facilities, 21% of respondents chose because of environmental health reasons, 19% of respondents chose because of security from natural disasters, 11% of respondents chose because of house prices and convenience, 3% others. The reasons for choosing a place to live based on the sub-district can be presented in Figure 4 and Table 11.

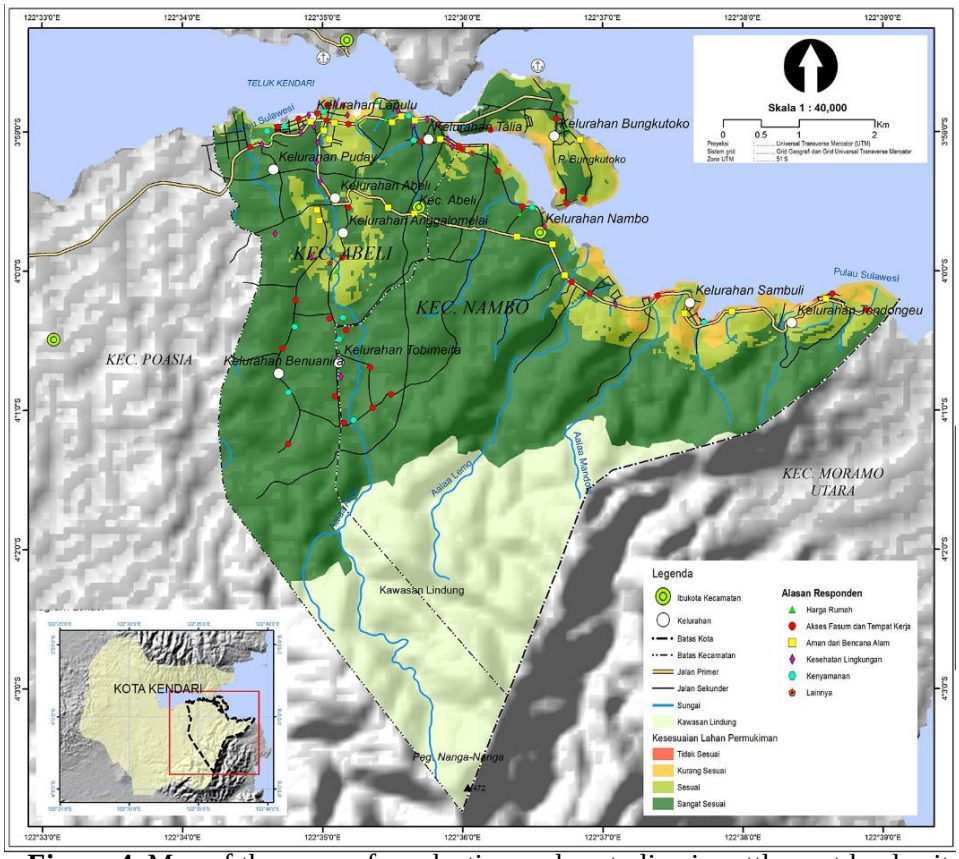

Figure 4. Map of the reason for selecting a place to live in settlement land suitability.

Table 11. The main requirement in selecting settlement location in Abeli and Nambo Sub-District

No.	Requirement	Abeli		Nambo		Total	
		Freq.	%	Freq.	%	Freq.	%
1	House Price	6	10	5	13	11	11
2	Location	16	27	18	46	34	34
3	Safety	12	20	7	18	19	19
4	Environmental Health	18	30	3	8	21	21
5	Convenience	7	12	4	10	11	11
6	Others	1	2	2	5	3	3
Total		60	100	39	100	99	100

While the reason for choosing a place to live based on Land Suitability can be seen in Table 12.

Table 12. Respondent Reason in Selecting House to Land Suitability

No.	Reason in Selecting House	Very Suitable	Suitable	Less Suitable	Not Suitable	Total	%
1	House Price	5	2	4	-	11	11
2	Access to office and public facilities	13	12	9	-	34	34
3	Safe from Natural Disaster	7	10	2	-	19	19
4	Environmental Health	8	8	5	-	21	21
5	Convenience	7	3	1	-	11	11
6	Others	-	2	-	1	3	3
Total		40	37	21	1	99	100

2.4. Discussion

The results of overlaying land suitability parameters for settlement was then overlaid with maps of forest areas because settlements must be outside of protected forests. Land Suitability in a suitable category for residential areas in Abeli sub-district generally also spread to the same coastal area as in the very suitable area. Area with this category is characterized by the following characteristics: 8-15% slope, 50-100 metes r from the coastal border, 5-10 meters river boundary, 500-1,000 meter from tsunami prone location, 300-500 m distance from flood location - 500 , 100-200 meters distance from mangrove ecosystem 100 - 200 meters, tide fluctuation is 0.5-2 m, and high floodwaters ROB is 0 - 1 mdpl.

Suitability land in the not suitable category was also spread in the same coastal areas as in the area with a very suitable category. Area with this category is characterized by the following characteristics: slope > 25%, 0-30 meters distance from coastal boundary, 0-3 meters distance from river border, 0-500 meters distance from tsunami-prone locations, 0-300 meters distance from flood location, 0-100 meters distance from mangrove ecosystem, having sea tide fluctuations > 2 m, and high floodwaters ROB (> 1 mdpl). The development of settlements in the coastal areas of Abeli and Nambo Sub-districts should be a part of the development process and the overall use of coastal areas where development of facilities and development infrastructure is also related to the development of settlements.

It refers to the definition of settlements according to [9], that is land use used for the development of housing, public facilities and infrastructure, trade, offices, recreational facilities and other interest related to community life activities. Residents who have been domiciled in coastal areas, generally use the land only based on aspects of ease in utilizing natural resources only. It is also accompanied by limited facilities and infrastructure as well as adequate information about the use of natural resources and the environment, thus encouraging the use of territories and natural resources that are not suitable with their designation and benefits.

This phenomenon encourages the growth of settlements and the efforts to handle and manage natural resources by prioritizing distances that are easily accessible and close to the market, but it is carried out in an uncontrolled and unplanned manner. As a result, the development of regional spatial planning is not integrated and not directed and still traditional and slum. Exiting conditions in the area were partly located in the area of mangrove forests and agricultural areas. In Abeli and Nambo Sub-districts, the land function of ±300 hectares had been managed by the community to become housing, tombs, places of worship, including fish ponds, aquaculture and industry.

According to [5], the form and nature of settlements and urban area in coastal areas must be an integral part and do not conflict with the overall ecological processes and coast phenomena. The principle thing is that the increasing need for settlements, demands an integrated spatial layout in coastal areas that is environmentally sound. Settlement in coastal areas that are chaotic and not environmentally sound will cause environmental degradation, namely erosion, sedimentation, environmental pollution and flood.

The policy-making process and the alternative development of the coastal area of Kendari City for the designation of residential areas should pay attention to various aspects related to this policy so that the development and sustainable utilization of the coastal area of Kendari City can be achieved optimally. Alternative regional development must also pay attention to the aspirations and opinions of various parties, especially those who are competent in the use of this region, so that conflict in spatial use between sectors can be avoided which in itself will have a good influence on the utilization of natural resources in the coastal areas of the Kendari.

The results showed that the community in selecting settlement locations is more influenced by factors of easy to access the source of livelihood so that they prefer the locations close to the coast because most respondents worked as fishermen, besides that it is also due to limited available land. Traditionally fishermen communities on the coast can adapt to natural conditions, but because of lack of good arrangement, the settlement environment becomes increasingly slum and creates other social problems such as health, social environment and discomfort.

3. Conclusion

Based on the results it can be concluded that:

1) Land suitability criteria of settlement in Abeli and Nambo Sub-District that were very suitable 2.382,87 Ha (80,44%), suitable 461,01 Ha (15,56%), less suitable 114,26 Ha (3,86%) and not suitable 0,14 Ha (0,14%).
2) In selecting the settlement location of the community living in Abeli Sub-District, it was affected by consideration of housing price (10%), consideration of location or access to workplaces and public facilities (27%), consideration of security against natural disaster (20%), consideration of environmental health (30%), consideration of comfort (12 %), and others (2%). Whereas in Nambo Sub-District it was affected by considerations of 13% house prices, consideration of location or access to workplaces and public facilities 46%, consideration of security against natural disasters 18%, consideration of environmental health 8%, consideration of convenience 10%, etc. 3 %. For people who live in locations that were not suitable (N) so that the Government needs to conduct socialization so that they no longer live in that location

4. References

[1]. Dahuri, R., et al., *Pengelolaan sumberdaya wilayah pesisir dan lautan secara terpadu.* PT. Pradnya Paramita. Jakarta, 2001. **328**.
[5]. Ward, P., et al., *Coastal inundation and damage exposure estimation: a case study for Jakarta.* Natural Hazards, 2011. **56**(3): p. 899-916.
[6]. Kendari, B.P.S.K., *Kota Kendari dalam Angka 2017*. Badan Pusat Statistik Kota Kendari, Kendari, 2017.
[8]. Perka, B., *No 2 Tahun 2012 Tentang Pedoman Umum Pengkajian Risiko*. 2012, Bencana.

Deforestation and carbon emissions at Poso Regency, Central Sulawesi Province, Indonesia

Jaka Suryanta, Irmadi Nahib, Turmudi

Centers for Research, Promotion and Cooperation, Geospasial Information Agency (BIG)
Jl Raya Jakarta Bogor KM 46 Cibinong, Jawa Barat, 16911, Indonesia

e-mail: irmadi.nahib@big.go.id

Abstract: Forests are natural resources that are very beneficial for livelihoods and also have a variety of ecological functions. One function of forests is to maintain the amount of carbon stored. Changing forest areas to non-forest areas has resulted in reduced forest function as a provider of environmental services. The forest conversion also has an impact on the total contribution of greenhouse gas (GHS) emissions. Central Sulawesi Province has quite extensive forest, which is 4,258 million ha, but needs to be paid attention in the period 2000-2009 deforestation has reached 432.111.50 Ha (10.15%). Significant deforestation has occurred in one district, namely in Poso with a contribution of 4.61% in the province of Central Sulawesi. This study aims to calculate the rate of deforestation and simulate carbon emissions in Poso District using the REDD + model. The main data used in this study are land use / cover maps (2003, 2009 and 2015), driving variables (distance from: forest edge, road, river flow, and slope) as explanatory deforestation variables. The results showed that deforestation in the period 2003-2015 reached 19,944.99 (3.58%) or the deforestation rate of 1,662.08 ha in the first year. Based on simulations and real change data, the logistic regression model for prediction of deforestation is Y1 = -1.0369 + 0.00146 * X1 - 0,000498 * X2 - 0,000237 * X3 + 0.04523 * X4 -0,0386X5 (ROC = 0 , 7408), while the amount of carbon to be protected by REDD projects is given a departure from the business-as-usual deforestation scenario up to 18,868 million tCO2e.

1. Introduction

Conversion of land cover from forest to other land is a contributor to total greenhouse gas (GHS) emissions, especially from the forestry sector. Emissions from factories and motorized vehicles have a greenhouse effect, however tropical deforestation is a major contributor to greenhouse gas emissions in developing countries. Incentive mechanisms, such as reducing emissions from deforestation and forest degradation (REDD+), are currently being considered as possible emissions reductions and off-set solutions [1].

Vegetation of tropical forests and undersea plants such as shrubs, bushes, grasslands and savannas also have a role in the process of global carbon sequestration and conservation and have great potential to reduce greenhouse gas emissions and global warming [2].

The United Nations in 2008 launched a REDD program (Reducing Emissions from Deforestation and Forest Degradation in Developing Countries) by setting up mechanisms for mitigating climate change by overriding forest carbon. REDD also shows the importance of secondary ecosystem services related to forest conservation, including protection of biodiversity and water quality [3].

Deforestation in Indonesia exceeds what happens in Brazil and is even in the highest category in the world, even though the forest area is smaller in the size of Brazil's forests [4]. Referring to [5] the annual average deforestation in Indonesia for the period 2000-2012 was 671,420 hectares, consisting of 525,516 ha of deforestation in mineral soils and 145,904 ha of deforestation on peatlands.

Further to Central Sulawesi Province with forests of around 4.258 million ha, it has a strategic role in implementing REDD +. Deforestation that occurred in this province in the period 2003-2009, reached 432.111.50 Ha (10.15%), so that changes in forest cover in 2009 reached 3.826 ha. Poso District, which is part of this Province, contributes 4.61% of total deforestation in Central Sulawesi Province. Forest cover in Poso Regency in 2003 was 561,811.86 ha or around 73.59% of the total area. Has decreased by 19,944.99 ha (3.55%) compared to 2015. The level of deforestation in the period 2003 - 2015 was around 1,662.08 ha of 1-year.

Poso regency consist Forest Reserve covering an area of 299,170 hectares, production forest area of 79,144 ha, limited production forest area of 271.747 ha, production forest area which can be converted forest area of 34 157 ha and Forest Nature Reserve as well as an area of 145 452 ha Forest Tourism. Forests are very spacious with a fortune in it, with proper management without damaging existing ecosystems is a major economic resource.

Referring to the forest and environmental conditions that have occurred in Poso, it is necessary to study and predict future deforestation and how carbon emissions will occur using the Redd++ scenarios model. This study will use land use / cover map data (2003, 2009 and 2015), as well as driving variables (distance from: forest edge, road, flow, and slope) as explanatory deforestation variables.

1.1. Objective
This study aims to calculate the rate of deforestation and simulation carbon emission in Poso District by using REDD+ model. The REDD project location for this study is the conservation forest area in Poso District.

1.2. Research area
Its geographical location is 1°06 '44,892 "- 2°12' 53,172" S and 120°05 '96 "- 120°52' 4.8" E

2. Materials and Methods

2.1. Tools and Data
The tool used in this study is ArcGIS 10.2 and Terrset software. Referring to [6], Terrset is an integrated geospatial software system designed to monitor and model the environment for sustainable development. The TerrSet system combines the IDRIS GIS Analysis and IDRISI Image processing tools along with a vertical application constellation.

Data used in this study: Indonesian topographic maps, Scale 1: 50,000, Geospatial Information Agency, Poso District land cover map, Scale 1: 250,000 (2000, 2009 and 2015), Directorate General of Forestry Planning - Ministry of Environment and Forestry.

Environmental variables (dependent variable): distance from the edge of the forest, distance from the road, distance from flow, altitude and slope, Indonesian Topographic Map, Scale 1: 50,000, Geospatial Information Agency. Methodology the Bio-Carbon Fund (BioCF) Project requires three basic spatial or geographical data inputs, project area, leakage area, and reference area.

2.2. Landuse analysis and prediction model
The 2003, 2009 and 2015 land use maps are the result of interpretation of Landsat images. covering five classes of land cover are: dry forest, wet forest, plantation, agriculture, non-forest, and water body. This analysis is done with a land change modifier module at TerrSet sotware. We can predict future land cover based on actual land cover and previ-sion, this module also considers several driving variables such as roads, rivers, settlements (distance), infrastructure, slopes, etc.

We were conducted the study in the area by cross tabulating the derived land cover map of 2003 as the land cover early input image and the 2015 land cover map as land cover the later input image. Refer [6] and [7], flowchart of the general procedure used in forest cover change modelling Figure 1.

Potential transition modelling was used to group land use transitions into a set of sub-models and then utilized to explore the potential power of the chosen explanatory variables. In the current study, the change analysis showed that there is only one set of transition, from forest to non-forest category.

The explanatory variables chosen for this study are distance from existing forest edge, distance from road, distance from streams, elevation and slope. In order to predict change, the transition was empirically modelled using multi-layer perception (MLP) neural network and logistic regression

Logistic regression model (LRM) was used to model and analyze the lancover change. The binary presence or absence is the dependent variable for the periods 2000–2009. The predicted landcover of 2015 was validated using ROC/AUC (Relative Operating Characteristic/Area Under Curve) module of IDRISI TerrSet.

The ROC module compares a suitability image by depicting the likelihood of that class occurrence (the input image) and a boolean image showing where that class actually exists (the reference image). Refer [6] and [9], the ROC module compares suitability image by depicting the likelihood of that class occurrence (the input image) and a boolean image showing where that class actually exists (the reference image).

The ROC curve is the true vs false positive fraction and the AUC is a measurement of overall performance. The REDD projects are modelled based on a 30 years projection with intermittent assessments every 5 years, that 6 prediction maps will be produced over the 30 years prediction between 2015 and 2045. The carbon reporting is done based on these intervals.

Reductions in GHG emissions are calculated by subtracting the estimated carbon that would be saved through REDD project intervention, along with the estimated carbon loss through leakage from the estimated carbon loss (in this case through land use and cover change) without the implementation of a REDD project intervention.

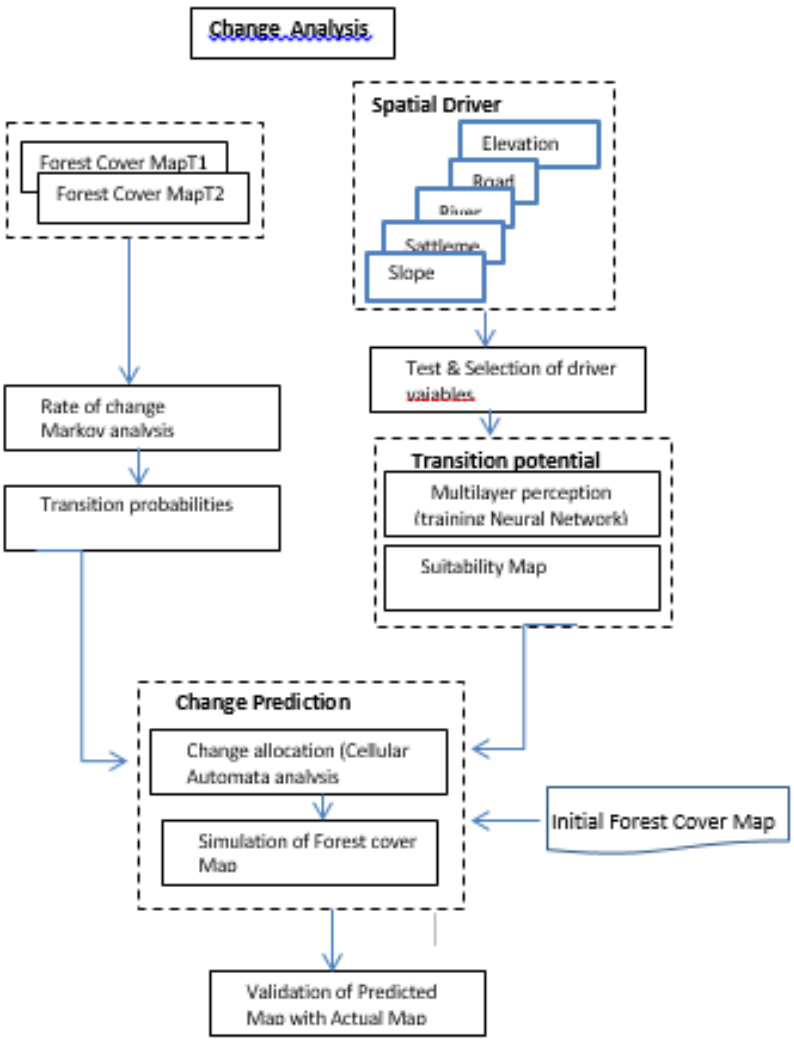

Figure 1. Flowchart of the general procedure used in forest cover change modelling.

The formula used in the calculation is: C-REDD = (C-Baseline) – (C-Actual) – (C-Leakage)

C-Baseline	=	Baseline greenhouse gas emissions within the project area; tCO2e
C-Actual	=	Actual greenhouse gas emissions within the project area; tCO2e
C-Leakage	=	Leakage greenhouse gas emissions; tCO2e
C-REDD	=	Net anthropogenic greenhouse gas emission reduction attributable to the REDD project activity; tCO2e

In this study, the conservation forest area is assumed to be a REDD project area, as wide as 298,052.73 ha.

3. Results and discussion

3.1. Landcover Change

Analysis of changes in the land cover of the Poso Regency area is based on multi-year data, namely from 2003 to 2015. Table 1, Table 2, and Figure 2 show land cover and changes from Poso Regency.

Table 1. Land cover changes of Poso Regency area in between year 2000 to year 2015.

No	Land Cover	Year 2000		Year 2009		Year 2015	
		Ha	%	Ha	%	Ha	%
1	Primary dryland forest (PF)	376,645.23	49.34	361,262.25	47.33	360,161.19	47.18
2	Secondary dryland forest (SF)	183,972.69	24.10	186,486.48	24.43	180,511.74	23.65
3	Primary mangrove forest(PMF)	219.15	0.03		-		-
4	Secondary mangrove forest (SMF)	974.79	0.13	1,193.94	0.16	1,193.94	0.16
5	Estate crop (EP)	2,072.52	0.27	2,072.52	0.27	2,072.52	0.27
6	Pure dry agriculture (AUA)	69,291.72	9.08	71,501.31	9.37	74,399.94	9.75
7	Mixed dry agriculture (MxUA)	36,487.26	4.78	35,778.78	4.69	39,840.03	5.22
9	Paddy Field (Rc)	6,879.87	0.90	6,879.87	0.90	6,879.87	0.90
10	Fish pond/aquaculture (Po)	252.45	0.03	252.45	0.03	252.45	0.03
11	Transmigration areas (Tr)	583.65	0.08	583.65	0.08	583.65	0.08
12	Settlement areas (Se)	3,067.20	0.40	3,067.20	0.40	3,067.20	0.40
13	Mining areas (Mn)	3,672.18	0.48	3,672.18	0.48	3,672.18	0.48
14	Bare ground (Br)	41,169.24	5.39	52,537.32	6.88	52,653.24	6.90
15	Open Swamp (WB)	38,045.16	4.98	38,045.16	4.98	38,045.16	4.98
		763,333.11	**100.00**	**763,333.11**	**100.00**	**763,333.11**	**100.00**

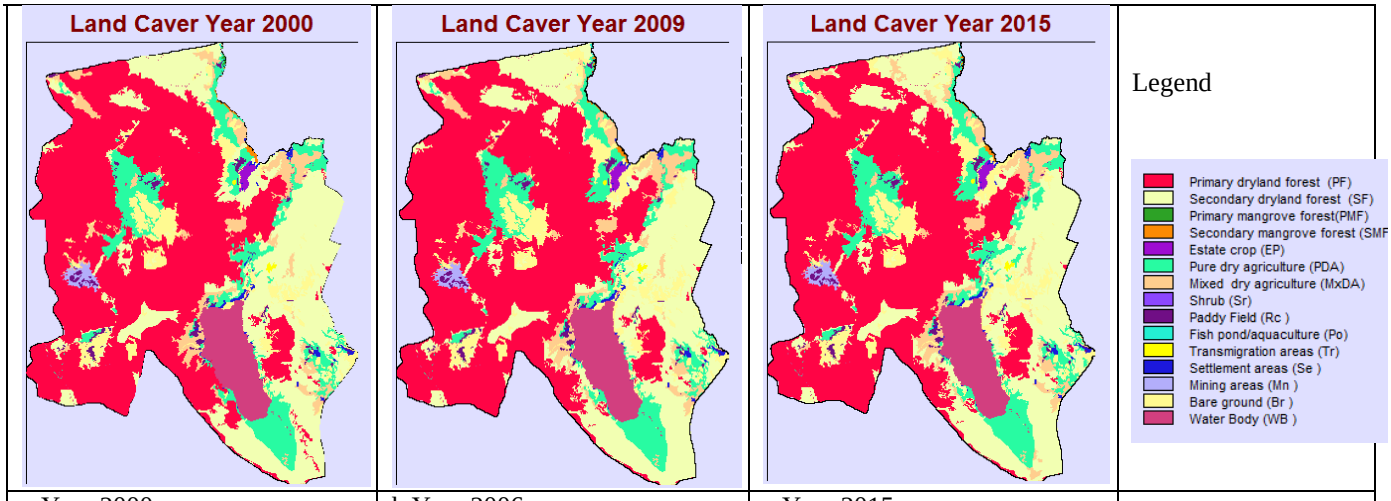

a.Year 2000 | b.Year 2006 | c.Year 2015

Figure 2. Poso District Landcover Map of years 2000, 2006 and 2015

The forest cover area in Poso district in 2015 was 612,472.50 ha or approximately 69.71% of the total area. It decreased by 62,017.74 ha (9.19%) compared to 2003. The rate of deforestation 5,168.14 ha year- 1. The rate of deforestation in this area is lower than deforestation in central sulawesi province. this condition is in accordance with Tumudi's research. Refer [8] Central Sulawesi province has forest area of 4.477 ha (year 2000) and 4.360 ha (year 2011). The rate of deforestation of Central Sulawesi Province in the period 2000-2011 amounted to 117,430 ha or 10.675 ha per year. The largest deforestation occurred in the Tojo Una-Una District up to 29,170 ha (25.01%) and the second, Poso with

17. 850 ha . This condition shows deforestation in Poso district contributes for about 15.20% of all deforestation in Central Sulawesi Province.
Dryland forest conditions in Poso District in 2003 covered 664,482.24 ha and reduced into 603,161.37 ha in 2015. The reduction of 61,320.87 ha or approximately 9.22 % over the 12 years. The average deforestation of dryland forest occurred in Poso was 0.76 % per year or about 5,110.07 ha per year. This reduction was caused by deforestation which has changed dryland forest into a non forest.

In 2003, wet forest area in Poso District was 10,007.73 ha and decreased to 9,311.13 ha in 2015. The reduction of wet forest area was 696.60 ha, or approximately 6.96 % over the 12 years. The average decrease of wet forest was 0.58 % per year, or about 58.05 ha per year. This reduction of wet forest was caused by the deforestation, which has changed the wet forest into non forest. Mostly occur in mangrove forests, converted into ponds.

Table 2. Changes of balancing forest and non forest at Poso Regency in between years 2003 - 2015.

No		2003 – 2009		2009 – 2015		2003 – 2015	
	Land Cover	Hectare	Percent	Hectare	Percent	Hectare	Percent
1	Forest	(12,869.19)	(2.29)	(7,075.80)	(1.29)	(19,944.99)	(3.55)
2	Non Forest	12,869.19	7.87	7,075.80	4.01	19,944.99	12.20
3	Water bodies	0.00	0.00	0.00	0.00	0.00	0.00

Source : Result of Analysis of Landcover Map from 2003 to 2015

Over 62,017.47 ha were lost between 2003 and 2015 inside the study area (25,590.16 ha between 2003-2009 and (36,437.31 ha between 2009-2015). This roughly corresponds to 9.19% of the forest area that existed in the year 2003 (674,489.97 ha). Annual deforestation occurred at the rate of 0.76 % between 2003-2015. Between 2003 and 2009 the deforestation gross rate was 0.63%, whereas between 2009-2015 reaching 0.93.

Over the 12 years (2003-2015) the increase of non-forest area was 65,984.67 ha or 33.69 % The cause of deforestation is mining activity. . Starting in 2009, there is a significant addition of mining company area. Up to 2016, in Poso district there are as many as 51 nickel mining companies, 29 of the company has production license and just 22 company has exploration license. Mining activities with open pit systems making forest cover changes into non-forest areas. Besides that also in Poso district there are about 30 plantation companies. Plantation activity also causes the change of forest to non-forest (plantation) cover compared to the condition of the land cover in 2003. The rate of change was 5,498.72 ha per year or the reduction was 2.81% per year compared to non-forest areas condition in 2003. The increase of non-forest areas was caused by the activity of forest land conversion into non-forest areas (other uses).

Meanwhile, there were no change on the water bodies. The water bodies category recorded neither increase nor decrease. Refer [10] conveys that no changes in the body of water in certain period of time indicate that the changes of land cover are mostly oriented on agriculture and new settlements.
Meanwhile [11] declare that the changes of forest cover were caused by the deforestation, either planned or not. Planned deforestation is usually in the form of changes planned by the government for the benefit of forest land for plantations, agricultural or residential development, which is carried out lawfully in accordance with the legislation. Unplanned deforestation is a deforestation through illegal activities. The forest degradation can be caused by illegal or unauthorized activities, such as harvesting and illegal logging.

3.2 Greenhouse Gas Emission
Based on the results of the land use c not equal change analysis for the period between 2003 and 2009, the evaluation of the 4 explanatory variables in the transition potential sub-model and the transition

potential surface that was subsequently created, the model was calibrated and employed to predict and simulate deforestation an 6-year period from 2009 until the year 2015. The model for predicting the forest cover change,

Y1 = -1.0369 + 0.00146 * X1 - 0.000498* X2 - 0.000237* X3 + 0.04523* X4 -0.0386X5

where :

x1 = distance from edge forest
x2 = distance from roads
x3 = distance from streams
x4 = elevation
x5 = slope

Table 3 . Calculation of ROC and AUC by model logistic regrestion base on forest changes in between 2000 years and 20015.

Statistic of logistic regression	Based on forest changes 2000- 2015
Number of total observations	6,802,813
-2logL0	370,966.1634
-2log(likelihood)	396.5673
Goodness of fit	456,068.7266
Pseudo R2	0.9989
Chi-square (df=5)	370,569.5961
ROC	0.7408
AUC	0.7782

The validation of the model was undertaken by computing the ROC statistic using a map of actual change between 2003 and 2009 as the reference image and the simulated land cover map of 2015 as the input image. The ROC statistic was obtained at 0.7408, a reasonably strong value that is good enough to make the results of the simulation acceptable. Pseudo R2 value greater (0.5946 and 0.3750) than 0.2 indicates that the model is a relatively good fit for the data. The simulated map is shown in figure 4. The result of that simulation shows that the forest category further decreased from 674,489.97 ha (77.11 %) to 612,472.50 Ha (69.71) invariably reducing the size of the non forest category by the same measure. The rate of deforestation 5,168.12 ha year-1 . This is the future business as usual scenario (figure 3). Deforestation has been observed mainly along the main road, in mining areas and close to previously deforested areas. The result of that simulation shows that the forest category further decreased from 674,489.97 ha (77.11 %) to 612,472.50 Ha (69.71) invariably reducing the size of the non forest category by the same measure.

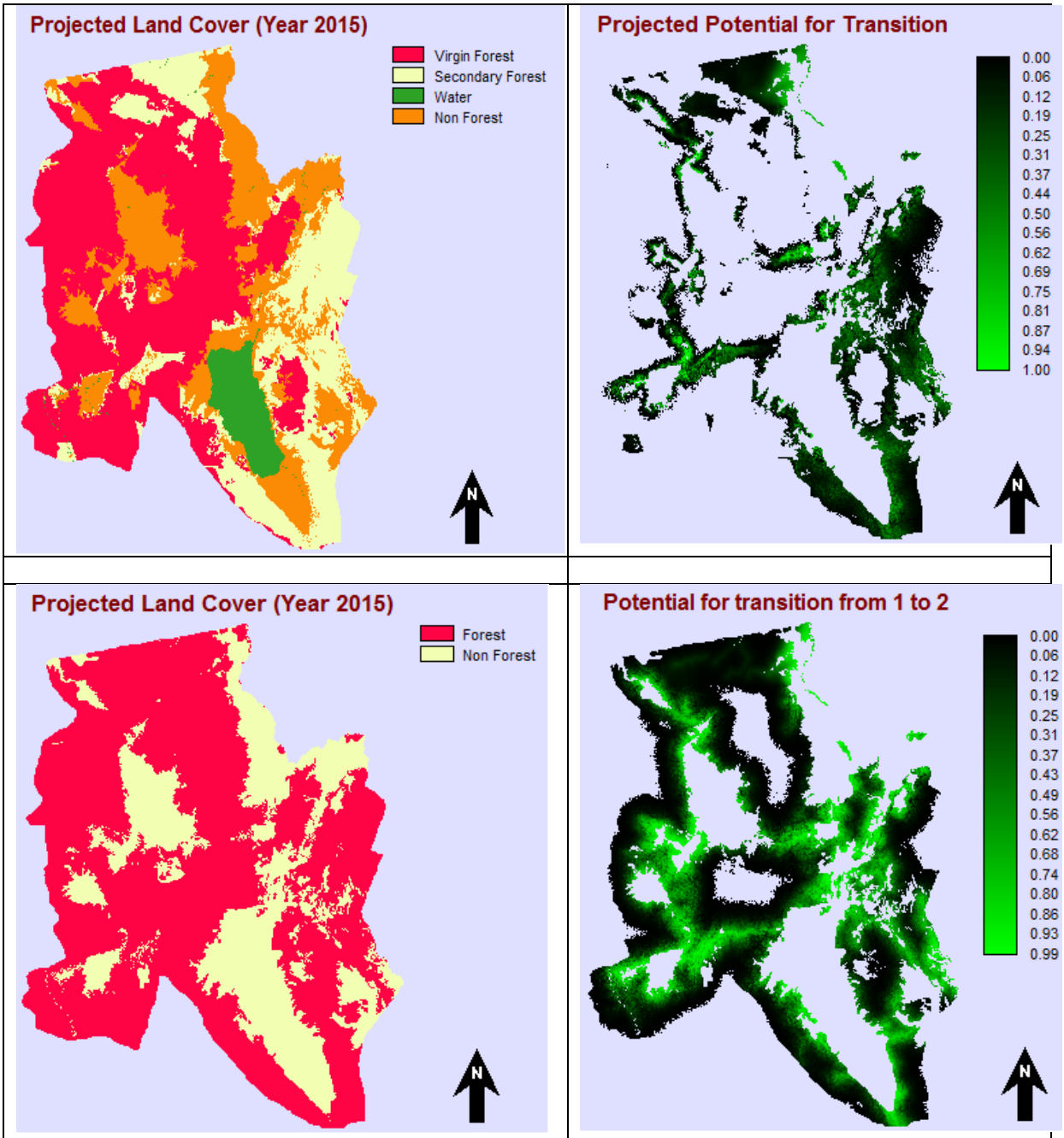

Figure 3: Simulated map and Transition potential Deforested of 2015

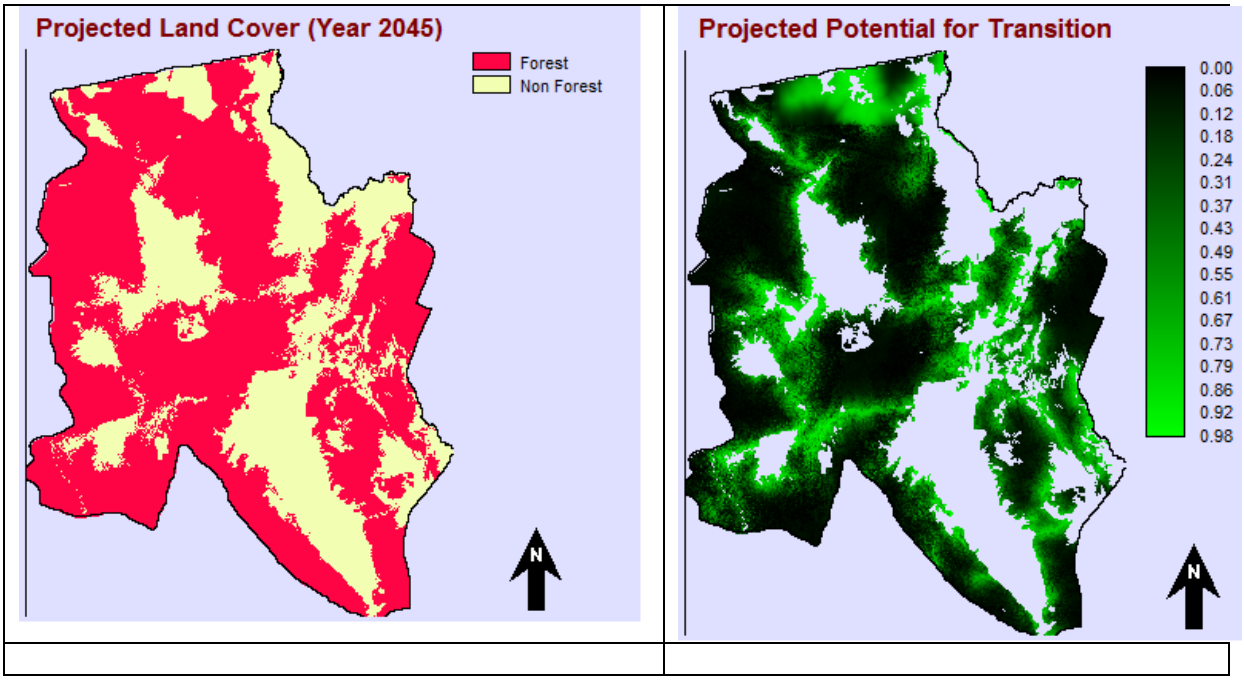

Figure 4. Future BAU and Suitable Deforestation

The result of REDD modeling that the scenario of future sustainable development with the protection of conservation forest area in Poso District as wide as 205,151.49 ha . For the next 30 years, the cumulative carbon is 18,868,706.00 tCO2e will be saved or prevented from being released into the atmosphere as the consequences of reduction conversion of forest cover categories to Non-Forest categories until 2045. While continuting usual business scenarios without REDD project intervention, only 26,533,552,00 tCO2e will be saved by 2045. Detail of deforestation and carbon emissions estimates base on time series presented in Table 4 and Figure 5.

Table 4. Comparison of Carbon emissions by Actual project and Redd model project base on years 2016 until 2045

Project Years	Year	Carbon Baseline	Carbon Actual	Carbon Leakage	Carbon REDD
1	2016	-0.20	-0.07	-0.04	-0.09
6	2021	-0.25	-0.38	-0.24	-0.60
11	2026	-0.25	-0.63	-0.47	-1.36
16	2031	-0.26	-0.85	-0.59	-2.26
21	2036	-0.27	-0.98	-0.72	-3.30
26	2041	-0.28	-1.12	-0.86	-4.39
30	2045	-0.28	-1.23	-0.97	-5.29

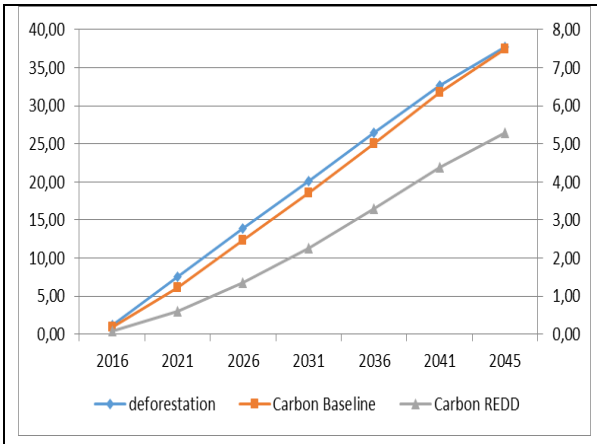

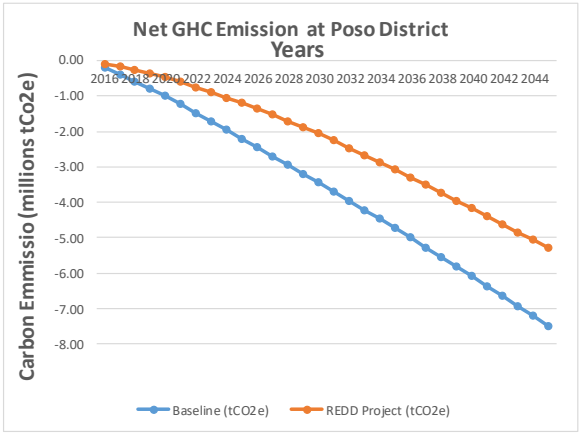

a. Deforestation and Carbon Emission | b. Net GHC Emission

Figure 5. Deforestation and Net Emisision at REDD Project, Poso Utara District

4. Conclusion

Results show that the deforestation on the period 2003-2015 reached 62,017.47 (9,19 %) or the rate of deforestation 1,662.08 ha of 1-year . The logistic regression model for prediction of deforestation is Y1 = -2.2649 + 0.001126X1 - 0.000152 X2 - 0.000225 X3 + 0.010704 X4 (ROC = 0,7408), while the amount of carbon that the REDD project will protect from the business as usual deforestation scenario up to 18.868 million tCO2e.

5. Acknowledgements

This paper is the development of the activities of " Data and Spatial Information Colllection for Natural Resources of Central Sulawesi Province", which is the cooperation of Development Planning Board of Central Sulawesi Province with Geospatial Information Agency. We are grateful to Head of Centers for Research, Promotion and Cooperation, Geospasial Information Agency (BIG) for the data and laboratory facilities, and to Head of the Regional Development Planning Board of Central Sulawesi Province, which has financed part of its funding activities

6. References

[1] Sangermano, F., Toledano, J., & Eastman, J. R. (2012). Land covers change in the Bolivian Amazon and its implications for REDD+ and endemic biodiversity. Landscape Ecology, 27(4), 571-584. DOI 10.1007/s10980-012-9710-y

[2] Bununu, Y. A., Ludin, A. N. M., & Hosni, N. Modelling Vegetation Loss And Greenhouse Gas Emissions In Kaduna, Nigeria. 10th SEATUC Symposium, 22nd – 24th February 2016, Shibaura Institute of Technology, Tokyo, Japan Gibson L, Lynam AJ, Bradshaw CJ, He F, Bickford DP, Woodruff DS, Bumrungsri S, Laurance WF. Near-complete extinction of native small mammal fauna 25 years after forest fragmentation. Science. 2013 Sep 27;341(6153):1508-10.

[3] Margono. B. A. et al. 2014. Primary forest covers loss in Indonesia over 2000- 2012.Nature Climate Change. Volume 4. pp. 730-735

[4] Government of Indonesia. 2014. National Forest Reference Emission Le,el for Deforestation and Forest Degradation in the Context of the Acti,ities Referred to Decision 1/CP.16. Paragraph 70 (REDD+) Under the UNFCCC. (Encourages developing country Parties to contribute to mitigation actions in the forest sector), Directorate General of Climate Change. The Ministry of Environment and Forestry. Indonesia

[5] Sumargo, W., Naggara, S. G., Nainggolan, F. A., & Apriani, I. (2011). Potret Keadaan Hutan Indonesia Periode Tahun 2000-2009 Edisi I. Forest Watch Indonesia Nomor ISBN, 978-979.
[6] Suryadi I, Rauf A, Maulida M. 2012. Provisional Reference Emission Level Provinsi Sulawesi Tengah. Tecnical Report. UN-REDD Indonesia Program
[7] Turmudi and Nahib, I. 2015. Potret Hutan Sulawesi Tengah Berdasarkan Data Geospasial. Buku Mosaik Informasi Geospasial Wilayah Sulawesi Tengah. IPB Press.
[8] Kumar, R., Nandy, S., Agarwal, R., & Kushwaha, S. P. S. (2014). Forest cover dynamics analysis and prediction modeling using logistic regression model. Ecological Indicators, 45, 444-455.
[9] Nahib, I., & Widjojo, S. (2016). The Impact of Landcover Changes on Carbon Stock: A Study Case In Central Kalimantan Forest. 36th Asian Conference on Remote Sensing 2015 (ACRS 2015) Quezon City, Metro Manila Philippines 19-23 October 2015 Volume 1 of 6. ISBN: 978-1-5108-1721-0.
[10] Chust, G., D. Ducrot, and J.L.I. Pretus. (2004). Land Cover Mapping with Patch-Derived Landscape Indices. Landscape and Urban Planning 67: 45-53. www.elsevier.com/locate/landurbplan
[11] S. M. Metev and V. P. Veiko, Laser Assisted Microtechnology, 2nd ed., R. M. Osgood, Jr., Ed. Berlin, Germany: Springer-Verlag, 1998.

Object detection of aerial image using mask-region convolutional neural network (mask-R CNN)

Musyarofah
Remote Sensing Technology and Data Center, National Institute of Aeronautics and Space (LAPAN),
70 LAPAN Street, Pekayon, Pasar Rebo, 13710 Jakarta Timur, Indonesia

musyarofah@lapan.go.id

Abstract. The most fundamental task in remote sensing data processing and analysis is object detection. It plays an important role in classification and very useful for various applications such as forestry, urban planning, agriculture, land use and land cover mapping, etc. However, it has many challenges to find an appropriate method due to many variations in the appearance of the object in image. The object may have occlusion, illumination, viewpoint variation, shadow, etc. Many object detection method has been researched and developed. Recently, the development of various machine learning-based methods for object detection has been increasing. Among of them are methods based on artificial neural network, deep learning and its derivatives. In this research, object detection method of aerial image by using mask-region convolutional neural network (mask-R CNN) is developed. The result shows that this method gives a significant accuracy by increasing the image training and epoch time.

1. Introduction

The use of remote sensing images has been increasing in recent years due to the advanced development of remote sensing technology that offers a better quality and higher resolution of image. The amount of availability of image data is going up, as well. Many various applications such as forestry, urban planning, agriculture, land use and land cover mapping, etc. can be applied by using remote sensing image. Therefore, the demand of remote sensing image data is also growing lately. In order to obtain a good result and get benefit from remote sensing image data, the data should be processed and analyzed carefully.

The most fundamental task in remote sensing data processing and analysis is object detection. It plays an important role in classification. The result and accuracy of object detection can influence the accuracy of image classification and gives a significant effect in image analysis. However, object detection is challenging because the object may has many variation of appearance in image caused by scale variation, occlusion, illumination condition, viewpoint variation, deformation, shadow, background clutter, etc [1].

In the last decades, many study and research have been conducted to find and develop an appropriate method to obtain higher accuracy and better result in object detection. Generally, there are four main categories in object detection method include template matching-based object detection methods, knowledge-based object detection methods, object-based image analysis (OBIA)-based object methods, and machine learning-based object detection [2]. Nowadays, the development of various machine learning-based methods for object detection is growing. The techniques using machine learning are more advanced and powerful. Therefore, the technique becomes popular and widely used in many applications including some applications that use remote sensing image and analysis. Among of them are methods based on artificial neural network, deep learning and its derivatives.
In remote sensing community, artificial neural network or neural networks, which is the basis of deep learning (DL) algorithm, was popular in 1980s and have been used for many years. And then it changed, another machine learning based methods like support vector machine (SVM), random forest (RF), etc. replaced neural networks in classification and change detection task. SVM has an ability to handle high

dimensionality data and perform well with limited training samples [3], while RF is easy to use and can obtain high accuracy [4]. However, since 2014, DL as the derivative of neural networks has returned the interest of the remote sensing community to neural networks. In image analysis tasks including object detection, land use and land cover (LULC) classification, etc., DL algorithms give significant achievements [5,6,7,8,9,10].

In this research, object detection method of aerial image by using mask-region convolutional neural network (mask-R CNN) is studied, developed and implemented.

2. Neural Networks

Neural networks are one type of machine learning model. Fundamentally, machine learning is using algorithms to extract information from raw data and represent it in some type of model [11] that can be used to infer things about other data. Neural networks or artificial neural networks (ANN) are a computational model used in machine learning both for classification or regression and are inspired by the function of the human brain. ANNs are composed by several layers of nodes that are connected by links with a weight attached to them. In the fully connected version of ANNs, every node is connected to all nodes in the layers behind and in front of it and to no node in its own layer, meaning nodes in one layer are completely independent of each other. It's a supervised learning algorithm where first the data is forward propagated in the network the error is being calculated and then back-propagated through the network while adjusting the weights [12].

3. Deep Learning (DL)

One definition says that deep learning is a neural network with more than two layers. The problematic aspect to this definition is that it sounds and makes deep learning created since the 1980s. After the arrival of deep learning, neural networks had many changes architecturally in network styles. It is also caused by the development of processing power that more powerful recently. Therefore, DL shows a spectacular result that transcends the earlier generation of neural networks. The evolution of neural networks includes the following facets [11]:

- More neurons than previous networks
- More complex ways of connecting layers/neurons in neural networks
- Explosion in the amount of computing power available to train
- Automatic feature extraction

By the evolution of neural networks, deep learning can be defined as neural networks with a large number of parameters and layers. There are four fundamental network architectures in DL:

- Unsupervised pre-trained networks
- Convolutional neural networks (CNN)
- Recurrent neural networks (RNN)
- Recursive neural networks

One of the great advantages of DL compared to another traditional machine learning algorithms is automatic feature extraction. By feature extraction, the networks process of deciding which characteristics of a dataset can be used as indicator to label that data reliably [11]. DL had reduced human effort in feature extraction which is an input of classification. Therefore, the accuracy gained by DL is higher than another conventional machine learning algorithms for almost every data type with minimal tuning and human role.

4. Convolutional Neural Networks (CNN)

Convolutional neural networks (CNN) are one of fundamental network architectures of deep learning. CNNs are a specialized kind of neural network for processing data that has a known, grid-like topology [13]. The network uses a mathematical operation, convolution, which the name of CNN comes from.

Therefore, CNNs can be defined as neural networks that employ convolution in place of general matrix multiplication in at least one of their layers. A convolution is a powerful concept for helping to build a more robust feature space based on a signal. So, by using convolution, CNNs obtain the goal to learn higher-order features in the data.

Since CNNs perform well in learning feature of the data, then CNNs are suitable for object recognition, object detection, and classification. In fact, the successful of CNNs in image recognition makes the power of deep learning is recognized. CNNs can identify faces, individuals, street signs, platypuses, and many other aspects of visual data and CNNs are good at building position and rotation invariant features from raw image data, as well [11]. CNNs are very advantageous for the input that has structure, repeating patterns and spatially distributed value like images and audio data. Besides that, CNNs also have been used in natural language translation and sentiment analysis.

CNNs transform the input data from the input layer through all connected layers into a set of class scores given by the output layer [11]. There are many variations of the CNN architecture, but they are based on the pattern of layers, as demonstrated in the following figure.

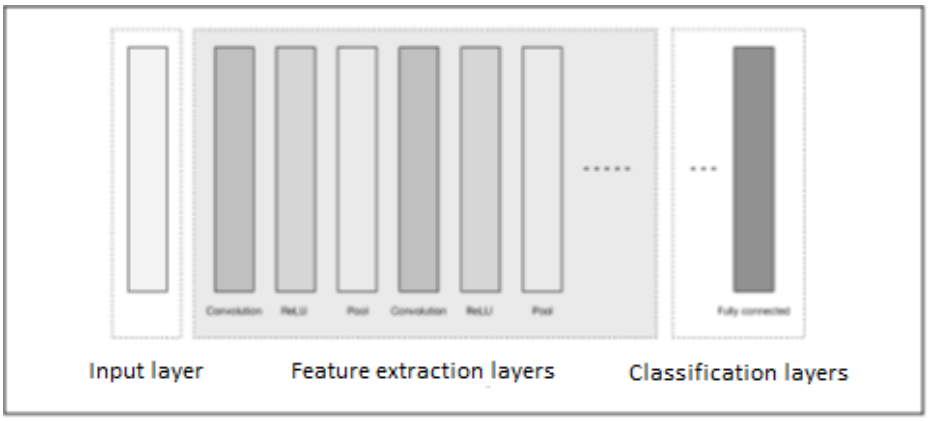

Figure. High-level general CNN architecture

The figure depicts three major groups:

1. Input layer
2. Feature-extraction (learning) layers
3. Classification layers

3.1. Convolution

A convolution is defined as a mathematical operation describing a rule for how to merge two sets of information. It is important in both physics and mathematics, defines a bridge between the space (time) domain and the frequency domain through the use of Fourier transforms. It takes input, applies a convolution kernel, and gives us a feature map as output. The convolution operation is known as the feature detector of a CNN. The input to a convolution can be raw data or a feature map output from another convolution. It is often interpreted as a filter in which the kernel filters input data for certain kinds of information.

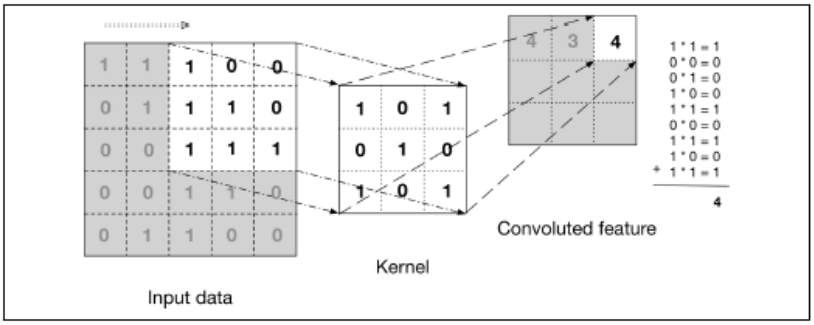

Figure. The convolution operation

5. Mask Region Convolutional Neural Networks (Mask R-CNN)

Mask region convolutional neural networks (Mask R-CNN) is a general framework that conceptually simple and flexible for object detection and object instance segmentation. Mask R-CNN efficiently detects objects in an image while simultaneously generating a high-quality segmentation mask for each instance [15]. The method of Mask R-CNN is an extension of earlier method, Faster Region Convolutional Neural Network (Faster R-CNN). In Mask R-CNN, a third branch is added for predicting segmentation masks on each Region of Interest (RoI), in parallel with the two existing branches for classification and bounding box regression. The mask branch which is the third branch, is a small fully convolutional network (FCN) applied to each RoI, predicting a segmentation mask in a pixel-to-pixel manner. Mask R-CNN is simple to train and adds only a small overhead to Faster R-CNN [15].

6. Methodology

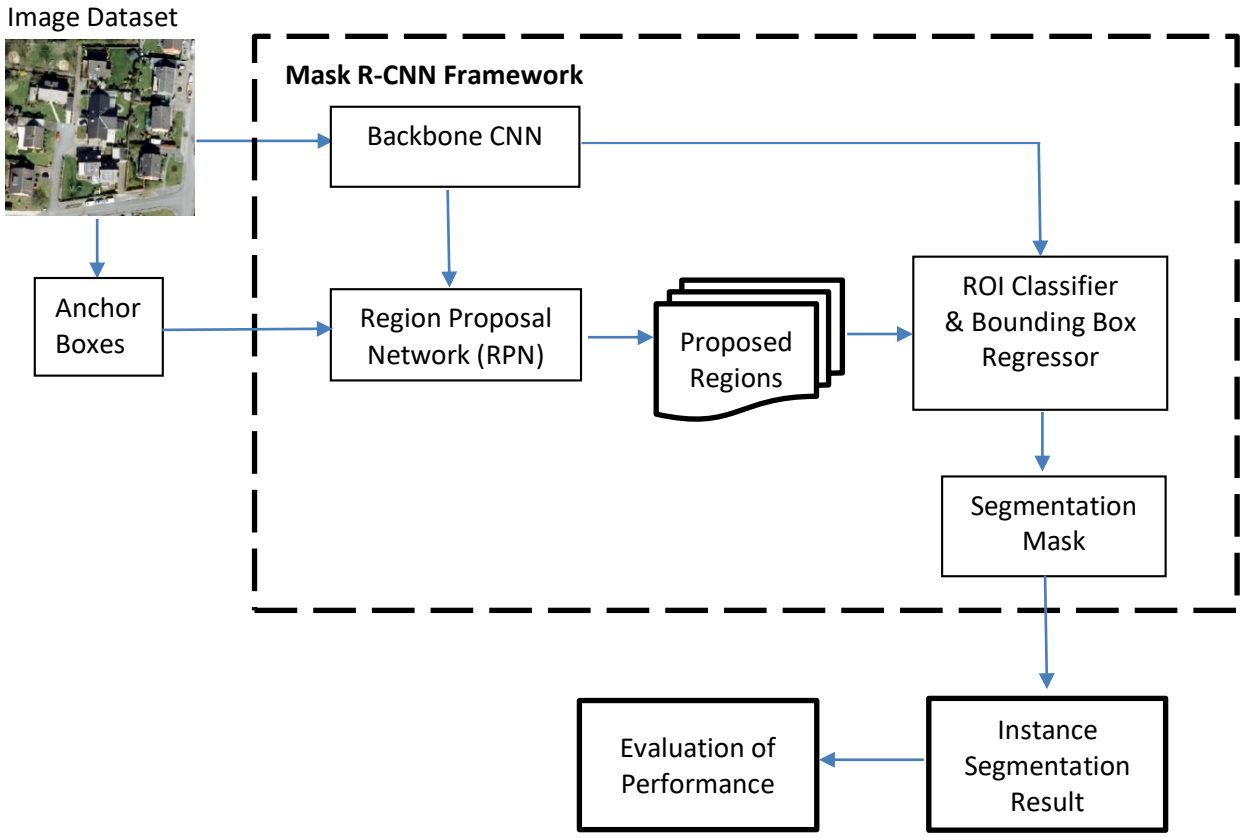

Mask R-CNN adopts the method from Faster R-CNN, which consists of two stages. The first stage, called a Region Proposal Network (RPN), proposes candidate object bounding boxes. The second stage is extracting features using RoIPool from each candidate box and performs classification and bounding

box regression. Mask R-CNN is a two stage framework. The first stage scans the image and generates proposals (areas likely to contain an object). And the second stage classifies the proposals and generates bounding boxes and masks.

Backbone CNN

Backbone is a standard convolutional neural network that serves as a feature extractor. The early layers detect low level features (edges and corners), and later layers successively detect higher level features (object like car, person, sky, etc.).

Region Proposal Network (RPN)

The RPN is a light-weight neural network that scans the image in a sliding-window fashion and find areas that contain objects.

Proposal ROI

Anchor boxes

Anchors are the regions that the RPN scans over, which are boxes which are distributed over the image area.

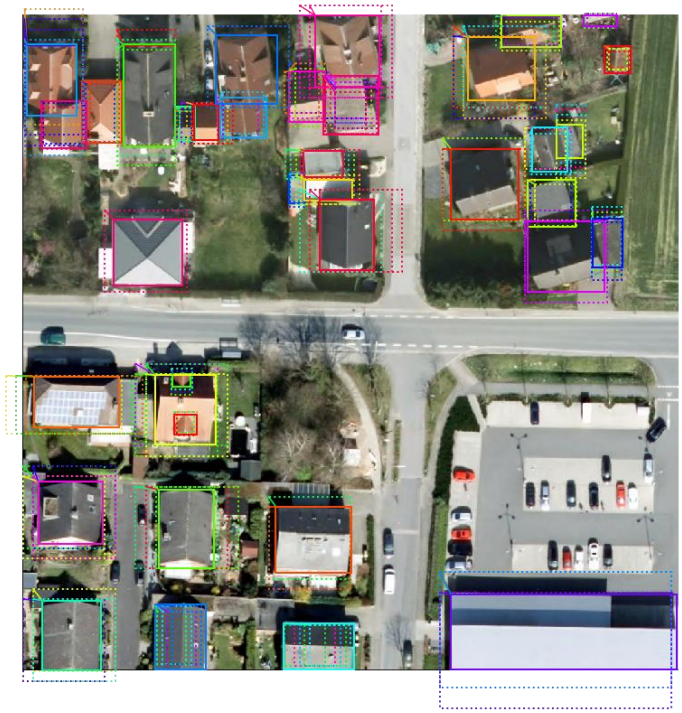

Positive anchor

Negative Anchor

Neutral Anchor

7. Results and Discussion

Temporary Result

Application of Dem TerraSAR-X to prospecting geothermal: Rajabasa Volcanic Complexs, Sumatra, Indonesia

Agustin, F.[1*], Sanjaya,I.[1], Hernawan, U.[1],Sidarto[1]

[1]Centre for Geological Survey, Indonesia Geological Agency, Jl.Diponegoro no.57 Bandung Indonesia 40122

e-mail: fitriani.agustin@esdm.go.id

Abstract. TerraSar-X radar produces ORRI (Ortho Rectified Radar Images) and DEM (Digital Elevation Model) images. The 9 meter DEM resolution is powerful tool for detailed geological mapping through topographic features interpretation. Based on the geological interpretation of the DEM image, the Rajabasa Volcanic Complex (RVC) consists of several (number) volcanic units. The oldest unit is an ancient Rajabasa Volcano (Late Miocene), underlain by Tarahan Tuff (Early Oligocene) that was intruded by Canti Dacite. In the western part of the Ancient Rajabasa Caldera, the Cukur Volcano splitted the Ancient Rajabasa Volcano; and around the Cukur caldera is found some volcanos, including Kelawi, Mengkudu, Tangkil volcanoes, Kepayang Basalt and Sumbersari Rhyollite; while in the eastern part there are Pandan, and Rajabasa Volcanoes. Geothermal system is natural heat transfer from rain waters that sink in the rocks and change to the steam by heat of magma. The steam is trapped in a reservoir (porous rocks), covered by seals or cap rocks (low permeability rocks). In Indonesia, geothermal is generally associated with volcanoes, forms in large rock formation traps which usually connected to the caldera system. The RajabasaVolcanic Complex (RCV) has a long series of volcanoes, from the Late Miocene to the Resen, the size of the oldest volcanic caldera is quite large, and four hot springs were found as geothermal surface manifestations. The RVC, therefore, expected to have large traps of heat flow for further geothermal exploitation.

1. Introduction

Geothermal generally relates to volcanoes, while the Indonesia is geologically located between threeactive plates in the world, namely the Eurasian Continent, the Indian-Australian and the Pacific Ocean Plates. Based on the position there are many volcanoes in this region that is rich in geothermal energy. However, the Indonesia which has abundant geothermal reserves (40% of the world's geothermal reserves) has not been maximally utilized. There are several obstacles to geothermal exploration in Indonesia, including the poor state of infrastructure in remote areas, local community resistance to this project, and the volcanic area is usually a natural reserve and covered by protected forest. Remote sensing technology is very useful for exploration. Whereas the geothermal power plants are non-polluting, noiseless and electricity produces around 90%, compared to 65-75% of fossil fuel power plants.

Rajabasa volcano is one of the volcanoes that is geographically located at the southeastern tip of Sumatra island and has a long live. This volcano is active since the Upper Miocene when Java and Sumatra were separated or the Sunda Strait opened [1]. Bronto et al. [2] stated that the diameter of ancient Rajabasa Caldera was 11 km, and Darmawan et al. [3] has discussed geology and geothermal systems in Rajabasa Volcano using field data, water geochemistry and magnetic data. This paper will discuss the geothermal potential in the Rajabasa volcano with the volcanostratigraphic approach, interpreted on the DEM (Digital Elevation Model) Terra-Sar-X image. According to Bronto et.al [4], the volcanostratigraphic classification is the systematic grouping of volcanic rock/deposit. Ranks of the volcanostratigraphic formal units, from high to low, are respectively Arc, Super Brigrade, Brigade, Crown, and Hummock. This technique is powerful for geothermal exploration. The Rajabasa Volcano is administratively situated in South Lampung Regency, and located in the southeastern tip of Sumatra Island, and on the edge of the Sunda Strait (Figure 1).

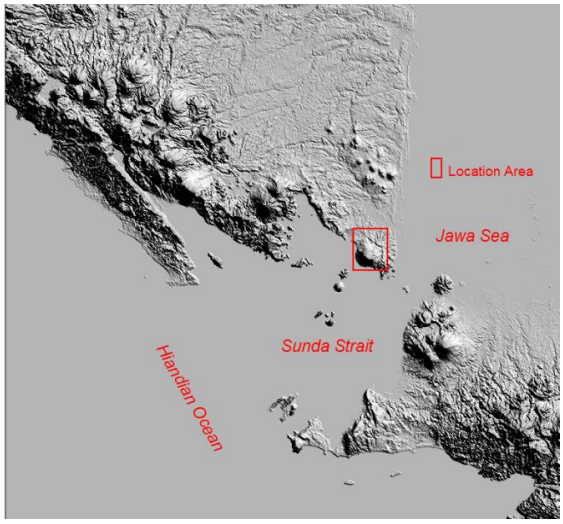

Figure 1. Location map of Rajabasa Volcano (red box)

2. Methodology

The TerraSar-X radar imageries owned by the Remote Sensing Laboratory, the Geological Survey Center, Geological Agency, Ministry of Energy and Mineral Resources, consists of a DEM (Digital Elevation Model) image that has a resolution of 9 meters, and an ORI (Orthorectified Image) with a resolution of 3 meters. The two imageries are utilized, however, only the DEM image showing the elevation of the earth's surface (Figure 2). This image is significant to geological interpretation, due to the fact that the image express thesurface topographic exposures. Before interpretation, some image processing is done in order the appearance of the image is clearer than before. Geological interpretation based on morphological appearances and drainage patterns, and it was carried out manually on a computer screen. For the validation of the interpretation results the field checks accompanied by rock sampling and photo capture of rock outcrops was done. The resulting map is a geological volcano map, arranged volcanostratigraphically. Based on the geological conditions and surface manifestations, the geothermal systems were analyzed.

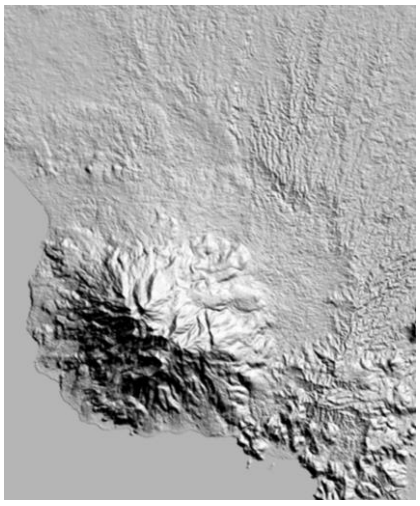

Figure 2. DEM TerraSar-X of Rajabasa Volcanoes Complex

3. Regional geology

Rajabasa Volcano is part of the Sumatra Island. The island of Sumatra is the southwestern edge of the Eurasian Continent Plate. The oceanic crust underlaying the Indian Ocean is part of the Indo-Australian Ocean Plate, and tilted northward northeast along the Sunda Trench [5]. This subduction causes the Sumatra island to be divided into 4 tectonic zones, namely the accretion prism, the forearc basin, the BarisanVolcanoArc, and the back arc basin (Figure 3). Rajabasa volcano is tectonically situated in the BarisanVolcanicArc, physiographically parts of the Lampung Heights, and based on 1: 250,000 scale of systematic geological mapping is located in the Geological map of Tanjungkarang Quadrangle.

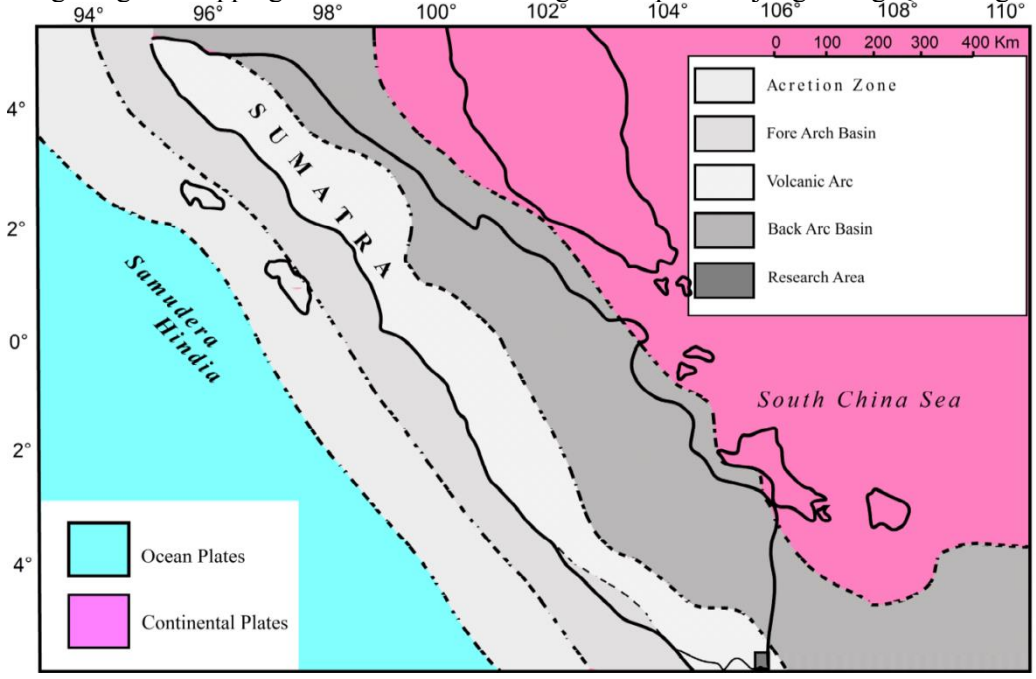

Figure 3. Kenozoic tectonic map of Sumatra [6]

According to Gafoer [7], the oldest rocks in the Lampung Heights are the Permo-Carbon Gunungkasih Complex consisting of metamorphic rocks (schist, gneiss, marble and quarzite).Unconformably overlaying the rocks is the Menanga Formation which is composed of Early Cretaceous marine sedimentary and a few volcanic rock [8], and followed by magmatism producing Middle Cretaceous - Late Cretaceous granitoid. The rocks are unconformably overlain by the Tarahan, Campang and Sabu Formations, each of which is locally distributed. The Hulusimpang Formation consisting of Oligo-Miocene volcanic rocks unconformably overlay the formations. In the Middle Miocene is followed by granite and andesite intruded the existing rocks. Mio-Pliocene the Contour and SurungBatangFormation filled local basins, and unconformably overlay the older rocks. Then, it followed the formation of lava (Tpv) and deposition of the Kasai Formation and the Tuf Lampung. Since Plio-Pleistocene, volcanic activity increased. Based on the Geological Map of Tanjungkarang Quardangle [8], the rocks exposed in the area are Pliocene andesite unit consisting of andesites, showing sheeting joints; Plio-Pleistocene Lampung Formation is composed of rhyolite-dacite tuffs and tuff volcanic clastics; the Holocene Rajabasa Young Volcanic rocks consist of andesitic lava – basalt lavas, breccias, and tuffs; the youngest rock unit is alluvium.

4. Geology of the area

4.1.1. Stratigraphy

The exposed rocks consist of volcanic sediments, intrusive rocks, volcanic rocks and rumble rocks. The volcanic sedimentary and intrusion rocks are described in lithostratigraphic, whereas stratigraphy of the volcanic rocks sequentially arranged in volcanostratigraphy, in accordance with the Indonesian

Stratigraphic Code [9]. The distribution of rocks and their sequence is shown in Figure 4, while the correlation of each unit is illustrated in Figure 5.

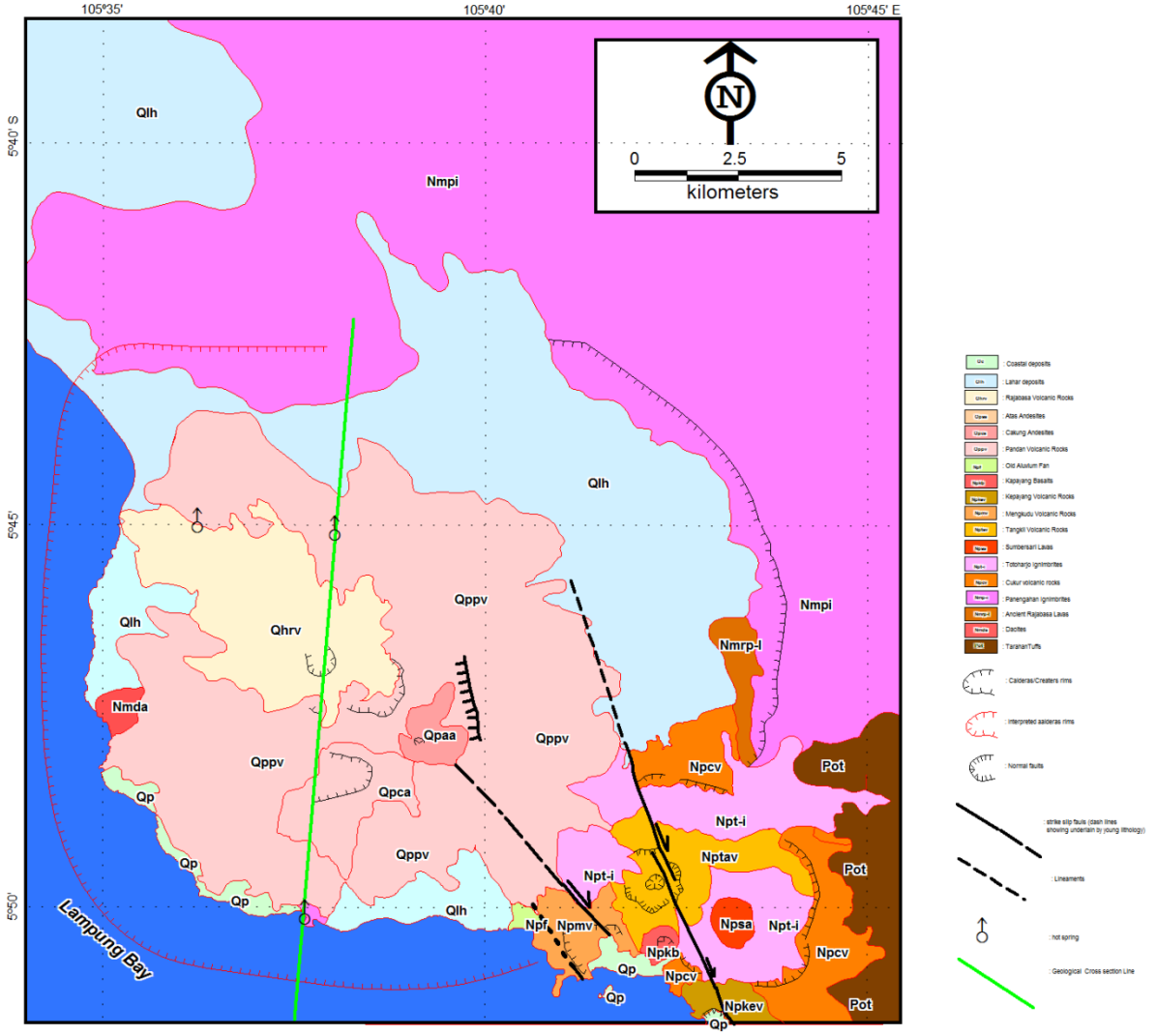

Figure 4. Geological Map of Rajabasa Volcano Complex interpreted on DEM.

Tarahan tuff is the oldest exposed rock on this area, whose distribution in the eastern part. The constituent rocks consist of alternating fine tuff and medium tuff, good sorting with parallel laminations. Sidarto et al [10] analyzed the fission track which showed the result of 31.5 ± 7.5 million years, or Rupelian equivalent (Early Oligocene). Based on the similarity of rocks and the age, the tuff can be correlated with the Tarahan Formation [8]. The TarahanTuff was intruded by Middle Miocene Dacite. These rock units were unconformably overlain by ancient Rajabasa volcanic rocks concisting of andesite lavas (contructiveperiode), and Panengahan Ignimbrites (distructiveperiode) comprises of various material breccias, lapili pumice, and rhyolite tuffs. The age of Panengahan Ignimbrite is 8,8 ± 2,3 million years or Tontonian equivalent (Upper Miocene) [10].

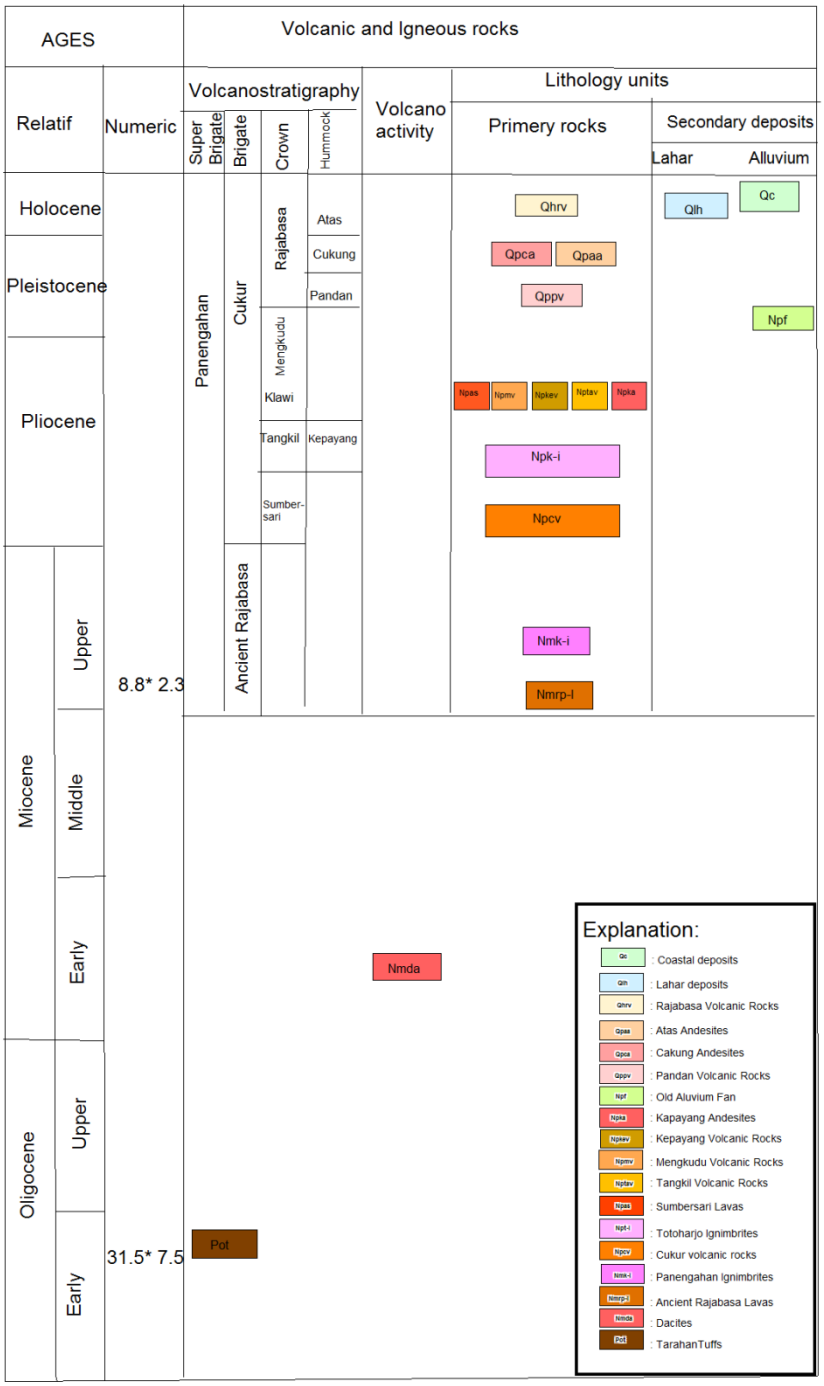

Figure 5. Correlation of each lithology units in Figure 4.

Based on the shape and size of caldera (Figure 6), the body of the Ancient Rajabasa Volcano is very large, which is classified as a brigade.The ancient Rajabasa volcanic rocks are overlaid by the Cukur, Pandan and RecentRajabasaVolcano, meanwhile the ancient Rajabasa volcanic rocks was underlain by Early Oligocene TarahanTuff, intruded by the Middle Miocene Dacite. In the southeastern part of the ancient Rajabasa Caldera, the Cukur Volcanco appeared, which had also a fairly large caldera. The product Cukur Volcano is divided also into two units, namely Cukur Volcanic Rock (constructive periode) and Totoharjo Ignimbrite (distructive periode). The Cukur Volcano is classified as brigate. Around the Cukur Caldera there are several volcanoes, namely the KelawiVolcano on the eastern wing, on the southwest wing there are the Mengkudu Volcano and Kapaya Lava, while in the caldera there are Tangkil Volcano and Sumbersari Riolite, that are classified as crown, except Kapaya and Sumbersari

Lava are classified ashummucks. Pandan Volcano appears in the middle of the ancient RajabasaCaldera, and on the wings of this volcano there are two volcanic cones, namely Mount Cukung and Atas, and inside the crater there is recentRajabasaVolcano. While Pandan, Cukung, and Atas volcanoes are classified as hummucks, while the RajabasaVolcano is as brigate.

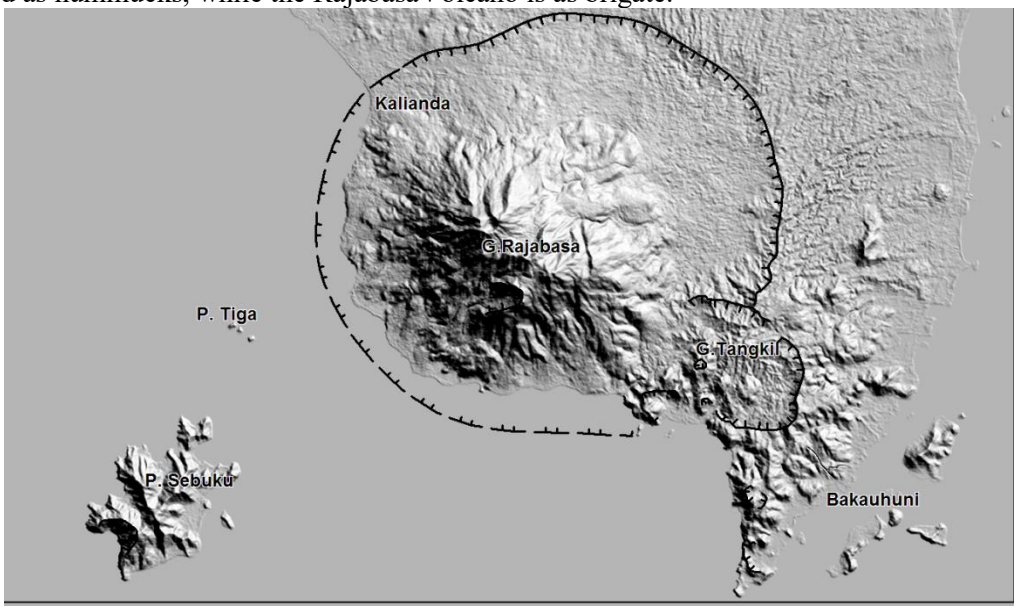

Figure 6. The shape of the ancient Rajabasa andCukur Volcano Calderas on the DEM image

5. Geological structures

The geological structures within the study area areconsist of calderas and craters, strike slip and normal faults (Figure 4). The calderas and the craters are characterized by circular shapes (rounded or elliptical) which are generally caused by volcanic activity. The two circulars are distinguished by their diameters, the caldera has a diameter greater than 2 km, while the crater has a smaller diameter (diameter less than 2 km). The observed calderas are the Ancient Rajabasa and the Cukur Volcano Calderas; while the crater consists of Kelawi, Tangkil, Cukung, Pandan and Rajabasa craters. The Tangkil strike slip faults are characterized by north southwest – southsoutheast valley alignments which cut through the Cukur, Tangkiland KelawiVolcanoes. There are some right displacements of normal faults around Tangkil and Kelawi Volcanoes. Based on features indicates that the Tangkil Fault is a right slip fault. While the right slip Hargopancaran Fault is characterized by valley alignment, and right displacement of the Mengkudu Crater. There is straightness of valleyand in the estuary there is an alluvium fan deposit indicating a fault, but along this alignment no data showing relative movement. This appearance is categorized as lineament. The normal faults show circular, observed around MountTangkil and Kelawi, which are relatively down inside, caused by eruption of volcanoes, resulting material inside the volcanoes are empty, and subsidence was occured. The north-northwest - south-east normal fault is located in the northeast of the AtasVolcano is characterized by very steep valley lineament, and west block was down. This fault is controlled by local tectonic activity. The fault formations are correlated to the regional fault. The faults are relatively the closest to the Panjang and the Tanjungan Faults. Both faults play a role in controlling the faults formation (Figure 7). Based on Reidel model [11], showing the Tangkil Fault as a Riedel Fault (R1), the Harjopancaran Fault is a P. Fault, while the normal fault controlled by very local tectonic.

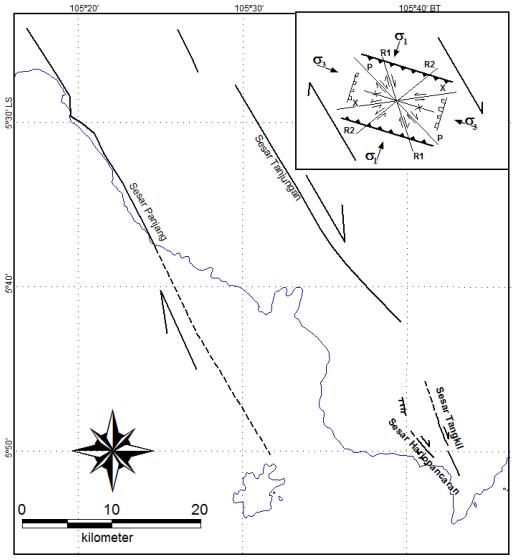

Figure 7. Modelling of fault formation in the area.

6. Geothermal Prospectivity

Geothermal systems in Indonesia are generally related to hydrothermalsystems. The formation of geothermal systems is primarily rain (meteoric) water, falling on the surface of the earth seep into the ground as a meteoric ground water (Figure 8). The groundwater is collected and heated by the magma. This heated water turns into a condensed liquid-vapor phase, and then changes into a vapor phase. The vaporis collected and trapped in a reservoir covered by seals. Fractured rocks (usually the old volcanic rocks) are generally act as reservoirs, whereas young volcanic rocks influenced by magma that rise to the surface alter into clay minerals (permeable zones), as seals. The existence of geothermal energy is usually indicated by the presence of geothermal manifestations that appear on the surface such as hot springs, fumaroles, mud pools, and others. This manifestation occurs due to fractures or faults that cuts through the reservoir, and allows fluids (steam and hot water) to flow to the surface. This surface manifestation should be determined by infrared thermal band remote sensing technique (Landsat or Aster). However, the volcanic areas in Indonesia having geothermal prospect are generally covered by dense forests, while the geothermal features are narrow, therefore these manifestations are difficult to detect from airplanes or satellites, and usually we obtain information from local people.

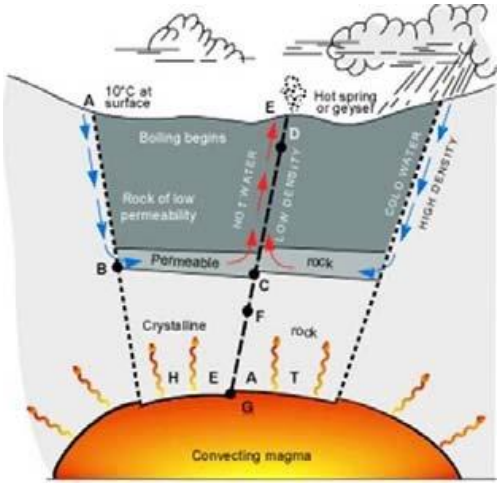

Figure 8. Model of geothermal system [12]

There are four hot springs inthe RajabasaVolcano Complex; they are Waymuli, Kalianda, Pematangpunduh, Waybelerang (Sumpur) hot springs..The Waymuli hot spring is quite large (Figure 9), and are situated in ancient RajabasaVolcanicRock outcrops that are fractured.Kalianda hot spring located in the sea, utilized for hot water bath (Figure 9).

Figure 9. Photo of the Waymuli hot spring (left) and Kalianda hot spring (right).

Pematangpunduh hot spring is located in the RajabasaVolcanicRock, and utilized hot water bathroom, and there are some clay mineral alteration (Figure 10), and Waybelerang hot spring shows high sulfur, very hot, big debit, situated in PandanVolcano, and intensive altered clay mineral (Figure 10).

Figure 10. Photos of the Pematang punduh hotspring and altered minerals into clay (left)

And Waybelerang hot springs (right).

7. Discussion

Rajabasa Volcano Complex have long live since Upper Miocene until recently [10] and are situated in the volcanic arc, having huge heat source [13]. The oldest volcanic rock complex are ancient Rajabasa Volcanic Rocks forming a big caldera and it is very possible as a caldera type of geothermal which has a large reserve [13]. The Pematangpunduh and Waybelerang hot springs showed that the Pandan and Rajabasa Volcanics cut through magma to the surface causing both rocks altered into clay minerals that are characterized by permeable rocks which are prominent as seal or cap rocks. While the Waymuli and Kalianda hot springs are located in the ancient Rajabasa Volcanic Rocks, showed fractures, it means that the rocks are considerable for reservoir. By a geological cross section through the Waymuli and Waybelerang hot springs, a geothermal model in the Rajabasa Volcano Complex can be constructed (Figure 11).

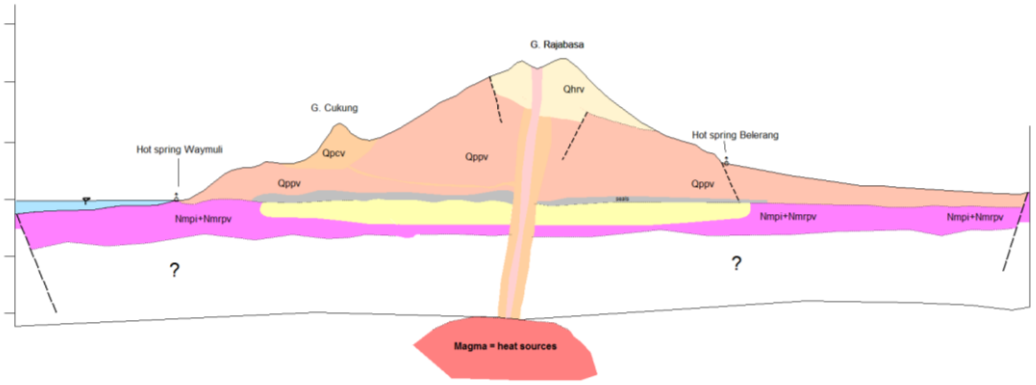

Figure 11. Geological cross section illustrates geothermal system in RajabasaVolcano Complex.

Combination of this technique with data from Darmawan et al. [3] will be significant for geothermal exploration.

8. Conclusion

The geology of Rajabasa Volcanic Complex concists of Brigate Ancient Rajabasa Volcanic Rocks (Late Miocene), underlain by Tarahan Tuff (Early Oligocene) that is intruded by Canti Dacite. In the western part of the Ancient Rajabasa Caldera, the Cukur Volcano (Brigate) splitted the Ancient caldera; and around the Cukur caldera is found some volcanoes, including Kelawi, Mengkudu, and Tangkil volcanoes (Crown), Kepayang Basalt and Sumbersari Riolite (Hummuck). While in the western part there are Pandan (Hummock), and Rajabasa Volcano (Crown). The geological structures discovered consists of calderas, craters, strike slip and normal faults. In terms of geothermal prospectivity, the reservoir is Ancient Rajabasa volcanic rocks, while the seals are Pandan and Recent Rajabasa Volcanic Rocks.

9. Acknowledgments

Authors would like to thanks principally to the Head of Geological Survey Institute, The Geological Agency, Ministry of Energy and Mineral Resources for the permission of the data to be published and also wish to thank the technical team of remote sensing geological map program during the field and mapping session until the map published.

10. References.

[1] Sidarto and A. Cita, *Geologi Selat Sunda. Pusat Air dan Lingkungan Geologi*. 2019: Bandung.
[2] Bronto, S., *Geologi Gunung api Purba: Publikasi Khusus*. 2010, Bandung: Badan Geologi, Kementrian Energi dan Sumberdaya Mineral.
[3] Darmawan, I.G.B., L.D. Setijadji, and D. Wintolo, *Geology and Geothermal System in Rajabasa Volcano South Lampung Regency, Indonesia (Approach to Field Observations, Water Geochemistry and Magnetic Methods).* Geology, 2015. **19**: p. 25.
[4] Bronto, S., J. Sianipar, and A. Pratopo. *Volcanostratigraphy for supporting geothermal exploration*. in *IOP Conference Series: Earth and Environmental Science*. 2016. IOP Publishing.
[5] Hamilton, W., *Tectonics of the Indonesian region. Professional Paper 1078.* US Geological Survey, Reston, VA, USA, 1979.
[6] Gafoer, S., G. Burhan, and J. Purnomo, *Peta Geologi Lembar Lahat Sumatera.* Bandung: Pusat Penelitian dan Pengembangan Geologi, 1986.

[7] Gafoer, S., *Tinjauan kembali tataan stratigrafi pra-Tersier Sumatera Bagian Selatan.* Prosiding Persidangan Sains Bumi dan Masyarakat, Malaysia National University, 1990.
[8] Geologi, P.P.d.P., et al., *Peta Geologi Lembar Jambi, Sumatera 1: 250,000*. 1993: Pusat Penelitian dan Pengembangan Geologi.
[9] Name, N., *Indonesian Stratigraphic Code*. 1990: Indonesian Geologist Association.
[10] Sidarto, S., I., , U. Margono, and D. Novita, *Peta Geologi Lembar Panengahan, skala 1:50.000* 2018, Pusat Survei Geologi: Bandung.
[11] McClay, K.R., *The mapping of geological structures*. 2013: John Wiley & Sons.
[12] Saptaji, N. *Sekilas Tentang Panas Bumi*. 2018.
[13] Kasbani, K., *Tipe Sistem Panas Bumi Di Indonesia Dan Estimasi Potensi Energinya.* Buletin Sumber Daya Geologi, 2009. **4**(3): p. 23-30.

Development of frame sample for estimating Corn crop area

Lena Sumargana[1], Heri Sadmono[1], Swasetyo Yulianto[1], Kadarmanto[2]

[1]Regional Resource Development Technology Center (PTPSW) Agency for Assessment and Application of Technology (BPPT)
[2] Directorate of Statistic for Food Crops, Horticulture, and Plantation Central Statistics agency (BPS)

e-mail: Lena.sumargana@bppt.go.id, herisadmono.hs@gmail.com, s_yulianto@yahoo.com, kadarmanto@bps.go.id

Abstract. Area Frame Sampling (KSA) is one of the methodologies to estimate crop area and furthermore crop production, Area frame sample methods have successes operated to monitor and estimated rice crop in Indonesia. with the same method, are being developed sampling frame of square segments by points for estimating corn crop area. Because there is no standard land map of corn comodity, the information on potential segment location is obtained from KSA rice survey data, field surveys, and maps of potential agricultural commodities. 100 m x 100 m segment unit built with 4 points as sample segment and using KSA apps, observation of the growing stage of corn was carried out directly at each midpoint of the subsegments that had been determined. There are 21965 segments that have been made as sample frame areas for observing the growing stage of corn in Indonesia and are expected to provide fast and accurate information about the area of corn plant

1. Introduction

Corn is a food crop as a source of staple food consumed by several countries, in addition to rice and wheat. Aside from being a staple food, corn is used as a material for cooking oil, ethanol, flour and animal feed.

Collection of harvested area data both paddy and secondary crops still uses conventional methods using the Agricultural Statistics (SP) questionnaire [1]. Harvest area data collection is still using the eye view of data collector (eye estimate). Practically, the method is easy to implement but has disadvantages. The low accuracy and long data collection time are some of the drawbacks of using this method.

One of the priority agenda of the government or nawacita is food self-sufficiency in Indonesia, can regulate and meet the food needs of its people sovereignly. the availability of agricultural data that is timely and accurate is the foundation to be able to realize agricultural policies that are targeted, then improving methodology in agricultural data collection must be done.

Data Collection on Integrated crop using the Area Frame Sample (Kerangka Sampel Area) method is a new method developed by BPPT in collaboration with BPS in order to improve the harvest area data collection method based on the results of the eye of the data collection officer (eye estimate). This method is more objective and modern by involving technological devices in it. So that the agricultural data collected becomes more accurate and timely [2].

The sample area framework method has been recommended by the Indonesian Statistics Society Forum to the government and the government to assign BPS to be able to produce accurate statistics on food crop production that is needed for proper government decision making related to efforts to maintain food security, especially regarding the national corn reserve policy, rice imports, and corn price

stabilization. The Area Frame Sample (KSA) method has been successfully implemented for the national rice commodity, so on October, 2018 the vice president presented the results of improved rice harvest area calculation using the Area Frame Sample method.

Area frame sampling of square segment by points (KSA) is a statistical procedure for measuring the quantity of rice/corn areas in geographical interest region by observing sample points within a square segment as a small part of the population [3]. Communication, observation and data transmission systems are carried out with the internet and Android devices. In this paper discuss the process of developing area frame sample for corn commodities.

2. Data and Methods

Development of Area Frame Sample for crop agriculture statistics is carried out using the area frame sample approach with point observations. The steps that will be carried out in the development of Area Frame Sample are:

a) Collecting administrative maps that contain administrative boundaries up to the district level for the entire Province.
b) Inventory data of corn harvest area per district from the Agriculture Survey report for the past 5 years;
c) Determine the consistency of corn harvested area in each district to obtain an indication that corn plants regularly planted in the region along with its area;
d) Calculation of segment allocation for corn crops per district;
e) KSA-paddy observations data inventory for the past 1 year, by checking all observations that are consistent with the growing stage of paddy fields are not planted with rice (code 7 in the KSA Paddy apps) to enable the availability of information on existing corn plants in the region;
f) Field observations with the use of open-camera applications to identify the distribution of corn crops;
g) Inventory data from other sources: Seralia and commodity potential maps from the ministry of agriculture
h) creating a 100 m x 100 m grid for the entire study area
i) Overlaying all layers of the results of the potential corn inventory, namely:
    a. KSA-paddy code 7 observations data (paddy fields are not planted with rice) that have corn crops.
    b. The results of field observations using OC applications from existing corn plants
    c. The results of the Cerealia project
    d. Map of potential agricultural crop commodities
j) Segment sample selection, by simple random sampling
k) Assign attributes to selected segments.

3. Development of Area Frame Sample

The use of an area Frame Sample in the estimation of food crop production (especially corn) in this activity is manifested in an approach to the design of frame sample based on observation points. The basic principle of this approach is the estimation of area based on direct observations in the field of the corn growing stage at the observation points that have been determined in selected samples. The proportion of the growing stage in the sample segment is extrapolated to obtain the population area of each growing stage.

In KSA-paddy the grid size is 300 x 300 meters but for this corn commodity, the frame sample grid size is 100 m x 100 m. This size was chosen to accommodate the area of corn planting, the number of segments and their distribution to obtain estimates up to the district level

3.1 Gridding and overlay

Development of Area Sample Framework based on information on the distribution of potential locations of corn plants and administrative area boundary maps. Preparation of a sample area framework begins by forming a square statistical unit in a particular administrative area.

The study area is divided into rectangular shaped boxes with a size of 100m x 100m, hereinafter referred to as segments. Segment boundaries are determined based on geographical coordinates with a fixed location. The boundaries of this study area follow the boundaries of the KSA-paddy segment.
The division of the study area into segments and sub-segments is shown in Figure 1.

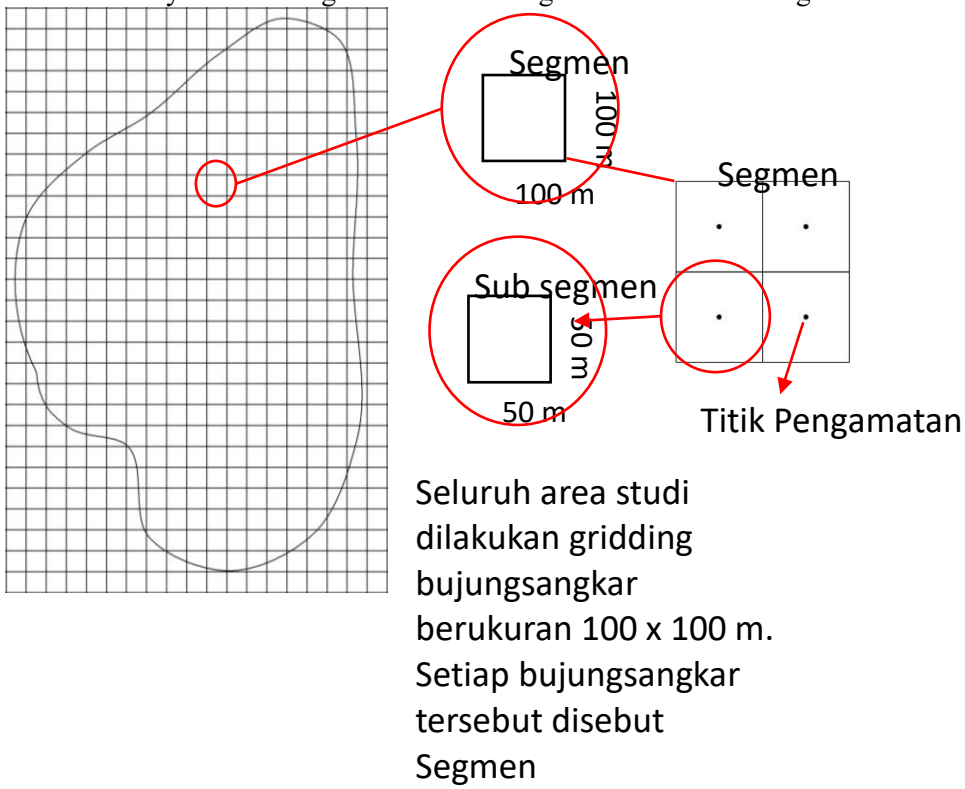

Figure 1. Division of regions in segments and subseges

the number of samples is determined based on the minimum dimension sample which is still possible in relation to the accuracy of data that is acceptable in the estimation at the district level. Consideration in determining sample dimensions mainly refers to the dimensions of the population, the difficulty of conducting the survey and relates to the constraints of activity management (coordination, number of personnel), costs and difficulties in the transfer of survey technique know-how. In this operational design, the number of 1% segment samples is the maximum planting area of corn in the sub rounds per district. The number of samples is also adjusted by considering the coefficient of variation to be achieved, knowledge held about local conditions.

There are four sources of corn location information that are used as a reference for stacking with the grid in the study area, while the results of the inventory layer of potential corn commodity are:

The results of the KSA-paddy code 7 (paddy fields are not planted with rice) observation inventory of existing corn plants were obtained from the survey results in 2018.

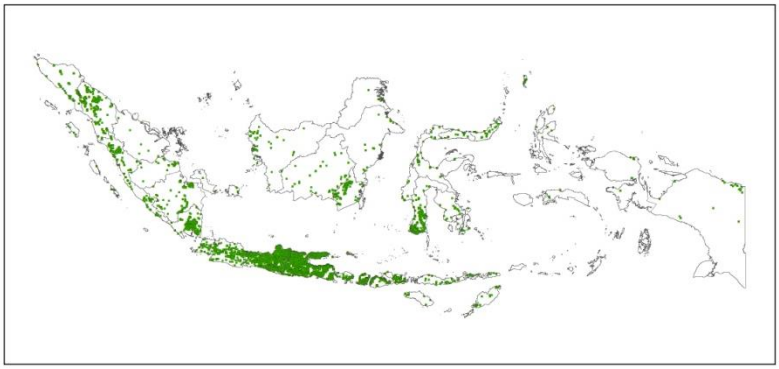

Figure 2. Distribution of corn locations from code 7 KSA-paddy

Field identification result by surveyors using open-camera apps or GPS device that have corn plants, containing information on the location of corn plants or geotagged photos

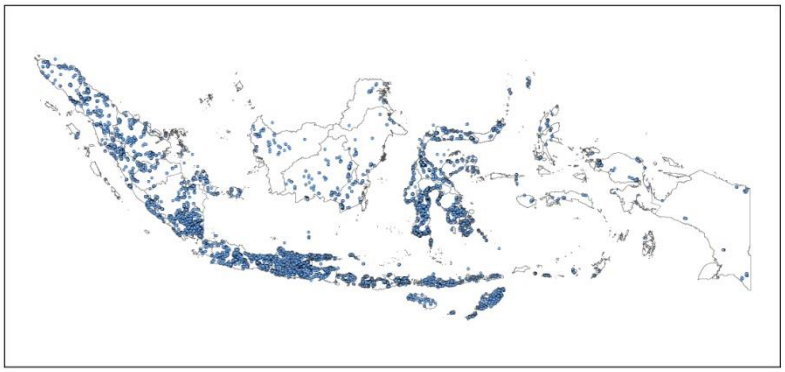

Figure 3. Distribution of corn location from field identification

The results of the Serealia project, containing the coordinates of the location of corn plants from the prospective farmer-prospective location (CPCL) data from the Directorate of Serealia Ministry of Agriculture.

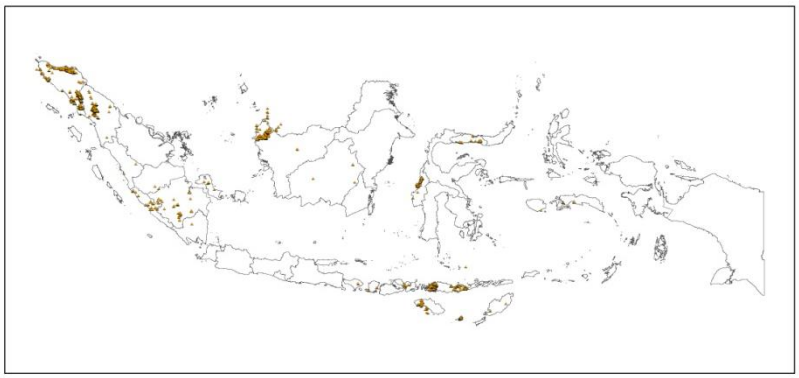

Figure 4. Distribution of corn location from CPCL data

Potential commodity polygon obtained from the Pusdatin Ministry of Agriculture, contains polygon areas of potential food crop commodities namely soybean, corn, peanuts, cassava, mustard greens, cucumbers, Chinese cabbage, tobacco, patchouli.

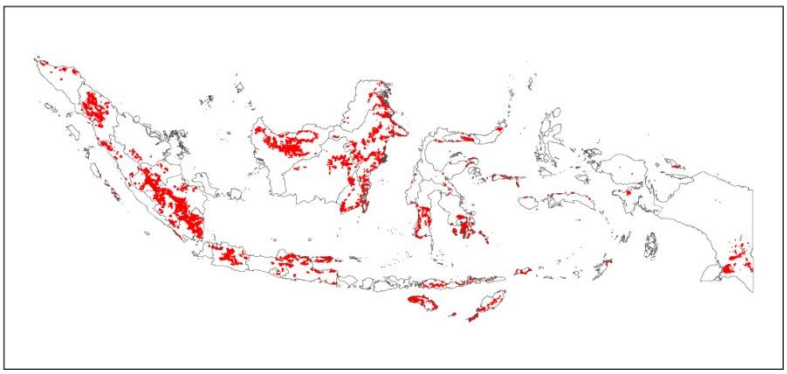

Figure 5. potential polygon data for some agricultural commodities

combining the four potential commodity corn data into a 100 m x 100 m grid segment, so that some information points on the potential for corn commodities are stored in the grid segment.

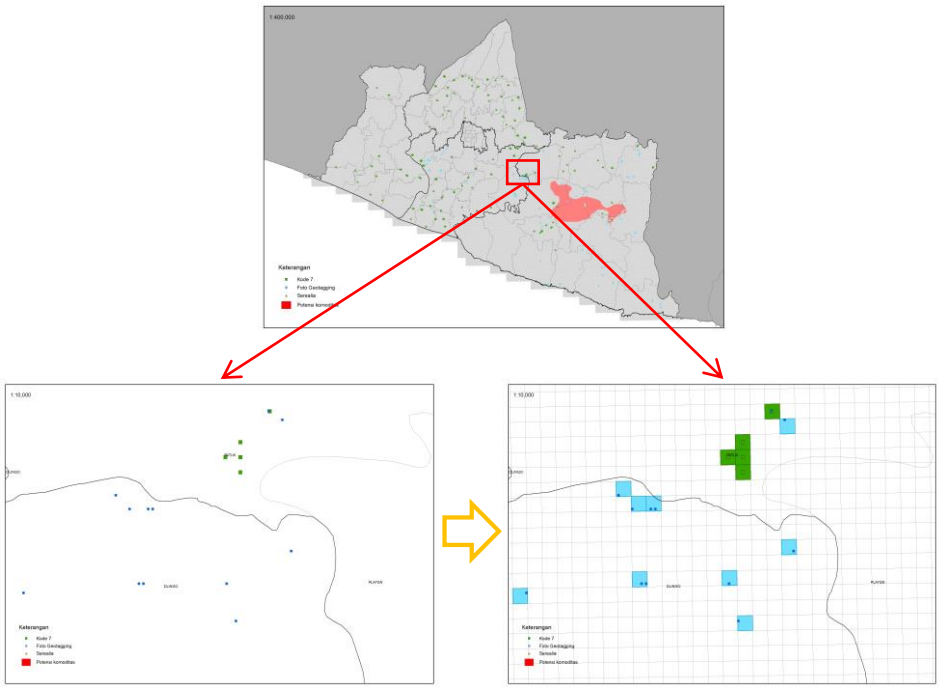

Figure 6. Combining 4 corn potential location information into segments

Determine information on the potential of corn commodities in each segment based on information on the overlay map. The segment contains some information on the potential of corn commodities based on the four corn data. Determination of information on the potential of commodities in the segment is determined using priority principles in the segment. The priority order is Observation of Code 7 KSA-paddy, Geotagged Photos, Serealia and polygon commodity potential. For example, if two points enter a segment consisting of kode 7 KSA-paddy and from a geotagged photo, the segment will have code 7 KSA-paddy information.

To obtain the representation of the observation points in each statistical unit (segment), in one segment a 50 m x 50 m grid is formed, hereinafter referred to as a subsegment. Each central point of the subsegment becomes Observation points that are regularly observed in the corn growing stage. Total Observation Points in one segment are four pieces that can represent information in one segment as a

whole. Figure 7 illustrates the distribution of Observation Points in a sample of selected segments measuring 100 m x 100 m. While the distance between observation points is 50 m.

Figure 7. Illustration of subsegment and center point for observation radius of corn growth stage

For data management, identification of each segment observed is done by coding. The segment code is adjusted to the province code, district code, sub-district code, and serial number of the selected segment per district. Provincial code, Regency code and sub-district code refer to the code used by the Central Statistics Agency (BPS).

The segment code consists of 10 digits, the first 2 digit sequence is the provincial code, the next 2 digits is the district code in the province, the next 3 digits is the sub-district code for the province and district, and the last 3 digits are this random number obtained from the sequence number for each district.

3.2 Defining the Number of Sample Segment

To estimate harvested area at the sub-district level, the area of each subdistrict (kecamatan) must be represented by a number of sample segments that are representative of the population. For this reason, segment representation must be calculated in each subdistrict. To estimate harvested area at the sub-district level, the area of each sub-district must be represented by a number of sample segments that are representative of the population. For this reason, segment representation must be calculated in each sub-district. Because there is no standard land map for corn commodities, an approach is carried out using a maximum planting area of subround in one year.

The population (number) of segments is the planting area of corn in the subdistrict (in hectares) divided by 1 hectare, which is the size of the segment 100m × 100m, and can be written as follows: $N_h = \text{roundup}\left(\frac{\text{Planting area (ha)}}{1\,\text{ha}}\right)$.

The number of segment samples for each subdistrict is determined by 1 percent of the segment population:

$$n_h = 1\% \text{ x } N_h$$

N_h: segment population in the stratum *h*,
n_h: the number of sample segments in the stratum *h*.

The number of sample segments identified from the selected extraction results is 21,965 segments spread throughout Indonesia. Table 1 shows the distribution of the number of segments for each province.

Tabel 1. Distribution of number of segments each province

Province	Segment Allocation	Province	Segment Allocation	Province	Segment Allocation
Aceh	820	Jawa Tengah	2224	Kalimantan Utara	132
Sumatera Utara	1538	DIY	282	Sulawesi Utara	572
Sumatera Barat	582	Jawa Timur	2894	Sulawesi Tengah	656
Riau	584	Banten	344	Sulawesi Selatan	1242
Jambi	504	Bali	138	Sulawesi Tenggara	792
Sumatera Selatan	702	NTB	566	Gorontalo	332
Bengkulu	442	NTT	1252	Sulawesi Barat	270
Lampung	900	Kalimantan Barat	492	Maluku	226
Kep Babel	112	Kalimantan Tengah	344	Maluku Utara	186
Kep. Riau	74	Kalimantan Selatan	440	Papua Barat	209
Jawa Barat	1421	Kalimantan Timur	280	Papua	413

All 100m x 100m square segments are not limited by physical appearance, but are limited by lines based on geographic coordinates, observers are tasked with observing the corn growth stage and land conditions at the center radius of the midpoint of the segment in the segment, it is necessary know the physical boundaries in the field in accordance with the geographical coordinates that have been set previously. Physical boundaries in this field can be determined by using the facilities on an android-based application that has been made

3.3 Sample Segment Selection

The method of selecting sample segments applied to KSA corn is simple random sampling by considering the distance from the distribution of segments obtained based on information on the potential of corn. The sample selection procedure is carried out for each study area in the Subdistrict with the following stages:

a) Random sequencing of the potential corn commodity segment resulting from code 7 KSA-paddy, and numbered
b) Random sequencing of the potential corn commodity segments resulting from the Geotagged Photo (Open camera application), and given an advanced sequential number from point a),
c) Random sequencing of the potential corn commodity segments resulting from cereal data, and given a sequential number from the stage point b),
d) Random sequencing of the potential corn commodity segments results from the commodity potential map data, and is given a sequential number from the stage point c),
e) Taken the first serial number as the selected segment to represent the segment in the sub-district,
f) The second segment is selected from the second sequence number from the sorting result, then the distance treshold is checked by 250 meters against the previous selected segment, if this second segment passes the distance limit then the second segment will be selected,
g) If the second segment does not pass the distance limit then a third segment will be selected, then a distance treshold of 250 meters is checked against the previously selected segment.
h) Stages f and g continue until the number of segment allocations in the sub-district is obtained.

Observation of the corn growth stage in each segment is represented by four observation points. Each of these observation points is determined to be in the middle of each subsection, so the distance from one point to the next is 50 m.

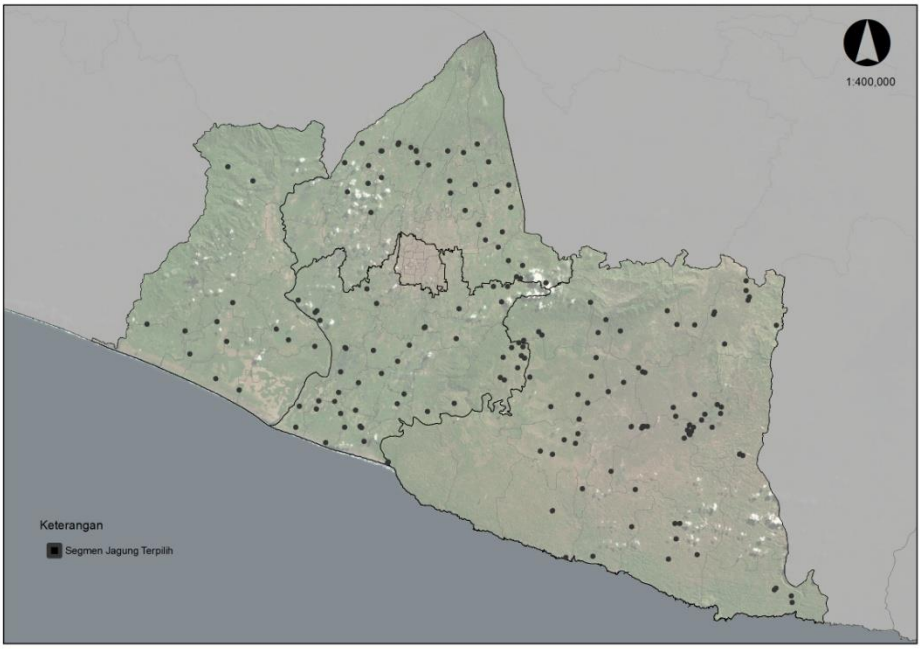

Figure 8. Example distribution of selected segments in the Province of DIY

3.3 Observing Growth Stage of Corn

Corn growth stage has the same growth pattern, but the time interval between growth stages and number of leaves that develop can be different. Corn growth can be grouped into three stages, namely (1) the germination phase, when the process of water imbibition is characterized by swelling of the seeds up to before the appearance of the first leaf; (2) vegetative growth phase, i.e. the phase from which the first leaves appear fully open until tasseling and before the female flowers (silking), this phase is identified by the number of leaves formed; and (3) the reproductive phase, which is the growth phase after silking to physiological cooking [4]. Table 2 is an indication table for the corn growing phase, which is used by observations to record the growing phase of corn at the observation point in the subsegment.

Tabel 2. Observatioan code and Growth stage of Corn

Code	Growing Stage	remark
1	Early Vegetatif (VA)	This phase begins after the plant is seen. the germination phase until the number of leaves is fully 3-5 leaves or up to about 8 days
2	Late Vegegatif (VR)	the number of leaves that are fully open 6 to n the last leaves or this phase takes place when the plant is 18-50 days after germination
3	Early Generatif (GA)	Taseling Stage (Flowering male) and Silking Stage
4	late Generatif (GR)	This stage takes place when the plant is aged from 24 days from out of silking stage to 65 days after silking
5	Panen Jagung Hijauan (PH)	corn plant is harvested as animal feed.
6	Fase Panen Jagung Muda (PM)	young corn plants are harvested as sweet corn or vegetable corn
7	Fase Panen Jagung Pipilan (PP)	corn plant is harvested as shelled corn
8	Land Preparation (PL)	land is being cultivated
9	No Corn Plant (BJ)	Phase where at the time of observation takes place the observation point is not planted with corn such as rice, soybeans, tobacco and so on
10	No Agriculture area	No Agriculture area

4. Discussions

The use of four sources of information on location information of corn plants, namely code 7 KSA-paddy, field observations with open camera applications, Serealia data and polygons of several commodities can help provide estimates of the location selection of corn segments. Simple random sampling results obtained by 21965 corn segments of size 100 x 100 meters spread across all provinces in Indonesia except DKI Jakarta, this number is expected to represent the distribution of existing corn commodity locations, with the method of data collection which is carried out following the data collection techniques on rice commodities it has been successfully carried out, the data transmission and data monitoring can be quickly carried out and the results of corn production can be quickly identified.

5. Acknowledgements

The authors would like to thank to the Regional Resource Development Technology Center for the Agency for the Assessment and Application of Technology (BPPT) and the Directorate of Statistics for food crops, Horticulture and Plantation Central Statistics Agency (BPS) for the implementation of the development activities of the area frame sample method for corn commodity.

6. References

[1] BPS, K.P., *Pedoman Pengumpulan Data Statistik Pertanian (SP) Tanaman Pangan.* 2015.
[2] Mubekti, M. and L. Sumargana, *Pendekatan kerangka sampel area untuk estimasi dan peramalan produksi padi.* Jurnal Pangan, 2016. **25**(2): p. 71-146.
[3] Munandar, M., *Sampling frame of square segment by points for rice area estimation.* Crop monitoring for improved food security, 2014.
[4] Subekti, N.A., R.E. Syafruddin, and S. Sunarti, *Morfologi tanaman dan fase pertumbuhan jagung.* Di dalam: Jagung, Teknik Produksi dan Pengembangan. Jakarta (ID): Pusat Penelitian dan Pengembangan Tanaman Pangan, 2007.

A comparative assessment on the applicability of UAV and TLS for estimating aboveground biomass of mangrove forest in Mahakam Delta, East Kalimantan, Indonesia

Md M Hossain[1]*, L van Leeuwen[1], Y A Hussin[1], Y B Sulistioadi[2]*

[1]Department of Natural Resources, Faculty of Geo-information Science and Earth Observation (ITC), University of Twente, Hengelostraat 99, 7511 AE Enschede, The Netherlands. Tel: +31534874293 Fax: +31534874399
[2]Soil and Water Conservation Laboratory, Forestry Faculty, Center of Geospatial Information Infrastructure Development (CGIID), Institute for Research and Community Services (IRCS), Mulawarman University, Samarinda, Indonesia.
author's e-mail: y.a.hussin@utwente.nl

Abstract. Mangrove forests are playing a vital role by storing and sequestering a large amount of global carbon that helps to reduce the GHG emission. Unfortunately, the global mangrove forests are decreasing rapidly due to agricultural expansion, illegal logging, mining, and palm oil production. The UNFCCC initiates REDD+ initiatives for reducing the GHG emission from deforestation and forest degradation. The aboveground biomass and carbon stock estimation is a prerequisite for an MRV system for complying such initiative. The use of UAV and TLS are considered as a popular remote sensing technique for estimating aboveground biomass and carbon stock appropriately. This study is aimed at a comparative assessment on the applicability of UAV and TLS for estimating aboveground biomass and carbon stock in the mangrove forest. The tree height extracted from CHM of UAV images can provide comparatively accurate tree height. The DBH and tree height measured from TLS 3D point clouds can also give a correct measurement of DBH and tree height. The aboveground biomass was estimated using a specific allometric equation developed for mangrove forests. The results show the accuracy of AGB estimated form UAV compared to TLS is achieved at R^2=0.9262 while RMSE=3.78 ton/ha.

1. Introduction

Mangrove forest is considered as a significant carbon sink of the terrestrial ecosystem as it can sequester and store an enormous volume of carbon compared to other forests. Mangrove forests can store three times higher carbon (including aboveground and belowground) as compared to terrestrial forests [1]. Besides, mangrove forests play an essential role in providing ecosystem services and functions including shelters for the birds and other animals, habitats for the plants, fish, invertebrates and amphibians and foods, woods and livelihoods for the local communities. This forest plays a crucial function for stabilizing alluvial sediments and protecting the coastline from erosion and natural hazards [2]. Unfortunately, global mangrove forests are degrading rapidly where half of the forest has been lost in the last four decades [3].

Mangrove forest has salt-tolerant trees that make it unique as compared to other forests. Also, mangrove forest is an ecosystem with rich biodiversity including various species of flora and fauna. In mangrove, some tree species have an intricate root system which is also the habitation of different aquatic species of flora and fauna. The flat and even canopy and intermingle crowns make it challenging to identify individual tree crowns in the mangrove. However, the advantage is that it has a single canopy, unlike the tropical forest which is multi-layered. The aboveground biomass estimation in mangrove forest is challenging due to accessibility interrupted by tides and congested roots for field data collection.
Nowadays, UAV is a popular technology for monitoring forest management as well as estimating aboveground biomass and carbon stock. The application of UAV technology especially in the forest sector is increasing dramatically over the last decades [4]. The UAV technique

can take imagery of a relatively large area within a short duration while the cost is lower compared to other remote sensing techniques. The UAV imagery has a very high spatial resolution which can be used to identify the small-scale objects in details. The 3D point clouds can be generated from the multiple partially overlapping images while applying the Structure from Motion (SfM) technique. The SfM technique is the process incomparable with stereographic analysis of aerial photographs to estimate the 3D structure of the object using a set of overlapping 2D images. The UAV can collect multiple images for certain objects, and the specific software can calculate camera position as well as the position of 3D points for overlapping, viewing rays of corresponding points [5]. Finally, it can generate 3D point clouds of the surface area. Digital Surface Model (DSM) and Digital Terrain Model (DTM) can be produced using 3D point clouds. Hence, Canopy Height Model (CHM) can also be generated by deducting DTM from DSM (Figure 1).

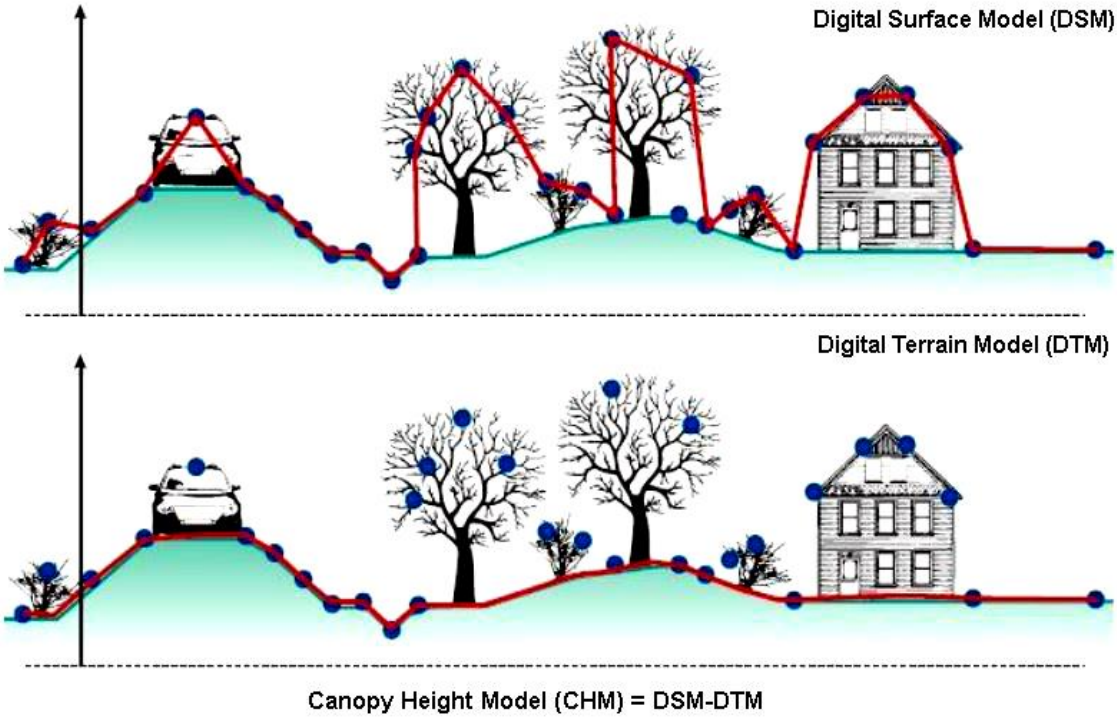

Figure 1. UAV DSM, DTM and CHM extraction from point cloud.

Another remote sensing instrument is the Terrestrial Laser Scanning (TLS), which is considered as one of the most useful and comparatively accurate techniques for measuring tree attributes in the forest. It is a ground-based active LiDAR instrument which uses laser beams to detect and measure surrounding objects and can generate 3D point clouds of the objects. TLS can provide an enormous amount of high-resolution 3D information on vegetation biophysical parameters. It can be applied for measuring crown structure, leaf area index, leaf area distribution, canopy radiation, and gap fraction. TLS can use simple allometric and isometric equations for assessing biomass, growth monitoring and disturbance of vegetation structure [6]. It can measure high-resolution 3D spatial data of forest structures as a ground-based active remote sensor. TLS can measure lower canopy more precisely compared to other techniques including manual measurement and satellite images. However, the use of TLS in the

mangrove forest for measuring biophysical parameters of trees is a big challenge. Because the weight of TLS instrument is almost 25 kilograms which is difficult to move from one scan position to another on the wet and muddy ground. Moreover, TLS is applicable only plot-based which is considered as a drawback for this technique.

In mangrove forests, several studies have been conducted for estimating aboveground biomass and carbon stock. Among them, satellite imagery or Airborne LiDAR data were mostly used. Some studies used UAV images for aboveground biomass and carbon stock estimation [7], [8], [9], [10]. However, no studies were found on the applicability of UAV and TLS for assessing aboveground biomass and carbon stock in the mangrove forest. In other studies, for example in tropical forest, UAV images were used to calculate height from CHM while UAV-DBH can be predicted from Crown Projection Area (CPA) based on a model developed from the relationship between CPA and field-measured DBH. On the other hand, TLS can estimate tree height and DBH of trees accurately from its 3D point clouds [6]. However, the use of TLS is difficult in the inaccessible area while UAV images can be collected easily from that area. Despite these drawbacks, both UAV and TLS are treated as a comparatively accurate technique for estimating aboveground biomass in the forest. This study will make a comparative assessment on the applicability of UAV and TLS for aboveground biomass and carbon stock estimation in a mangrove forest. The accuracy of UAV derived aboveground biomass depends to a large extent on the accuracy of image segmentation.

2. Materials and Methods

2.1. Study Area

Indonesia is a Southeast Asian country located in between the Pacific, and the Indian Ocean which has almost 23 percent of the world's mangrove ecosystems [3]. East Kalimantan is one out of 34 provinces in East Kalimantan. It has a total area of 129,066 square kilometers (49,832 sq. mi) and is the fourth largest province in Indonesia. The study is conducted in the mangrove forest of Mahakam Delta in East Kalimantan. The study area is situated between 0°32′18.20″ S and 117°34′3.87″ E. The size of the study area is approximately 47 hectares. In East Kalimantan, there are various mangrove swamp forests located far inland up to the Mahakam River [11]. A simplified map of the study area is shown in Figure 2.

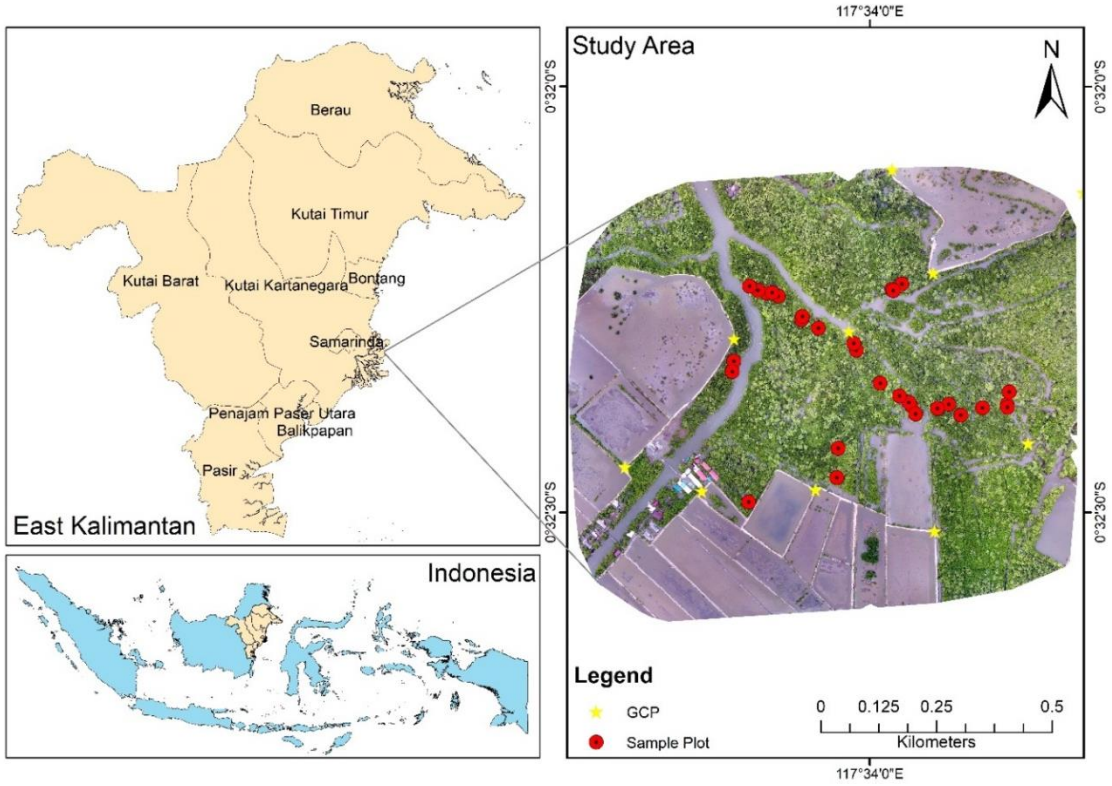

Figure 2. Location map of the study area.

The mangrove forest in Mahakam delta has diversified tree species. Among them, several tree species are considered as dominating species including *avicennia*, *rhizophora*, *bruguiera*, *xylocarpus*, and *sonneratia*, [12]. Among those, *avicennia* is the most common genus in Mahakam Delta which is known as 'api api' means 'fires' in the Malay language. It is a flowering plant with aerial roots which is included under the family Acanthaceae. Generally, it is available in the intertidal area of estuarine. *Rhizophora* and *bruguiera* are another genus included in Rhizophoraceae family which are common in the mangrove forest. Like to *avicennia*, it is also found in the intertidal zone of estuarine. It has intricate roots with up to 2.5-meter-high from the ground. X*ylocarpus* is another dominating species under the Meliaceae family. *Sonneratia* is also found in mangrove which is included as a genus under Lythraceae family. It has spread aerial roots similar to *avicennia*. Among these species, three species including *avicennia*, *rhizophora* and *xylocarpus* were identified in the field. The rooting and aeration system of the dominating species are illustrated in Figure 3.

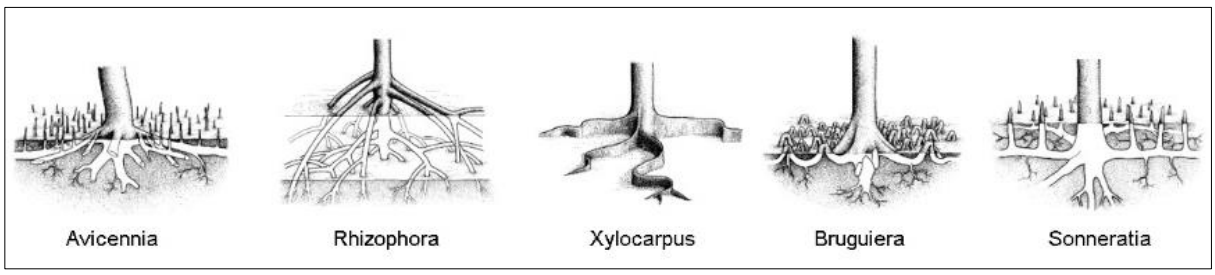

Figure 3. Rooting and aeration system of dominating species in mangrove forest. Adapted from: Göltenboth and Schoppe (2006).

2.2. Datasets

The study is based on three types of dataset including field-measured data, UAV and TLS data. Both field-measured and TLS data was collected from the same sample plots while UAV images were taken for the overall area. Later, these sample plots (same as biometric and TLS plot) were identified and extracted from the UAV images. The field-measured data and TLS data was collected between 14 to 22 October 2018, and UAV images were acquired on 21 December 2018. The list of datasets, source, and their characteristics are illustrated in Table 1:

Table 1. List of the dataset, their characteristics, and sources

SN	Data type	Characteristics	Data source
	Field-measured data	Biometric data of tree species, tree height, and DBH	Fieldwork (October 2018)
	TLS data	3D point clouds	Fieldwork (October 2018)
	UAV data	UAV-RGB images	Fieldwork (December 2018)

2.3. Materials

2.3.1. Field Equipment's and Instruments

There are different field equipment's were used during the field work to measure forest attributes including tree height, DBH, navigation, positioning, and setting sample plots. The list of field equipment required for the study is illustrated in Table 2:

Table 2. List of equipment's/instrument's used in the fieldwork and their application

SN	Equipment's/instruments	Application
	RIEGL VZ-400-TLS	Tree scanning within sample plots
	Phantom 4 DJI Drone	Acquisition of UAV-RGB Images
	Differential GPS	GCP Positioning
	Garmin eTrex GPS	Navigation and positioning
	Leica Disto D510	Tree height measurement
	Measuring Tape (30m)	Setting plot area
	Diameter Tape (5 m)	DBH measurement
	Data Recording Sheet	Data recording

2.3.2. Software and Tools

Different type of software and tools were used for processing and analyzing of UAV imagery, TLS, and field-measured data. The list of required software and tools are illustrated in Table 3.

Table 3. List of required software and tools

SN	Software and tools	Purpose/use
	Pix4D Mapper 4.2.27	Photogrammetric processing of UAV imagery
	RiSCAN Pro 2.5.2	TLS data processing and extraction of tree height and DBH
	eCognition Developer 9.4.0	Tree crown segmentation
	Cloud Compare 2.10	View point clouds

ArcGIS 10.6	Data processing and visualization
MS Office (Word, Excel) 2016	Thesis writing and statistical analysis

2.4. Methods

The research method is an essential step to response the research objectives and questions of the study. It comprises fieldwork design, sampling method, data collection, processing, data analysis, and findings. The methods used in this study are categorized into five steps:

1. The first step was related to fieldwork for collecting the required data and information from the study area. The biometric, TLS and UAV data were collected from the fieldwork. A total of 30 sample plots were identified as purposively for collecting field data.
2. The second step was based on TLS data processing for co-registration and point clouds generation and extraction of all individual trees for measuring tree height and DBH. Aboveground biomass and carbon stock is estimated from TLS data using an allometric equation based on mangrove forest.
3. The third step was involved in the preparation and analysis of field-measured biometric data for estimating aboveground biomass and carbon stock. Biometric data is considered as ground truth for comparing the accuracy of tree height, DBH and aboveground biomass/carbon stock for UAV and TLS data.
4. The fourth step was related to processing and analyzing of UAV data for accurate CPA segmentation for estimating DBH and exploring different segmentation algorithms. The CHM was generated for estimating tree height of the sample plots. Aboveground biomass and carbon stock were calculated from the processed data using the specific allometric equation for mangrove forest.
5. The fifth and final step was based on assessing the accuracy of tree height, DBH and estimated aboveground biomass/carbon stock measured from TLS and UAV using field-measured data and allometric equation as the reference.

The key process of the methods followed in the study is illustrated in Figure 4.

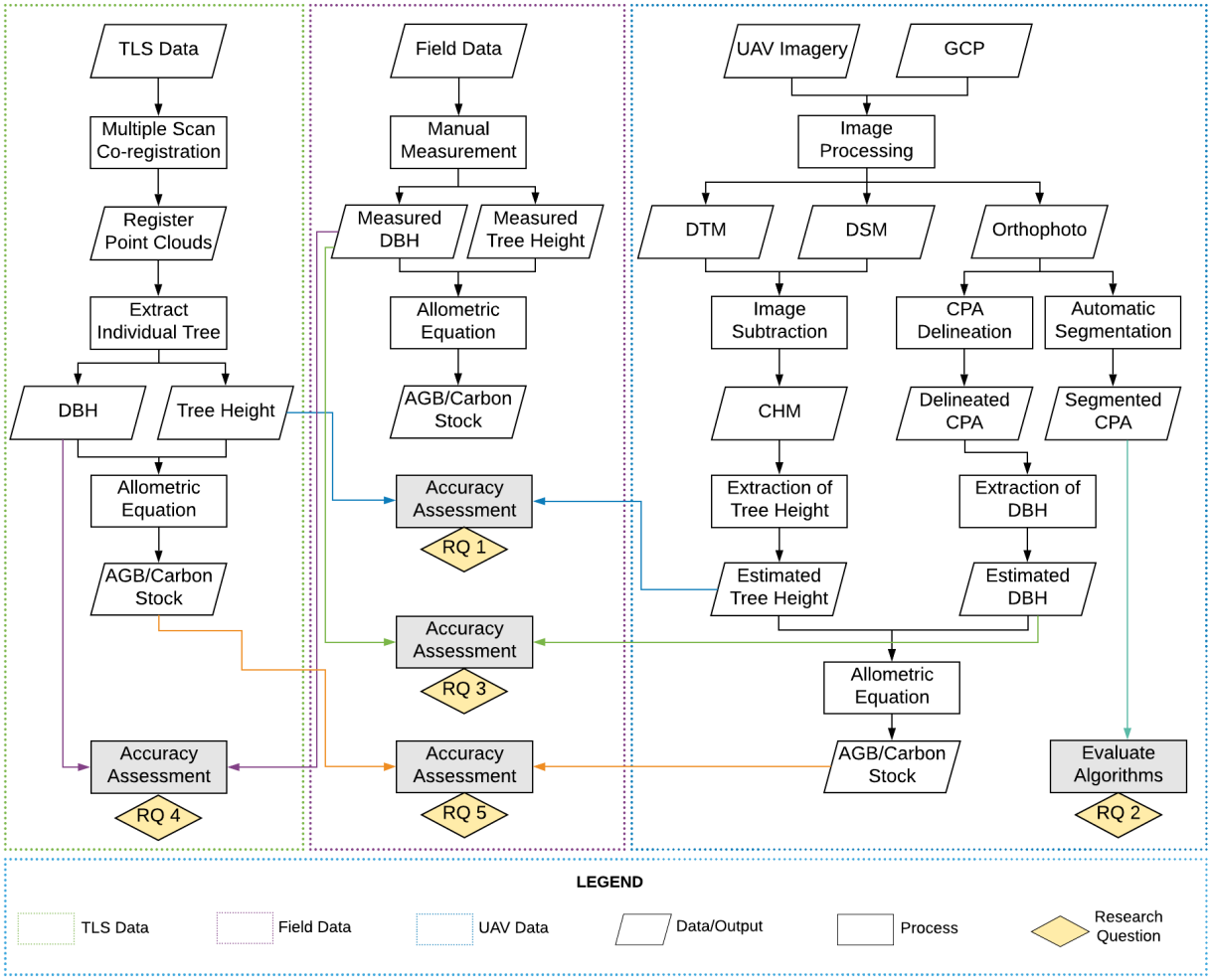

Figure 4. Research workflow diagram.

2.4.1. Sampling design and biometric data collection

The Sampling design is an essential part of a research study. A purposive sampling method was followed in this study. Mangrove forest is difficult for data collection due to wet ground and complex root system. Carrying a TLS in mangrove forest is very difficult for its weight (almost 25 kg). Therefore, the purposive sampling method was applied to ensure full utilization of the limited time and minimize the risks to collect data from inaccessible places.

Biometric data (tree species, height, and DBH) was measured by following the purposive sampling method. A Circular plot with 12.62 m radius (500 m^2) was used for both biometric and TLS data collections. A circular plot is convenient to identify in the field and can provide comparatively few errors [6]. Moreover, the circular plot is convenient and easy for Terrestrial Laser Scanning. The forest type and species distribution of the study area were almost homogeneous. So a circular plot with 12.62 m radius was used for minimizing the required time as well as labour.

2.4.2. TLS Data Collection

The TLS (Figure 5a) was used to scan the same 30 sample plots which were used for biometric data collection at the same time. It is generally mounted on a tripod on the ground. It emits a laser beam to the objects around the scanning positions and receives the reflected beams with 3D points of those

objects. A multiple scan approach was followed with 4 (four) different scan positions for each plot. Because four scan position (1 center and three outers) is easy to identify in the field as well as can reduce the scan duration compared to more scan position in each plot. The center position of each plot was used as the first scan position. The three other scan positions were set outside of the perimeter of the circular plot which is 15 m away from the center scan position with an angle of 120 degrees (Figure 5b). Because scanning from center position with three other positions can scan the objects from a 360-degree angle and can generate comparatively accurate 3D point clouds of those objects. A multiple scan position can minimize the occlusion problem and can produce a sufficiently dense 3D point cloud that can be used as an accurate measurement of tree height and DBH [13].

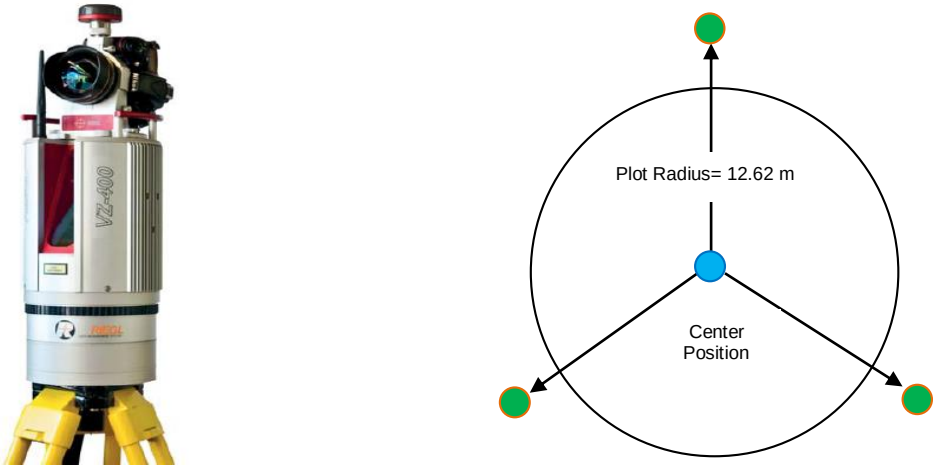

(a) (b)

Figure 5. (a) RIEGL VZ-400 TLS ; (b) Diagram of TLS multiple scan position

2.4.3. Setting the Retro-reflectors

The retro-reflectors were used as tie points among the multiple scan positions. It improves the accuracy of the scanning as well as regulate the alignment of each scan. The reflectors are required for accurate co-registration of all scans for generating 3D point clouds. Both circular and cylindrical reflectors were used for scanning of each plot in the fieldwork. A total of 10-12 cylindrical reflectors were placed on the top of sticks for their visibility from all scan positions. Moreover, 8-10 circular reflectors were tagged (Figure 6a) on the tree trunk facing to the center position with a clear view.

Figure 6. (a) Plot preparation before TLS Scanning and setting the reflectors; (b) TLS scanning

2.4.4. UAV data acquisition

A Phantom 4 DJI Drone with an RGB camera was used for UAV image acquisition in the study area. A UAV flight was operated for covering 0.47 ha area located in Tani Baru village in Mahakam Delta. A total of two UAV flight plan fulfilling the research requirements were prepared to acquire UAV imagery covering 30 sample plots in the study area. The Pix4D capture android application was used to prepare these flight plan. The duration of the UAV flight mission was considered according to UAV battery capacity. The UAV flight parameters used for image acquisition is illustrated in Table 4.

Table 4. UAV flight parameters used for image acquisition

Parameter		**Value**
Flight Mission	:	Grid
Flight Speed	:	Moderate (10 m/sec)
Angle	:	90^0
Flight Height	:	164.58 – 172.63 meter
Front Overlap	:	85%
Side Overlap	:	75%
Image Size	:	4000x3000

2.4.5. Allocation of GCP Markers

A total of 8 (eight) GCP markers were allocated in the study area for identifying accurate spatial reference of 3D maps generated from the UAV images. Differential GPS was used to measure the accurate position of all GCPs in the study area. The GCP marker allocation and model of the Phantom 4 DJI drone are illustrated in Figure 7.

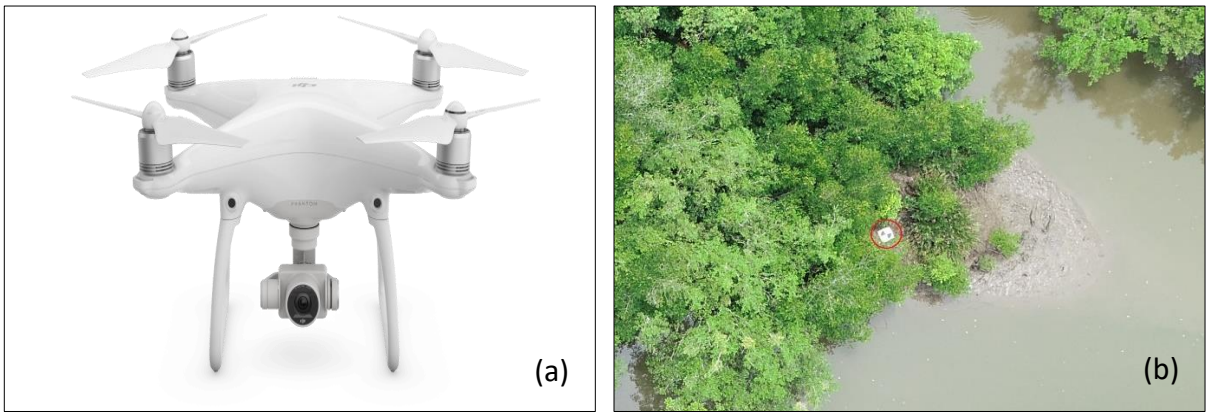

Figure 7. (a) A Phantom 4 DJI Drone; (b) A GCP marker placed in the study area

2.4.6. TLS Data Processing

RiScan Pro software was used to process field acquired TLS data. A process flow diagram for UAV image processing is illustrated in the following diagram.

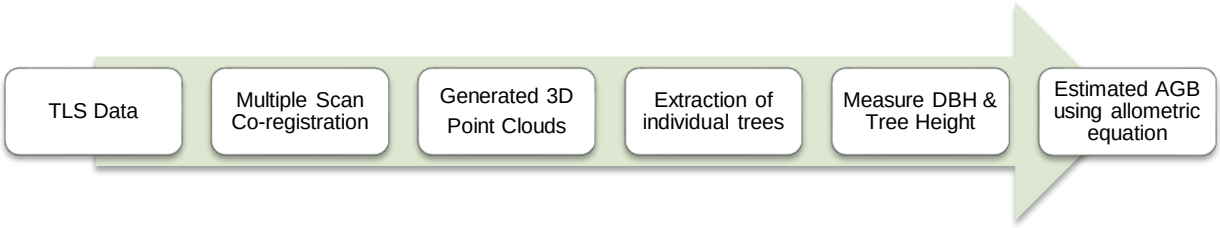

2.4.7. DBH and tree height Measurement

RiSCAN Pro software was used for extracting individual trees from the 3D point clouds generated from multiple co-registration. For the identification and separation of a particular tree, the extracted plot was displayed in true color mode for enhancing the visualization of the tree label. The individual trees were identified based on their color and shape with selection tools. After that, the trees were extracted and saved as new point clouds.

The DBH can be measured using different methods including distance measurement tool and circle fitting. The circle fitting method is based on a circle center that can adjust to projected points of the stem for structuring a radius to measure DBH while the distance measure tool calculates the distance between two points to measure DBH. The distance measure tool in RiSCAN Pro was used to measure DBH in this study. The DBH was computed at the height of 1.3m from the base (Figure 8a and 8b). The measured DBH of all individual trees were manually entered into MS Excel for analysis.

Similar to DBH measurement, the tree height was also measured with measure distance tools in RiSCAN Pro software. The highest point and lowest point of individual trees were identified and calculate the distance between two points. The resultant distance was considered as the tree height. The species *rhizophora* has a long and congested root system. Sometimes its aboveground roots are up to 2.5m high from the ground. The tree height of *rhizophora* was measured including the height of the root (Figure 8c).

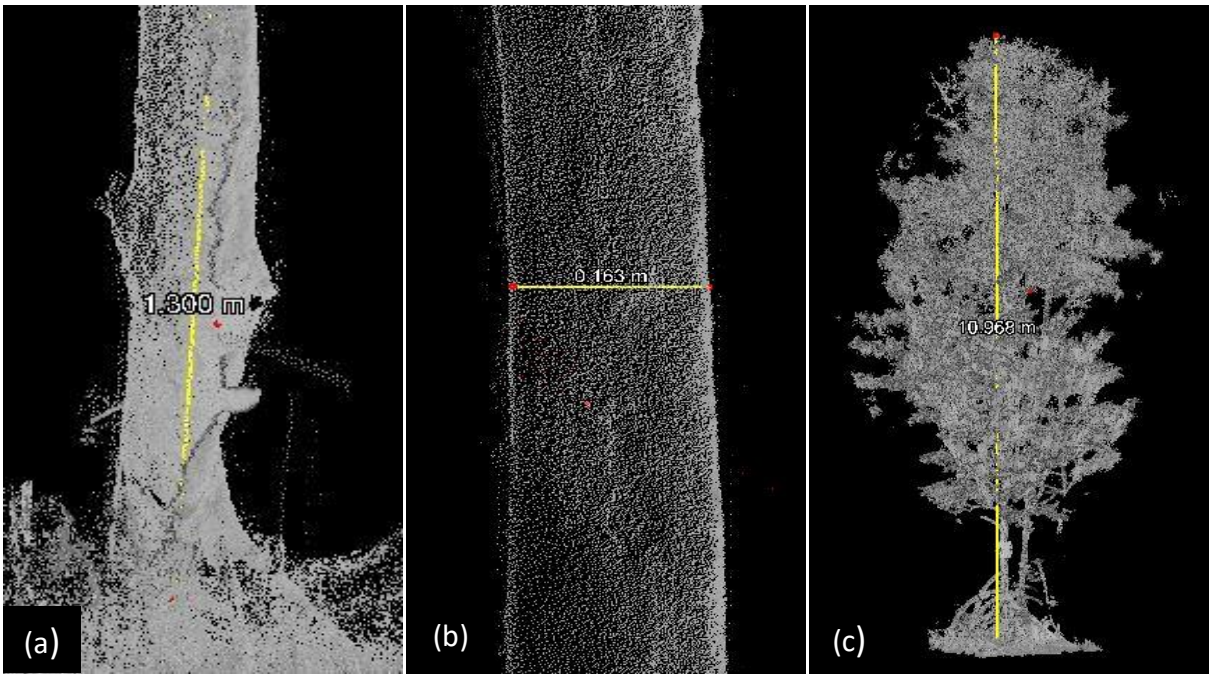

Figure 8. Measurement of (a) 1.3m height from ground; (b) DBH; and (c) height.

2.4.8. UAV Image Processing

The photogrammetric software Pix4D Mapper Pro was used to process the UAV images for generating DSM, DTM, and orthophoto. The following is the process flow diagram for UAV image processing.

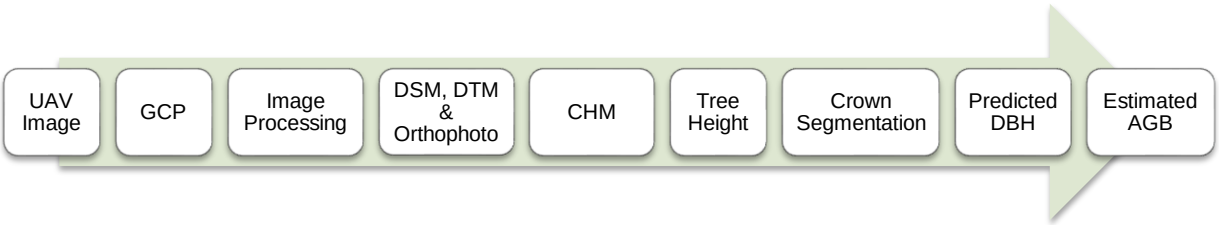

2.4.9. Generation of Digital Surface Model, Digital Terrain Model, and Orthophoto

After generating 3D point clouds, Pix4D Mapper can generate orthophoto, DSM and DTM. The orthophoto is a geometrically corrected image, made from multiple raw images using a uniform scale. The orthophoto was used to identify the crown projection area (CPA) for estimating DBH for individual trees. Besides, a DSM is a surface model considering the height value of objects while DTM is a terrain which represents the terrain heights originated on the surface of the earth. The DSM and DTM are illustrated in Figure. centre position of the area. Thus, the negative values do not affect the height measurement of the plot area. The DSM and DTM show negative values here because the edges do not have sufficient image matching. Therefore, the point clouds were not densely generated in that area. As a result, the lowest values of DSM and DTM were calculated as negative. All of the sample plots are located around the centre position of the area.

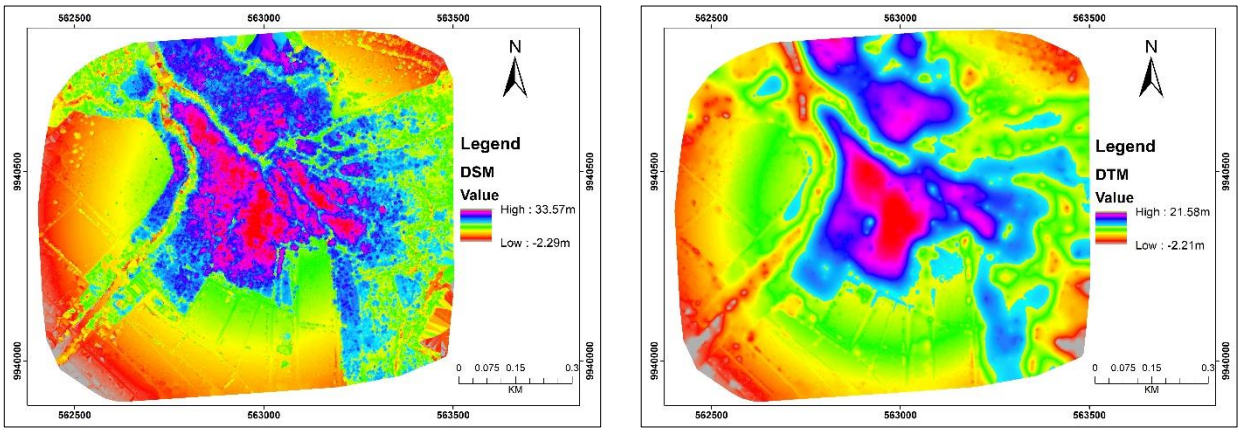

(a) (b)

Figure 9. (a) DSM of the study area; (b) DTM of the study area

2.4.10. Generation of Canopy Height Model and Extraction of Tree Height

The Canopy Height Model was generated by subtracting the DTM from the DSM. The Raster Calculator tool in ArcGIS was used to calculate the Canopy Height Model using DTM and DSM. The Canopy Height Model was used to estimate individual tree height from the sample plots. For tree height estimation, field-measured trees were identified and matched with corresponding tree crown in Canopy Height Model.

2.4.11. Above Ground Biomass Data Analysis

2.4.11.1 Allometric Equation

The allometric equation is a commonly used method to estimate aboveground biomass using forest biophysical parameters including tree height and DBH. Several researchers have developed some equations for simplifying biomass estimation using wood density, tree height and DBH [14]. However, site-specific allometric equation needs to be applied for accurate estimation of aboveground biomass [15]. Among different allometric equations for estimating aboveground biomass, the equation developed by Chave et al. [16] specified for mangrove forest is comparatively simple and renown to estimate aboveground biomass in a mangrove forest.

Equation 1. Allometric equation for AGB estimation

$$AGB_{est} = \exp(-2.977 + in(\rho D^2 H)) \equiv 0.0509 x \rho D^2 H \quad (1)$$

Where;

AGB_{est} = Estimated aboveground biomass in kg;

D = Tree DBH in cm (measured at 1.3m from ground but some cases at above prop root);

H = Tree Height in meter (measured from the ground);

p = Wood Specific Gravity in g/c3.

For estimating carbon stock, a carbon fraction (CF) of 0.47 [17] was used to calculate carbon stock using aboveground biomass.

Equation 2. Carbon stock calculation from AGB

$$C = AGBxCF \quad (2)$$

Where;

C = Carbon Stock,

AGB = Aboveground Biomass, and

CF = Carbon Fraction

2.4.11.2 Aboveground Biomass and Carbon Stock Estimation

Aboveground biomass and carbon stock was estimated using three different datasets including field-measured biometric data, TLS and UAV data. The above-mentioned specified allometric equation developed for mangrove forest, was applied to calculate AGB in this study. Besides, specific wood density for specific tree species was also used to estimate aboveground biomass accurately. The specific wood density used for *avicennia*, *rhizophora* and *xylocarpus* species are 0.6987 g/cm3, 0.9204 g/cm3 and 0.6721 g/cm3 respectively.

2.4.11.3 Aboveground Biomass and Carbon Stock Estimation using Biometric Data

The field-measured tree height and DBH were used to estimate aboveground biomass and carbon stock from field-measured. The abovementioned allometric equation was applied to calculate the AGB from biometric data. The carbon stock was also estimated from aboveground biomass.

2.4.11.4 Aboveground Biomass and Carbon Stock Estimation using TLS

The tree height and DBH measured from TLS point clouds were used to estimate aboveground biomass and carbon stock for TLS dataset.

2.4.11.5 Aboveground Biomass and Carbon Stock Estimation from UAV

The tree height extracted from UAV-CHM and DBH predicted from UAV-CPA were used for estimating aboveground biomass and carbon stock for UAV dataset.

3. Results and Discussions

3.1. The Accuracy of Tree Height Extracted from UAV-CHM Compared to Tree Height Measured from TLS 3D Point Clouds

The accuracy of UAV-CHM extracted tree height compared to tree height measured from TLS point clouds (as reference height) was conducted using a scatter plot based on these two tree heights. A total of 874 trees were considered for evaluating the accuracy of tree height extracted from UAV-CHM compared to tree height extracted from TLS point clouds. The result (Figure 10) shows that there is a strong correlation of 0.90 with R^2 (coefficient of determination) 0.8182. The Root Mean Square Error (RMSE) is 1.44m that is equivalent to 9.75% of total tree height measured from TLS point clouds.

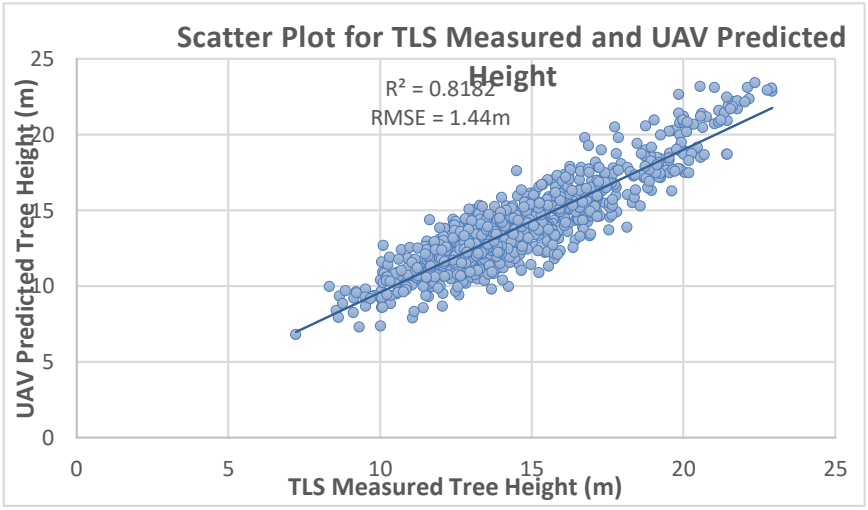

Figure 10. The relationship between tree height extracted from UAV-CHM and TLS point cloud

3.2. CPA-DBH Model development and validation

Several models were developed and validated for predicting DBH of individual trees using field-measured biometric DBH. A total of 90 trees were selected for model development and validation. Among them, 54 trees (60%) were selected for model development, and 36 trees (40%) were chosen for model validation. A total of 54 trees were randomly selected from 18 sample plots for model development. The trees were selected with biometric DBH (ranging from 10.00cm to 58.80cm) for representing field-measured DBH with a different range. It is found that most of the trees have DBH within 30cm while very few (42 out of 893) have higher DBH. A relationship between the UAV derived CPA, and field-measured biometric DBH was developed in a scatter plot. Four different regression functions, i.e., linear, logarithm, power and quadratic were developed. The results are illustrated in Figure 11.

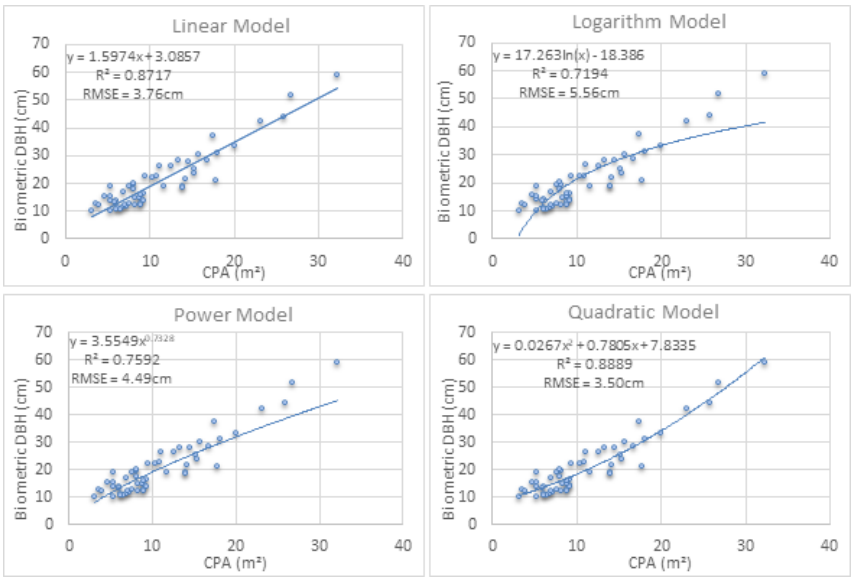

Figure 11. Different regression model for predicting DBH from CPA.

3.3. The accuracy of DBH derived from TLS 3D point clouds

The accuracy of DBH derived from TLS 3D point clouds was assessed with biometric DBH (referenced DBH) using a scatter plot based on these two measured DBH. A total of 874 trees were considered for this assessment. The result (Figure 12) shows that there is a correlation of 0.99 where the coefficient of determination (R^2) is 0.9985. The RMSE is 0.30 cm which is equivalent to 1.87% of biometric DBH. Therefore, there is a strong correlation between biometric DBH and TLS measured DBH.

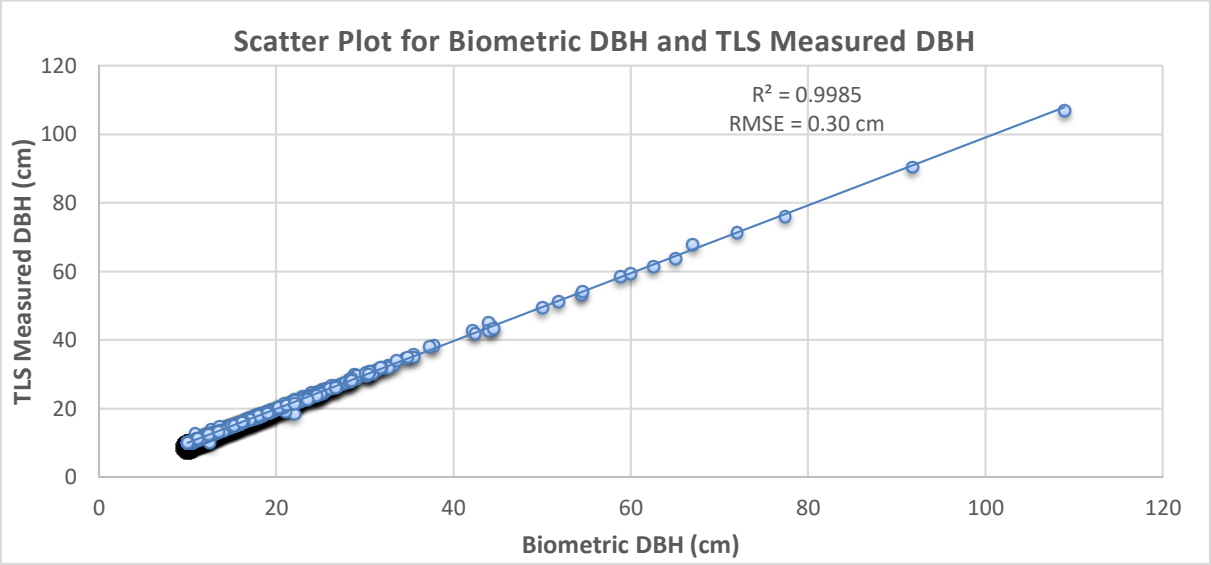

Figure 12. Scatter plot for biometric DBH and TLS measured DBH

3.4. The Accuracy of AGB Estimated from UAV Compared to AGB Estimated from TLS

The UAV and TLS estimated AGB were placed in a scatter plot for evaluating the accuracy of UAV estimated AGB compared to TLS measured AGB. The TLS scanned 30 sample plots data (reference data) were considered for developing this assessment. The result (Figure 13) shows that there is a strong correlation with 0.96 where the coefficient of determination (R2) is 0.9262. The Root Mean Square Error (RMSE) is found as 3.78 ton/ha which is equivalent to 3.25% of TLS estimated AGB.

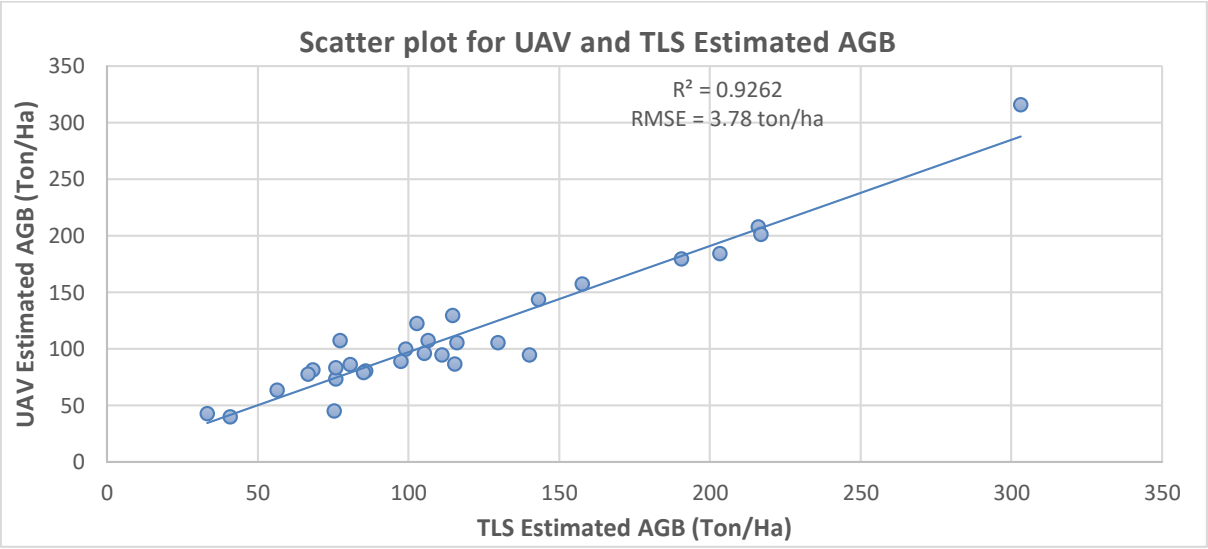

Figure 13. Scatter plot for UAV and TLS estimated AGB

3.5. Carbon stock estimation using UAV, TLS and the reference

The carbon stock estimation was conducted to identify the amount of carbon in the study area. The carbon stock was estimated using Equation 2 provided by [17]. The carbon stock was calculated from stand-alone biometric, UAV and TLS dataset. The plot-wise estimated carbon stock for field-measured biometric, TLS and UAV are illustrated in Figure 14. The result shows that most of the plots have carbon stock below 60 tons/ha while only five plots have more than 80 ton/ha carbon. But two plots (plot 12

and 18) have carbon stock below 20 tons/ha. The average carbon stock (ton/ha) for biometric, TLS and UAV are 52.24, 55.26 and 53.38 respectively.

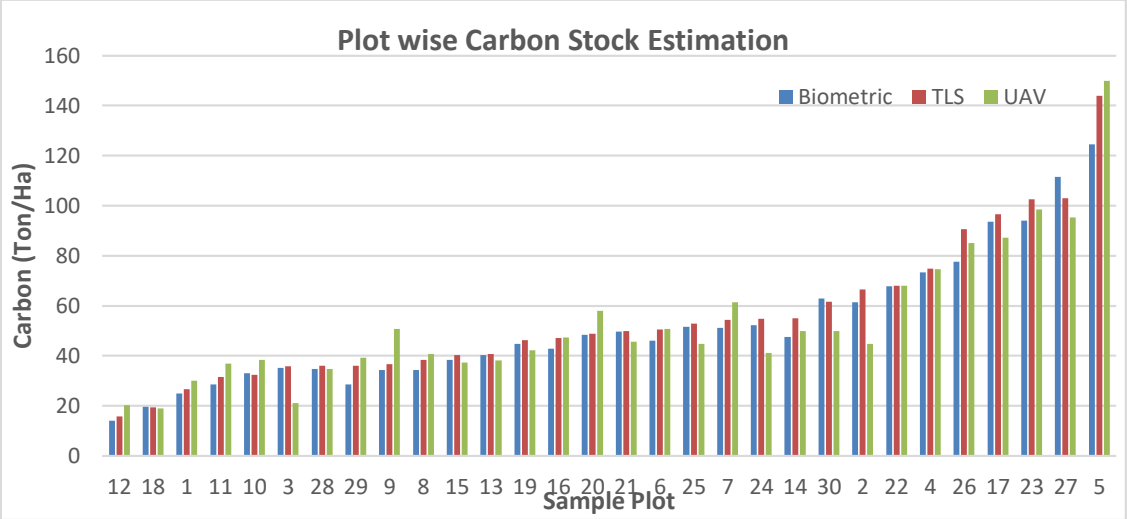

Figure 14 Plot-wise carbon stock of biometric, TLS and UAV.

3.6. Aboveground Biomass and Carbon Stock

The aboveground biomass and carbon stock was estimated with biometric, TLS and UAV datasets. The maximum aboveground biomass was estimated as 303.10 ton/ha (in plot 5) and minimum as 33.25 ton/ha (in plot 12) by TLS. This is because aboveground biomass is dependent on DBH, tree height, wood density and number of trees inside the plot area. It is observed that higher aboveground biomass was estimated in the plots which are dominated by *Rhizophora*. Also, the number of trees are found comparatively more in the plots having higher aboveground biomass. The DBH and tree height also has significant influences on estimating aboveground biomass in the plots.

In this study, average aboveground biomass was estimated as 112.38 ton/ha and 116.33 ton/ha from UAV and TLS respectively. The aboveground biomass estimation from UAV data was found consistent with related some past studies. Among them, Otero et al. [18] estimated aboveground biomass from UAV as 143 Mg/ha (equivalent to 157.63 ton/ha) in Matang mangrove forest in Malaysia while Lucas et al., [19] found 81 Mg/ha (equivalent to 89.29 ton/ha) AGB in Mozambique's mangrove forest using TLS. Apart from UAV and TLS, Hamdan et al., [20] estimated 133.97 Mg/ha (equivalent to 147.68 ton/ha) AGB using SPOT-5 image of Kuala Sepetang forest reserve in Malaysia. Also, Pham and Brabyn [21] got 150 Mg/Ha (equivalent to 165.35 ton/ha) AGB in Quang Ninh mangrove forest in Vietnam using ALOS PALSAR.

3.7. AGB Estimation by Tree Species

The mangrove trees are different from other forests for its aerial and long congested roots. The tree height and DBH need to be measured accurately for estimating AGB accurately. The average predicted DBH of UAV was found underestimated for *avicennia* while it was overestimated for *rhizophora* compared to TLS and biometric DBH. Because the *avicennia* has a sparse canopy which resultant less dense point clouds that may influence to underestimation in tree height. On the contrary, UAV-CHM derived tree height including all trees were found underestimated compared to height extracted from TLS point clouds. The percentage of deviation of tree height extracted from UAV-CHM compared to TLS measured height was found as -2.59 and -7.03 for *avicennia* and *rhizophora* respectively. The deviation of tree height of *rhizophora* was higher due to its congested root system. Also, there are some differences in the canopy and leave density among those species. The species *avicennia* has a spread canopy with leathery leaves while the *rhizophora* has a dense canopy with elliptic leaves (Figure 15).

Figure 15. Physical structure of *Rhizophora* and *Avicennia.*

The species *rhizophora* has long and congested aboveground roots up to 2.5-meter high from the ground. The DBH was measured at 1.3m from the ground or above the highest stilt root. Because the allometric equation followed in this study was developed including aboveground roots for such type of tree species. But the other species, i.e., *avicennia* and *xylocarpus* have no congested aboveground roots like *rhizophora*. The measurement of DBH and tree height can be affected through the irregular structures as well as the quantity of leaves. In this study, the deviation of tree height of *rhizophora* derived from UAV-CHM was found higher than *avicennia* and *xylocarpus* because the dense canopy structure of *rhizophora* is different from the other two species which may affect to height measurement [22].

4. Conclusions

The accuracy of tree height extracted from UAV-CHM compared to tree height measured from 3D point clouds of TLS is attained at $R^2 = 0.8182$ and RMSE = 1.44m (%RMSE = 9.7%). Therefore, the accuracy of tree height extracted from UAV-CHM is 90.3% accurate compared to tree height resultant from 3D point clouds of TLS data. So, the null hypothesis was not rejected. Therefore, there is no significant difference between tree height estimated from CHM of UAV imagery and tree height resultant from TLS.

The accuracy of DBH predicted from CPA segmentation of UAV imagery compared to field-measured DBH is achieved at $R^2 = 0.87$ and RMSE = 3.21cm (%RMSE = 19.97%). The DBH extracted from CPA segmentation of UAV imagery was 80.03% accurate compared to field-measured DBH. Consequently, the null hypothesis was not rejected. Therefore, there is no significant difference between DBH derived from CPA segmentation of UAV imagery and field-measured DBH.

The accuracy of DBH measured in 3D point clouds of TLS compared to field-measured DBH is achieved at $R^2 = 0.9985$ and RMSE of 0.30cm (%RMSE = 1.87%). So the DBH extracted from TLS 3D point clouds was 98.13% accurately measured in TLS point clouds compared to field-measured DBH. So, the null hypothesis was accepted. Therefore, there is no significant difference observed between the TLS measured DBH and field-measured biometric DBH.

The accuracy of aboveground biomass estimated from UAV imagery compared to aboveground biomass measured from TLS is attained at $R^2 = 0.926$ and RMSE of 3.78 ton/ha (%RMSE = 3.25%). Therefore, 96.75% of the aboveground biomass estimated from UAV imagery was accurate compared to aboveground biomass estimated from 3D point clouds of TLS data. Consequently, the null hypothesis

was not rejected. Therefore, there is no significant difference between aboveground biomass estimated from UAV imagery and TLS point clouds.

5. Acknowledgment

The Authors would like to highly acknowledge and appreciate the research permit issued by the Indonesian Ministry of Science and Technology and Higher Education. They would like to highly Acknowledge the support and contribution of Dr. Y. Budi Sulistioadi and the Faculty of Forestry University of Mulawarman, Samarinda, Indonesia for facilitating our research work, helping us with the logistic, collecting image and ground truth data in Tani Baru mangrove forest. We highly appreciate the support of the team of Mita Priskawanti and Muhammad Lutfi Hamdani for their continuous help during October 2018. We acknowledged the UAV data collection by Dr. Y. Budi Sulistioadi in 2017 and 2018. Without the data and support, our research could not have been done.

6. References

[1] Alongi, D M (2012). Carbon sequestration in mangrove forests. *Carbon Management*, *3*(3), 313–322. https://doi.org/10.4155/cmt.12.20

[2] Boone, J K, & Bhomia, R K (2017). Ecosystem carbon stocks of mangroves across broad environmental gradients in West-Central Africa: Global and regional comparisons. *PLoS ONE*, *12*(11), 1–17. https://doi.org/10.1371/journal.pone.0187749

[3] Giri, C, Ochieng, E, Tieszen, L L, Zhu, Z, Singh, A, Loveland, T, Duke, N (2011). Status and distribution of mangrove forests of the world using earth observation satellite data. *Global Ecology and Biogeography*, *20*(1), 154–159. https://doi.org/10.1111/j.1466-8238.2010.00584.x

[4] Anderson, K, & Gaston, K J (2013). Lightweight unmanned aerial vehicles will revolutionize spatial ecology. *Frontiers in Ecology and the Environment*, *11*(3), 138–146. https://doi.org/10.1890/120150

[5] Westoby, M J, Brasington, J, Glasser, N F, Hambrey, M J, & Reynolds, J M (2012). "Structure-from-Motion" photogrammetry: A low-cost, effective tool for geoscience applications. *Geomorphology*, *179*(June 2018), 300–314. https://doi.org/10.1016/j.geomorph.2012.08.021

[6] Newnham, G J, Armston, J D, Calders, K, Disney, M I, Lovell, J L, Schaaf, C B, Danson, F M (2015). Terrestrial laser scanning for plot-scale forest measurement. *Current Forestry Reports*, *2*(3), 214–214. https://doi.org/10.1007/s40725-016-0039-7

[7] Husson, E, Lindgren, F, & Ecke, F (2014). Assessing biomass and metal contents in riparian vegetation along a pollution gradient using an unmanned aircraft system. *Water, Air, and Soil Pollution*, *225*(6). https://doi.org/10.1007/s11270-014-1957-2

[8] Zahawi, R A, Reid, J L, Dandois, J P, Ellis, E C, Holl, K D, & Nadwodny, D (2015). Using lightweight unmanned aerial vehicles to monitor tropical forest recovery. *Biological Conservation*, *186*, 287–295. https://doi.org/10.1016/j.biocon.2015.03.031

[9] Wahyuni, S, Jaya, I N S, & Puspaningsih, N (2016). Model for estimating above ground biomass of reclamation forest using unmanned aerial vehicles. *Indonesian Journal of Electrical Engineering and Computer Science*, *4*(3), 586–593. https://doi.org/10.11591/ijeecs.v4.i3.pp586-593

[10] Messinger, M, Asner, G P, & Silman, M (2016). Rapid assessments of Amazon forest structure and biomass using small unmanned aerial systems. *Remote Sensing*, *8*(8), 1–15. https://doi.org/10.3390/rs8080615

[11] Choong, E T, Wirakusumah, R S, & Achmadi, S S (1990). Mangrove forest resources in Indonesia. *Forest Ecology and Management Elsevier Science Publishers*, *3334*, 45–57.

[12] Food and Agriculture Organization. (2018). Mangrove management. Retrieved August 22, 2018, from http://www.fao.org/forestry/mangrove/vegetation/en/idn/

[13] Liu, J, Liang, X, Hyyppä, J, Yu, X, Lehtomäki, M, Pyörälä, J, Chen, R (2017). Automated matching of multiple terrestrial laser scans for stem mapping without the use of artificial references. *International Journal of Applied Earth Observation and Geoinformation*, *56*, 13–23. https://doi.org/10.1016/j.jag.2016.11.003

[14] Nam, V T, Van Kuijk, M, & Anten, N P R (2016). Allometric equations for aboveground and belowground biomass estimations in an evergreen forest in Vietnam. *PLoS ONE*, *11*(6), 6–9. https://doi.org/10.1371/journal.pone.0156827

[15] Basuki, T M, van Laake, P E, Skidmore, A K, & Hussin, Y A (2009). Allometric equations for estimating the aboveground biomass in tropical lowland Dipterocarp forests. *Forest Ecology and Management*, *257*(8), 1684–1694. https://doi.org/10.1016/j.foreco.2009.01.027

[16] Chave, J, Andalo, C, Brown, S, Cairns, M A, Chambers, J Q, Eamus, D, Yamakura, T (2005). Tree allometry and improved estimation of carbon stocks and balance in tropical forests. *Oecologia*, *145*(1), 87–99. https://doi.org/10.1007/s00442-005-0100-x

[17] IPCC (2006). 2006 IPCC guidelines for national greenhouse gas inventories. Retrieved from https://www.ipcc-nggip.iges.or.jp/public/2006gl/vol4.html

[18] Otero, V, Van De Kerchove, R, Satyanarayana, B, Martínez-Espinosa, C, Fisol, M A Bin, Ibrahim, M R Bin, Dahdouh-Guebas, F (2018). Managing mangrove forests from the sky: Forest inventory using field data and Unmanned Aerial Vehicle (UAV) imagery in the Matang Mangrove Forest Reserve, peninsular Malaysia. *Forest Ecology and Management*, *411*(December 2017), 35–45. https://doi.org/10.1016/j.foreco.2017.12.049

[19] Lucas, R M, Mitchell, A L, & Armston, J (2015). Measurement of forest above-ground biomass using active and passive remote sensing at large (subnational to global) scales. *Current Forestry Reports*, *1*(3), 162–177. https://doi.org/10.1007/s40725-015-0021-9

[20] Hamdan, O, Khali Aziz, H, & Mohd Hasmadi, I (2014). L-band ALOS PALSAR for biomass estimation of Matang Mangroves, Malaysia. *Remote Sensing of Environment*, *155*(April 2018), 69–78. https://doi.org/10.1016/j.rse.2014.04.029

[21] Pham, L T H, and Brabyn, L (2017). Monitoring mangrove biomass change in Vietnam using SPOT images and an object-based approach combined with machine learning algorithms. *ISPRS Journal of Photogrammetry and Remote Sensing*, *128*, 86–97. https://doi.org/10.1016/j.isprsjprs.2017.03.013

[22] Taureau, F, Robin, M, Proisy, C, Fromard, F, Imbert, D, Debaine, F, Debaine, F (2019). Mapping the mangrove forest canopy using spectral unmixing of very high spatial resolution satellite images. *Remote Sensing*, *11*(3), 367. https://doi.org/10.3390/RS11030367

The classification of oil palm plantations derived from Landsat 8 OLI images using Google Earth Engine

Sri Mulyati , Iksal Yanuarsyah, Sahid Hudjimartsu

Geoinformatic of Informatics Engineering Department, Faculty of Engineering and science, Ibn Khaldun University, Jalan KH Soleh Iskandar KM 2, Tanah Sereal, Bogor, West Jawa, Indonesia,
sri.soniqbale@gmail.com

Abstract: Oil palm plantations are increasing rapidly in the tropics, especially in Indonesia. The development of oil palm plantations needs to be monitored to detect how wide the area of oil palm plantations in the area. In addition, many researchers and forestry practitioners need tools to monitor the development of oil palm which is simple and easy to use. Google Earth Engine (GEE) is a cloud computing platform that provides a lot of remote sensing data and can be classified using the algorithm provided in GEE. The remote sensing data used is Landsat 8 to classify a palm oil plantation using Random Forests Algorithm. The results showed that the classification accuracy for oil palm plantations was around 81%. GEE has the potential to be upgraded as a tool to detect and monitor the expansion of oil palm plantations in Indonesia and does not require programming skills.

Keywords: oil palm, classification, algorithm, random forest, google earth engine

1. Introduction

Central Kalimantan is one of the provinces in Indonesia located on the island of Borneo. The capital is the City of Palangka Raya. Central Kalimantan has an area of 157,983 km². and has a large oil palm plantation area, which is 1,142,004 Ha [1]. Therefore, Central Kalimantan is taken as a case study in the research that is being developed at this time, to make land cover classifications (Oil Palm, Non Palm Oil, and Water).

The emergence of revolution 4.0, and the emergence of the development of big data with cloud computing, and the need for methods to monitor forestry practitioners, the authors tried to process data and conduct data sampling for classification using the Google Earth Engine.

Google Earth Engine is a platform that provides big data and various analytical methods that make it easy for us to do analysis. Google Earth Engine itself is a platform for scientific analysis and visualization of geospatial data sets, for academic, non-profit, business, and government users [2].

The Earth Engine is also a host of satellite imagery and stores it in public data archives covering historical earth images that will return more than forty years. Images, taken daily, are then available for global data mining [4] [3].

In this land use classification analysis the method used is random foretst. Random Forest (RF) method is a method that can improve the results of accuracy, because in generating conclusions for each node is done randomly. This method is used to build decision trees consisting of root nodes, internal nodes, and leaf nodes by randomly retrieving attributes and data according to the provisions in force [11][4].

So from that research will develop a system that can be used by the forestry practitioner to analyze the classification of land cover, to become easier and faster with webgis which will later be made.

2. Methodology

This research is carried out from January to May 2019 in the geoinformatics lab of the Ibn Khaldun University Engineering Faculty. The research data used in this study is the 2015 Austin sample data and 2017 visual sample data.

The sampling area is the Central Kalimantan region which has an area of 1,142,004 Ha of oil palm plantations [1][5]. The data used is obtained from the 2015 outsat sample data and 2017 visual sample data, using the Google Earth Engine software, aarcgis 10.3. Image classification process is a process of grouping all pixels in an image into groups so that it can be interpreted as a specific object [7][6]. Image classification is divided into two classifications, namely Supervised Classification and Unsupervised Classification. In this study, Unsupervised Classification used the classification process in each pixel to compare to see which pixels have high similarities and grouped in clusters [8][7]

The method used in this analysis is random forest:
Random Forest (RF) method is a method that can improve the results of accuracy, because in generating conclusions for each node is done randomly. This method is used to build decision trees consisting of root nodes, internal nodes, and leaf nodes by randomly retrieving attributes and data in accordance with the provisions in force. The root node is the topmost node, or commonly referred to as the root of the decision tree. Internal node is a branching node, where this node has a minimum output of two and there is only one input. While leaf nodes or terminal nodes are the last nodes which have only one input and do not have output. The decision tree starts by calculating the entropy value as a determinant of the level of impurity of the attribute and information gain value. To calculate the entropy value, use the formula as in equation 1, while the other information values use equation 2.

$$Entropy\ (Y) = -\sum (c|Y)\log 2\ p(c|Y)\ i \qquad (1)$$

Where Y is the set of cases and p (c|Y) is the proportion of the value of Y to class c.

$$InformationGain\ (Y,a) = Entropy\ (Y) - \sum |Yv|\ |Ya|\ Entropy\ (Yv) v \epsilon Values\ (a) \qquad (2)$$

Where Values (a) are all possible values in the set of cases a. Yv is a sub class of Y with class v related to class a. Y is all values that correspond to a.

3. Results and Discussion

3. 1 Analysis
In this study the classification of oil-palm, non-palm and water was carried out in Google Earth Engine, using 30 sample points in each class. The results can be seen in Figure 3.1

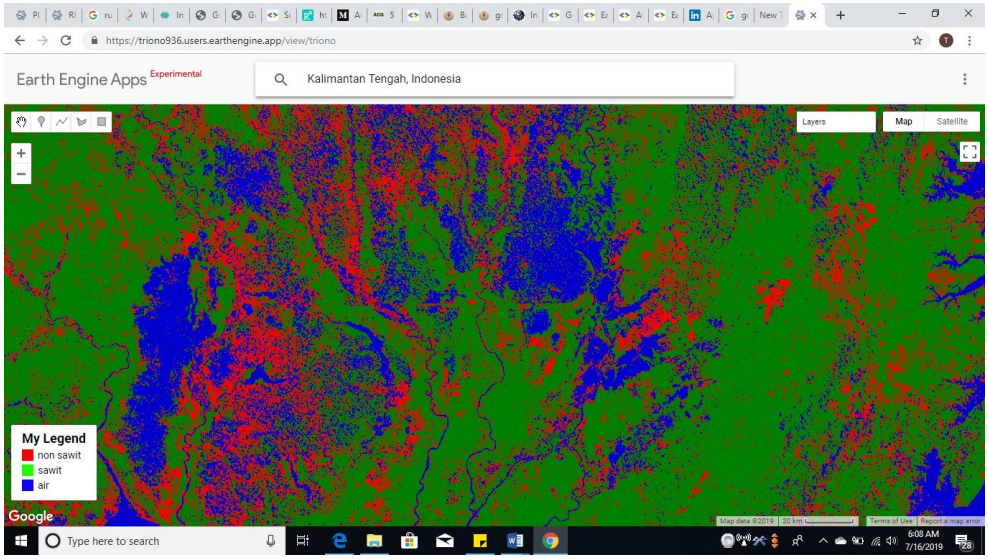

Figure 3.1 results from classification

From Figure 3.1 the results of the classification and have been published with the link https://triono936.users.earthengine.app/view/mulyatisri

Making this web using php and CI framework, and this web display can be seen in Figure 3.2 which contains the home page.

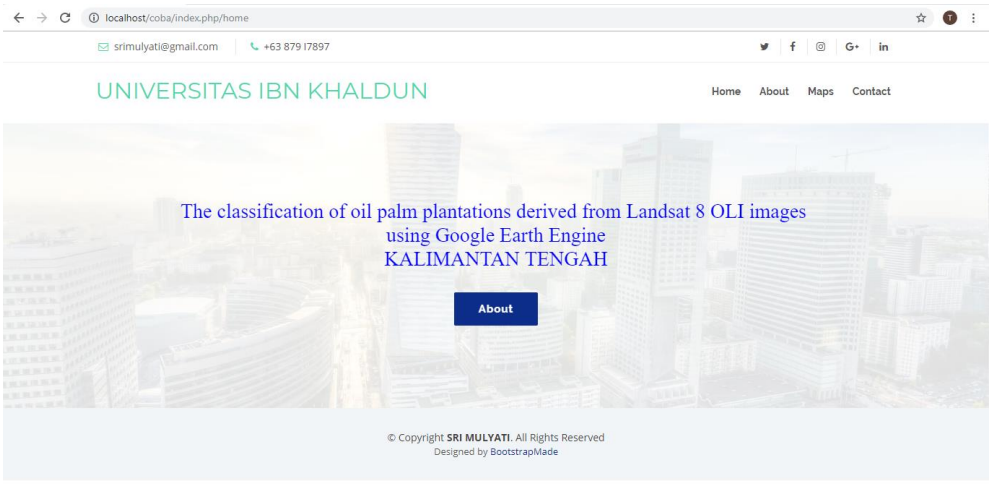

Figure 3.2 home view

After the home view there is a display about which explains a little about the analysis that is being made, as in Figure 3.3.

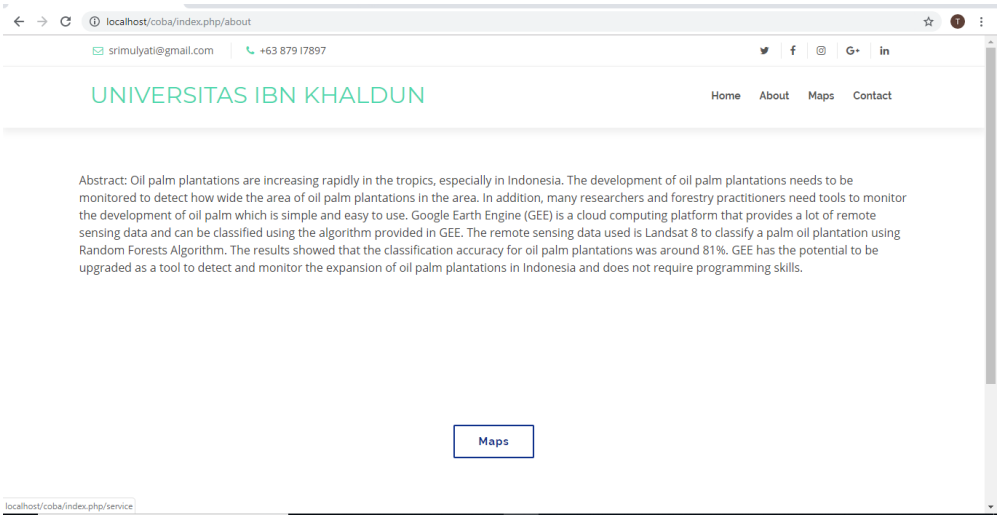

Figure 3.3 about view

After the display About, there is a map display in which there is an analysis button will contect to the link https://triono936.users.earthengine.app/view/sri, as shown in Figure 3.4

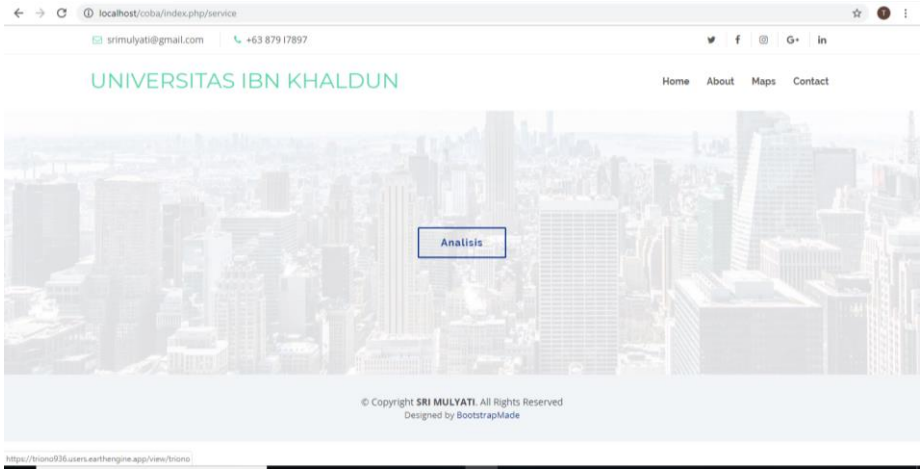

Figure 3.4 Analysis view

After the Maps view there is a contact view to send a message of criticism or suggestion made, as in figure 4.5

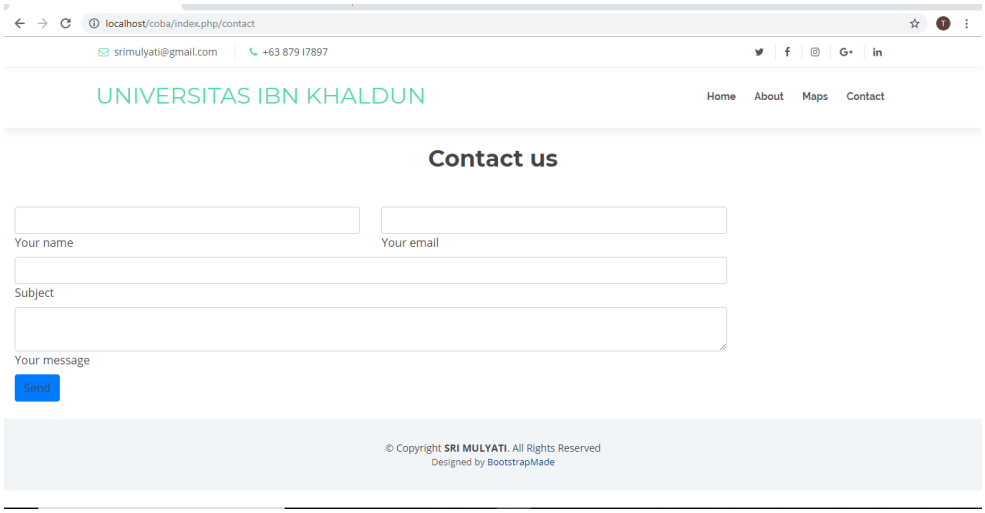

Gambar 4.5 View Contact

In this analysis a random forest method is used, with a sample of 30 in each class, the accuracy obtained from the analysis of classification of oil, non-palm oil and water is 83.33% as shown in Figure 3.6 below :

	Oil Palm	Non Oil Palm	Water	Sample Point
Oil Palm	30	0	0	30
Non Oil palm	0	16	14	30
Water	0	1	29	30
Total	30	17	43	90
User Accuracy	100	94.11764706	67.44186	
Over All Accuracy	83.33333			
N	90			
Xij	75			
X	2700			
KAPPA *Amount*	4050			
KAPPA *Dividers*	5400			
KAPPA Accuracy	75			

Figure 3.6 results from accuracy

From the results of the Kappa accuracy, there have been 14 sample errors in the Non Palm sample of 14 samples which in fact in the field of 14 samples are Water, why did an error occur? Because when sampling there are similarities in hue or color so that an error occurs or is not appropriate when in the field. and in water samples as many as 17 samples which after 17 samples were seen to be Non Palm, due to the similarity of hue or color when taking samples.

4. Conclusion

Based on the results of the classification of non-palm oil and water can be concluded:

1. Cloud computing is a new technology in this era 4.0, it can save a lot of data even though it's big data, so I use this compilation for analysts of land cover classification with the google earth engine.
2. This classification uses the google earth engine platform, Earth Engine, is a tool for analyzing geospatial information. You can analyze forest and water coverage, changes in land use, or assess the health of agricultural land, among many other possible analyzes.
3. Classifications taken include Oil Palm, Non Palm Oil, Water.

5.References

[1] Data BPS 2017 Luas Kelapa Sawit Di Indonesia

[2] Noel Gorelick, Matt Hancher , Mike Dixon , Simon Ilyushchenko , David Thau, Rebecca Moore, 2017. *Google Earth Engine: Planetary-scale geospatial analysis for everyone*. Googl Inc., 1600 Amphitheater Parkway, Mountain View, CA, 94043, US.

[3] Jun Xiong , Prasad S. Thenkabail, Murali K. Gumma , Pardhasaradhi Teluguntla , Justin Poehnelt, Russell G. Congalton, Kamini Yadav, David Thau, 2017. *Automated cropland mapping of continental Africa using Google Earth Engine cloud computing. aU.S. Geological Survey (USGS), 2255, N*. Gemini Drive, Flagstaff, AZ 86001, USA.

[4] Andrii Shelestov, Mykola Lavreniuk, Nataliia Kussul, Alexei Novikov and Sergi Skakun. 2017, *Exploring Google Earth Engine Platform for Big Data Processing: Classification of Multi-Temporal Satellite Imagery for Crop Mapping*, Department of Geographical Sciences, University of Maryland

[5] Data BPS 2017 Luas Kelapa Sawit Di Kalimantan

[6] Janice Ser Huay Lee, Serge Wich, Atiek Widayati, Lian Pin Koh, 2016. *Detecting industrial oil palm plantations on Landsat images with Google Earth Engine*. Asian School of the Environment, Nanyang Technological University of Singapore, Singapore

[7] C. Chein-I and R. H., *"An Experiment-Based Quantitative and Comparative Analysis of Target Detection and Image Classification Algorithms for Hyperspectral Imagery,"* in on *Geoscience and Remote Sensing*, IEEE Trans. , 2000.

[8] Fransiska Amalia Kurniawan, Adiwijawa, Angelina Prima Kurniati, 2011. *Analisis Dan Implementasi Random Forest Dan Classification Dan Regression Tree (Cart) Untuk Klasifikasi Pada Misuse Intrusion Detection System*. Teknik Informatika, Fakultas Teknik Informatika, Universitas Telkom.

[9] Lillesand and Kiefer, "Penginderaan Jauh dan Interpretasi Citra Penginderaan Jauh," in *Penginderaan Jauh dan Interpretasi Citra Penginderaan Jauh*, Yogyakarta, Gadjah mada University Press, 1998.

[10] Andrii Shelestov, Mykola Lavreniuk, Nataliia Kussul, Alexei Novikov, and Sergii Skakun, 2017. *Exploring Google Earth Engine Platform for Big Data Processing: Classification of Multi-Temporal Satellite Imagery for Crop Mapping.* Department of Space Information Technologies and Systems, Space Research Institute (NASU-SSAU), Kyiv, Ukraine

[11] Rizky Mulya Sampurno, Ahmad Thoriq, 2016. *Klasifikasi Tutupan Lahan Menggunakan Citra Landsat 8 Operational Land Imager (Oli) Di Kabupaten Sumedang (Land Cover) Classification using Landsat 8 Operational Land Imager (OLI) Data in Sumedang Regency)* Departemen Teknik Pertanian dan Biosistem, Fakultas Teknologi Industri Pertanian, Universitas Padjadjaran

[12] Heru Noviar,Ita Carolita, Joko Santo Cahyono, 2012. *Uji Akurasi Training Sampel Berbasis Objek Citra Landsat Di Kawasan Hutan Provinsi Kalimantan Tengah*. Pusat Pemanfaatan Penginderaan Jauh, LAPAN .

Consecutive Dry Days and Peatland Fires in Ogan Komering Ilir Regency

Winarno*, Siti Arfah, Anisah, Afifuddin, and Syaefudin
Agency for The Assessment and Application of Technology (BPPT)
Jakarta, 10340, Indonesia
winarno@bppt.go.id

Abstract. The most influential factors on causing peatland fires in Ogan Komering Ilir Regency is the human factor. However, the climate factor such as temperature, humidity, rainfall, and wind play an important role to trigger a fire. The absence of rainfall, as one of the main forms of precipitation, causing a drought. Drought is indicated by Consecutive Dry Days (CDDs). Precipitation data from the European Centre for Medium-Range Weather Forecasts (ECMWF) and peatland fires occurrence data from the Regional Disaster Management Agency (Badan Penanggulangan Bencana Daerah - BPBD) from 2016 to 2018 has been used. Spatial analysis with spatial join analysis and statistical analysis with correlation analysis was used to know the relationship between CDDs and peatland fires. The result showed that there was a weak correlation between burned area and total precipitation in 2017. The burned area and CDDs in 2016-2018 also show weak correlation, and there was no significant correlation between CDDs and total fire occurrence in 2016-2018. Hence, CDDs did not directly influence the occurrence of peatland fires but can indicate how wide the burned area. Hopefully, this study would provide the stakeholders with appropriate policies in handling peatland fires based more on human activities and dry days.

Keywords: Consecutive Dry Days, Peatland Fire, Burned Area, Precipitation

1. Introduction

The peatland fires occur nearly every year in Indonesia. The most severe fire occurred in 1997 and 2015, coinciding with the peak event of El Nino. It was recorded that in the latest El Nino, about 850.000 ha of peatland in Sumatera and Kalimantan had burnt, including in commercial plantations and degraded peat landscapes [1]. The losses are extremely high, not only affect environmental damage but also affect human health. The occurrence of peatland fires is influenced by many factors including weather conditions, human activities, land use, fuel characteristics, fire management activities, and climate change [2,3]. Although human activity is a significant driver for the fire activity, there is an inter-annual variability that suggests that external factors may also be influencing the number of fires such as rainfall anomalies [4]. Many studies showed that drought or less precipitation has a positive correlation with the occurrence of peatland fires [e.g.:2-5].

Drought or less precipitation could be explained by Consecutive Dry Days (CDDs). CDDs means the maximum number of consecutive days with precipitation less than a certain threshold which varies [6,7]. The fire which burns certain area on a day without precipitation is more than ten times larger than the fire on a day with precipitation before the fire occurrence [2]. The study showed that the number of consecutive days has a greater association with the size of large fires (>100 ha) but has less influence on the size of small fires [2].

Ogan Komering Ilir (OKI) is one of the regency in South Sumatera which experienced the biggest fire in 2015. About 377.335 hectares was burnt or 51,23% of the total burnt area in South Sumatera [8]. According to the Regional Disaster Management Agency (BPBD) data from 2016 to 2018, there are 300 peatland fire occurrences in OKI and mostly happen in the dry season. Based on many studies, weather conditions surely play a critical role in setting conditions favorable for fire occurrences, and their effect on particular fire can be inferred from antecedent weather conditions at the time when a fire occurs [2].

Therefore this study aims to find the relationship between precipitation and peatland fire occurrences in OKI, based on historic fire data from 2016 to 2018. We hypothesis that the peatland fire occurrences will be correlated with the precipitation, where the lower precipitation the wider area will be burned, the more Consecutive Dry Days happen the more fire will occur and the wider area will be burned. If there is a significant correlation, the losses could be reduced with the development of the technological instrument and forecasting method to prevent the fire.

2. Material and Methods

2.1. Study Area

The study area was located in OKI, South Sumatera. It lies between $2^0$30' N – $4^0$15' S and $104^0$20' – $106^0$00' E. It has 1.704.202,96 hectare which about 54% of its area is peatland [9]. Generally, the area of OKI has a flat up to tilted topographic shape with a slope for about 0-3% and a wavy topographic shape for about 15-25%. OKI is a swampy lowland area with a swamp area approximately 75% and a land area of 25% with an average height of 10 meters above sea level. OKI has a tropical climate with temperature ranging from 24,4^{0}C – 32,9^{0}C. The dry season occurs from May to October and the rainy season start from November to April [10]. The figure below shows the location of the study area.

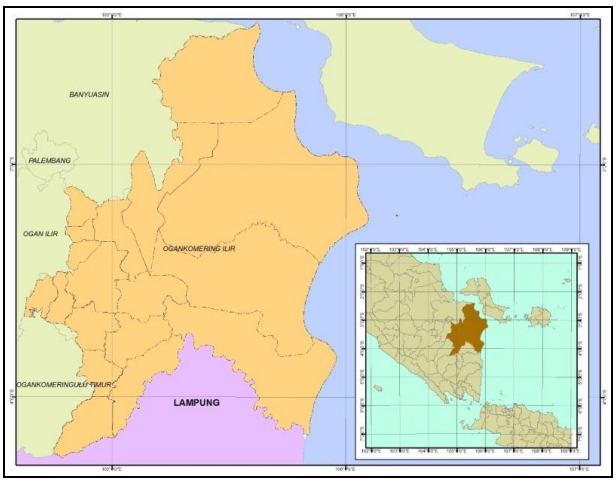

Figure 1. Study area

2.2. Peatland Fire Occurrence and Precipitation Data

In this study, the peatland fires occurrence and burned area data were collected from BPBD and Manggala Agni OKI Daops III. While the precipitation data were collected from the ERA-Interim European Centre for Medium-Range Weather Forecasts (ECMWF). ERA-Interim is the latest global atmospheric reanalysis produced by the ECMWF. Reanalysis is a process of assimilation from various models and observations which produce the best global estimation of atmospheric, wave, and oceanographic parameters [11]. From 2016 to 2018, there are a total number of 300 peatland fires occurrence spread in 12 of 18 districts in OKI. For total burned area data per year scattered in several districts as follows:

Table 1. Burned area data

District	Burned area (ha)			
	2016	2017	2018	Total
Cengal	1	31.68	181.5	214.18
Jejawi	0	23.6	27.75	51.35
Kayu Agung	0.5	0.75	8	9.25
Lempuing	0	96	0	96
Pampangan	0	6.5	24	30.5

District	Burned area (ha)			
	2016	**2017**	**2018**	**Total**
Pangkalan Lampam	4.31	51.3	240.2	295.81
Pedamaran	0	0.5	191.5	192
Pedamaran Timur	5.5	7	106.25	118.75
Sungai Menang	4	10.5	136.5	151
Tanjung Lubuk	6	345.159	108.5	459.659
Teluk Gelam	0	2	6.5	8.5
Tulung Selapan	0	7.65	280.2	287.85
Total	21.31	582.639	1310.9	1914.849

The precipitation dataset that collected in daily precipitation come from 2016 to 2018. Precipitation in the day fire occurs and total precipitation from 30 days before the fire was used to be analysed. Moreover, the CDDs is counted from precipitation data with the threshold of 6 mm/day also had been used. This threshold was selected by some consideration. In the United States's national fire danger rating system (NFDRS), a drought index is calculated based on the number of consecutive days with precipitation 5.0 mm. In the Canadian fire danger rating system (CFDRS), the threshold precipitation for drought was 2.8 mm [2]. In Indonesia, the standard drought index from the Indonesia Weather and Meteorology Bureau (BMKG) was below 1.0 mm. All of the three standard use precipitation data acquired from the weather station which has less error. Considering the ECMWF data is an assimilation data which could have more errors, therefore the threshold below 6.0 mm is chosen.

2.3. Spatial and Statistical Method

2.3.1. Spatial Analysis

The spatial analysis used in this study was spatial join analysis, which correlating fire occurrences location, a grid of total precipitation and CDDs based on their nearest neighbor. Fire occurrences data are in the form of points and contain information such as location geometric, administrative, date of fire occurrence and burned area in 2016-2018. Meanwhile the precipitation data in the form of grid point which covers OKI and its surrounding regency. The available precipitation data in the form of 3-hour daily data. Therefore to get precipitation data when a fire occurs, spatial join using the nearest neighbor had been used, so that the precipitation data ID is obtained closest to the fire location. This ID is used to retrieve precipitation data for the past 30 days only at the fire location.

2.3.2. Statistical Analysis

To measure linear relationships between two random variables, correlation analysis was used. Correlation analysis attempts to measure the strength of relationships between two variables and its direction through a single number called a correlation coefficient and measure the significance of the relationship. According to Walpole et al [12], the definition of correlation as follows: Let X and Y be a random variable with covariance σ_{XY} and standard deviations σ_X and σ_Y respectively. The correlation coefficient of X and Y is:

$$\rho_{XY} = \frac{\sigma_{XY}}{\sigma_X \sigma_Y}$$

The correlation coefficient satisfies the inequality $-1 \leq \rho_{XY} \leq 1$. It assumes a value of zero when σ_{XY} = 0. Where there is an exact linear dependency, say $Y = a + bX$, ρ_{XY} = 1 if $b > 0$ and ρ_{XY} = -1 if $b < 0$. It is important to remember that the correlation coefficient between two variables is a measure of their linear relationship and that a value of $\rho = 0$ implies a lack of linearity and not a lack of association.

3. Result and Discussion

The number of peatland fire in OKI based on the data are 11 occurrences in 2016, 70 occurrences in 2017 and 219 occurrences in 2018. In Figure 2, it can be seen that peatland fire in OKI commonly occurred in July until October with different peak time. In 2016 the most peatland fire occurred in August, while in 2017 and 2018 most peatland fire occurred in September. The difference peak time in 2016 could happen because the weak La Nina event occurs in the last quartile in 2016. The weak La Nina caused increasing precipitation start from September to December 2016 [13]. This also explains why the precipitation during the fire period in 2016 in no zero precipitation (Figure 4).

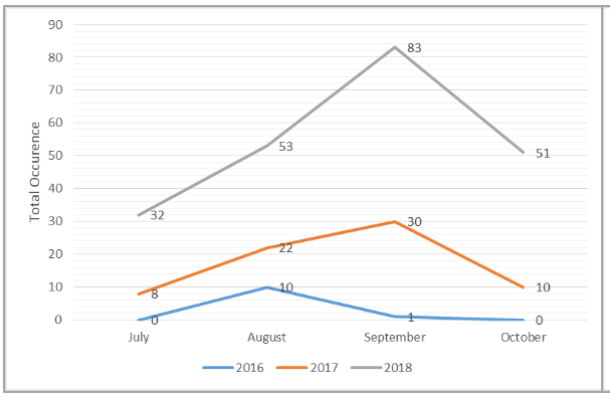

Figure 2. Peatland fire occurrence

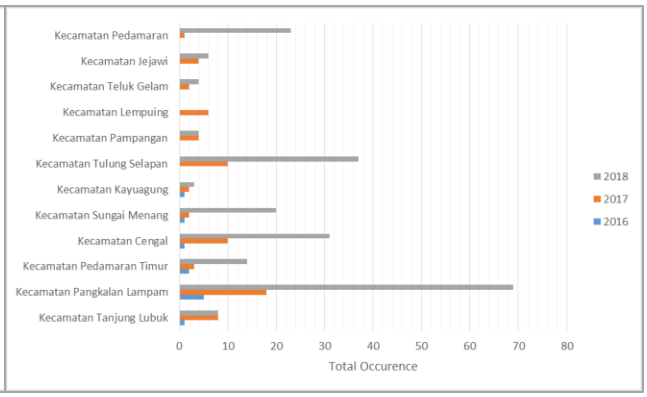

Figure 3. Peatland fire location

Based on the location, peatland fires in OKI mostly occurred in Pangkalan Lampam District, Tulung Selapan District, and Cengal District as can be seen in Figure 3. The three districts are known as an with a vast swamp. Moreover, there are rice fields landuse in several areas in these districts. The presence of rice field indicates that areas in OKI Regency are prone to burn because of the existence of sonor farming system. Sonor is a local knowledge of farming system which is the cultivation of rice in peatlands by burning - seed sowing - and harvesting mechanism with no land preparation [14]. As the most fire happens in Pangkalan Lampam district, which around one three of its area is rice fields.

Related to precipitation and CDDs, the peatland fire occurence each year was made as follows:

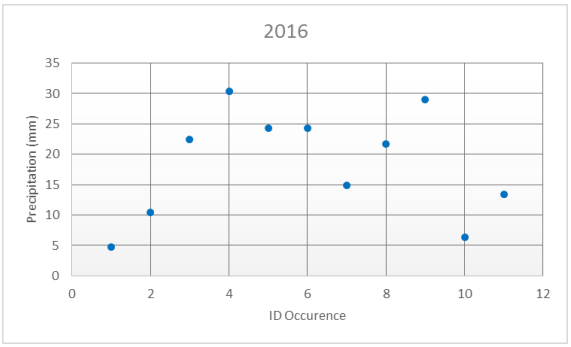

(a)

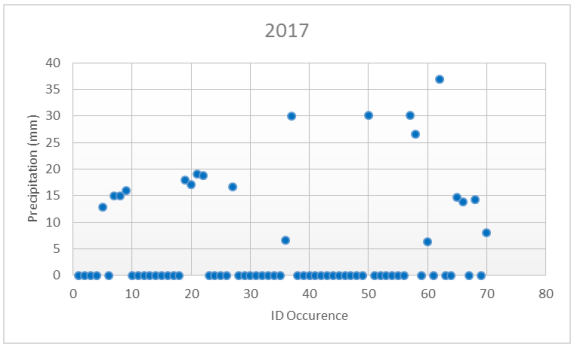

(b)

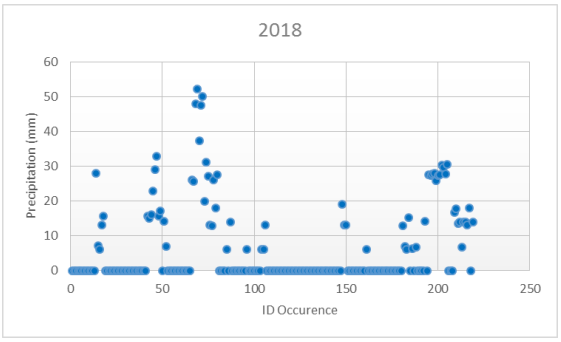

(c)

Figure 4. Profile of ID Occurrence and Precipitation based on year, (a). 2016, (b). 2017, (c). 2018

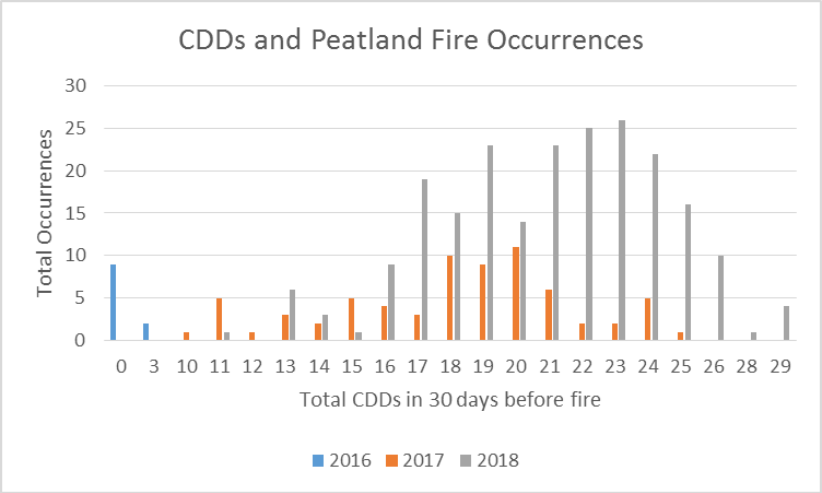

Figure 5. CDDs and Peatland Fire Occurrences

The precipitation in Figure 4 was obtained from precipitation on the day of each fire occurences, while the CDDs in Figure 5 calculated based on a predetermined threshold. It can be seen that according to point peatland fire location (ID Occurrence), there is no data with zero precipitation in 2016 (La Nina effect). Whereas in 2017, there are 50 of 70 occurrences or more than 71% which have zero precipitation. In 2018, there are 151 from 219 occurrences or more than 68% which have zero precipitation. In terms of CDDs, the most fire occurs with 17-25 CDDs.

From these data, we can see that mostly fire happen in zero precipitation and many days of CDDs. Our hypothesis that it should be the more zero precipitation and CDDs occur the more peatland fire will occur. Furthermore the more peatland fire occur the more burned area. But as could be seen in Figure 4, there are also some fire occur in no zero precipitation. If the data showed like this, will there be a correlation? To confirm this, the correlation between the burned area and the total precipitation for 30 days ago before the fire, CDDs and total occurrence, and CDDs and burned area was made. The result can be seen in Table 2 and Table 3 below:

Table 2. Correlation between burned area and total precipitation 30 days ago before fire

Correlation	**Burned Area**			
	2016 (N=11)	2017 (N=70)	2018 (N=219)	2016-2018 (N=300)
Total Precipitation	0,085	**-0,301**	0,007	-0,108

Table 3. Correlation between CDDs and total occurrences, CDDs and burned area

Correlation	CDDs			
	2016 (N=11)	**2017 (N=70)**	**2018 (N=219)**	**2016-2018 (N=300)**
Total Occurence	-	0,169	0,214	0,200
Burned Area	0,192	**0,434**	0,001	**0,136**

In the two tables above, correlation coefficient that accepted only the one with bold. The other correlation value has no significance. The correlation between total precipitation and burned area has value -0,301 which can be said as weak correlation. The negative sign showed that the lower precipitation the wider area will be burned, which is consistent with our hypothesis. However the correlation only valid in 2017 data.

The correlation between CDDs and total occurrence has no significance at all. As for CDDs and burned area, the correlation has value 0,434 for 2017 data and 0,136 for 2016-2018 data. The positive sign in this correlation showed that the more CDDs happen the wider area will be burned. The same problem like the previous correlation, the value only valid for 2017 data and total data this time, this indicates some possibility about the data as well as the fire occurrence.

First, the quality of peatland fires data needs to be checked and validated. As the data were made in daily of fire occurrence by the field officer, it could be the fire that can not be extinguished in a day being recorded again in the next day with different size of burned area. If this happen, then fires data would not give a valid correlation. Second, we found that many of burned areas in OKI have a size of fewer than 10 hectares. According to Chen [2], drought has a significant influence on the size of large fires (>50 ha) but not much effect on the size of small or moderate fires. Therefore, this could explain why the correlation is hard to find. Last, it is commonly known that most of the peatland fires caused by human. The weather condition by this case is precipitation has a role only in setting conditions favorable for fire occurrences. So, it is possible in 2018 for example human just trigger a fire randomly.

The correlation between precipitation and burned area or CDDs and burned area by this calculation has small value but it doesn't mean precipitation has no influent in peatland fire. Precipitation influences on peatland fire through changing fuel moisture content [15]. Besides that, the study in Yunan [2] about the correlation between CDDs and forest fire from 1.983 historic fires data showed the correlation value around 0,29-0,33. This means that correlation between weather condition and fire is about that number.

However, peatland fires that happen in OKI surely have a weak correlation. This also convinced by Figure 6 below that showed accumulative month precipitation toward the fire location. The dots which show fire location lies in variate precipitation. At first, we would think that fires will happen only in less precipitation, but even in high precipitation the fire still occurs.

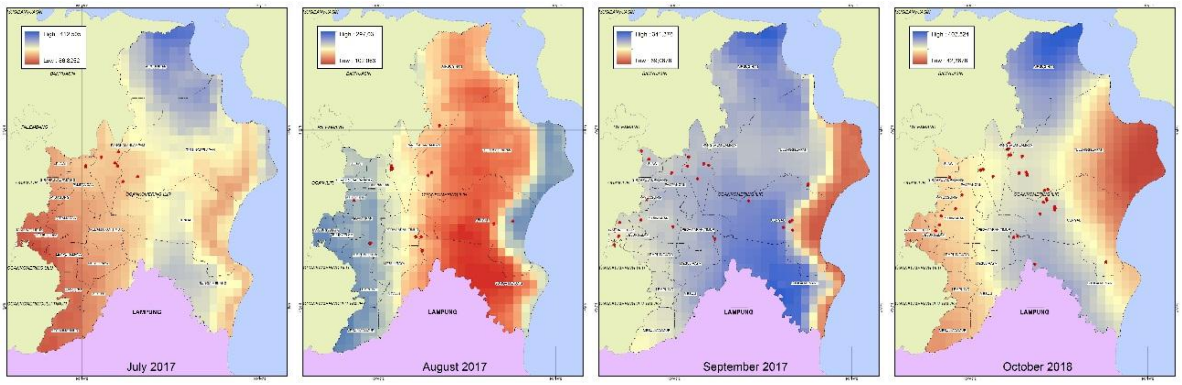

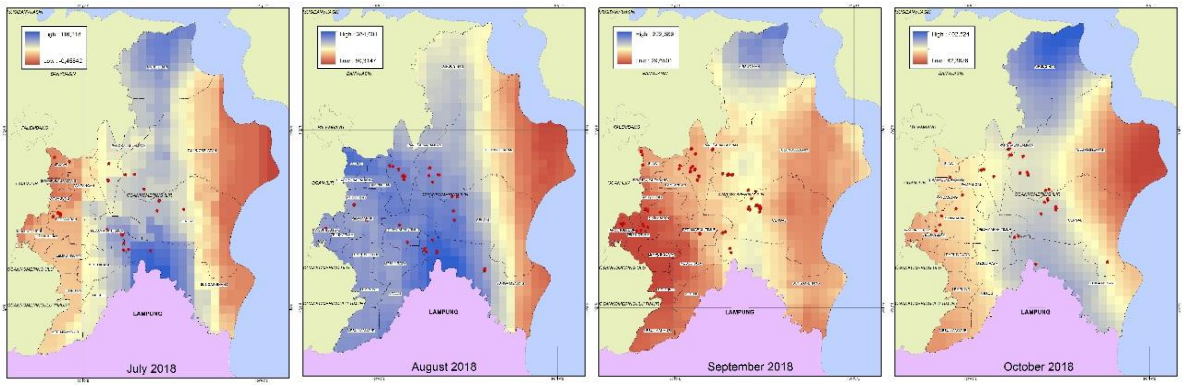

Figure 6. Accumulative month precipitation and fire location in 2017 and 2018

4. Conclusions

According to the result, the following conclusion were drawn.

- Total precipitation 30 days before fire occurrences have a weak correlation with burned area. However, this correlation showed the negative sign which means the lower precipitation the wider area will be burned.
- Total CDDs that count from 30 days before fire occurrences have no correlation with total occurrence. Peatland fire could occur anytime even in high precipitation.
- Total CDDs that count from 30 days before fire occurrences have a weak correlation with burned area. The correlation has a positive sign which means more CDDs happen the wider area will be burned.

Acknowledgment

This research was funded by the Agency for The Assessment and Application of Technology (BPPT). The authors would like to thank all reviewer of *Center for Regional Resources Development of Technology* (PTPSW) for warm discussions.

References

[1]. Giesen, W., and Sari, E.N.N., 2018. *Tropical Peatland Restoration: The Indonesian Case. Technical Report for Tropical Peatland Restoration*. doi: 10.13140/rg.2.2.30049.40808

[2]. Chen, F., Fan, Z., Niu, S. and Zheng, J., 2014. *The Influence of Precipitation and Consecutive Dry Days on Burned Areas in Yunnan Province, Southwestern China*. Hindawi Open Access: Research Article of Advance in Meteorology Volume 2014. doi:10.1155/2014/748923.

[3]. Thoha, A.S., Saharjo, B.H., Boer, R., and Ardiansyah, M., 2019. *Characteristics and Causes of Forest and Land Fires in Kapuas District, Central Kalimantan Province, Indonesia*. Biodiversitas. Volume 20 No. 1.pp. 110-117. doi: 10.13057/biodiv/d200113.

[4]. Ceccato, P, I.N., Jaya, S., Qian, J.H., Tippet, M.K., Robertson, A.W., and Someshwar, S., 2010. *Early Warning and Response to Fires in Kalimantan, Indonesia*. IRI Technical Report 10-14. International Research Institute for Climate and Society, Palisades, New York (US).

[5]. Thoha, A.S., Saharjo, B.H., Boer, R., and Ardiansyah, M., 2014. Spatiotemporal Distribution of Peatland Fires in Kapuas District, Central Kalimantan Province, Indonesia. Journal od Agriculture, Forestry and Fisheries. Volume 3 No. 3 pp.163-170. doi: 10.11648/j.aff.20140303.14.

[6]. Duan, Y., Ma, Z., and Yang, Q., 2017. *Characteristics of consecutive dry days variation in China*. Theoritical and Applied Climatology 130: 701-709. doi: 10.1007/s00704-016-1984-6.

[7]. Zolina, O., et al, 2012. *Chsanges in the Duration of European Wet and Dry Spells during the Last 60 Years*. Journal of Climate Volume 26.
[8]. Dinas Kehutanan Provinsi Sumatera Selatan, 2016. *Penyusunan Informasi Areal Bekas Terbakar Tahun 2015 Provinsi Sumatera Selatan*.
[9]. Peta Gambut Skala 1:50.000. Balai Besar Litbang Sumber Daya Lahan Pertanian (BBSDLP)
[10]. Badan Pusat Statistik Kabupaten Ogan Komering Ilir. 2018. *Ogan Komering Ilir dalam Angka 2018*. Ogan Komering Ilir Regency.
[11]. D.P. Dee, et al. 2011. *The ERA-Interim reanalysis: configuration and performance of the data assimilation system*", Quarterly Journal of the Royal Meteorological Society, pp 553-598.
[12]. Walpole, R. E., Myers, R. H.,Myers, S. L., Ye, K, 2007. *Probability & Statistics for Engineers & Scientists*. Eight Edition, Pearson Education International.
[13]. Athoillah, I., Sibarani, R.M., and Doloksaribu, D.E. 2017. *Spatial Analysis of the 2015 Strong El Nino and the 2016 Weak La Nina (Their Influence on Humidity, Wind and Rainfall Conditions in Indonesia)*. Jurnal Sains dan Teknologi Modifikasi Cuaca, Vol. 18 No. 1, hal 33-41.
[14]. Mulyanto. 2018. *The Sonor Farming Tradition on Forest and Land Fire in Ogan Komering Ilir Regency, South Sumatera*. Advance in Social Science, Education and Humanities Research, volume 323.
[15]. Van Wagner, C.E. 1974. *Structure of the Canadian Forest Fire Weather Index*. Canadian Forestry Service, Ottawa, Canada.

The evaluation of changes in land values at Wonorejo Mangrove tourism area (case study: Rungkut Sub-district, Surabaya District)

Udiana Wahyu Deviantari[1], **Yanto Budisusanto**[1], **Yaasmiin Pratita Apsari**[1]

Department of Geomatics Engineering, Institute of Technology Sepuluh Nopember Surabaya, ITS Raya Street, 60111 Surabaya, Indonesia

e-mail: dianada87@gmail.com

Abstract. Rungkut Subdistrict is one of the sub-districts that experienced rapid economic and development. This can be proven by the existence of a recreational facility in Rungkut Sub-district, namely Mangrove Wonorejo Tourism. The impact of the development of Wonorejo Mangrove Tourism as a public facility, will affect changes in the surrounding land value. In knowing the magnitude influence of Wonorejo Mangrove Tourism development on changes in the value of surrounding land, it was carried out through the calculation of land value changes in the area around Mangrove Tourism. By comparing the 2018 Tax Object Selling Value (NJOP 2018) with the Market Value in 2019. The results of the evaluation of changes in land values using spatial analysis obtained by Zone Y23 on Wonorejo Timur Street as a residential zone with the highest increased by 1345%, Zone Y30 on Raya Wonorejo Street as residential zone with the lowest increased by 74.19%, and the rest of the other zones who also experienced a percentage increase in the value of the land. This proves that the development of Wonorejo Mangrove Tourism has an influence on the value of surrounding land and also influences the increase of Tax Object Selling Value in the region. The changes value that occur due to several factors, such as changes in land functions, infrastructure development, location factors, and development of Mangrove Tourism, and etc.

1. Introduction

Rungkut sub-district, is increasingly in demand by the community. This can be proven by the development in one of the Rungkut sub-districts, namely around Mangrove Tourism. The impact of the development of Mangrove Tourism as a tourist facility and recreational facility in Rungkut Sub-district will affect the land value pattern around it. The land value pattern around Mangrove Tourism also affects the market prices around the area in the form of changes in land values. The market price is a price that is used as a reference for the community to make buying and selling transactions [1] Changes in land values that occur can be influenced by several factors, among factors that influence is the location factor. Location includes availability of accessibility and nature/environment situation [2].

In this study a calculation of land value changes in the area around Mangrove Tourism was carried out. By comparing the 2018 Tax Object Selling Value of the 2019 Land Market Value obtained after processing the sample data obtained during the field survey. This was done to evaluate changes in the value of land in the Wonorejo Mangrove Tourism Area in addition to knowing the percentage increase in land value of the 2018 Tax Object Selling Value (NJOP) in the area determined by PERWALI Kota Surabaya.

The existence of this research is expected to be able to help the planning and development of Wonorejo Mangrove Tourism in Rungkut Subdistrict and to provide a policy direction on land related to the development and solutions to the utilization of land area around Mangrove Tourism obtained from field surveys such as improving the facilities.

2. The Methods

2.1. Study Area

The location used in this research is in Rungkut Sub-district, Surabaya District. Rungkut Sub-district has an area of 2,104,182 Ha, as the fourth largest of the 31 Sub-Districts in Surabaya District which is geographically located at coordinates 07˚18`20 "- 07˚20`00" LS and 112˚46`- 112˚50 `BT.

Rungkut consists of several urban villages including Penjaringansari, Kedungbaruk, Kali Rungkut, Wonorejo Urban village, Rungkut Kidul, and Medokanayu Urban village. This research center is centered around Mangrove Tourism and the data used in the study were high resolution photo imagery for Surabaya District as shown in Figure 1 below:

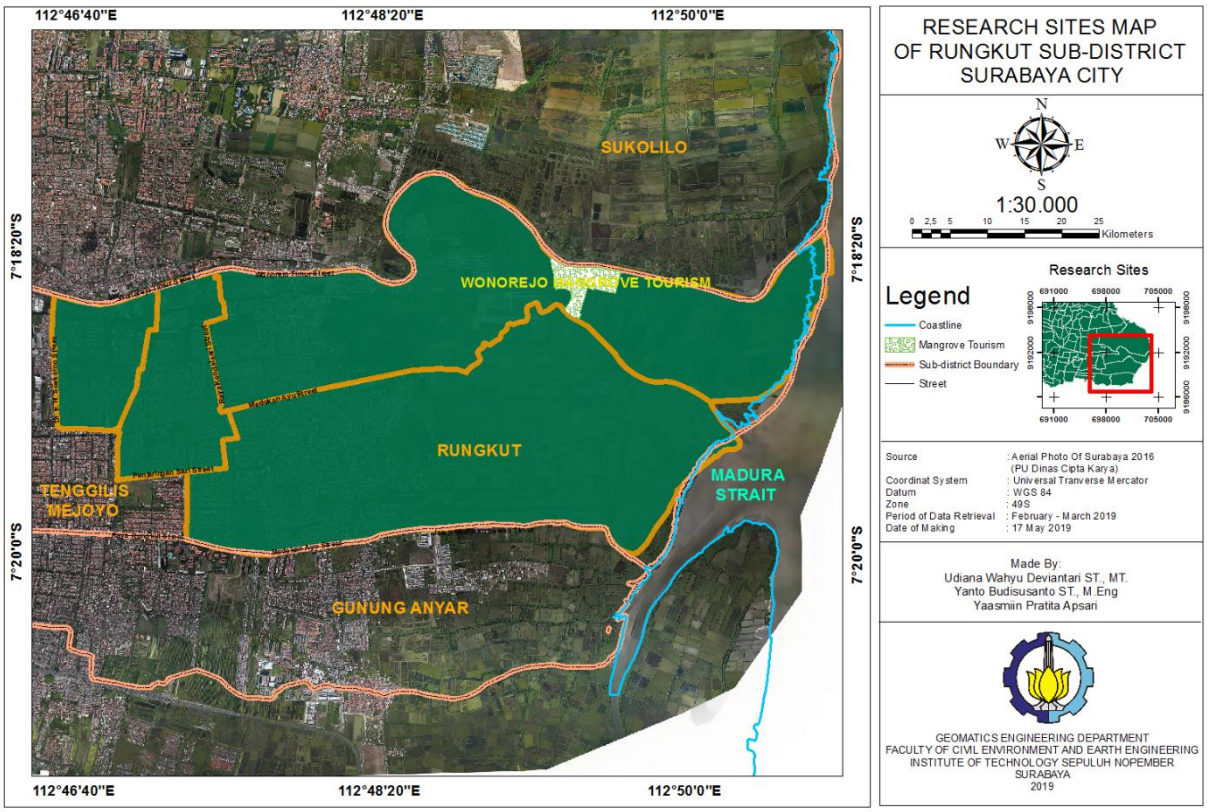

Figure 1. Rungkut Sub-district in Surabaya District.

2.2. Zone Delineation

At this stage a new zone imaginary boundary is created that contains land value data. The making of this new zone is based on the principle of making an imaginary boundary of ZNT in the [3] which groups land parcels in one ZNT by considering the following matters:

1. Indications of similar land values
2. Has similar characteristics
   - Accessibility
   - Land allotment (zoning)
   - Identification of land value determinants

   Zone delineations are used for planning field surveys in taking sample points in the field [4].

2.3. Land Value Data
Collecting information on land values is obtained through surveys directly in the field. Then processing the data is grouped according to each zone formed based on the similarity of characteristics/types of use of the land.

2.3.1. Calculation of NIR In Each Zone
After obtaining the appropriate land and zoning values, then the determination of the Average Indication Value (NIR) is done by summing at least 3 values of the land data and taking the average so that it gets the NIR in each zone. If in the delineation of the new zone there are several zones that do not have data on selling prices, then for ZNT, the determination of NIR is done by using comparative data from the existing zone, the data used as a comparison of at least 3 zones around (ZNT).

2.3.2. Comparing NIR of NJOP 2018 Zone to Market Price 2019 Zone
The NIR results obtained from the calculation of 2019 market prices in each zone that has been formed are then compared with the NIR from NJOP 2018 obtained from the Surabaya City Tax Service, to evaluate changes in land values in the Mangrove Tourism Area.

2.3.3. Analysis and Evaluation of Changes in Land Value Around Mangrove Tourism
Analysis was carried out by spatial analysis of the area studied around the Mangrove Tourism District of Rungkut Surabaya in 2019 against the influencing factors. A plot of land will have a high value or price if it is located in a strategic location (high economic activity, easily accessible location and complete infrastructure available) [5]. This is done to see whether there is a significant influence on the surrounding land values from several factors such as accessibility, distance to the CBD, type of land use, tourism and so on.

3. Results and Discussion

3.1. Result of Zone Delineation
The delineation of this zone is based on the [6] where the zone of land value is limited by the limits of ownership/ownership of tax objects or natural borders (Imaginary). In making this new zone, the grouping of plots of land in one zone of land value is carried out by paying attention to things like the following:
a) Indications of similar land values
b) Having similar characteristics, including:
- Land Position.
- Land allotment (Zoning).
- Data source
- Land Status in this study is limited to SHM, HGB, Check, Girik, Bank Certificates.

As shown in Figure 2 below:

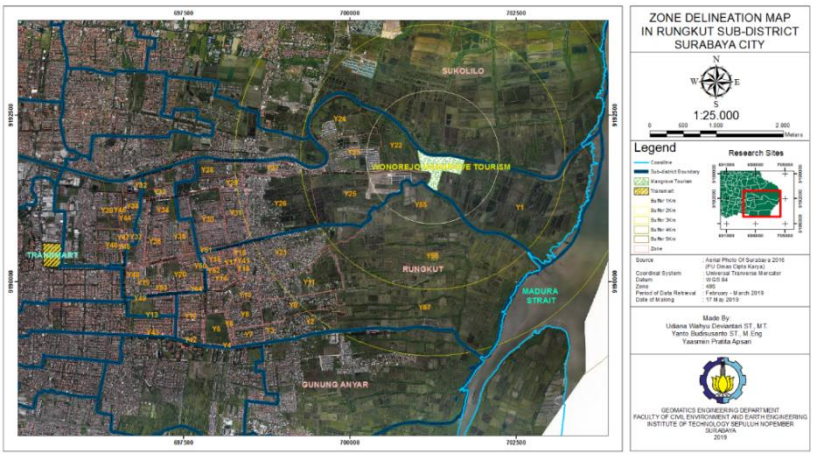

Figure 2. Result of Zone Delineation.

3.2. *Calculation of Land Market Value*

From the indications the value of the land obtained has not yet been immediately processed. The processing is carried out to obtain data in the form of Land Market Value Indications. The results of processing Land Market Value Indications can be seen in table 1 below.

Table 1. The Results of Calculation of Land Market Value

Sample Point	***Zone***	***Location***	***Type of Use***	***Indication of Land Market Value/m²***
ID230	Y1	East Wonorejo Street, Wonorejo	Pond	Rp. 916.667
ID239				Rp. 1.200.000
ID240				Rp. 1.649.000
ID9	Y26	Medayu Utara Street, Wonorejo	Settlement	Rp. 6.665.005
ID12				Rp. 7.713.280
ID19				Rp. 7.504.441
ID160	Y44	Dr.Ir.H.Soekarno Street, Kedung Baruk	Commercial	Rp. 43.364.571
ID187				Rp. 41.817.030
ID188				Rp. 40.227.120
ID56	Y15	Pandugo Street, Medokan Ayu	Housing	Rp. 6.565.000
ID57				Rp. 6.600.000
ID58				Rp. 6.333.333

From the calculation of the sample data, the highest Land Market Value is obtained in zone Y44 with a value of Rp.43.364.571/ m^2 located on Dr. Ir. H. Soekarno Street. The highest value can be obtained because the sample is a commersial zone located on the edge of the main road, with a strategic location, close to Dr. Ir. H. Soekarno Street, and has the main access to go to Mangrove Tourism and CBD in the form of Transmart Rungkut. For the lowest Land Market Value at zone Y1 with a value of Rp. 916.667/m^2 located on East Wonorejo Street. This value is obtained because the sample points in the form of ponds with limited access to roads and far from the CBD center as well as settlements and plantations are some of the supporting factors towards the high value of land in the region.

3.3. Calculation of Average Indication Value (NIR)

The calculation of the Average Indication Value (NIR) in the zone can be done using the zone around it, this is based on the [3] concerning the arrangement of calculation of the Land Value Zone. Some of the NIR Calculation Results from other NIR Zones can be seen in table 2 below:

Table 2. The Results of Calculation of Average Indication Value (NIR)

Zone	***Location***	***Comparison Zone***	***Average Indication Value (NIR) (Rp/m²)***
Y6	Medokan Sawah Street, Medokan Ayu	Y4 Y42 Y43	Rp. 22.299.088
Y17	Medokan Asri Utara Street, Medokan Ayu	Y14 Y15 Y16	Rp. 5.819.929
Y47	Dr.Ir.H.Soekarno Street, Kedung Baruk	Y44 Y45 Y46	Rp. 35.299.354
Y52	Penjaringan Sari Street, Penjaringan Sari	Y50 Y51 Y53	Rp. 14.756.098
Y49	Penjaringan Sari Street, Penjaringan Sari	Y42 Y43 Y48	Rp. 26.755.271
Y18	Wonoayu Street Medokan Ayu	Y16 Y17 Y51	Rp. 11.063.478

3.4. The Evaluation of Changes Land Value

The results of the Map of Land Value Changes in Mangrove Tourism Area were obtained by comparing NIR Results from processing Market Prices after processing sample data obtained when conducting 2019 field surveys of NIR from NJOP 2018, the resulting map is one form of Thematic Map, in general This map represents statistical data in the form of value levels. In this study, the representation of the colors displayed on the map can support and simplify the analysis in evaluating changes in land values that occur in the area around the Mangrove Tourism District of Rungkut. Changes in land values that occur due to several factors, such as changes in land functions, development of infrastructure, location factors, accessibility factors, distance factors to the market center / Central Business District (CBD) and development of Mangrove Tourism, and so forth. Making a Map of Changing Land Values in the Mangrove Tourism Area was conducted to determine the effect of land values on the development of Wonorejo Mangrove Tourism, also to find out the percentage increase in the value of land to NJOP in the region. The following is a figure 3 Results of Map of Changes in Land Value in Mangrove Tourism Areas to NJOP of 2019 below:

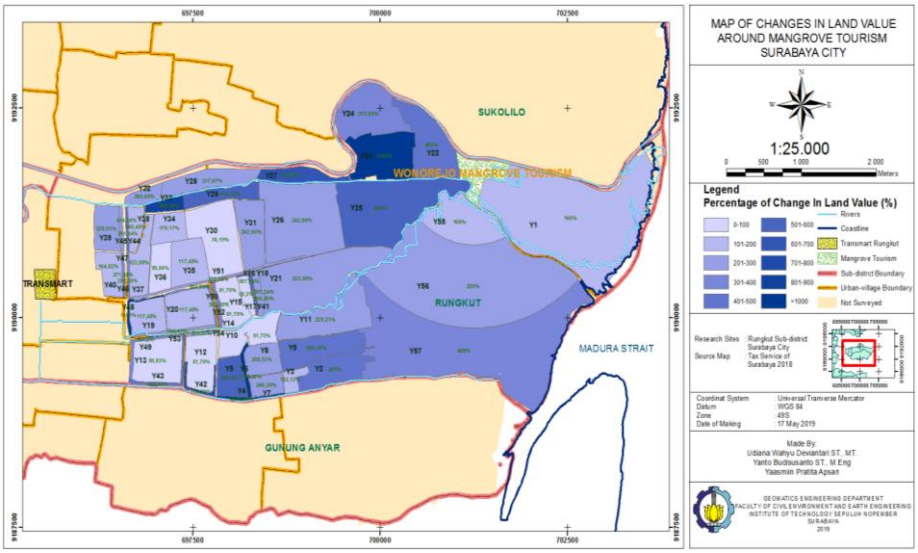

Figure 3. Map of Changes in Land Value in Mangrove Tourism.

Based on Article 6 paragraph 1 of Law No. 12 of 1985, the basis for imposition of Land and Building Tax is the Tax Object Selling Value (NJOP). The NJOP is determined through a particular analysis model based on the technical provisions in force at the Directorate General of Taxes. The procedure for determining NJOP is regulated in the Director General of Tax Decree Number: KEP.533/PJ/2000 which has been amended by the Director General of Tax Decree Number: KEP.115/PJ/2002. NJOP which is the basis for imposing Land and Building Taxes, should be in accordance with market prices (which apply in the relevant region). If NJOP does not match market prices, then market prices that should be represent land values, cannot represent land values in a particular zone. The zone is a geographical zone consisting of a group of land that has the same land value, so-called Land Value Zone (ZNT). If the average market price cannot represent the value of land in a zone it can result in mismatches in the formation of ZNT, and UN designation on several parcels of land [7].

So that, it is necessary to evaluate the percentage change in land value to determine the effect of mangrove tourism development on the surrounding land values. The results of the calculation of value changes indicate that Mangrove Tourism has an effect on the increase in NJOP Value. This is because market prices are more representative of the conditions on the ground with more determinants of land values. The highest change in land value is in zone Y23 and the lowest change in land value is found in zone Y30, both zones have the same designation as housing zone. Zone Y23 is a new zone located on Jalan Wonorejo Timur with land allotment as housing. There is a change in land value between ZNT Zone and NJOP Zone with an increase in land value of 1345%, as in table 4.10 calculation below.

Table 3. The Highest Percentage Change in Land Value of Zone 23

Zone of NJOP 2018	***Zone of ZNT 2019***	***Changes***
Rp. 614.000		
Rp. 614.000	Rp. 8.875.000	1345%
Rp. 614.000		

This highest percentage changes in Land Value can occur due to a change in land function in zone Y23 which was previously a pond land into a residential land. Changes in the function of this land are very reasonable, considering that every year population growth in each region is increasing. As well as a

factor that the Sub-district of Rungkut is one of the Sub-districts whose development is very rapid in the second largest city of Indonesia [8]. So many entrepreneurs and investors are developing their businesses, especially housing around the research area. For the lowest percentage changes in land value is at zone Y30. Zone Y30 is a new zone located on Jalan Raya Wonorejo, the land area in this zone as housing. There is no change in land function between the 2019 ZNT Zone and 2018 NJOP Zone. With an increase in land value of 74.19% as the lowest percentage increase compared to other zones, the increase calculation as in table 4.11 below.

Table 4. The Lowest Percentage Change in Land Value of Zone 30

Zone of NJOP 2018	***Zone of ZNT 2019***	***Changes***
Rp. 5.095.000		
Rp. 5.095.000	Rp. 8.875.000	74,19%
Rp. 5.095.000		

These changes are not as big as the changes in other zones, this could be due to the absence of changes in land functions between the 2019 ZNT Zone and 2018 NJOP Zone, as well as the absence of developments in the area around the Y30 zone in the form of improved road access, CBD development or physical land changes which is almost the same as the old zone (NJOP 2018). Thus, a fixed percentage increase occurs with an increase in value that is less than the other zones.

In addition to these two zones, other zones also experienced a percentage increase in the value of their land. Overall the percentage increase occurred in all zones formed as in table 5 below, it shows that there is a positive influence between the tourist areas of mangroves on the increase of the Tax Object Selling Value in 2018. Changes in values that occur can be due to several factors, such as changes in land functions, development of infrastructure, spatial utilization and development of Mangrove Tourism.

Table 5. The Evaluation of Changes in Land Values in Several Zones

Zone	***Zone of NJOP 2018***	***Zone of ZNT 2019***	***Changes***
Y4	Rp. 3.100.000	Rp. 24.625.000	694,35%
Y5	Rp. 1.032.000	Rp. 6.805.000	559,399%
Y6	Rp. 1.722.000	Rp. 22.005.000	1177,87%
Y18	Rp. 1.722.000	Rp. 11.305.000	556,504%
Y21	Rp. 1.573.000	Rp. 5.095.000	223,90%
Y22	Rp. 614.000	Rp. 4.605.000	650%
Y23	Rp. 614.000	Rp. 8.875.000	1345%
Y24	Rp. 1.573.000	Rp. 7.455.000	373,93%
Y25	Rp. 537.000	Rp. 2.508.000	367,04%
Y31	Rp. 2.176.000	Rp. 7.455.000	242,60%
Y32	Rp. 5.095.000	Rp. 18.375.000	260,65%
Y33	Rp. 1.862.000	Rp. 18.375.000	886,84%
Y35	Rp. 3.745.000	Rp. 8.145.000	117,489%
Y36	Rp. 3.745.000	Rp. 7.455.000	99,06%
Y40	Rp. 4.605.000	Rp. 12.195.000	164,820%
Y41	Rp. 1.416.000	Rp. 5.625.000	297,245%
Y43	Rp. 5.625.000	Rp. 30.345.000	439,46%
Y46	Rp. 8.145.000	Rp. 38.395.000	371,39%
Y47	Rp. 8.145.000	Rp. 35.055.000	330,387%
Y52	Rp. 3.745.000	Rp. 15.105.000	303,33%

4. Conclusion

Based on the results Changes in land values in the area around Mangrove Tourism experienced a significant increase, namely: the highest increase in the Y23 zone of the residential area by 1345%, and the lowest increase in the Y30 zone of the housing area by 74.19%. Value changes that occur can be due to several factors, such as changes in land functions, infrastructure development, spatial use and development of Mangrove Tourism. From the analysis of the Land Value Change Map it is known that there is a relationship between regional development (Mangrove Tourism) and the increase in land values around the area. This is indicated by an increase in the percentage of land values against the Tax Object Selling Value in all zones formed at the study site.

5. References

Adrian, Sutawijaya. 2000. "Development Economics Analysis of Factors Affecting Land Value as the Baseline for Assessing the Selling Value of Tax Objects (Njop) in the City of Semarang. "Development Economy: 65–78.

Deborah, B. 1996. "Agricultural Location Theory: Von Thunen Contribution to Economic Geography."

Fahirah, F. 2011. "Identification of Variable Housing Property Valuation Based on Perception of Housing Residents." *SMARTek*.

Kahar, Sutomo, and Sawitri Subiyanto. 2016. "Making a Land Value Zone Map with a Bulk Assessment Approach to Increase the Potential of PAD (Regional Original Revenue) especially on PBB and BPHTB." 5: 122–31.

Kusumo; 2015. "Analysis of Changes in Land Value Zones Due to Changes in Land Use in Tembalang District, Semarang City." 7: 109–19.

Minister of Finance of the Republic of Indonesia. (2000). Decree of the Director General of Taxes No. KEP-533 / PJ. / 2000 concerning Registration Instructions, Data Collection and Assessment of Objects and Subjects of Land and Building Taxes in the Formation and or Maintenance of Tax Object Information Management Database Systems.

Minister of Finance of the Republic of Indonesia. (2006). Decree of the Director General of Tax No. SE-25 / PJ.6 / 2006 concerning Procedures for Establishing / Improving ZNT / NIR.

Nathania. 2017. "Analysis of Land Changes and Land Value Zones of East Ungaran District Due to the Construction of Semarang - Solo Toll Road (Year 2008 - 2017)." 6: 433–42.

Estimating and mapping aboveground biomass/carbon stock using ALOS-2 PALSAR-2 of the mangrove forests in East Kalimantan, Indonesia

M K Nesha[1]*, Y A Hussin[1], L. van Leeuwen[1], Y B Sulistioadi[2]*

[1]Department of Natural Resources, Faculty of Geo-information Science and Earth Observation (ITC), University of Twente, Hengelostraat 99, 7511 AE Enschede, The Netherlands, Tel: +31534874293 Fax: +31534874399
[2]Soil and Water Conservation Laboratory, Forestry Faculty, Center of Geospatial Information Infrastructure Development (CGIID), Institute for Research and Community Services (IRCS), Mulawarman University, Samarinda, Indonesia,

e-mail: y.a.hussin@utwente.nl

Abstract. UN-REDD+ program introduces the MRV mechanism for AGB/carbon stock estimation to reduce the emissions from deforestation and forest degradation in the tropics. The MRV mechanism is required a low cost and robust technique to estimate AGB/carbon stock with reasonable accuracy in the tropical forests. Among the different RS techniques, L-band SAR estimates AGB with high accuracy in the inland tropical forests. However, the accuracy of AGB estimation in the tropical mangrove forests is relatively low according to the literature. In this context, this study was carried out to estimate AGB/carbon stock using HV radar backscatter coefficients of ALOS-2 PALSAR-2 in part of the planted mangrove forest at Mahakam Delta, East Kalimantan, Indonesia. A linear regression model was applied to estimate AGB in the study area (105 ha) using HV polarization backscatter of PALSAR-2. The accuracy of the AGB estimation was assessed in terms of R^2, RMSE, and p-value. The results of the linear regression models revealed that HV backscatter coefficients estimate AGB with high accuracy at R^2 of 0.89, RMSE of 23.16 tons ha^{-1} and p-value < 0.01. Therefore, the equation derived from the simple linear regression model was used to map the AGB and carbon stock in the study area.

1. Introduction

Mangrove is a unique and complex ecosystem, flooded during high tide and the ground is a layer of dense mud, with soil containing high levels of organic materials during low tide. Mangrove forest has zonations where the types of plants change with different water and salinity level moving away from the sea to inland. All these unique attributes in the mangrove forests lead to uncertainty in estimating AGB with high accuracy and low cost. As a result, this has partly resulted in difficulties to assess AGB for MRV mechanism of UN-REDD+ program following a unique methodology in diverse forests regions in the tropics including mangroves.

Most of the studies on AGB/carbon stock estimation in mangrove forests have been done using optical images [1, 2]. However, mangrove forests are situated in tropical and sub-tropical regions, thus affected by cloud condition for most of the year, making it difficult to obtain clear passive optical images from the satellite. In contrast, L-band SAR is an active sensor which can be used in all weather conditions, making it more reliable for accurate estimation of AGB/carbon stock.

L-band SAR backscatter is depicted to estimate higher AGB with reasonable accuracy in the terrestrial forests in the tropics. On the contrary, the use of L-band SAR for AGB estimation are surprisingly lacking for the mangroves, although mangroves have high carbon assimilation and flux rates [3]. Until today, only a few studies have been conducted to estimate AGB in the mangrove forest using L-band SAR backscatter data [4-7]. Again, the accuracy of AGB estimation in these studies is lower than that of inland forests in the tropics. In this context, we studied the relationship between PALSAR-2

backscatter coefficients and AGB in the mangroves of Mahakam Delta, in East Kalimantan, Indonesia to examine if backscatter coefficients of PALSAR-2 can estimate AGB with higher accuracy in the mangrove forest.

The findings of our study may prove a way forward towards a system using L-band SAR for modeling and estimating AGB in the mangroves with reasonable accuracy. Therefore, it may promote the implementation of REDD+ and Payment for Ecosystem Services strategies (PES), thus providing practical implications for developing regional and national Blue Carbon trading markets and guiding mangrove management and conservation.

2. Materials and Methods

2.1 Study Area

When it comes to the distribution of mangroves, Indonesia alone accounts for more than 30% of the entire world's mangrove carbon stock. However, most of Indonesia's mangrove forests are destroyed or severely degraded, and nearly half of the mangroves have been lost mostly to aquaculture and coastal development during the past 50 years [8]. Of the 31,894 km^2 of existing mangrove wetland in Indonesia, 31% are in good condition, 27% are moderately degraded, and the remaining 42% of mangrove forests are heavily degraded.

Despite sheltering almost one-third of the global mangrove forest, information on AGB estimation of mangrove forests is limited in Indonesia. East Kalimantan province has a second-largest area of mangroves in Indonesia. Mangroves in East Kalimantan covers over 11% of Indonesia's total mangrove forest [9]. Most of East Kalimantan's mangroves originated from the Mahakam Delta. In Mahakam Delta, mangrove covers nearly 1,500 km^2. However, most of the mangrove area has been lost mainly due to conversion to fish and shrimp ponds. The total area deforested was estimated to be 85,000 ha in 2001 representing about 75% of the mangrove forest in Mahakam Delta [10].

In an effort to restore the mangroves in Mahakam Delta, plantation took place since 2002 by both government and private companies at some sites of the Mahakam Delta. However, no studies have been conducted so far to quantify the AGB of the regrowth mangrove in the Mahakam Delta using L-band SAR. Thus, estimating AGB in the mangroves forests of Mahakam Delta using L-band SAR may help to elucidate the spatial distribution patterns of AGB in that region.

The study site was an area of young and reforested mangrove forest in the sea-front areas in north distributary zones of the Mahakam Delta in East Kalimantan, Indonesia. The study was conducted on a mangrove forest since L-band SAR has been less exploited to estimate its AGB/carbon stock though mangrove forest has high potential to sequester more carbon than any other forest ecosystem. The young mangrove forest was chosen as L-band SAR saturates at higher AGB estimates. Also, Mulawarman University, Samarinda, Indonesia provided us with the logistic support and two undergrad students in executing the fieldwork. A brief description of the study area is given in the following subsections.

2.1.1 Geographic Location

The study site covered an area of 105 ha in the mangrove forest located between W longitude 117.560366° to E longitude 117.573216° and N latitude -0.533392° to S latitude -0.543048° at Mahakam Delta, in the East Kalimantan province, Indonesia (Figure 1). East Kalimantan is one of the provinces in the Indonesian part of Borneo Island. It has the second largest area of mangroves representing about 11% of total mangrove forest in Indonesia [9, 11]. Most of the mangroves of East Kalimantan originated from the Mahakam Delta [11, 12]. Mahakam Delta comprises of 46 small islands forming an exceptional fan-shaped lobate and extends to the coastal area of the Makassar Strait of East Kalimantan. It is approximately 20 km from the capital city of East Kalimantan, Samarinda, Indonesia.

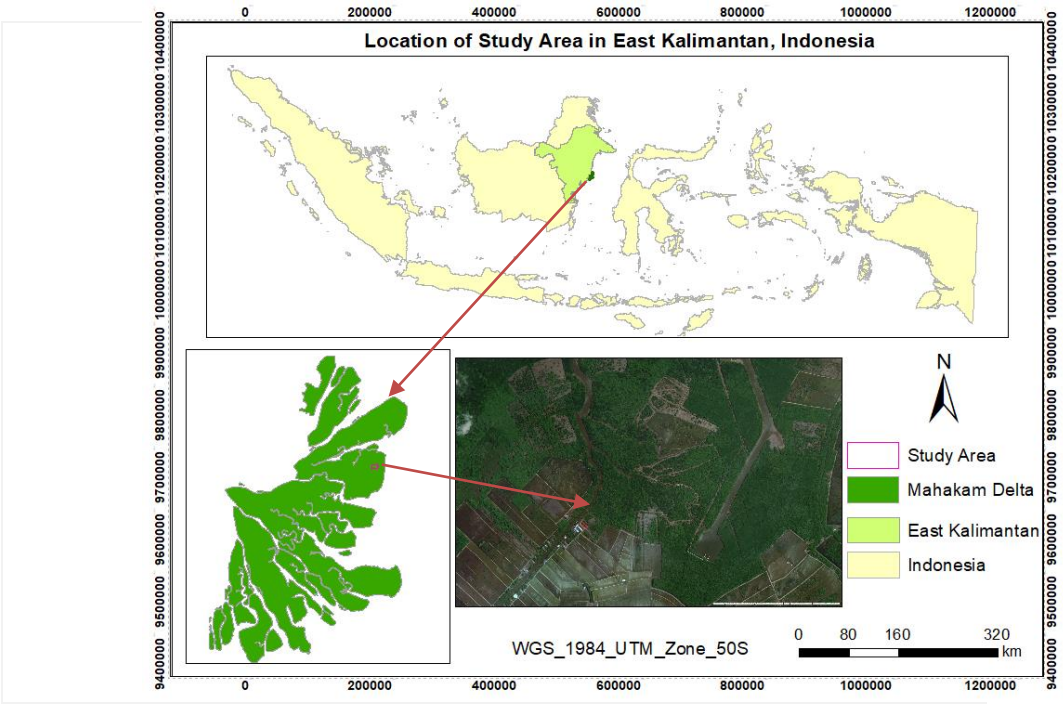

Figure 1. Location map of the study area.

Mahakam delta has very flat topography with around 0.1% slope. Several vegetation zones can be identified in the mangrove forest of the Mahakam Delta [12]. For instance, the pedada zone is located close to the delta front and is characterized by *Sonneratia alba* and *Avicennia spp.* The bakau (*Rhizophora*) zone is found mostly along the bank of distributaries of the lower delta area. The transition zone is a mixed zone where *Avicennia* sp., *Sonneratia caseolaris, Rhizophora* sp., *Bruguiera* sp., *Xylocarpus granatum,* and *Nypa fruticans* grow together. The nibung zone is in the uppermost area of the delta and is characterized by species of *Oncosperma* sp., *Heritiera littolaris, Gruguiera sexangula*, and *Excoecaria agallocha* [12]. Tidal current occurs due to a combination of diurnal and semi-diurnal component and can reach up to 2.5 m height. This tidal current is combined with high current from the Mahakam River at 1,500 m^3/sec. [13].

2.2 Materials

Study materials such as software, field equipment, and data are of paramount importance to conduct any research study. The following subsections highlight the materials used in this study.

2.2.1 Field Equipment

Several field equipment was used to collect primary data in the field sample plots. The list of all field equipment and their purpose are explained in Table 1.

Table 1. A list of field study equipment with their purpose.

Field Equipment	Purpose
Diameter Tape	Measuring tree diameter at breast height (DBH).
Leica DISTO D510 laser instrument	Measuring tree height.
Field data sheet and pencil	Record keeping of the field data.
Measuring Tape	Defining the perimeter of the field sample plots.
Garmin GPS	Measuring coordinates of the field sample plots.

2.2.2 Data and Purpose of Use

ALOS-2 PALSAR-2 backscatter coefficients were used to estimate and map AGB in the study area. DBH and height of the trees were measured in the field while the Basal Area (BA) was calculated from field-measured tree DBH. Moreover, wood density was collected from the World Agroforestry Centre. These data and their purpose in the study are described in Table 2.

Table 2. A list of data used in this research.

Data	Purpose
ALOS-2 PALSAR-2	To extract HV and HH backscatter coefficients for the field plots and derive their relationship with field-measured AGB, BA, tree DBH and tree height.
DBH	To be used in the allometric equation for calculating field-measured AGB.
Tree Height	To be used in the allometric equation for calculating field-measured AGB.
BA	To derive the relationship between BA and backscatter coefficients.
Wood Density	To be used in the allometric equation for calculating field-measured AGB.

2.2.3 Software

Few software was used for processing and analyzing data in this research. One of them was the Sentinel Application Platform (SNAP) which is an open source software developed for the European Space Agency (ESA). SNAP is a typical platform for all Sentinel Toolboxes. The Sentinel-1 Toolbox (S1TBX) supports an extensive collection of data for processing, display, and analysis from ESA SAR missions as well as third-party SAR data, for example, ALOS PALSAR.

ArcGIS-ArcMap 10.6.1 was used for performing all GIS-based analysis including retrieval of the PALSAR-2 backscatter coefficients. Statistical analysis was conducted using both Microsoft Excel and R programming Language in RStudio. Finally, Microsoft Office was used for writing the report and presentation. Table 3 lists all the software and its application in this study.

Table 3. A list of software used in this research.

Software	Purpose
SNAP	Sub-setting the ALOS-2 PALSAR-2 image for the study area Pre-processing of ALOS-2 PALSAR-2 data Calibration of PALSAR-2 data, i.e., conversion of DN values to backscatter coefficients Geometric correction and georeferencing of PALSAR-2 image Speckle filtering of PALSAR-2 image
ArcGIS	Extraction of backscatter coefficients from PALSAR-2 subset in the field plots Producing AGB/carbon stock map
R studio	Statistical analysis Correlation analysis Regression analysis Model development and validation Accuracy check (R^2, RMSE and p-value)
MSOffice	Statistical analysis Report writing Presentation

2.3 Methods

This study was designed to estimate AGB using HV and HH polarization backscatter data from ALOS-2 PALSAR-2 in the mangroves of Mahakam Delta in East Kalimantan, Indonesia. Linear regression was used to model AGB in the mangrove forest using the backscatter coefficients of PALSAR-2. The main steps of the study are shown in the flowchart in Figure 2 and briefly described below.

Step 1: This step involved the collection of trees DBH, tree height, wood density, and PALSAR-2 data.
Step 2: The biometric data was processed, and field-measured AGB/carbon stock was calculated using the allometric equation by Chave et al., [14] in this step. BA was also calculated in this step.
Step: 3: This step involved the calibration of PALSAR-2 data in retrieving the backscatter coefficients, geometric correction and georeferencing, and speckle filtering of the PALSAR-2 image.
Step 4: This step included regression analysis between PALSAR-2 backscatter coefficients and forest parameters (BA, DBH and tree height). It also included regression analysis between forest parameters.
Step 5: This step depicted the model development and validation between HV polarization backscatter coefficients of PALSAR-2 and field measured AGB.
Step 6: This step dealt with the saturation point determination of AGB estimation in relation to HV backscatter coefficients of PALSAR-2.
Step 7: This step involved in AGB/carbon stock mapping using the equation derived from the best model in terms of R^2, and RMSE resulted from step 5.

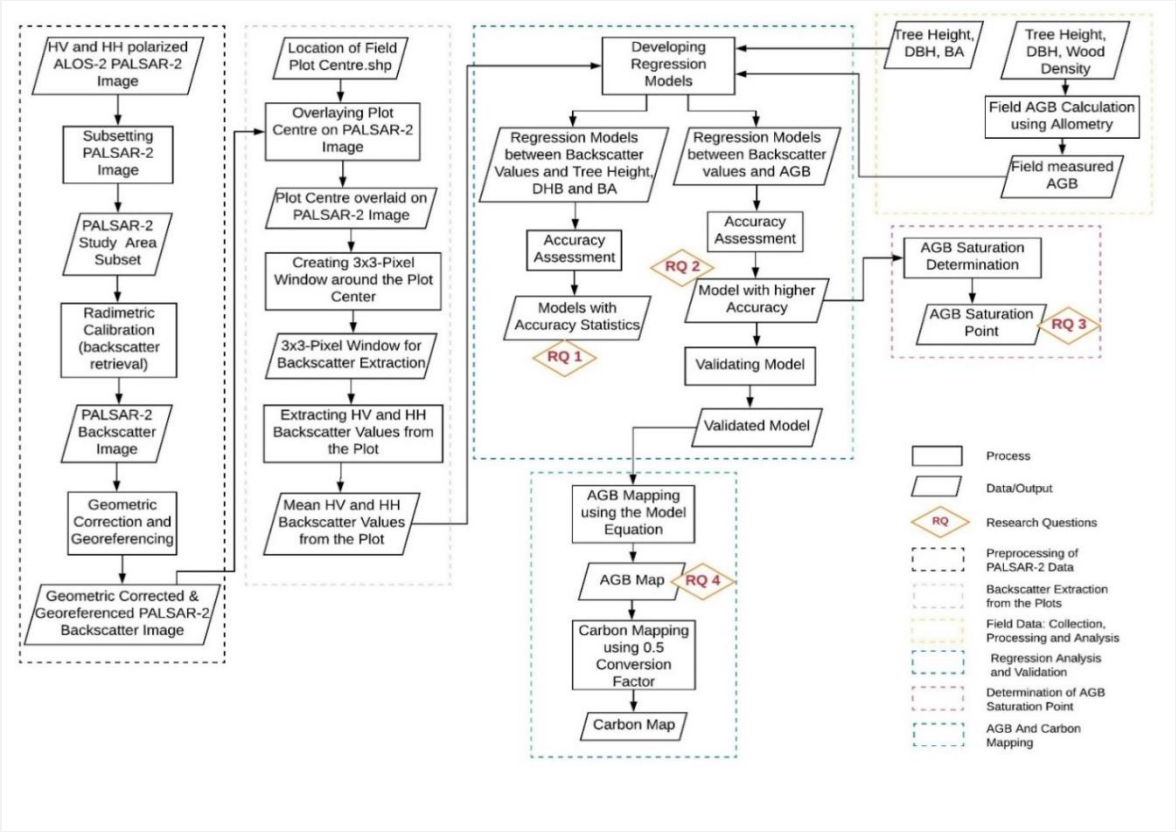

Figure 2. Methodological flowchart of the study.

2.3.1 Sampling plot

Purposive sampling was used for determining the sample plots in the study area. In total, 71 sample plots were selected. The main reasons for using purposive sampling are as followed.

Accessibility: Sample plots were selected in the study area where it was accessible by the boat through rivers and small water channels. It was very challenging and in some places, impossible to walk through the excessive muddy ground. Therefore, some areas of the mangrove forest were excluded due to the excessive muddy surface.

Time and Cost: Several plots were also chosen in the mangrove forest close to the school (where our team and we were staying during the period of data collection) and accessible by walking to reduce the boat hiring cost. Time was a crucial factor as we had to collect data during peak hours of low tide.

Administrative Permission: Access was restricted in some parts of the mangrove forest in the study area particularly close to an oil company property. Therefore, we selected the sample plots in areas where we had full access from the authority.

2.3.2 Field Plot Establishment

The size of the plot also affects AGB estimation and the optimum plot size varies in different regions and types of vegetation. However, AGB estimation was depicted to be the most accurate with the plot size of 500 m^2 since the plot size > 500 – 600 m^2 does not significantly improve the result of AGB estimation . Moreover, the plot size of 500 m^2 was demonstrated as a cost-effective plot size as it tends to sample a reasonable number of trees in each plot. Therefore, a circular plot of 500 m^2 (0.05 ha) with a radius of 12.62 m was established in our study area. The circular plots of 500 m^2 were established

using a measuring tape. Then, each tree >= 10 cm in diameter was tagged in the plot. This is because trees < 10 cm in diameter have no significant contribution to AGB estimates [15]. Therefore, tree height and DBH were measured only for the trees with diameter >= 10 cm. Several tree species were present in the study area. Among them, *Avicennia Alba* and *Rhizophora spp*. were the dominant tree species. in case of *Rhizophora spp.* the tree DBH is measured at 1.3 m height from the stem base/buttress over the prop roots which represents the distance at 10-20 cm above the topmost prop-root attached to the stem of the tree. The main stem height over the prop-roots of the *Rhizophora spp.* varies from trees to trees. Measuring DBH at 1.3 height from the buttress crossed the uppermost prop-root and represented the main stem between 10-20 cm above the upmost prop-root. Some field photos of DBH measurement of *Rhizophora spp*. are shown in Figure 3.

Figure3. DBH measurement of *Rhizophora* Species, the measurement was taken at 1.3 m height from the stem base/junction over the prop roots.

In the case of *Avicennia alba* tree species, DBH was measured at 1.3 m height from the ground. The height of 1.3 m was used to minimize the variation in DBH measurement and to be consistent with the point of measurement. Similarly, the tree height was measured from the ground to the top of the trees.

2.3.3 Acquisition of ALOS-2 PALSAR-2 Data

The ALOS-2 is an Advanced Land Observation Satellite 2 which carries the Phase Array L-band Synthetic Aperture Radar 2 (PALSAR-2) Sensor on board. ALOS-2 is a Japanese satellite launched by the Japan Aerospace Exploration Agency (JAXA). One dual-polarized (HV and HH) ALOS-2 PALSAR-2 image was acquired from JAXA through the Remote Sensing Technology Center of Japan (RESTEC). The mangrove forest in the study area is inundated up to 2.5 m during high tide [13]. The time of scene observation of the PALSAR-2 image was chosen during peak hours of low tide to minimize the effects of inundation on the backscattering.

2.3.4 Extraction of the PALSAR-2 backscatter coefficients from the plots

The plot centers were overlaid on the PALSAR-2 image in ArcGIS. Around the plot center, a polygon was created with the 3 by 3 pixels for each plot. Thus, 71 polygons were created for 71 plots, and later these were combined into one shapefile. The establishment of the 3 by 3 pixels window to cover the plot area is illustrated in Figure 4.

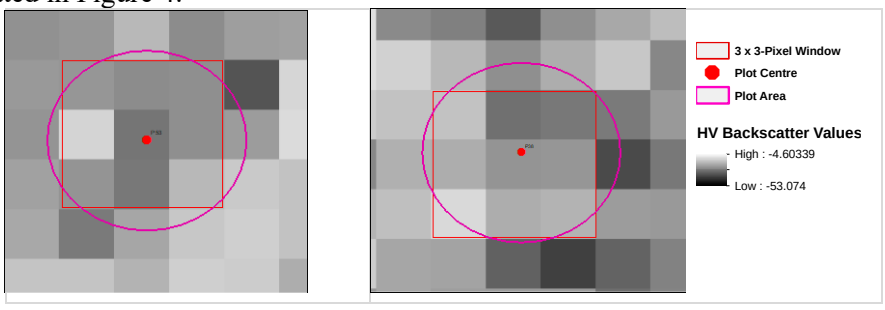

Figure 4. Establishment of the 3 by 3 pixels for extraction of backscatter values from the plot.

The average backscatter coefficient for 3 by 3 pixels window was extracted using zonal statistics under spatial analyst tool in ArcGIS. The polygons of 3 by 3 pixels window were linked to the Plot_ID following the Plot_ID of the coordinates of the plot center. This is to note that all the field-measured data had the same Plot_ID and accordingly, the window of 3 by 3 pixels window was also linked to the same plot. As a result, the extracted backscatter coefficients from the 3 by 3 pixels window were associated with the field-measured data. This was important to be able to analyze the relationship between the field-measured data and backscatter coefficients.

However, not all the plot centers perfectly fitted inside the center of 3 by 3 pixels window. Some plot center points fell between the edge of two pixels. Some of the plot centers were also found at the intersection of four pixels. It created a problem to identify the center of the pixel, thus placement of the 3 by 3 pixels window for the plot. This has been illustrated in Figure 5.

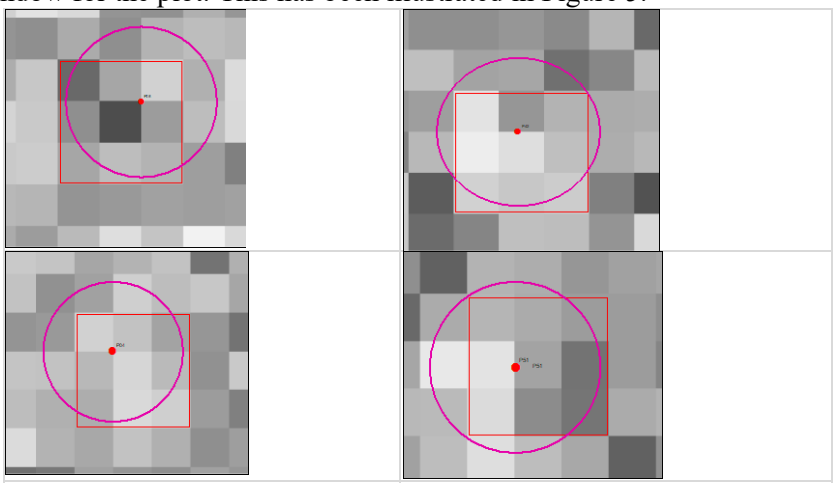

(a)Plot center at the intersection of four pixels.

(b) Plot center at the edge of two pixels.

Figure 5. Location of plot center between two or more pixels.

Drone images provided information on the canopy density of the plot and major species types as well as the position of the plot. The ground photos of the plot taken during data collection were also used to support the visual analysis with the drone images. Based on this analysis, plot center at the intersection of four pixels/at the edge of two pixels was shifted to the most suitable pixel among the shared pixels, and then the window of the 3 by 3 pixels was established. The shifting of the plot center of plot 3 and plot 4 and subsequent establishment of their 3 by 3 pixels window is illustrated in Figure 6. The dimension of 3 by 3 pixels covered 9 pixels of the PALSAR-2 image. An average value of the extracted backscatter coefficients within the 9 pixels was used for AGB model development and validation. NRCS/backscatter coefficients were the predictor or estimator for the field-measured AGB.

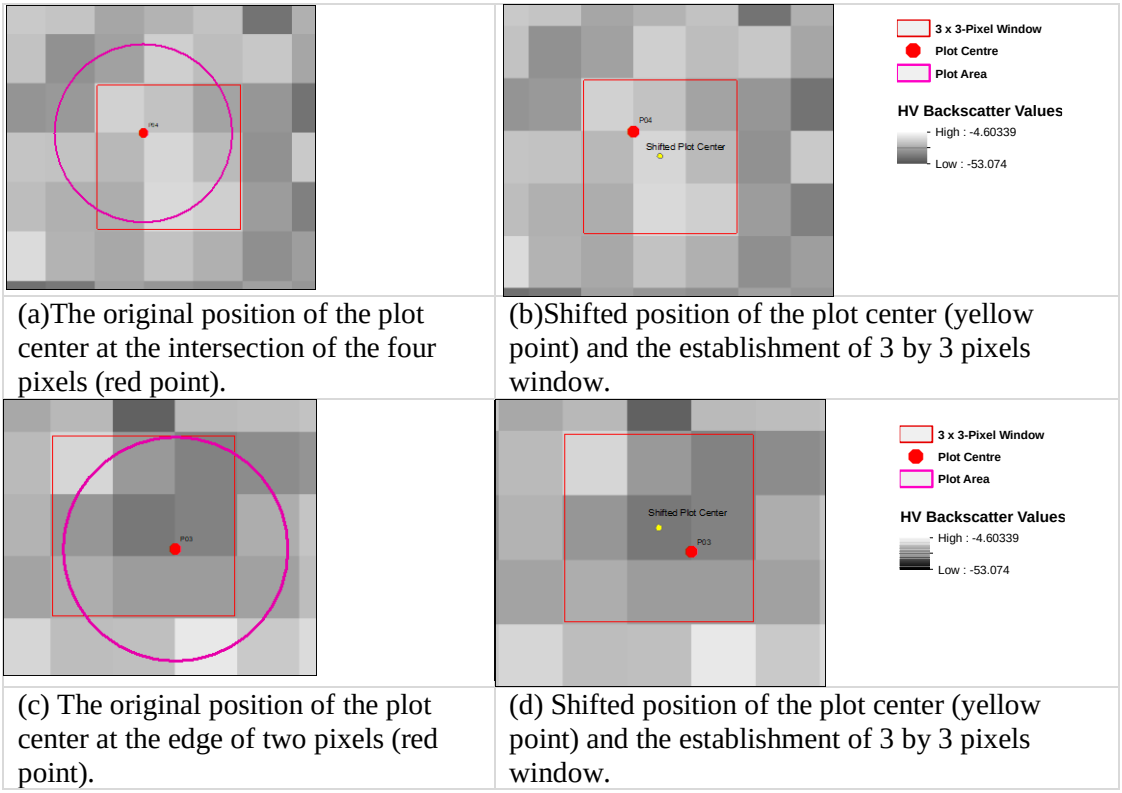

(a)The original position of the plot center at the intersection of the four pixels (red point).

(b)Shifted position of the plot center (yellow point) and the establishment of 3 by 3 pixels window.

(c) The original position of the plot center at the edge of two pixels (red point).

(d) Shifted position of the plot center (yellow point) and the establishment of 3 by 3 pixels window.

Figure 1. The shifting of the plot center for establishment 3 by 3 pixels window. The red points mark the original position, and the yellow points represent the final position of the plot center after shifting.

2.3.5 Sampling Plot AGB Calculation

AGB was calculated using tree DBH, tree height and wood density data in an allometric equation proposed by Chave et al., [14] for the mangrove forests. AGB was calculated for each tree in each plot. The allometric equation used for AGB calculation is given in Equation 1.

Equation 1. Allometric Equation for Calculation of AGB.

$$\text{Mangroves, AGB} = 0.0509\ \rho\ \text{D}\hat{}2\ \text{H} \qquad (1)$$

Where:

AGB = aboveground biomass estimated in kilogram
D = diameter at breast height in centimeter
ρ = wood density in gcm^{-3}
H = tree height in meter

The total AGB was calculated for individual plots using equation 2 in kilogram per 500 m^2 plot. Then, it was converted to tons per hectare using equation 2.

Equation 2. AGB Calculation in tons per ha.

$$AGB\ (tons/ha\text{-}1) = (Total\ AGB\ (kg/plot) * 20)/1000 \qquad (2)$$

2.3.6 Plot Carbon Calculation

Carbon was calculated from the AGB using the conversion factor of 0.5 and is expressed in tons ha-1. The conversion factor may vary from plant to plant, species to species and site to site. Therefore, the global default conversion factor of 50% was used to convert AGB to carbon stock followed by the

Intergovernmental Panel on Climate Change [16]. The equation to calculate carbon using the conversion factor of 0.5 is given in equation 3.
Equation 3. Calculation of Carbon using Conversion Factor.

$$C = AGB * CF \quad (3)$$

Where: C is the carbon stock in tons ha^{-1}
AGB is the aboveground biomass in tons ha^{-1}
CF is the carbon fraction (0.5)

3. Results and Discussions

3.1 The Relationship between HV Backscatter and Field-measured AGB

The linear regression analysis showed a strong relationship between HV backscatter and field measured AGB with R^2 of 0.89 and RMSE of 23.72 tons ha^{-1} at a p-value of 2.58755E-34. This result depicts that HV backscatter can significantly explain 89% variation in AGB using linear regression. The scatterplot of linear regression between HV backscatter and field measured AGB is presented in Figure 7.

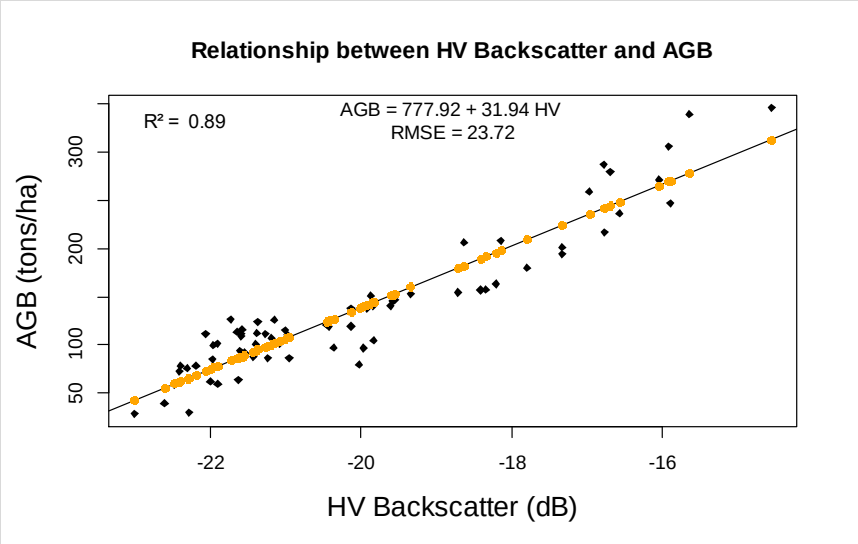

Figure 7. Simple linear regression using HV backscatter coefficients to predict AGB, the black dots represent field measured AGB and orange dots on the regression line (solid line) represents predicted AGB by the regression.

3.2 Model Development

A linear regression model to estimate AGB using HV backscatter depicted a very high accuracy with R^2 of 0.89. This implies that HV backscatter can explain 89% of the variation in AGB. The RMSE of the model accounted for 23.16 tons ha^{-1}. The RMSE was calculated based on the validation data. The graphical presentation of the model is shown in Figure 8.

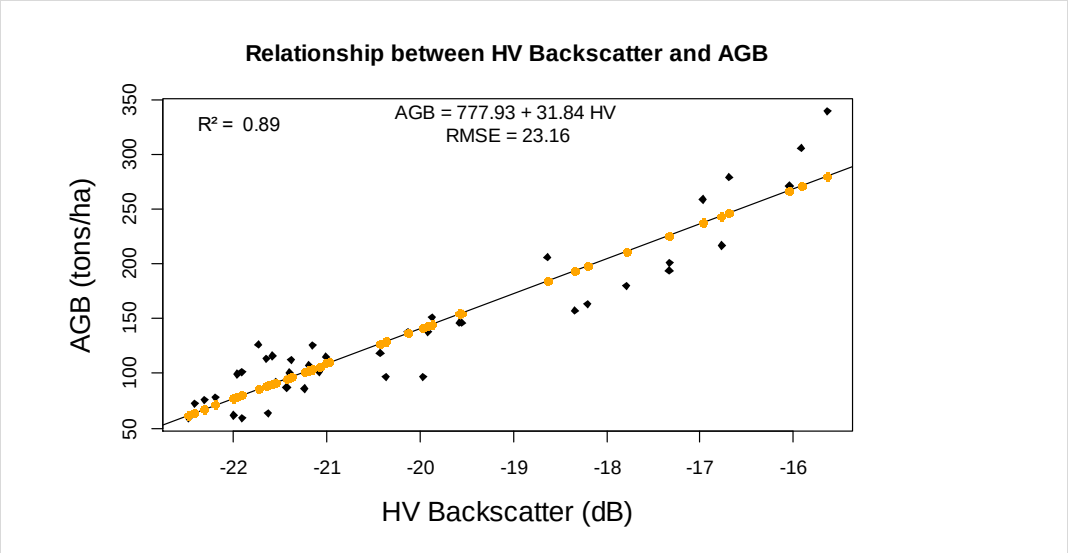

Figure 2. The scatter plot of the regression model between HV Backscatter and field measured AGB, the black dots represent field measured AGB while the purple dots represent the predicted AGB along the regression line by the regression model.

3.3. Model Validation and Accuracy Assessment

The equation derived from the model was used to estimate AGB of the study area. The average estimated AGB from the 29 validation plots was used to validate the model. In other words, estimated AGB from the 29 plots (40% of the dataset) was used to measure the predictive accuracy of AGB by regression model using HV backscatter. The validation dataset was independent of the data used for model development.

The regression results of the model validation between the observed (field-measured) AGB and estimated AGB depicted a strong coefficient of determination at R^2 of 0.89. Thus, we concluded that estimated AGB using HV backscatter can explain 89% of the observed AGB. The RMSE of the model validation was calculated at 22.69 tons ha^{-1} which is approximately similar to the model RMSE. The scatterplot of the relationship between the observed and estimated AGB is presented in Figure 9.

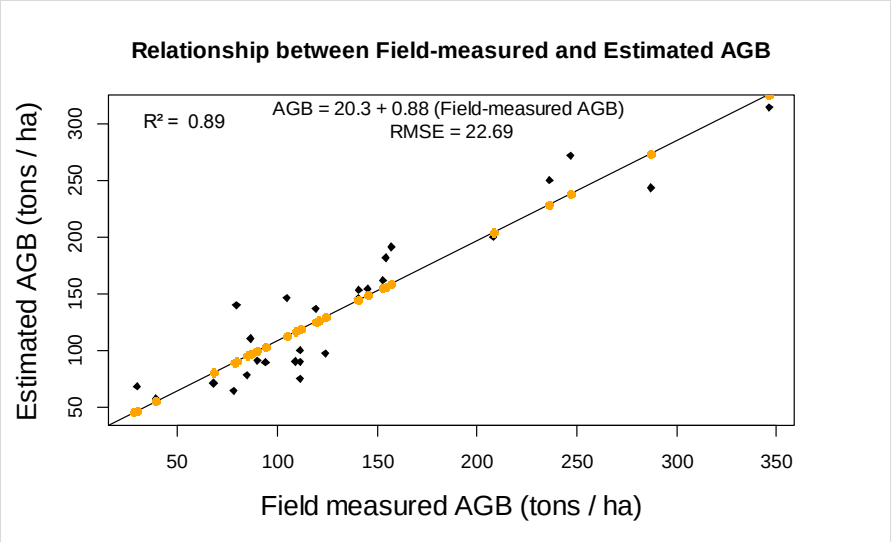

Figure 9.3 The scatterplot of the regression model validation between observed AGB and estimated AGB, the black points represent field measured AGB while the orange line represents the AGB predicted by the regression model validation.

3.4 AGB and Carbon Stock Map of the Study Area

AGB of the study area was mapped using the equation, AGB = 777.93 + 31.84 HV derived from simple linear regression model developed from the relationship between HV backscatter and AGB. Out of 105 ha of the study area, 75 ha was mangrove forest, and 20 ha was water bodies. Therefore, a separate group was created representing water bodies.

The map of estimated AGB of the study area is shown in Figure 10. It can be observed from the AGB map that most of the AGB ranged between 100 tons ha^{-1} and 200 tons ha^{-1} followed by 200-300 tons ha^{-1}. The amount of AGB higher than 300 tons ha^{-1} was mostly found in some areas along the river and scattered in some places over the study area. The average AGB of study area accounted for 181 tons ha^{-1}. The total AGB was estimated at 13,719 tons in the study area.

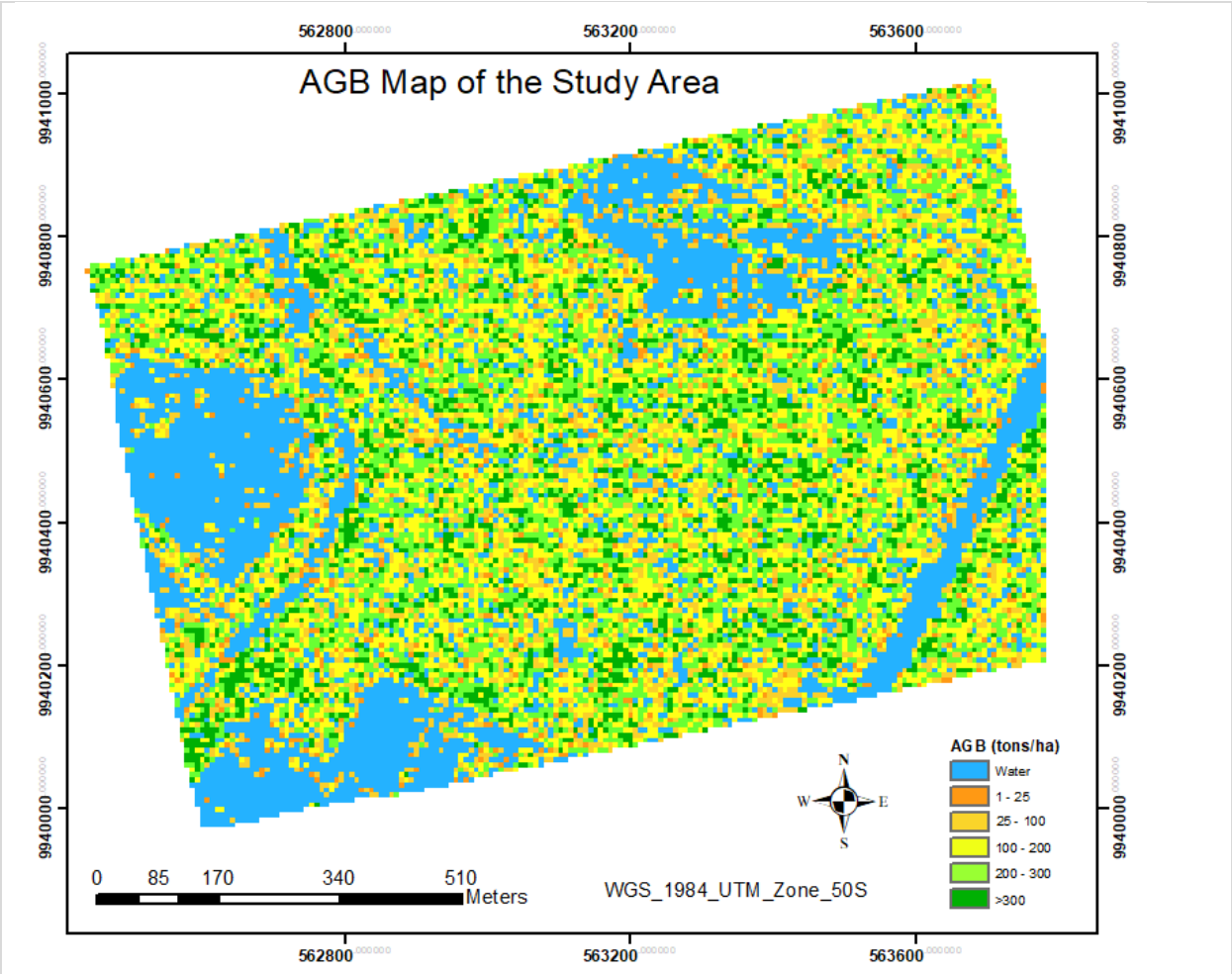

Figure 10. AGB map of the study area at Mahakam mangrove forest, East Kalimantan, Indonesia

It can also be seen from the frequency distribution of the estimated AGB in Figure 32 that AGB range from 100-200 tons ha^{-1} had the highest frequency followed by AGB at 200-300 tons ha^{-1}. The total number of pixels for the range from 100-200 tons ha^{-1} accounted for 5082, and the total AGB for this range summed to 3773.57 tons. It was followed by 4300 pixels for the AGB range from 200-300 tons ha^{-1} with total AGB at 5193.97 tons. The negative values represented water with a total of 5750 pixels covering an area of 20 ha.

The carbon stock map of the study area followed the same pattern as the AGB map. This is because the carbon stock map of the study area was produced by converting the AGB estimates using the conversion factor of 0.5 as 50% of forest biomass represents the carbon stock [16]. The average estimated carbon stock stood at 91 tons ha^{-1} in the study area. The total estimated carbon stock was estimated at 6860 tons. The carbon stock map of the study area is depicted in Figure 11.

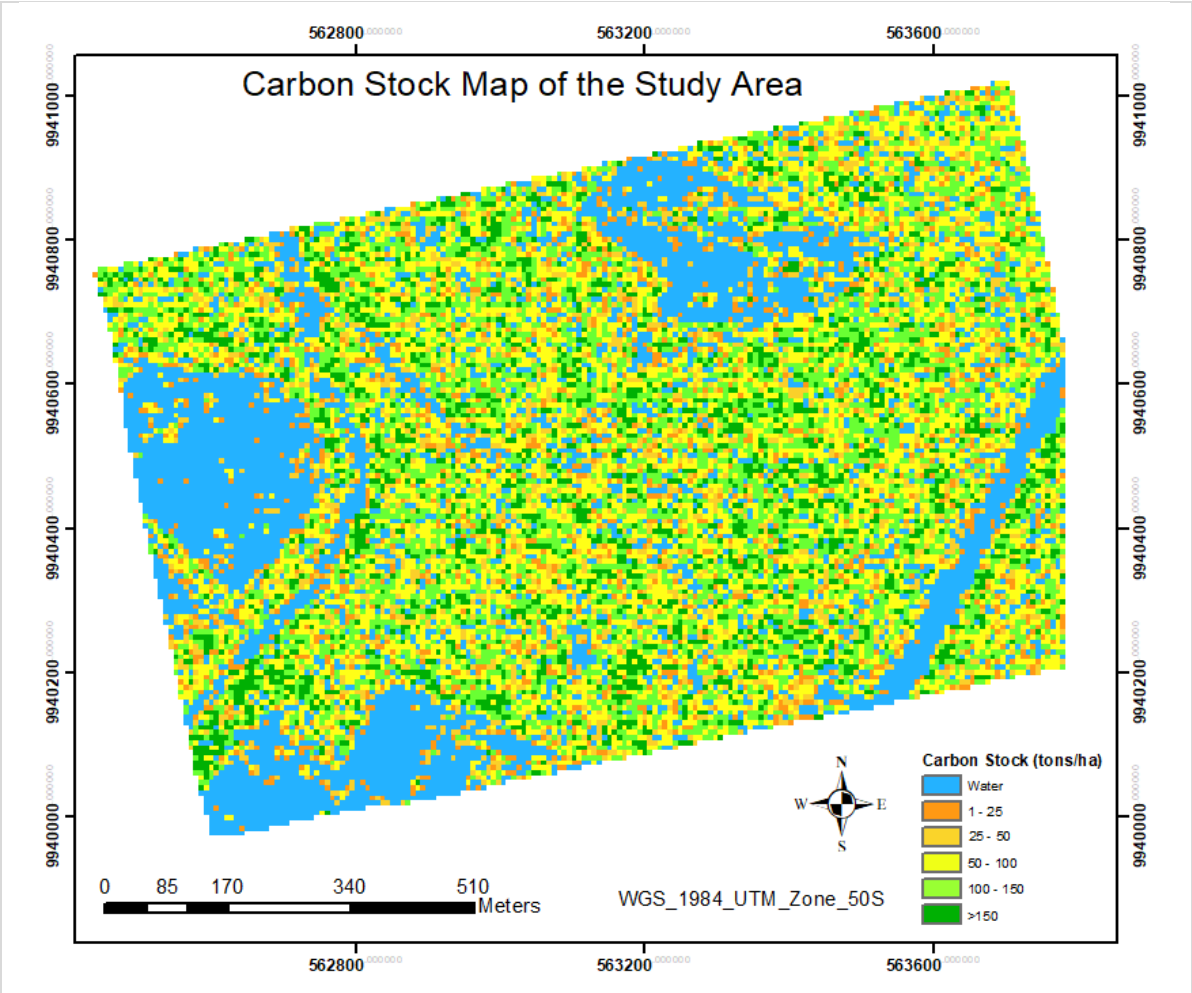

Figure 11. Carbon stock map of the study area at Mahakam Delta mangrove forest.

3.5 The relationship between AGB and Backscatter Coefficients

The enhanced backscattering in the mangrove areas has an important contribution to the AGB estimation in our study. The enhanced backscattering is mainly observed in the forest areas with the muddy ground floor having high water content and higher vegetation in our study, which is related to the time of image acquisition. The image scene acquisition time of PALSAR-2 in our study is 16:26:06 (UTC) on 30 July 2018. This is equivalent to 1:26 (am) local East Kalimantan time which represents the peak hours of the first low tide started at 12. 28 am at Balikpapan, East Kalimantan on 30 July 2018. Our study area is inundated 2.5 m during the high tide. The inundation of the forest affects the backscattering of the L-band SAR. Therefore, PALSAR-2 image acquisition during the low tide condition contributes to the enhanced backscattering as observed by other studies. According to Ormsby et al., [17], Imhoff et al., [18], Imhoff et al., [19], Hussin, [20], Wang & Imhoff, [21] and Henderson & Lewis [22], L-band cross-polarized backscatter of the flooded forest is enhanced because of the wet stems and the wet condition of forest ground. As L-band has a longer wavelength and can penetrate down to the ground surface in the forests, backscatter from L-band radar is enhanced from flooded forest vegetation because of the high dielectric constant of the ground floor and wet stems.

The growth of the trees can also contribute to the AGB estimation in our study. The age of the mangrove trees in our study area is approximately 16 years which is similar to the studies in Vietnam [5-7] and Malaysia [4]. However, the average height of the trees in our study area is comparatively higher ranging from 10.5 m to 18.3 m while the height of the trees ranged from 2.84 m to 7.61 m in the studies in

Vietnam [5-7]. The tree diameter in our study differs from the study by Hamdan et al. (2014) where the tree diameter in the sample plots ranges from 5.0 to 48.8 cm. Although, the range of the AGB of our study is similar to the study by Hamdan et al., [4], the majority of the plots have higher AGB in our study (>115 tons ha^{-1}) than that of Hamdan et al., [4], with (<100 tons ha^{-1}). As there is an increase in volume scattering with the growth of the trees [23], it can influence the AGB estimation using HV backscatter coefficients in our study. This is because the HV polarization of L-band is related to the volume scattering from the forests.

However, the majority of the plots in our study has AGB greater than 115 tons ha^{-1} whereas it is below 100 tons ha^{-1} in the study by Hamdan et al., [4]. On the contrary, the range of AGB is higher in our study compared to the studies in Vietnam [5-7] where the AGB of the mangrove forest ranges from 36.22 to 230.14 Mg ha^{-1} with a mean of 87.67 Mg ha^{-1}.

It should be mentioned here that our mangrove forest at Mahakam is about 16 years old with natural style plantations. On the other hand, the mangrove in Malaysia is a planted and sustainably managed mangrove forest. Also, it is a planted mangrove with community-based forest management in Vietnam. Therefore, the differences mentioned in the range of biomass and forest parameters are because of the differences in the characteristics of the mangrove forests. The range of field measured AGB in our study is comparable with the study conducted to estimate AGB in the Matang mangrove forest in Malaysia where AGB ranges between 9.53 and 340.82 Mg ha^{-1} [4]. Some of the species in our study area are similar to those reported in the study by Hamdan et al., [4] where 85% of the species were *Rhizophora murconata and Rhizophora apiculata.* However, the tree species are different in the studies in Vietnam [5-7].

Moreover, the diameter of the trees could play a role in AGB estimation in our study. It has been reported that tress <10 cm in diameter does not contribute significantly to biomass estimation [15]. Therefore, we included trees >= 10 cm diameter in our study. However, the studies conducted in Malaysia and Vietnam include trees from 5 cm in diameter for AGB estimation [4-7].

The distribution of sample plots in the study area might be another reason. We have a small study area covering nearly 105 ha. The number of sample plots in this small study area was 71 which shows a homogenous distribution of the plots over the study area. Thus, it covers all the variations in the study area. In other studies, the area is larger, but the sample plots are less and scattered over the study areas. This might not cover all the variations in their study area. In the study in Malaysia [4], 320 sample plots are scattered over 41,000 ha of mangrove forest. While in the study in Vietnam, the number of sample plots is 25 covering the mangrove forest of about 125 km along the Hai Phong coast [5-7].

4. Conclusions

The relationship between BA, DBH and Tree Height with PALSAR-2 backscatter values were modeled using linear regression model. Among them, BA showed a high correlation with HV backscatter values at R^2 of 0.78. The tree DBH and HV polarized backscatter had a moderate relationship at R^2 of 0.51. However, the relationship between the tree height and HV backscatter values was quite weak at R^2 of 0.25. On the contrary, the relationship between all these forest parameters and HH backscatter values showed very weak relationships.

The relationship between cross (HV) polarized L-band PALSAR-2, and AGB showed high accuracy with R^2 of 0.89 and RMSE of 23 tons/ha. The inclusion of like polarized (HH) backscatter values in the model did not improve the accuracy of the model prediction; rather it was the same as the simple linear regression model.

The L-band HV polarized backscatter values depicted the presence of saturation to estimate AGB at 216.9 tons/ha. This is an indication of the limitation of AGB estimation > 216.9 tons/ha using L-band SAR.

The amount of estimated AGB in the study area ranged between 1 and 350 tons/ha. The estimated AGB was classified into five classes, and the majority of AGB estimates were found to be ranged from 100 to 200 tons/ha. The total amount of AGB in the study area is 13,719 tons, and the corresponding figure for carbon was 6860 tons. The accuracy of the estimation was observed at R^2 of 0.89 and RMSE of 22.69.

5. Acknowledgment

The Authors would like to highly acknowledge and appreciate the research permit issued by the Indonesian Ministry of Science and Technology and Higher Education. They would like to highly Acknowledge the support and contribution of Dr. Y. Budi Sulistioadi and the Faculty of Forestry University of Mulawarman, Samarinda, Indonesia for facilitating our research work, helping us with the logistic, collecting image and ground truth data in Tani Baru mangrove forest. We highly appreciate the support of the team of Mita Priskawanti and Muhammad Lutfi Hamdani for their continuous help during October 2018. We acknowledged the UAV data collection by Dr. Y. Budi Sulistioadi in 2017 and 2018. Without the data and support, our research could not have been done.

6. References

[1] Dube, T. and O. Mutanga, *Evaluating the utility of the medium-spatial resolution Landsat 8 multispectral sensor in quantifying aboveground biomass in uMgeni catchment, South Africa.* ISPRS Journal of Photogrammetry and Remote Sensing, 2015. **101**: p. 36-46.

[2] Gibbs, H.K., et al., *Monitoring and estimating tropical forest carbon stocks: making REDD a reality.* Environmental Research Letters, 2007. **2**(4): p. 045023.

[3] Komiyama, A., J.E. Ong, and S. Poungparn, *Allometry, biomass, and productivity of mangrove forests: A review.* Aquatic Botany, 2008. **89**(2): p. 128-137.

[4] Hamdan, O., H.K. Aziz, and I.M. Hasmadi, *L-band ALOS PALSAR for biomass estimation of Matang Mangroves, Malaysia.* Remote Sensing of Environment, 2014. **155**: p. 69-78.

[5] Pham, T.D. and K. Yoshino, *Aboveground biomass estimation of mangrove species using ALOS-2 PALSAR imagery in Hai Phong City, Vietnam.* Journal of Applied Remote Sensing, 2017. **11**(2): p. 026010.

[6] Pham, T.D., K. Yoshino, and D.T. Bui, *Biomass estimation of Sonneratia caseolaris (l.) Engler at a coastal area of Hai Phong city (Vietnam) using ALOS-2 PALSAR imagery and GIS-based multi-layer perceptron neural networks.* GIScience & Remote Sensing, 2017. **54**(3): p. 329-353.

[7] Pham, T.D., et al., *Estimating aboveground biomass of a mangrove plantation on the Northern coast of Vietnam using machine learning techniques with an integration of ALOS-2 PALSAR-2 and Sentinel-2A data.* International journal of remote sensing, 2018. **39**(22): p. 7761-7788.

[8] Kusmana, C., *Distribution and current status of mangrove forests in Indonesia*, in *Mangrove ecosystems of Asia*. 2014, Springer. p. 37-60.

[9] Hartini, S., G.B. Saputro, and M. Yulianto. *Assessing the used of remotely sensed data for mapping mangroves Indonesia*. in *SELECTED TOPICS in POWER SYSTEMS and REMOTE SENSING. Available [online] also at: http://www. wseas. us/e-library/conferences/2010/Japan/POWREM/POWREM-34. pdf [accessed in Bogor, Indonesia: August 25, 2014]*. 2009.

[10] Van Zwieten, P., et al., *Aquatic food production in the coastal zone: data-based perceptions on the trade-off between mariculture and fisheries production of the Mahakam delta and estuary, East Kalimantan, Indonesia*, in *Environment and Livelihoods in Tropical Coastal Zones: Managing agriculture-fishery-aquaculture-conflicts*. 2006. p. 219-236.

[11] Susilo, H., Y. Takahashi, and M. Yabe, *Evidence for mangrove restoration in the Mahakam Delta, Indonesia, based on households' willingness to pay.* J. Agric. Sci, 2017. **9**: p. 30-41.

[12] Sidik, A.S., *The Changes of Mangrove Ecosystem in Mahakam Delta.* Indonesia: A Complex Social–Environmental Pattern of Linkages in Resources Utilization, The South China Sea: Sustaining Ocean Productivities, Maritime Communities and the Climate, Kuantan, Malaysia, 2008.
[13] Zain, Z., et al., *Potency of Mahakam Delta in East Kalimantan, Indonesia.* International Journal of Science and Engineering, 2014. **6**(2): p. 126-130.
[14] Chave, J.r., et al., *Tree allometry and improved estimation of carbon stocks and balance in tropical forests.* Oecologia, 2005. **145**(1): p. 87-99.
[15] Brown, S., *Measuring carbon in forests: current status and future challenges.* Environmental pollution, 2002. **116**(3): p. 363-372.
[16] IPCC, *Climate change 2007: Synthesis report. Contribution of Working Groups I, II and III to the Fourth Assessment Report of the Intergovernmental Panel on Climate Change.* IPCC Geneva, Switzerland., 2007.
[17] Ormsby, J.P., B.J. Blanchard, and A.J. Blanchard, *Detection of lowland flooding using active microwave systems.* 1985.
[18] Imhoff, M., et al., *Forest canopy characterization and vegetation penetration assessment with space-borne radar.* IEEE Transactions on Geoscience and Remote Sensing, 1986(4): p. 535-542.
[19] Polcyn, F., *Monsoon flood boundary delineation and damage assessment using space borne imaging radar and Landsat data.* Photogrammetric Engineering and Remote Sensing, 1987. **53**(4): p. 405-413.
[20] Hussin, Y.A., *The effects of polarization and incidence angle on radar backscatter from forest cover.* 1991.
[21] Wang, Y. and M. Imhoff, *Simulated and observed L-HH radar backscatter from tropical mangrove forests.* International Journal of Remote Sensing, 1993. **14**(15): p. 2819-2828.
[22] Henderson, F.M. and A.J. Lewis, *Principles and applications of imaging radar. Manual of remote sensing: Volume 2.* 1998.
[23] Le Toan, T., et al., *Relating forest biomass to SAR data.* IEEE Transactions on Geoscience and Remote Sensing, 1992. **30**(2): p. 403-411.

Aboveground mangrove forest biomass and carbon stock assessment with terrestrial laser scanner (TLS) using quantitative structure model (QSM) in East Kalimantan, Indonesia

G. K. Beyene, Y A Hussin, I van Duren

Department of Natural Resources, Faculty of Geo-information Science and Earth Observation (ITC), University of Twente, Hengelostraat 99, 7511 AE Enschede, The Netherlands, Tel: +31534874293 Fax: +31534874399

e-mail: y.a.hussin@utwente.nl

Y B Sulistioadi

Soil and Water Conservation Laboratory, Forestry Faculty, Center of Geospatial Information Infrastructure Development (CGIID), Institute for Research and Community Services (IRCS), Mulawarman University, Samarinda, Indonesia

e-mail: bsulistioadi@gmail.com

Abstract. Mangroves are highly valuable green vegetation types that enhance ecological diversity in the coastal areas and support socio-economic activities. From the total world mangroves, Indonesian share is 22.6% which is around 3.11 million ha area coverage. Mangroves are a unique ecosystem that provides goods and services to society. However, the rate at which mangroves degraded and disappeared have enormous consequences on the aquatic ecosystems, atmospheric condition and climate. In most cases, estimation of above ground biomass/carbon stock relies on allometric equations. Application of terrestrial laser scanner (TLS) using quantitative structural model (QSM) focus on common areas such as the inland forest. In this study, we used TLS to estimate above ground biomass (AGB) of mangrove forest in the coastal area using QSM which is independent of diameter at breast height (DBH). The DBH and tree height from TLS showed high agreement with DBH and height from filed with R^2 0.978 and RMSE of 0.62 cm, and R2 0.73 with RMSE of 1.93 m respectively. The tree parameters measured in the field were used to estimate AGB/carbon stock using allometric equation and used as a reference to AGB/carbon stock derived from TLS and QSM.

1. Introduction

To provid information about mangroves forest ecosystems, it requires a lot of data which is difficult to assess directly. Estimation of mangrove biomass/carbon stock is needed an accurate measurement of diameter at breast height (DBH) and tree height. Precise measurement of tree stem volume is desirable for sustainable forest resource planning, which is strongly linked to biomass and carbon stock of the forest [1]. Accurate measurement of AGB/carbon stock is essential characteristics to understanding the effects of climate change [2]. Even though forest parameters are critical to model carbon stock/biomass of forest, but inaccurate measurement of tree parameters leads to overestimation or underestimation of AGB/carbon stock [3]. Allometric equations which convert tree height and DBH to biomass/carbon stock directly is uncertain, because, it depends on the capability of the equation to manage variation [4] and difference of biomass/carbon stock in different parts of the tree [5].

Terrestrial Laser Scanner can determine high-quality tree attributes that are important in estimating biomass with high accuracy level [1]. But there is no research conducted on assessment of mangrove

forest AGB/carbon stock with TLS using QSM. However, there is one research done by Feliciano et al., [6] on the assessment of AGB with TLS only. As Newnham et al., [7] showed Terrestrial Laser Scanning ‘‘presents an opportunity to go beyond simple empirical isometric and allometric equations to the point where three-dimensional measurements could use as a basis for assessing tree volume,”. It shows the specific implication of considering an increase in the importance of AGB assessments and forest carbon stock inventories [8].

According to Zianis & Seura, [9] “The simplified statistical models are limited in accuracy, and cannot give accurate quantitative and geometric information on a single tree, especially in the branch level.” From TLS point cloud branch distribution can be reconstructed using QSM algorithms [10]. Therefore, combining TLS with QSM provides a detailed structure of the trees that enables us to estimate biomass. QSM gives complete data on branch size to calculate AGB accurately. A study conducted to estimates AGB of mangrove forests using TLS done at Everglades National Park, Southwestern coast of South Florida [6] showed that TLS is a promising option for non-destructive sampling to measure AGB. However, estimating AGB in tropical mangroves by TLS using QSM is entirely new. We do not know yet if and to what extent TLS using QSM can improve the accuracy of biomass and carbon estimates. Therefore, this research will assess the applicability of TLS using QSM to estimate AGB in tropical mangroves of the delta of Mahakam River, East Kalimantan, Indonesia.

2. Materials and Methods

2.1. Study Area

The location of the study area is in Mahakam delta east coast of Borneo Island specifically in the province of East Kalimantan, Indonesian, between 0°21' and 0°10' South and between 117° 15' and 117" 40' East, placed at the mouth of the Mahakam River [11] (Figure 1). The area is slightly larger than one square kilometre and consists of a collection of islands. The delta of the Mahakam comprises some 42 islands with a total land surface of about 1100 km2 [12]. All weather and dirt roads are present only on the delta’s fringe; they lead to the main villages, poor in infrastructure, and are accessible by boat only [11]. The disturbance of this ecosystem started with the introduction of a shrimp farm, and the expansion of human settlements related to the oil and gas exploration and exploitation, which attracted both workers and land speculators [11].

The province of East Kalimantan is characterised by a tropical rainforest climate, with a dry condition starting from May to September and a wet from October to April, governed by the Monsoons [12]. According to Bosma et al., [11] “The annual rainfall of the area exceeds 2,500 mm within the 25,000 km^2 catchment of the Mahakam river that discharges into the Makassar Strait”. The delta of Mahakam River is covered by dense mangrove, composed of mainly Avicennia, Sonneratia (Sonneratia alba), Rhizophora (Rhizophora spp.), and Nypa species (Nypa fruticans) and nibung (Oncosoerma spp.); which are freshwater mangroves [12].

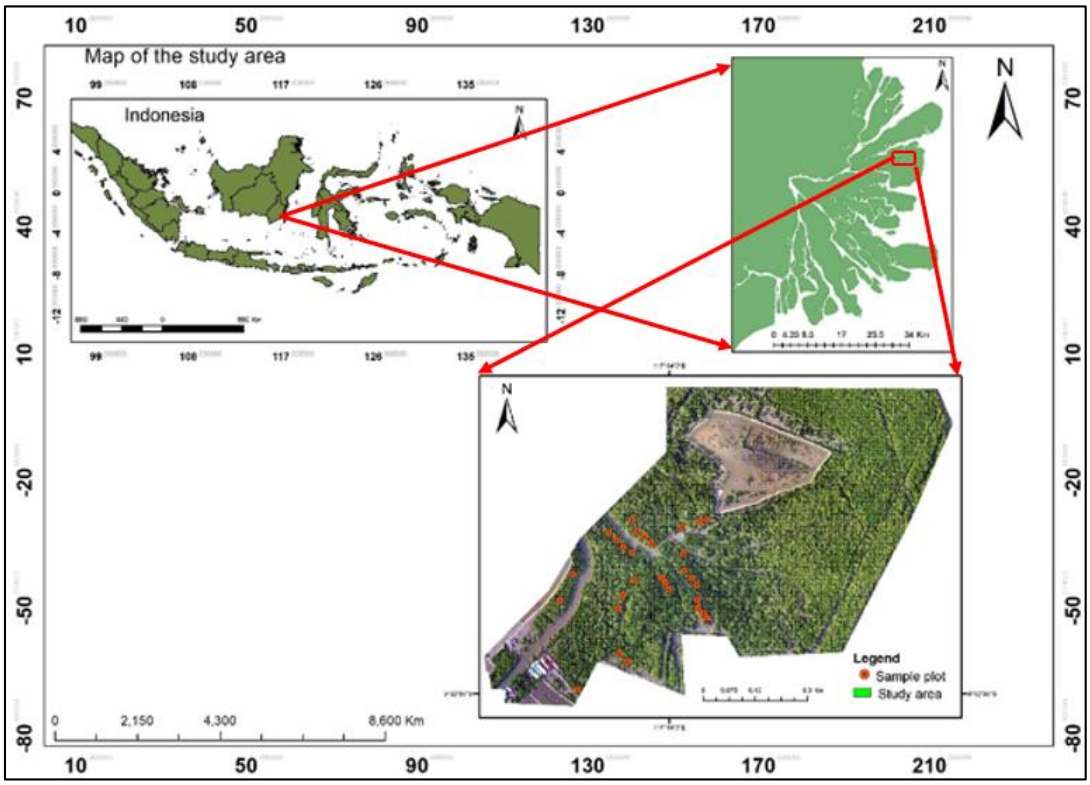

Figure 1. Map of the study area in Angan district. The overview map shows the location of the study area relative to the country (Indonesia) and Mahakam delta east coast of Borneo. The red points on the figure show the location of the plot centre.

2.2. Materials

Different hardware and software and field equipment used for the study during data collection and processing.

Collection of data in the field was performed using the right instruments and materials to minimise uncertainty during field data collection. Table 1 shows materials used during sample collection and the description of its functions.

Table 1. Field equipment used for biometric data collection, tree structure scanning, and field data recording.

No	Instrument	Function
1	TLS (RIEGL VZ 400)	Tree scanning
2	Diameter Tape	Measure DBH
3	Clinometer	Measure slope
4	Field sheet	Record data
5	Tablet	Navigation
6	Leica DISTO D510	Measure the height
7	Handheld GPS	Take point location
8	Laminated paper	Tree labelling

Different software was used to process and analyse the collected data from the field listed in Table 2.

Table 2. Software used for data process and analysis

No	Software	Function
1	RiSCAN PRO v2.4.2	Register and extract individual trees
2	MATLAB R2018b	Ran QSM algorithm
3	ArcGIS 10.5.1	Map generation
4	Lucid chart	Flowchart drawing
5	MS office 2010	Data analysis and thesis writing
6	Mendeley	Citation and reference

2.3. Methods

The appropriate method was designed to answer research questions, in such a way that divided into different stages which are namely; pre-field, field data collection, data processing, analysis and AGB estimation using volume derived from QSM. Pre-field activities were practical activities done to facilitate fieldwork preparation. Practising different field instruments were done such as Leica DISTO D510, GPS, Haga and Clinometer; differential GPS set up and TLS operation to collect point cloud and point cloud processing using RISCAN PRO software. Apart from pre-field, the method used in this research comprised of four main steps. The first step was field data collection, that is a collection of tree parameters (DBH and height) in the sample plot using diameter tape and Leica. Diameter tape was used to measure the DBH of all trees with DBH ≥ 10cm in the sample, and Leica DISTO D510 used for height measurement of trees. Field measured AGB/carbon stock was estimated using DBH measured by diameter tape and Height from Leica multiplied by specific and generic wood density.

The second step was data acquisition using TLS. In this stage, multiple scanning positions were used to scan all plots and generate the points cloud. RiSCAN PRO software was used to register the four scanning position sequentially using the centre scanning position as a reference. Individual trees were extracted manually to measure DBH and height of the tree using measuring tools. The DBH and height of tree derived from TLS multiplied by specific and generic wood density were used to estimate AGB/carbon stock from TLS. The third step in this research was identifying individual trees which are visible, have dense point cloud and not intermingling with others and exported as ASCII file. Then the exported tree point clouds as ASCII file was imported into MATLAB, and the data ran to generate tree volume using QSM algorithm. To estimate AGB/carbon stock of individual tree that derived from QSM tree volume generated was multiplied by wood density. The final stage in this research was to compare AGB/carbon stock that obtained from QSM and TLS with estimated from filed measured tree

parameters. Figure 4 shows the flowchart of a method that has been used to address each specific objective of this study.

Figure 2. Tree labelled in the sample plot with laminated paper has a number on it to identify trees having DBH of ≥ 10cm to estimate AGB/carbon stocks per tree.

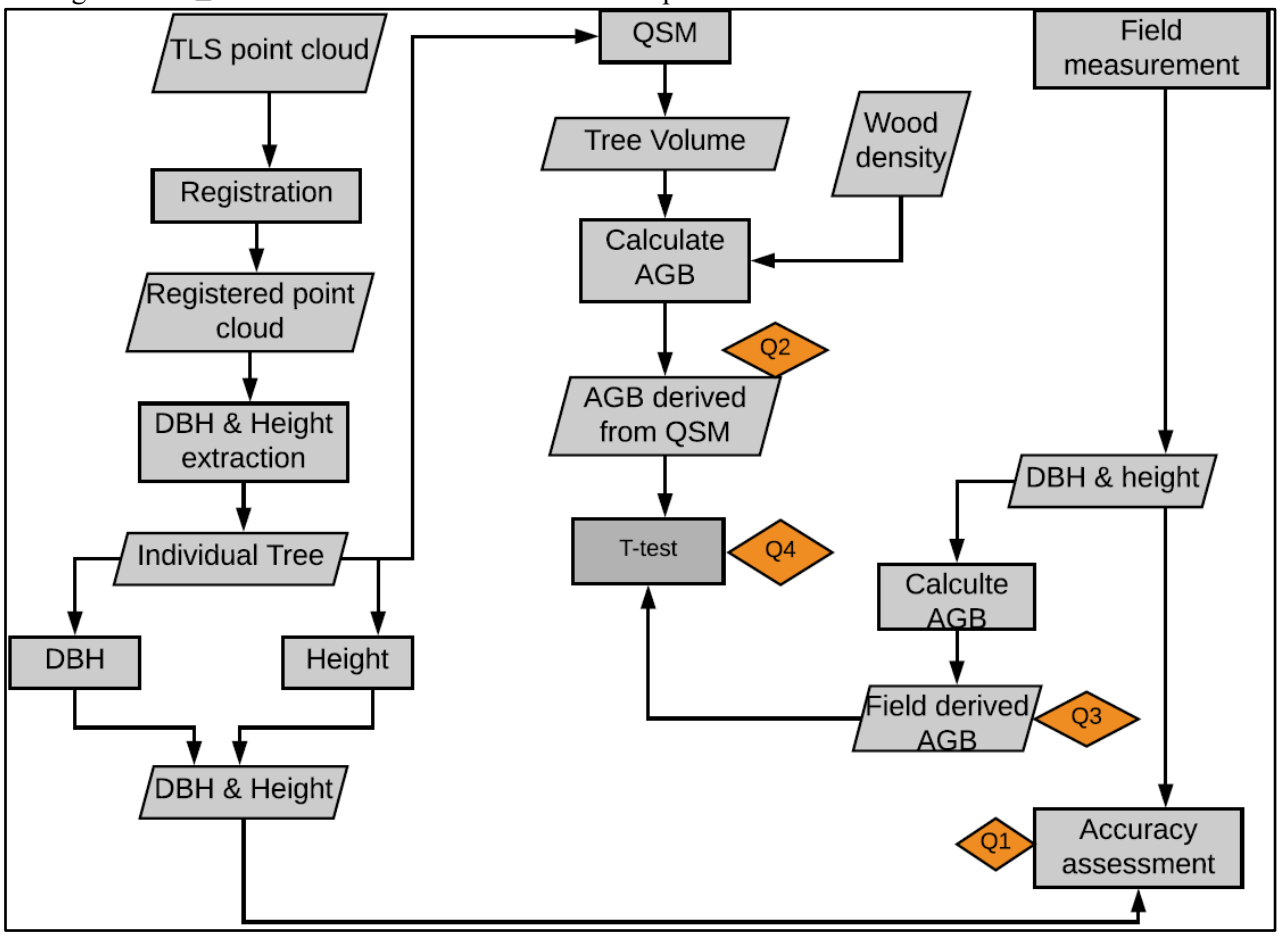

2.3.1. Sampling Design and determination of sample plot

Mangroves are not an easily accessible ecosystem, and it is difficult to apply a random or grid sampling strategy to estimate biomass/carbon stock. By taking the study area into consideration and homogeneity of the population, purposive sampling was selected to address the research objectives. The weight of TLS, time for TLS installation in the coastal area, travel time from plot to plot and the low and high tides were also considered to select purposive sampling. In purposive sampling, the sample chosen from the entire populations based on researcher interest and accessibility [13], but it includes all diversities.

A circular sampling plot of 500m^2 with a radius of 12.62m was recommended for biomass/carbon estimation. The area of the sampling plot was adjusted in line with a slope of the terrain using the slope correction factor. Due to the flat train of the study area, we are not using the slope correction factor to arrange the radius of our sample plot. The sample size that has greater than 600m^2 does not significantly improve the accuracy of the result; instead, it increases operational cost. Also, the circular plot has less error as compared to the rectangular plot. Therefore, a circular plot of 500m^2 selected in which multiple scanning positions applied.

Because of the unstable nature of the area and the mud, water, pneumatophores and aerial roots of *Rhizophora* the centre of the plot where selected on relatively stable and able to hold a tripod. By measuring a radius of 12.62m from the centre to the border of the bounder of the plot was demarked by check and all the trees inside the plot that have ≥ 10cm DBH were measured and considered for AGB estimation. All the trees inside the plot that have DBH of ≥ 10cm were labelled using laminated paper that has a number on it (Figure 3).

Figure 3. Tree labelling to identify trees in the sample plot that have DBH ≥ 10cm used for AGB/carbon stock estimation with laminated paper have a number on it attached to individual trees.

2.3.2. Terrestrial Laser Scanner data acquisition

The use of LiDAR (Light Detection and Ranging) to estimate forest parameter started later 2000s. Similarly, the use of TLS mounted on the tripod utilises a LiDAR system which collects multiple millions of point clouds within a minute. There are two approaches that we followed when applying TLS for point clouds collections which performed based on the objective that we try to achieve. These two approaches are single and multiple scanning modes [14]. During this study multiple scanning were performed, one at the centre of the plot and the rest (three) at different outer positions of the sample plot 2.5 m from the border of the plot (Figure 4). Total of four scanning locations within the sample plot was undertaken to get the best point cloud coverage. Trees within the plot with a DBH of ≥ 10cm were marked to distinguish the trees extracted from the sample to measure tree parameters, e.g., DBH, height, volume, etc. The point clouds which are collected from different positions in the sample plot help to get the 3D structure of the mangrove tree.

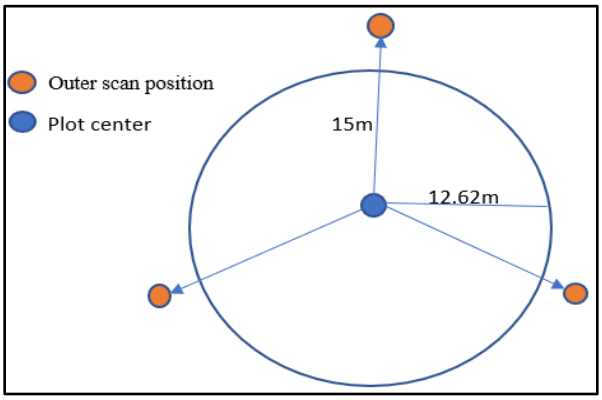

Figure 4. Multiple TLS scanning position one at the centre and the rest three approximately at 120o from each other with a radius of 12.62m to include the tree on the border of the plot it extends to 15m from the centre to have dense point clouds and the whole structure of the tree.

2.3.3. Retroreflectors

In multi-scanning retroreflectors used as tie points to merge all (four) scanning position data into one single point cloud by geometric transformation using RiSCAN PRO software [15]. Two types of retro-reflectors are used in this study; twelve cylindrical and six circulars (Figure 5). When we adjusted the scanning position within the plot four cylindrical and two circular retro-reflector were placed on a place that visible to two scanning locations. Circular reflectors were attached to the individual tree, and cylindrical one was fixed on sticks distributed in the plot. However, each retro-reflectors must be visible at least between the two scanning positions and central position.

Figure 5. Both circular and cylindrical retroreflectors that used as a reference (the common point between the two-scanning position) to register the four-scanning position in sample plot. Circular (left) and cylindrical (right) retroreflectors used.

2.3.4. Biometric Field Data Collection

Field data collection in the study area was performed from September 26 to October 28, 2018. Mangrove trees that have a DBH of ≥ to 10cm within the sample plot were measured and considered for biomass/carbon stock estimation. A DBH of the trees estimated at a 1.3m height above the ground and a stick having 1.3m height was used for consistent measurements (Figure 6). The contribution of the trees that have less than 10cm in diameter is insignificant to the biomass/carbon stock [16]. The tree that has a fork below 1.3m were also considered as two different trees, but that have above 1.3m was recognised as one. Tree height was measured using Leica DISTO D510.

Figure 6. *Rhizophora* species that need to climb them to measure DBH in the field using diameter tape.

2.3.5. Extraction of individual tree

After the registration of pint clouds of four scanning positions, individual trees were extracted manually to measure DBH and height using measuring tool in RiSCAN PRO (Figure 7). The biomass of single tree estimated by allometric equations and compared with biomass that derived from field measured and QSM derived.

Figure 7. Manually extracted individual tree with true-colour and saved as poly data for further analysis.

2.3.6. Tree parameters extraction and measurement

Individual tree DBH and height measured from a manually extracted tree in RiSCAN PRO software using measuring tools. The extracted tree saved as ploy data after removing noise (i.e., point clouds that is not part of the tree or from the nearby tree) and branches and canopy of another surrounding or overlapping trees. Two different approaches were used to measure DBH of the trees depending on the species of mangroves. Commonly *Avicennia* and *Rhizophora* are the two species in the study area. *Rhizophora* species have prop root to cope up with the high tide and aeration they rise their root above the ground; in some cases, it goes up to 2m. As a result, DBH measurement of *Rhizophora* spp. was measured from the end of the upper prop root 20-30cm [17] but in *Avicennia* spp., it starts from the ground, and we have used 1.3m above the ground to measure DBH (Figure 8). The height of the trees also measured by using the highest and lowest two points from the point clouds of the individual tree using the measuring tools in RiSCAN PRO software. Figure 13 shows the tree extracted and how its height was measured.

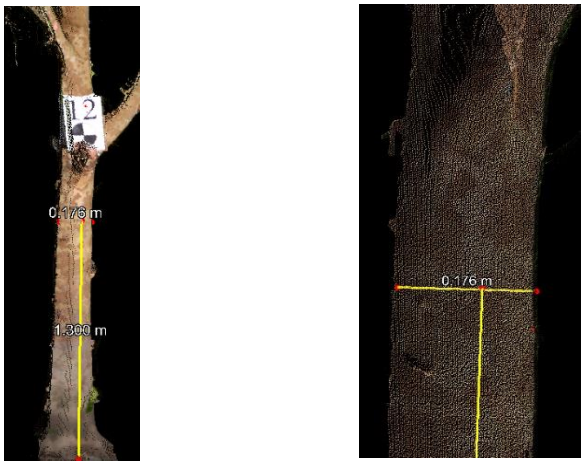

Figure 8. Individual tree DBH measured from manually extracted point clouds using measuring tools in RiSCAN PRO software.

2.3.7. Conversion of point clouds into ASCII format and QSM

The extracted individual trees point cloud converted and exported as an ASCII text file, that is a readable file format in MATLAB software. All individual trees data were exported and changed to x, y, z which makes it ready for 3D tree structure construction using the export function in RiSCAN PRO software. Reconstruction of the individual tree using QSM, done after TLS point clouds of each tree were exported as an ASCII and imported/loaded to MATLAB (R2018b) software. The procedural step that was taken during we performed tree QSM in MATLAB listed in the following sub-sections.

2.3.8. Steps of the reconstruction process.

Figure 9 shows the main steps in the reconstruction process of individuals tree in MATLAB using the QSM algorithm. The flow chart in Figure 9 and subsections describe the procedure followed in the reconstruction of the individual tree to generate volume in detail.

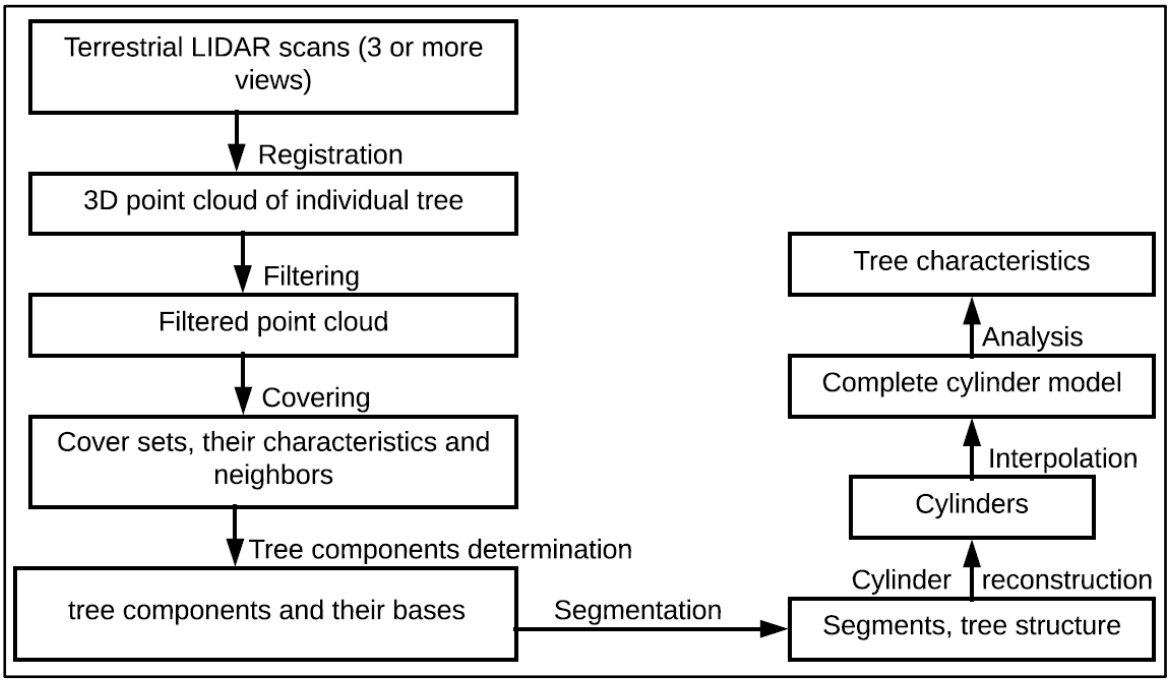

Figure 9. Main steps of reconstruction a tree using QSM [10].

3. Results and Discussions

3.1. The relationship between TLS derived, and field measured DBH and height

The estimated DBH and height derived from TLS and field measurement (Figure 10 & 11) show a strong relation. The two figures showed a very high correlation between the two methods with a coefficient of determination of (R^2) 0.978 for DBH, while a reasonable R^2 0.73 was found between the TLS height and field measured one. To confirm that the relation between the two methods, a t-test was performed at a confidence interval of 95% ($\alpha = 0.05$). These results suggest that there is no significant difference between DBH derived from TLS and DBH that measured in the field using diameter tape.

Similarly, there is no significant difference between height measured by Leica DISTO D510 and derived from TLS point clouds. As a result, the null hypothesis that stated, there is no significant difference between the two methods was accepted at a 95 % confidence interval.

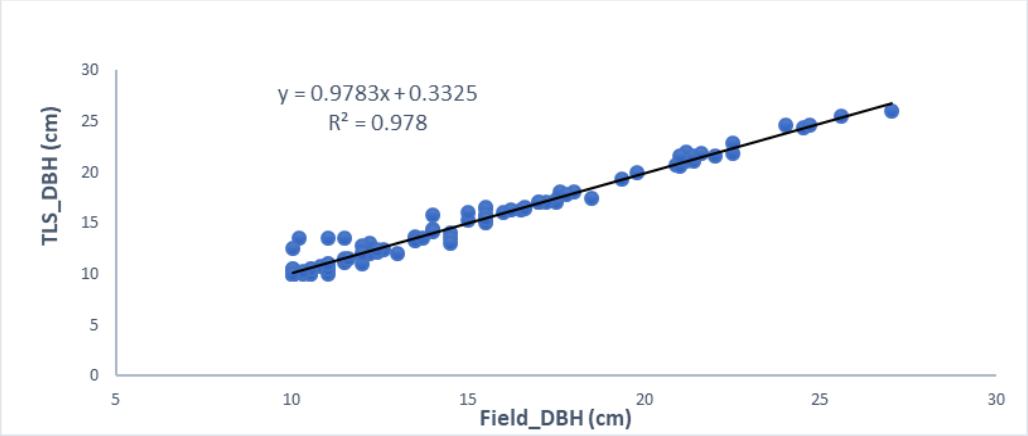

Figure 10. The relationship between field measured and TLS derived DBH

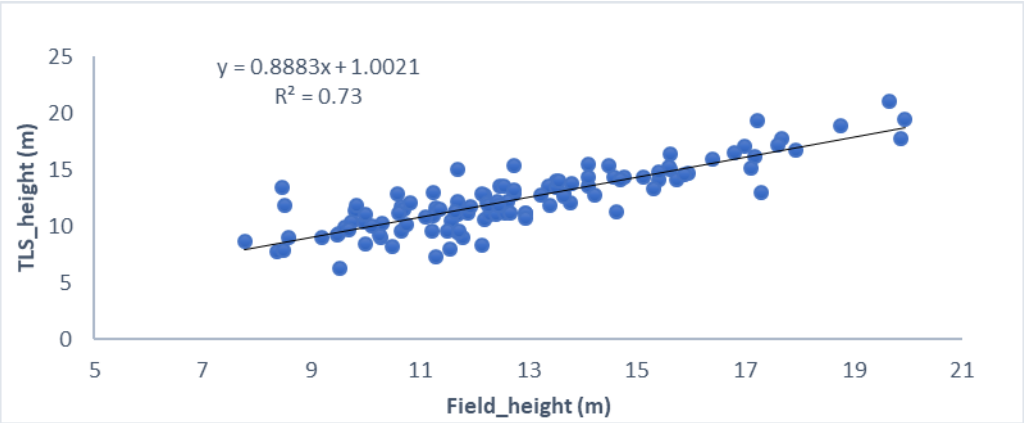

Figure 11. The relationship between field measured and TLS derived height

3.2. The relationship between AGB derived from TLS point clouds and field-measured tree parameters
The estimated AGB in both general and specific wood density using allometric equations do not show a significant difference between AGB derived from TLS estimated tree parameters and from field measured tree parameters. Figures 12 & 13 show the relation between AGB derived from TLS and field measured with the coefficient of determination R^2 0.978 with RMSE of 14. 49 kg/tree and R^2 0.9779 with RMSE of 11.41 kg/tee using specific and generic wood density respectively. These results suggest that estimation of AGB in both methods are highly correlated.

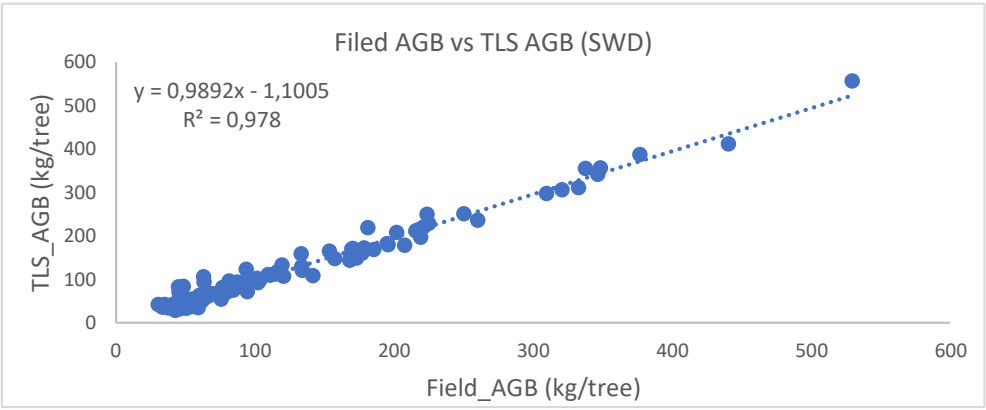

Figure 121. The relationship between field measured and TLS derived AGB using specific wood density.

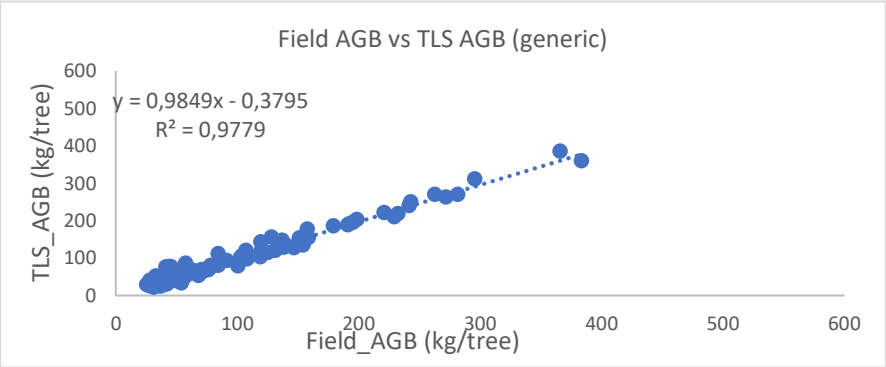

Figure 13. The relationship between field measured and TLS derived AGB using general wood density.

3.3. The Relationship between AGB derived from QSM and field measured

The relation between above ground biomass derived from QSM and field measurements using allometric equation resulted in a coefficient of determination R^2 0.9638 with RMSE of 15.05 kg/tree and R^2 0.9649 with RMSE of 21.08 kg/tree for general and specific wood density (SWD) respectively. Figures 14 & 15 show the relation between AGB derived from QSM and field measurements using specific and generic wood density respectively. These results suggest that estimation of AGB using specific and generic wood density multiplied by field-measured tree parameters and tree volume derived from QSM shows there is no significant difference, but specifically, the result suggests that when specific wood density used, there are high correlations between AGB estimated from QSM derived tree volume and field-measured tree parameters.

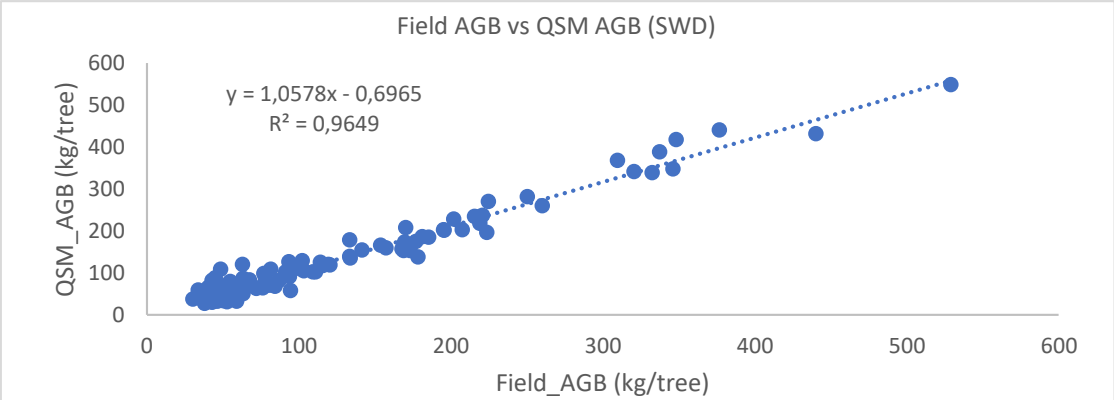

Figure 14. The relationship between field measured and QSM derived AGB using specific wood density.

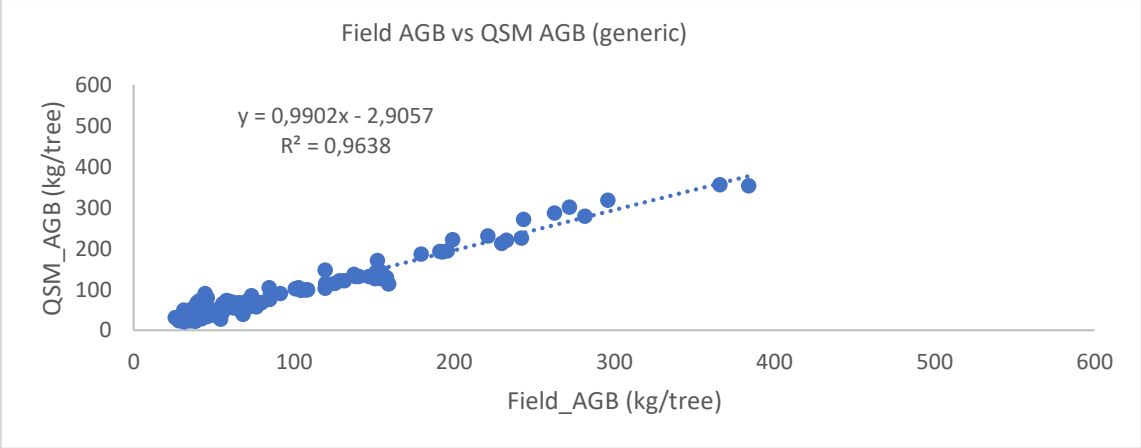

Figure 15. The relationship between field measured and QSM derived AGB using general wood density.

3.4. The Relationship between AGB derived from QSM and TLS point clouds

DBH and height of individual trees were extracted and measured using measuring tools in RiSCAN PRO to estimate AGB/carbon stock using generic wood density allometric equation and specific wood density allometric equation from global wood density. The allometric equation used is from Chave et al., [18]. Estimation of AGB/carbon stock obtained from QSM done by multiplying total tree volume generated through reconstruction algorithm with specific wood density 0.6987 and 0.8814 for *Avicennia*

and *Rhizophora* respectively and 0.57 for generic wood density for both species. AGB derived from TLS with allomeric equation was compared with AGB derived from QSM. Figures 16 and 17 show the relationship between AGB derived from TLS and derived from QSM with a coefficient of determination (R^2) 0.9757 and 0.9741 for general and specific wood density respectively. These results suggest that wood density does not significantly effect on the estimation of AGB using QSM derived tree volume and TLS derived tree parameters.

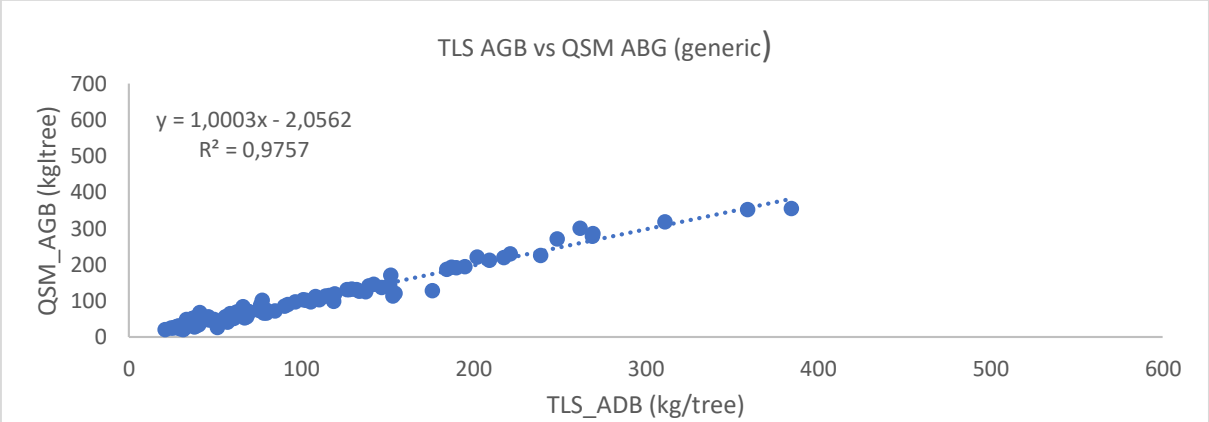

Figure 16. The relationship between TLS and QSM derived AGB using general wood density.

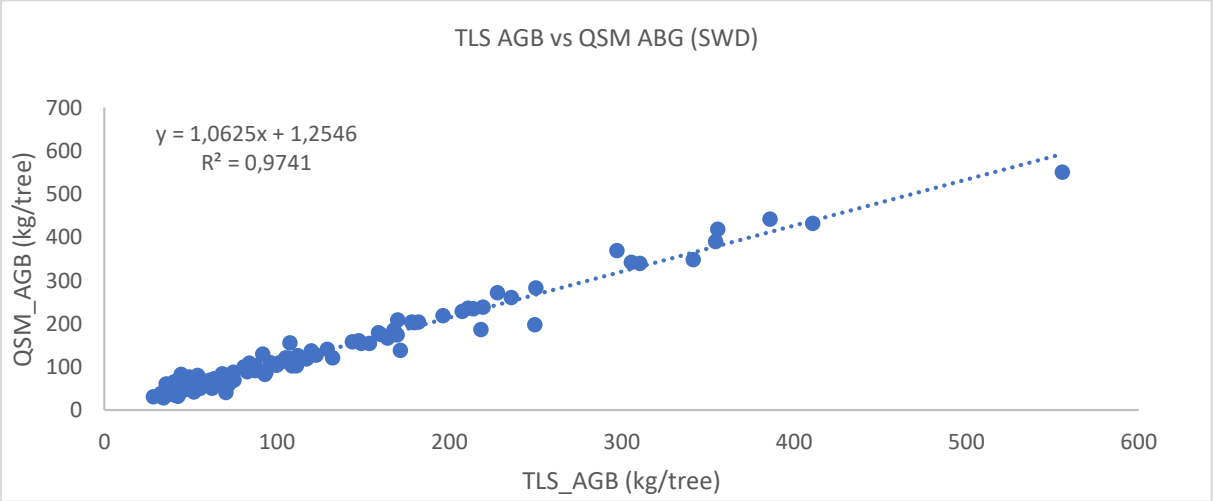

Figure 17. The relationship between TLS and QSM derived AGB using specific wood density.

3.5. Above ground biomass estimation

3.5.1. Above ground biomass estimated from field measured compared with derived from TLS point clouds

Above ground biomass/carbon stock of the study area estimated using generic/default and specific wood density. The AGB/carbon stock per trees varied from 25.8 kg/tree to 383.88 kg/tree and an average of 94.59 kg/tree when calculated from the field measured parameter using generic allometric equation but when species-specific allometry used the amount of AGB kg /tree increase to some extent, i.e. 30.3 kg/tree to 529.16 kg/tree and an average of 116.86 kg/tree. A similar case happened when AGB of the study area estimated using TLS derived parameters in both generic and species-specific allometry. When the generic allometry used AGB kg/tree range from 20.98 kg/tree to 384.35 kg/tree with an average of 92.79 kg/tree. For species-specific allometry, it ranges from 28.26 kg/tree to 555.89 kg/tree and an

average of 114.5 kg/tree. In both TLS derived and field-measured tree parameters, AGB estimated using species-specific is higher than the generic one. The result presented in section 3.3.3 shows there is no significant difference between AGB estimated from field measured DBH and height with AGB estimated using TLS derived DBH and height. Ghebremichael, [19]; Bazezew, [20] and Edward, [21] have got the same result in tropical inland forests.

3.5.2. Above ground biomass estimated from field measured compared with derived from QSM
To estimate AGB obtained from QSM total tree volume generated by reconstruction algorithm in MATLAB was multiplied by wood density (i.e., both general and specific wood density) and compared with the AGB that estimated by an allometric equation using tree parameter measured in the field. These results suggest that there is no significant difference between AGB derived from QSM compared to AGB from field measured. The same result obtained by Edward, [21] and Madhibha, [22] in a tropical forest in Malaysia. Madhibha, [22] used the same method with this research to estimate AGB of tropical forest in Ayer Hitam Forets Reserve, Malaysia and she got coefficient of determination or R^2 of 0.81 using default wood density and 0.797 for species-specific wood density which is slightly different with the average results 0.9638 of generic and 0.9649 specific in this study. The difference in results happened due to more young trees and open canopies of mangrove and not very high and intermingling tree canopies in this study area. Thus, it was easier for the laser beams of the TLS to reach the stems and canopies of the trees, and consequently, the point clouds were able to estimate the tree parameters better than the tropical in-land forest. Therefore, the AGB in this study estimated with higher accuracy. AGB obtained from QSM overestimated by 5.18 %, and allometric equations underestimate by 1.9%. Calderas et al., [23] obtained QSM overestimates the AGB by 9.68% and underestimation range between 36.57% - 29.85% for allometric equations in a Eucalyptus open forest. AGB estimated using allometric equations are DBH dependent and the error increase exponentially with increasing DBH, whereas AGB derived from QSM is DBH independent.

3.5.3. Above ground biomass derived from QSM compared with derived from TLS
Tree parameters DBH and height derived from TLS were used in the allometric equation to estimate above ground biomass. One hundred fifteen trees were used to assess AGB/carbon stock from both QSM and TLS. The result presented in section 3.3.8 showed that there is no significant difference found between AGB derived from QSM compared to AGB estimated form TLS with R^2 of 0.9757 and R^2 of 0.9741 by using general and specific wood density respectively. As the reconstruction of the tree in QSM depends on the point cloud from the TLS, these results were expected.

Madhibha, [22]; Tilon, [24] and Edward, [21] found the same result with this research when they compare AGB derived from QSM and TLS in the tropical and temperate forest. Madhibha, [22] reported that error in the estimation of AGB which was found in height estimations that is the same in this study. Therefore, the major issue contributing to error which affects allometric equations is the use of DBH and height, especially when there is an error in measuring these two parameters. To estimate AGB/carbon stock in this study both DBH and height were used. The same problem happened in this study as in Madhibha, [22] to estimate AGB/carbon stock due to error from height estimation. Calders et al., [23] found R^2 of 0.98 between AGB derived from QSM compared to destructive method but a lower R^2 of 0.78 when compared to AGB, derived from the allometric equation. The potential sources of error mentioned by Calders et al. [23] are wrongly chosen QSM parameters and basic wood density values that were derived from a range of DBH value which is not a source of error in this study as a result of using single wood density to estimate AGB/ carbon stock.

4. Conclusions
DBH and height of individual trees were measured in the field using diameter tape and Leica DISTO D510 respectively and compared with DBH derived from TLS point cloud in RiSCAN PRO software using measuring tools. Scatter plots (Figures 10 and 11) were constructed between DBH and height derived from TLS and field measured DBH and height. R^2 of 0.978 and 0.73 were obtained from

regression analysis for DBH and height. The level of significance was tested using a t-test, and it shows there is no significant difference between both method (TLS derived, and field measured) in DBH and height measurements. Therefore, the null hypothesis was accepted at a 95% confidence interval (there is no significant difference between DBH, and height derived from TLS and field measurement).

Height and DBH of individual trees measured in the field was used in the allometric equation to estimate AGB/carbon stock and compared with AGB derived from TLS using its measured DBH and height. The significant difference between AGB/carbon stock derived from TLS and AGB/carbon stock measured from the field was tested using t-test statistics. The results showed (Figures 12 and 13) that there is no significant difference between AGB/carbon stock estimated by both TLS and field methods using default/generic and specific wood density. As a result, the null hypothesis was accepted at a 95% confidence interval.

Above ground biomass/carbon stock derived from QSM method have shown no significant difference from above ground biomass/carbon stock estimated from field measured tree parameters using the allometric equation ($P>0.05$). This means that the null hypothesis is accepted. Figures 14 and 15 show the relationship between AGB/carbon stock derived from QSM and field measurements using the allometric equation. The result of this study shows that QSM can accurately estimate AGB/carbon stock of mangrove forest in the coastal area.

5. Acknowledgment

The Authors would like to highly acknowledge and appreciate the research permit issued by the Indonesian Ministry of Science and Technology and Higher Education. They would like to highly Acknowledge the support and contribution of Dr. Y. Budi Sulistioadi and the Faculty of Forestry University of Mulawarman, Samarinda, Indonesia for facilitating our research work, helping us with the logistic, collecting image and ground truth data in Tani Baru mangrove forest. We highly appreciate the support of the team of Mita Priskawanti and Muhammad Lutfi Hamdani for their continuous help during October 2018. We acknowledged the UAV data collection by Dr. Y. Budi Sulistioadi in 2017 and 2018. Without the data and support, our research could not have been done.

6. References

[1] Yu, X., et al., *Stem biomass estimation based on stem reconstruction from terrestrial laser scanning point clouds.* Remote Sensing Letters, 2013. **4**(4): p. 344-353.

[2] Penman, J., et al., *Good practice guidance for land use, land-use change and forestry.* Good practice guidance for land use, land-use change and forestry., 2003.

[3] Næsset, E., et al., *Laser scanning of forest resources: the Nordic experience.* Scandinavian Journal of Forest Research, 2004. **19**(6): p. 482-499.

[4] Chave, J., et al., *Improved allometric models to estimate the aboveground biomass of tropical trees.* Global change biology, 2014. **20**(10): p. 3177-3190.

[5] Raumonen, P., *Quantitative structure tree models from terrestrial laser scanner data.* Proceedings of Silvilaser, 2015: p. 28-30.

[6] Feliciano, E.A., S. Wdowinski, and M.D. Potts, *Assessing mangrove above-ground biomass and structure using terrestrial laser scanning: A case study in the Everglades National Park.* Wetlands, 2014. **34**(5): p. 955-968.

[7] Newnham, G.J., et al., *Erratum to: Terrestrial Laser Scanning for Plot-Scale Forest Measurement.* Current Forestry Reports, 2016. **2**(3): p. 214-214.

[8] Eggleston, H., et al., *IPCC Guidelines for National Greenhouse Gas Inventories. Volume 4: Agriculture, Forestry and Other Land Use.* Hayama: IPCC, 2006.

[9] Zianis, D., et al., *Biomass and stem volume equations for tree species in Europe*. 2005: FI.

[10] Raumonen, P., et al., *Fast automatic precision tree models from terrestrial laser scanner data*. Remote Sensing, 2013. **5**(2): p. 491-520.
[11] Bosma, R., et al., *Challenges of a transition to a sustainably managed shrimp culture agro-ecosystem in the Mahakam delta, East Kalimantan, Indonesia*. Wetlands ecology and management, 2012. **20**(2): p. 89-99.
[12] Persoon, G.A. and R. Simarmata, *Undoing 'marginality': the islands of the Mahakam delta, East Kalimantan (Indonesia).* Journal of Marine and Island Cultures, 2014. **3**(2): p. 43-53.
[13] Teddlie, C. and F. Yu, *Mixed methods sampling: A typology with examples.* Journal of mixed methods research, 2007. **1**(1): p. 77-100.
[14] Maas, H.G., et al., *Automatic forest inventory parameter determination from terrestrial laser scanner data.* International journal of remote sensing, 2008. **29**(5): p. 1579-1593.
[15] Wilkes, P., et al., *Data acquisition considerations for terrestrial laser scanning of forest plots.* Remote Sensing of Environment, 2017. **196**: p. 140-153.
[16] Brown, S., *Measuring carbon in forests: current status and future challenges.* Environmental pollution, 2002. **116**(3): p. 363-372.
[17] Kangkuso, A., et al., *Trends in allometric models and aboveground biomass of family Rhizophoraceae mangroves in the Coral Triangle ecoregion, Southeast Sulawesi, Indonesia.* Journal of Sustainable Forestry, 2018. **37**(7): p. 691-711.
[18] Chave, J.r., et al., *Tree allometry and improved estimation of carbon stocks and balance in tropical forests.* Oecologia, 2005. **145**(1): p. 87-99.
[19] Ghebremichael, Z., *Airborne LiDAR and terrestrial laser scanner (TLS) in assessing above ground biomass/carbon stock in tropical rainforest of Ayer Hitam forest reserve, Malaysia*. 2016, M. Sc. thesis, University of Twente, Faculty of Geo-Information Science and Earth Observation, Enschede, The Netherlands. Retrieved from http://www. itc. nl/library/papers_2016/msc/nrm/ghebremichael. pdf).
[20] Bazezew, M.N., *Integrating airborne lidar and terrestrial laser scanner forest parameters for accurate estimation of above-ground biomass/carbon in Ayer Hitam tropical forest reserve, Malaysia*. 2017, M. Sc. thesis, University of Twente, Faculty of Geo-Information Science and Earth Observation, Enschede, The Netherlands. Retrieved from http://www. itc. nl/library/papers_2017/msc/nrm/bazezew. pdf).
[21] Edward, J., *The effect of tree density on the assessment of above ground biomass using Terrestrial Laser Scanner and Quantitative Structure Modelling in Berkelah Tropical Forest, Malaysia*. 2018, The University of Twente.
[22] Madhibha, T., *Assessment of Above Ground Biomass with Terrestrial Lidar using 3D Quantitative Structure Modelling in Tropical Rain Forest of Ayer Hitam Forest Reserve, Malaysia*. 2016, MSc thesis, University of Twente Faculity of Geo-information and Earth Observation Science (ITC). Enschede, The Netherlands. Retrieved from http://www. itc. nl/library/papers_2016/msc/nrm/madhibha. pdf).
[23] Calders, K., et al., *Nondestructive estimates of above-ground biomass using terrestrial laser scanning.* Methods in Ecology and Evolution, 2015. **6**(2): p. 198-208.
[24] Tilon, S., *The Effect of Foliage on Estimating Above Ground Forest Biomass Using Terrestrial Laser Scanning and Quantitative Structure Modelling in Gronau.* The University of Twente, Faculty of Geo-Information Science and Earth Observation, Natural Resource Management, 2017. **73**.

Estimation of aboveground biomass/ carbon stock and carbon sequestration using UAV images at Kebun Raya Unmul Samarinda (KRUS) education forest, East Kalimantan, Indonesia

MD A Hashem[1]*, L van Leeuwen[1], Y A Hussin[1], Y B Sulistioadi[2]

[1]Department of Natural Resources, Faculty of Geo-information Science and Earth Observation (ITC), University of Twente, Hengelostraat 99, 7511 AE Enschede, The Netherlands
[2]Soil and Water Conservation Laboratory, Forestry Faculty, Center of Geospatial Information Infrastructure Development (CGIID), Institute for Research and Community Services (IRCS), Mulawarman University,

e-mail: y.a.hussin@utwente.nl

Abstract. The accurate assessment of AGB/ carbon stock and carbon sequestration in the forest is the burning issue to the global community for taking mitigation and adaptation measures. REDD+ activities need to be evaluated scientifically which requires MRV mechanism of carbon emissions to follow the UNFCCC principles that would be transparent, consistent, comparable, complete and accurate. Quantification and monitoring of tropical rainforest carbon sequestration are essential to understanding the role of the tropical rainforest on the global carbon cycle. The application of UAV is effective and efficient in assessing biomass with a relatively low cost for a small area at regular intervals. The purpose of this study is to assess forest aboveground biomass/carbon stock and carbon sequestration using high-resolution UAV images. The DSM, DTM, and orthomosaic were generated based on structure from motion (SfM) and 3D point clouds filtering techniques. The canopy height model (CHM) was generated from the DSM and DTM. The height extracted from the CHM and the predicted DBH calculated from the CPA based on the quadratic model were used as input in the generic allometric equation to estimate AGB and carbon stock. The results revealed that there was no statistically significant difference between field-based AGB and UAV-based AGB.

1. Introduction

Most of the studies on assessment of AGB/carbon stock and carbon sequestration in tropical rainforest has been conducted using optical images [1-4]. The data collected from optical remote sensing can have problems due to clouds, shadows, high saturation, low spectral variability, 2-D in nature and it is quite challenging to assess AGB and carbon stock using these data [5]. Although some medium-resolution remote sensing data such as Landsat, Sentinel, etc. are freely available, it is difficult to use them to assess the forest aboveground biomass and carbon stock due to pixel size, resolution versus tree crown size. Some very high-resolution data such as QuickBird, IKONOS, etc. can estimate biomass accurately, but they are costly and need highly technical knowledge to process [6]. The application of radar backscatter to estimate AGB/carbon stock is challenging and leads to underestimation of AGB in the tropical forest because of its high density and complex structure [7]. L-band radar data can be used to estimate AGB accurately up to 150 Mg ha^{-1} and it tends to saturate with AGB is greater than 150 Mg ha^{-1} [7]. The decrease of intensity of radar backscatter also known as saturation effect is the main reason for under-estimation of AGB. Recently, Lidar has proved to be the best remote sensing technique to estimate biomass/ carbon stock accurately and precisely. However, it is very expensive to assess biomass and carbon stock over a large area. Unmanned aerial vehicles (UAVs) can acquire high resolution remotely sensed data to estimate biomass and carbon stock. The application of UAV is effective and efficient in

assessing biomass with a relatively low cost for a small area [8]. Furthermore, limited expertise is good enough to operate and acquire data from the UAV platform.

Conventional remote sensing techniques can provide horizontal forest structure accurately rather than vertical forest structure. On the contrary, UAV is capable of providing horizontal and vertical forest structure. In tropical rainforests, the estimation of above ground biomass and carbon stock is quite challenging because of its complex stand structure and plentiful verities of species composition. A very limited number of researches were carried out using UAV images and Lidar in a tropical forest. However, the research on carbon flux and atmosphere is still insufficient in a tropical forest. Based on that reason, it is essential to conduct research on quantifying and monitoring carbon sequestration in a tropical forest. Few studies were carried out to estimate carbon sequestration annually using high resolution remotely sensed data. The research on the accuracy of the assessment of the AGB and carbon stock and specifically carbon sequestration using high-resolution UAV images of two consecutive years would be helpful in the decision-making process to implement the REDD+ initiatives, sustainable forest management and eventually natural resources management using its mechanism on MRV.

Despite having some benefits UAV also has limitations. The captured images by the UAV can only cover the upper canopy of the tree. In the tropical forest, the lower canopy of trees is not visible because it is fully or partially covered by the upper canopy trees. The point clouds are generated based on the captured images that covered upper canopy, and it has an impact on assessing the total AGB and carbon stock. The different sources of error or uncertainty have direct effects on AGB/ carbon stock and especially sequestration estimation. The choice of remote sensing techniques influences the level of uncertainty in the estimate of biomass. The major sources of error in assessing AGB/carbon stock and carbon sequestration are UAV data processing, tree parameter collection, allometric equations, ground-based sampling, regression modeling. In a tropical forest, the measurement of height is challenging because of the complex nature of the structure. It is quite challenging to extract accurate height form UAV-derived point clouds. The height variation affects the total AGB/carbon stock estimation, and finally, it influences assessing carbon sequestration. The variation of the amount of AGB and carbon stock of two years due to height error might be affected more on carbon sequestration estimation. The manually delineated CPA or automatic segmented CPA might have a certain level of inaccuracy, and it also has effects on biomass and carbon sequestration estimation because the predicted DBH is found based on CPA. In order to have complete and accurate biomass and carbon stock estimation, the identification and estimates of error is an essential part of the process [9]. Therefore, it is significant to identify and quantify these errors and analyze the effect on biomass estimation and more specifically, how will that affect the carbon sequestration.

This study is aiming at the assessing of AGB/ carbon stock, carbon sequestration and evaluating the effects of height and CPA delineation error on biomass estimation from very high-resolution UAV images based on SfM photogrammetry approach at Kebun Raya UNMUL (University of Mulawarman) Samarinda (KRUS) Education Forests, East Kalimantan, Indonesia.

2. Materials and Methods

2.1 Study Area

UNMUL Samarinda botanical garden also known as 'KRUS' located in the Samarinda City of East Kalimantan province, Indonesia which was belonging to CV. Mahakam wood before 1974. CV. Mahakam wood handed over an area of 300 hectares to the rector of Mulawarman University in 1974. Then the area was used as a conservation forest area and a suitable place for conducting research and educational activities on tropical forest. On 9 July 1974, the area was inaugurated as educational forests. In 2001, 300 hectares was reduced by 62 hectares because the area was allocated for a recreational botanical garden tourist spot. The map of the study area is shown in Figure 1.

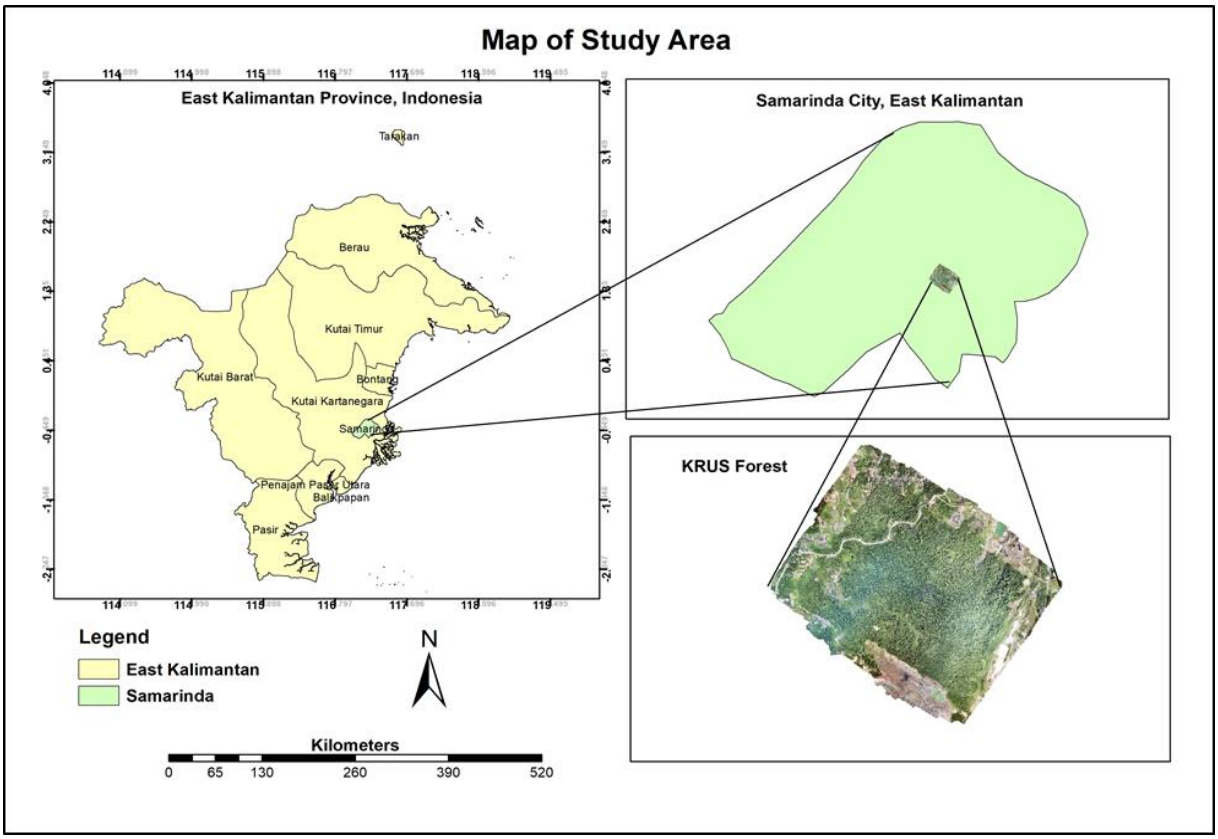

Figure 1. Map showing the study area

Kebun Raya Unmul Samarinda education forest is located between 117° 12' 15.388" E - 117° 13' 35.786" E and 0° 26' 17.435" N - 0° 27' 32.769" N. The study area is located in urban villages namely Laterite and Mugirejo under the North Samarinda and Sungai Pinang administrative districts respectively [10]. The average annual rainfall is 2000 mm while the rainfall is observed slightly lower from June to October. The daily maximum temperature is observed 33.20^0 C while 24.50^0 C is observed as the daily minimum temperature [10]. Very dry years occasionally occur due to the effect of the Southern Oscillation phenomenon and El Niño [11]. The soils of the study area are Podzolic Kandic, Podromolic Chromic, and Cambisol. The 60-70% of the study area consists of forest areas with ramps up rather steep slope.

The study area is largely a forest area with vegetation cover logged secondary dry forest (logged-over areas), and thickets with an area covering around 209 hectares while 29% of the area is the non-forested area. Among the 70% of secondary forests, the dominant species are Artocarpus spp, Macaranga spp, Eusideroxylon zwageri, Pentace spp., etc [10].

2.2 Materials

2.2.1 Field Equipment. The tools and equipment mentioned in Table 1 were used in the study to measure and collect the required data from the field.

Table 1: List of field equipment and its uses

Name of tools/ equipment	Uses
UAV Phanton4 DJI	2-D image capturing
Measuring tape (50m)	Identification of the outer boundary of plots
Diameter tape (5m)	Measurement of tree DBH
Handheld GPS (Garmin)	Navigation and X, Y coordinate reading
Field data sheet and pencil	Data recording
Range finder/ Haga altimeter	Measurement of tree height
Leica DISTO D5	Height measurement
Tablet	Navigation
Santo Clinometer	Slope measurement
DGPS	GCPs and plot center location

2.2.2 Data Processing Software. The different types of software were used to process and analyze the collected data from the study area. The list of software and their uses are mentioned in Table 2.

Table 2: List of software and uses

Name of software	Uses
ArcMap 10.6.1	Data processing and visualization
Pix4D	Photogrammetry processing
Erdas Imagine	Resampling of ortho-mosaic image
Microsoft Excel	Data analysis
Cloud compare	3-D point cloud visualization
Microsoft Word	Reports and thesis writing
Mendeley Desktop	Citation and references
Lucidchart	Flowchart drawing
Microsoft power point	Presentation of thesis

2.3 Methods

The research method encompasses the fieldwork design, spatial and statistical analysis and estimating the AGB/AGC and carbon sequestration and lastly evaluating the influence of height and CPA delineation error on assessing AGB. The research method of this study was comprised of five parts (Figure 2):

(i) The first part was the biometric data collection, processing, and analysis. It involved the field observation and acquiring required tree parameters using the above-mentioned instruments in Table-1;

(ii) The second part was capturing digital images using a UAV platform. Then the data was processed by Pix4D software to generate DSM, DTM and orthophoto;

(iii) The third part was the extraction of tree height from CHM generated from DSM and DTM;

(iv) In the fourth part, aboveground biomass (AGB)/ carbon stock and carbon sequestration were assessed using tree height and predicted DBH extracted from UAV data in the third part.

(v) In the fifth and the last part, the effect of the height and CPA delineation error on aboveground biomass was assessed.

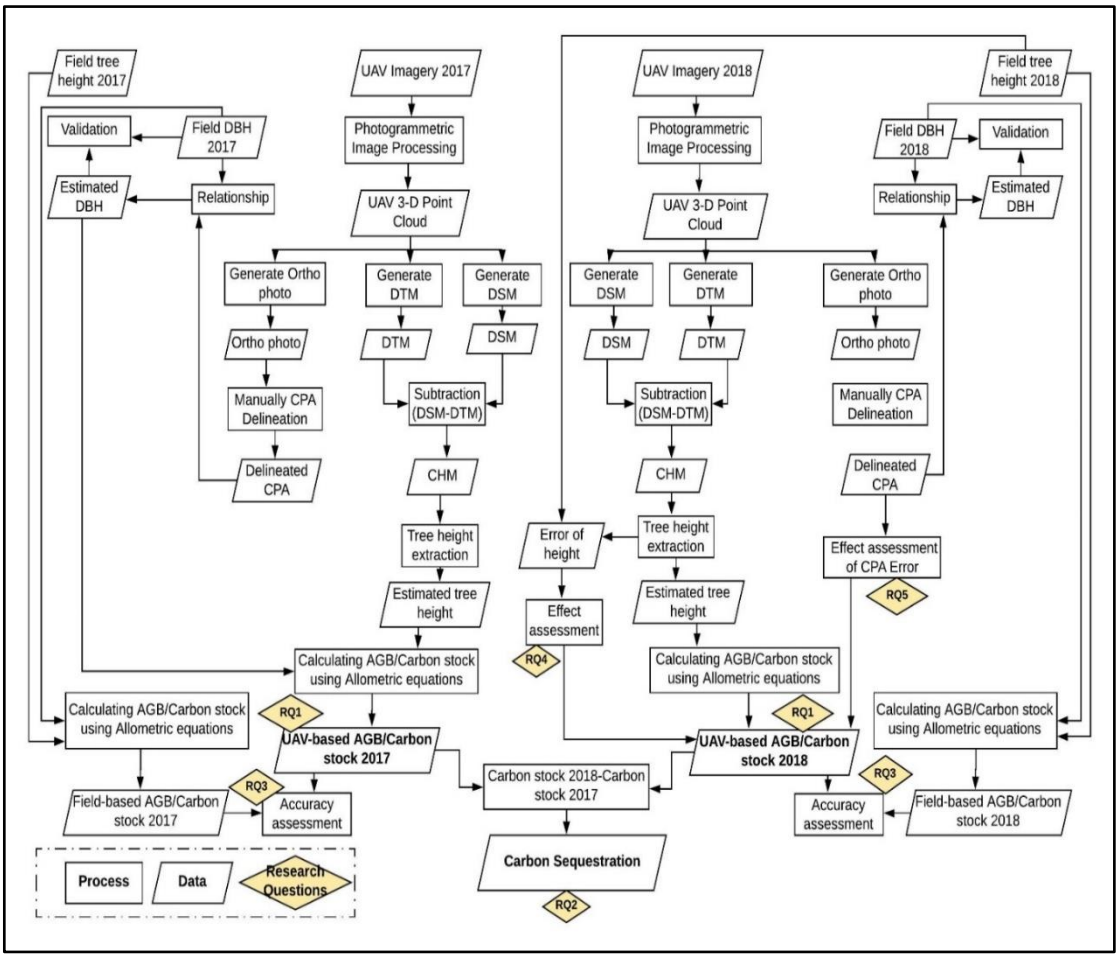

Figure 2. Research methods diagram.

2.4 Sampling design and plot size

In this study, a purposive sampling method was used to collect the field data. This sampling method is a non-probability method based on the judgment of researchers. The purposive sampling method was chosen considering the time limitation, inaccessibility in the forest, covering the variation of all forest structure, terrain conditions, UAV flight planning, etc. The total of 41 plots was selected to collect the biometric data. The distribution of sampling plots is shown in Figure 3.

Circular plots with an area of 500 m^2 (radius 12.62m) were used in flat terrain to collect the biophysical parameters of trees. Circular plots are preferred compared to square and rectangular plots because of delineating the outline of the plots is relatively easy and less error-prone. A study conducted by Ruiz et al., [12] brought to light that no significant difference in results could be found if the plot size is increased beyond 500 m^2. The radius of the plots was adjusted using a slope correction table if any slopes existed inside the plots.

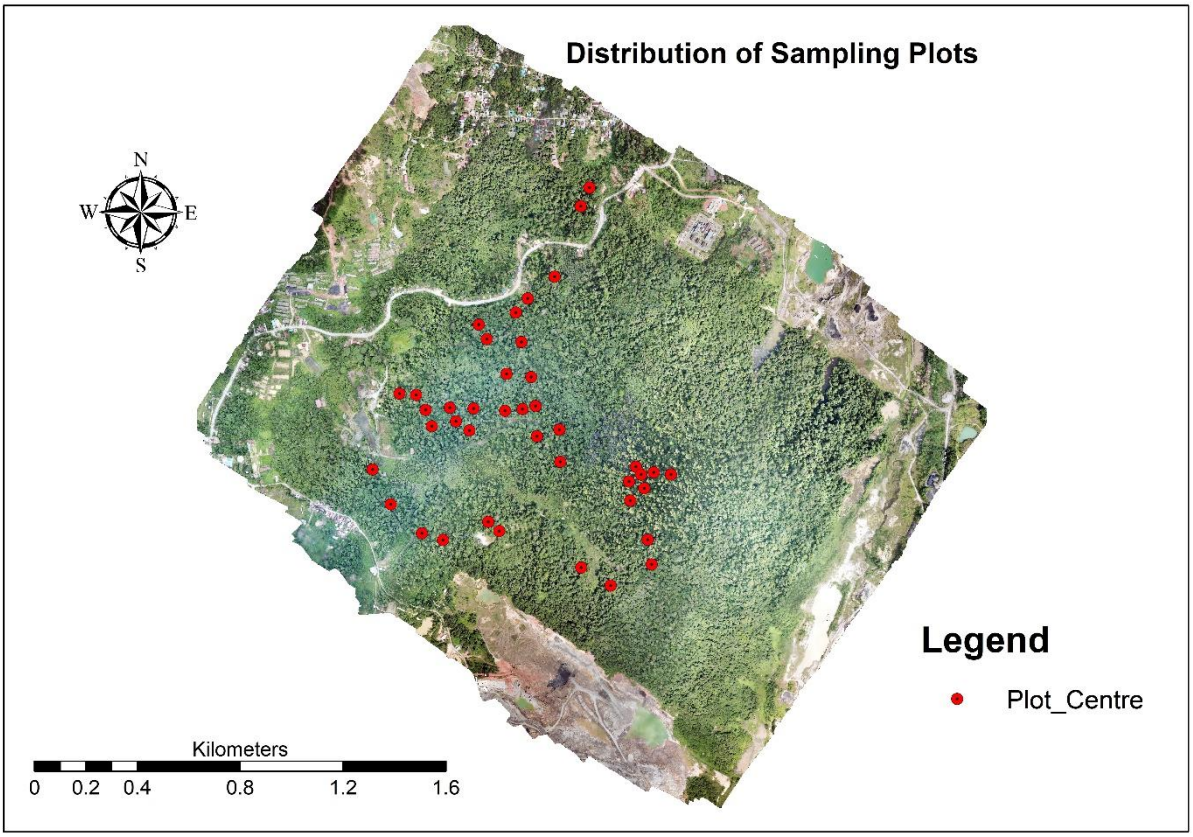

Figure 3. Distribution of sampling plots in the study area.

2.5 Biometric data collection

In this study, the primary, as well as secondary data were used to achieve the objectives of the research. The UAV images for 2017 obtained by the University of Mulawarman, Indonesia were used as secondary data. The following sub-sections illustrate the procedures and methods of field data as well as UAV data collection including the recording of the ground control point (GCP) using differential global positioning system (DGPS).

Fieldwork was conducted from 01 October 2018 to 25 October 2018. First, the center of the plot was fixed; then the measuring tape was used to delineate the outline of the plot with a 12.62m radius which covers 500 m^2. The XY coordinate of the center of the plots and the tree location was recorded by Garmin GPS. The diameter of breast height (DBH) was measured using diameter tape at 1.3m above ground. The height of the trees was measured using a Leica DISTO D510. The tree is having DBH equal to or greater than 10 cm was considered because the trees that have DBH less than 10 cm cannot contribute a role significantly in assessing aboveground biomass [9]. The tree height and DBH were recorded for 943 trees from the 41 plots. All the measured tree parameters were documented in a datasheet that was prepared before going to the field and later the data were transferred into the excel sheet for analysis. The captured photograph during the collection of biometric data is shown in Figure 4.

Figure 4. Biometric data collection

2.6 UAV Flight Planning

In this study, the UAV imagery was collected from the Kebun Raya UNMUL Samarinda (KRUS) education forest. The flight areas were selected based on the availability of enough open space to set the ground control points (GCPs) as well as landing and taking off UAV. The images were collected using Phantom-4 DJI UAV/ Drones. The mission planning was done setting flight parameters using Pix4D capture app. The spatial quality of the images acquired from the UAV platform depends on flight height and front and side overlap. There is a significant relationship between flight height, overlap, weather conditions and the quality of the point clouds [13]. Table shows the image acquisition parameters that were set-up to obtain the high-quality photogrammetric output.

Table 3. UAV flight planning

Parameter	**Value**
Speed	Moderate
Angle	90^0 (Nadir)
Front Overlap	75%
Side Overlap	65%
Flight Height	160 m -180 m

2.7 Ground Control Point

The UAV flight areas were selected in such a way that enough open spaces were available to place the ground control points. The ground control points were used for geo-referencing. The number and distribution of GCPs influence image orientation. So, the GCPs were evenly distributed using black and white spray paint in the study area. The minimum number of GCPs would be 3 and the larger the number of GCPS the better the accuracy [14]. The total 12 ground control point (GCP) were put in the study area. The coordinates of the GCPs were recorded using a differential global positioning system (DGPS). The distribution of GCP is shown in Figure 5.

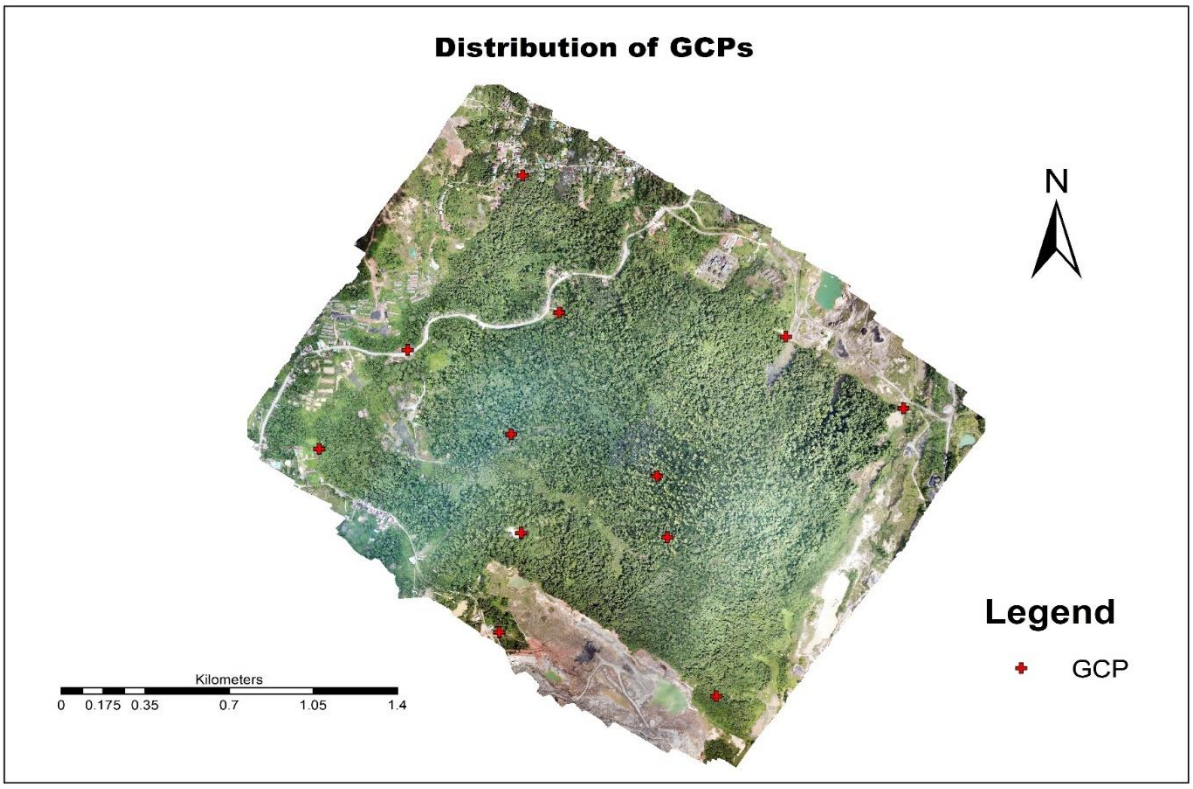

Figure 5. Distribution of ground control points (GCPs).

2.8 UAV Image Processing

The photogrammetric software Pix4D was used to generate 3-D dense point cloud, DSM, DTM and orthophoto from UAV-derived images. This software used SfM and stereo-matching algorithms for 3-D reconstructions. Structure for motion (SfM) represents the process to obtain a three-dimensional structure of a scene of an object as well as the camera motion from a series of two-dimensional digital images. SfM used a sequence of overlapping images which has a minimum number of common matching points to produce a sparse 3D model of the scene and camera parameters [15]. In the initial processing, the Pix4D software executed the computation of key points, image matching, and camera calibration. The key points are the common points between the two images that are matched. In the figure, the light green images are already matched and calibrated, and the software is being tried to calibrate and match the dark green images. The blue points indicated the location of the GCP. After loading the images in the Pix4D software, the processing options were set up; then the GCPs were loaded for the geo-referencing. In the first stage, the software computed the key points of different images of the same scene, and then image matching was performed based on key points. In the second stage, the software generated the sparse point clouds along with camera calibration. The high-quality point cloud was generated based on the estimated camera positions where the software computed depth information also. The point cloud was used to develop a digital surface model (DSM), digital terrain model (DTM),

and orthophoto. The canopy height model (CHM) was extracted by subtracting DTM from DSM. The process of producing DSM, DTM, orthomosaic and CHM were described in the following two sub-sections.

2.9 DSM, DTM, and Orthophoto Generation

The digital surface model (DSM) is a representation of the terrain relief that includes the topography and all natural (trees etc.) and man-made (buildings, bridges, etc.) objects. On the other hand, the digital terrain model (DTM) is a representation of the terrain relief in a digital form without any objects on the earth surface. A canopy height model (CHM) is generated from the difference between DSM and DTM [16]. Digital terrain model, digital surface model, and orthomosaic were generated automatically after producing dense point clouds using the Pix4D software. The software generated the DTM based on ground pixels only using an algorithm. A DSM represents the surface model as a regular grid that contains the height values. A DSM can be generated from the dense point cloud, sparse point cloud or a mesh. The quality of DSM is also dependent on the quality of the point cloud. The DSM was generated by interpolation using a delaunay triangulation method. Delaunay triangulation is a geometric structure that generates meshes and maximizes the minimum angles [17]. This method is recommended because of considering the suitability in the forestry applications. Finally, the orthomosaic was produced from the mosaicking of the geometrically corrected images. The schematic representation of DSM and DTM is shown in Figure 6.

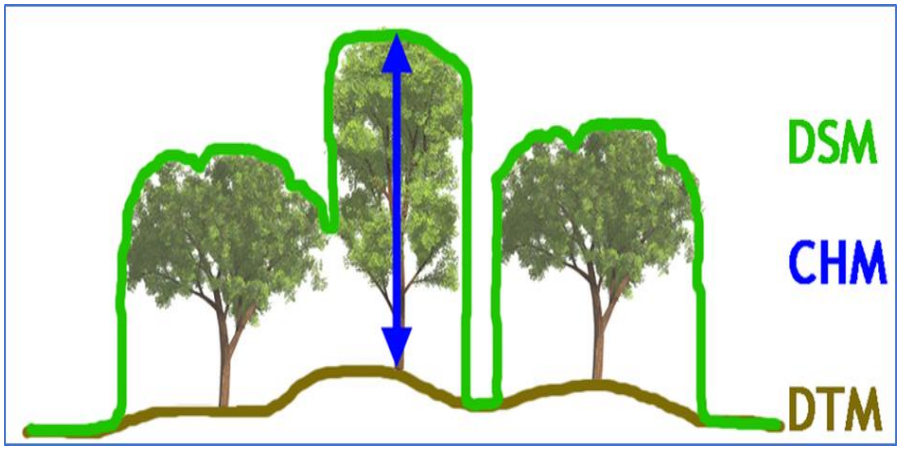

Figure 6. Generating canopy height model CHM= DSM – DTM.

2.10 Relationship between DBH and CPA

For model development the CPA obtained from manual digitization was used as input to predict DBH. In this study, the linear, power, quadratic and logarithmic model was tested to choose the suitable model for establishing the relationship between CPA and DBH. To perform this, the area of a delineated shapefile was calculated using ArcMap software. The DBH of matched trees was regressed with the corresponding CPA using quadratic relationship. The scatter plot was plotted while the trend line was fitted. The RMSE and %RMSE were calculated to observe and evaluate the relationship between CPA and DBH.

2.11 Estimation of Aboveground Biomass (AGB) for 2017 and 2018

The allometric equation is the commonly used method to estimate forest biomass in a non-destructive way. Various researchers have developed allometric equation based on a destructive method to estimate biomass and carbon in the different forest ecosystem and different tree species [18]. The region or site-specific allometric equations must be considered to assess the biomass accurately as the equations consider the site effects [19]. Application of regionally or locally developed allometric equations are not

recommended due to high species-diversity in tropical forest [2]. The generic allometric equations developed by [20] was considered a suitable equation to estimate above ground biomass in a tropical forest. The allometric equation developed by [20] is shown in Equation 1.

Equation 1: Allometric Equation for AGB Calculation

$AGB_{est} = 0.0673 \times (\rho D^2 H)^{0.976}$……..……. (1) Source: [20]

Where AGB_{est} is the estimated above ground biomass in kilograms (kg),
D is the diameter at breast height (DBH) in centimeter (cm),
H is the tree height in meter (m),
and ρ is wood density in gram per cubic centimeters (gcm^{-3}),
0.0673 and 0.976 are constant.

The aboveground biomass (AGB) was estimated for the year 2017 and 2018 using this allometric equation. The AGB was calculated and assessed for each plot.

Estimation of Aboveground Carbon for 2017 and 2018

The carbon stock was calculated from the estimated AGB. 50% of the estimated biomass is considered as carbon [21]. The carbon stock was calculated using Equation 2.

Equation 2: AGC Calculation from AGB

$AGC = AGB \times CF$…… (2)

Where,
AGC is aboveground carbon stock (Mg),
CF is the carbon fraction (0.5)

The total amount of sequestered carbon was assessed from the difference between the estimated amount of carbon for 2017 and 2018.

2.12 Comparison of UAV-based AGB and Field-based AGB

The height derived from UAV-CHM and predicted DBH based on UAV CPA were used as an input parameter to estimate the UAV-based AGB. The field-derived tree height and DBH were used as input parameter for estimation of field-based AGB. The UAV-based AGB and Field-based AGB were compared using a scatter plot and RMSE. Furthermore, the F-test and t-test were performed to test if there is a significant difference between UAV-based AGB and Field-based AGB. Lastly, the mean difference between the UAV-based AGB and Field-based AGB was assessed and evaluated.

3. Results and Discussions

3.1 Accuracy of UAV-derived Tree Height with Field-derived Tree Height 2017

A total of 569 identified trees were used to compare the UAV-derived height and field-measured height. The scatter plot demonstrated the relationship between UAV-derived height and field-measured height and showed a strong correlation of 0.92 and coefficient of determination (R^2) of 0.89. The root mean square error (RMSE) was ±1.57 m which is equivalent to 9.24 % of the measured tree height from the field. The scatter plot and regression statistics are shown in Figure 7.

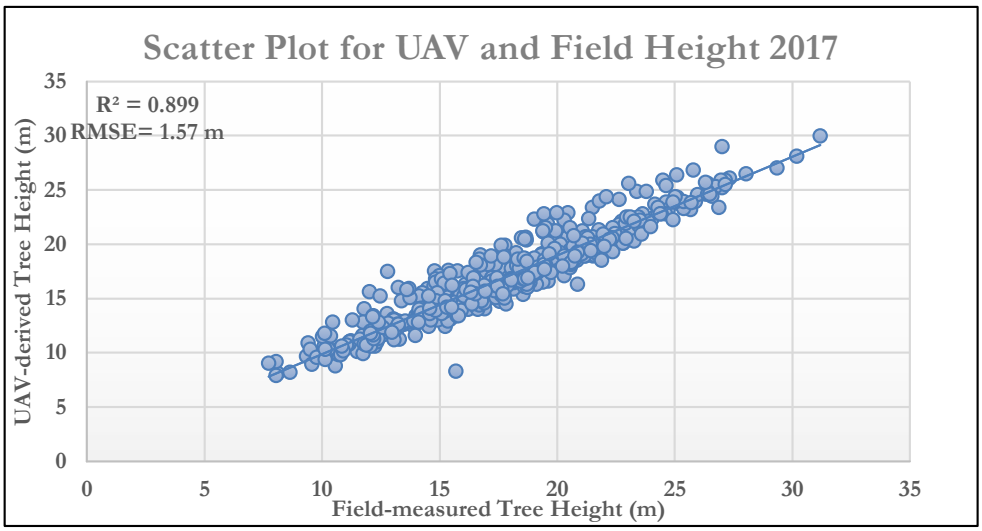

Figure 7. Scatter plot of field-measured and UAV-derived tree height.

3.2 Accuracy of UAV-derived Tree Height with Field-derived Tree Height 2018

A total of 590 identified trees were used for descriptive statistics as well as making a comparison with field-measured tree height. The same number of trees was considered to compare the UAV-derived tree height and field-measured tree height. The scatter plot demonstrated the relationship between UAV-derived height and field-measured height and showed a strong correlation of 0.93 and coefficient of determination (R^2) of 0.86. The root mean square error (RMSE) was ±1.58 m which is equivalent to 8.94 % of the measured tree height from the field.

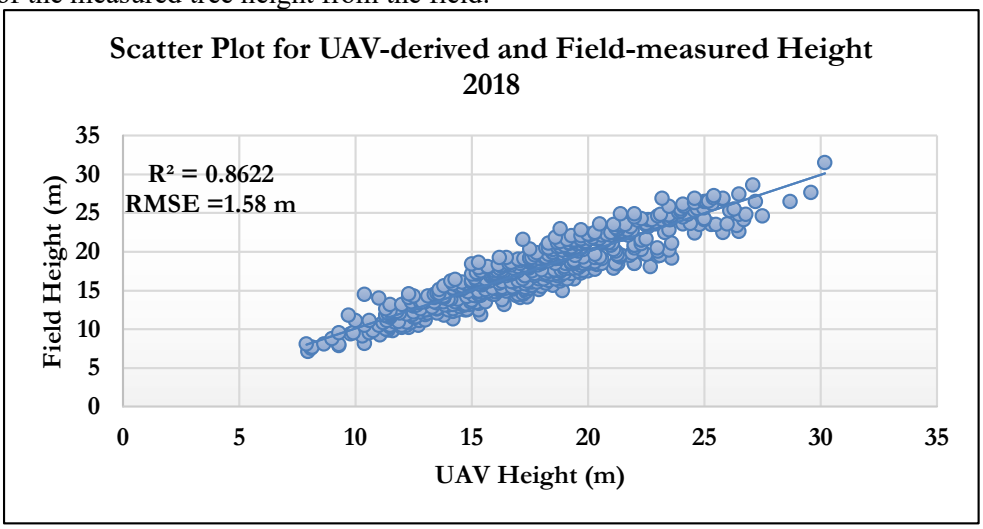

Figure 8. Scatter plot of UAV-derived and field-measured tree height 2018

3.3 Model Development between CPA and DBH for the Data of 2017 and 2018

The manually delineated CPA and corresponding field DBH of 75 trees were chosen from the randomly selected 123 trees which were picked from the 41 plots to model the relationship between CPA and DBH. The trees were also selected in such a way that covers all size classes of CPA and DBH. The results of the developed model are shown in Figure 9 and 10.

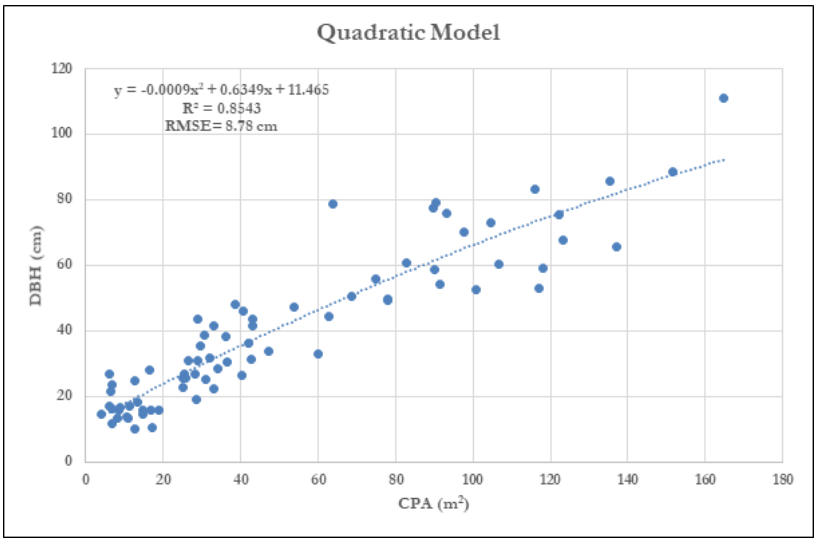

Figure 9. Quadratic model between CPA and DBH, 2017

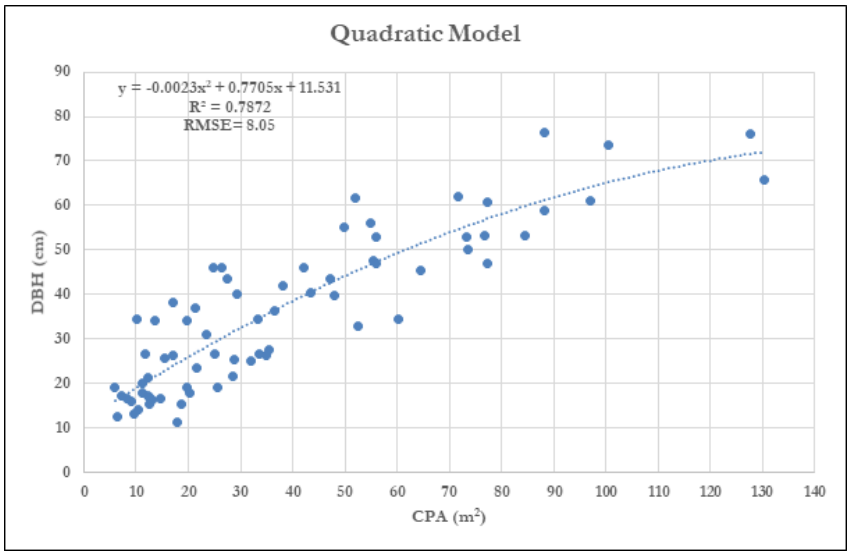

Figure 10. Quadratic model between CPA and DBH, 2018

3.4 AGB estimated using UAV in comparison to field AGB

The field-based AGB was found higher than the estimated UAV-based AGB because the number of trees was higher to calculate the field-based AGB than the number of trees for estimating UAV-based AGB. All trees within the plots were considered to assess field-based AGB while some of the trees were missing in every plot to estimate UAV-based AGB because the UAV can only observe the upper canopy. Out of 41 plots, the UAV-based AGB was higher than field-based AGB in 18 plots. The amount of UAV-based AGB is dependent on the predicted DBH that was calculated based on CPA using the quadratic model. The comparison between field-based AGB/AGC and UAV-based AGB/AGC are presented in Figure 11.

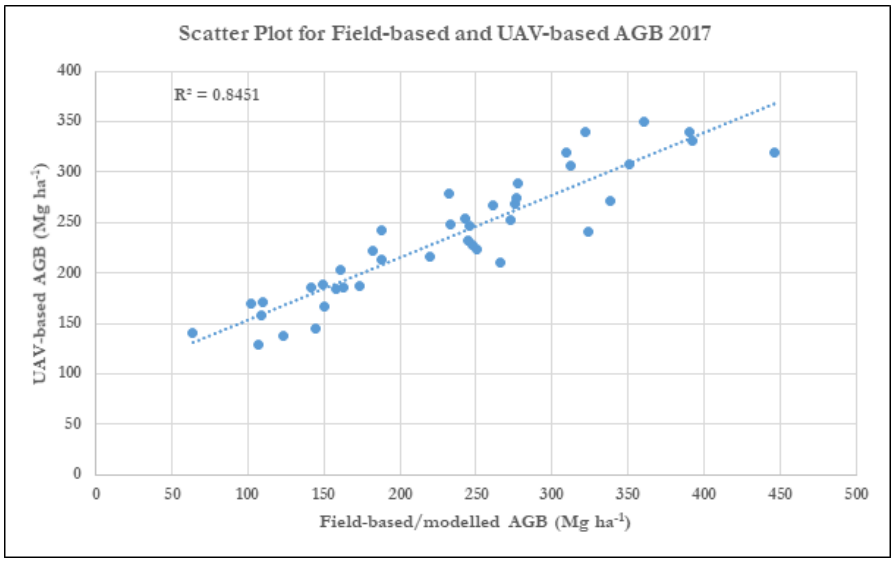

Figure 11. Scatter plot for accuracy assessment between field-based/modelled and UAV-based AGB 2017.

3.5 Comparison of Field-based AGB and UAV-based AGB 2018

Like the comparison of 2017, the field-based AGB was generally higher than the estimated UAV-based AGB because the number of trees was higher to calculate field-based AGB than the UAV-based AGB. In 14 plots, the UAV-based AGB was higher than the field-based AGB out of 41 plots. The variation of the amount of UAV-based AGB is dependent on the predicted DBH that was calculated based on CPA using the quadratic model. The detailed results of the comparison between field-based AGB/AGC and UAV-based AGB /AGC are illustrated in Figure 12.

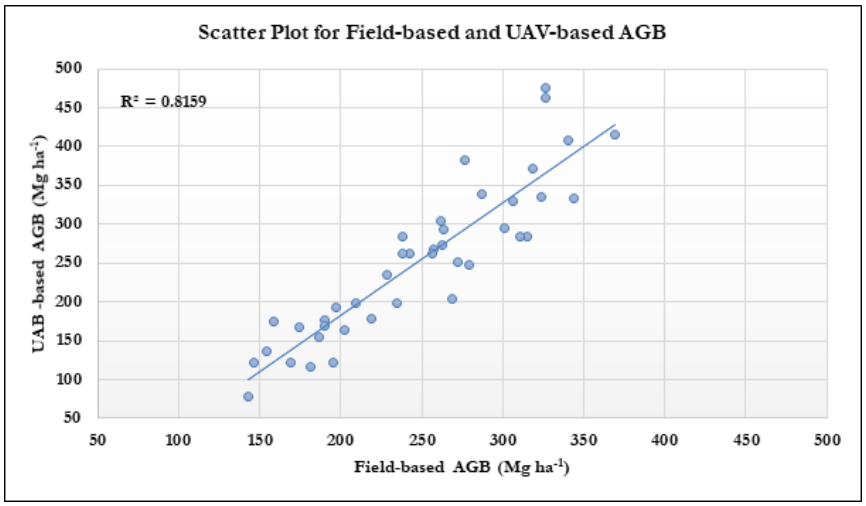

Figure 12. Scatter plot for field-based AGB and UAV-based AGB 2018

3.6 Comparison of UAV-based AGB 2017 and UAV-based AGB 2018

The UAV-based AGB for the year 2017 and 2018 were estimated and assessed for the 41 plots. The average UAV-based AGB for 2017 was estimated 235.37 Mg ha^{-1} while the mean UAV-based AGB for the year 2018 was assessed 248.01 Mg ha^{-1}. The difference between two means of UAV-based AGB for the year 2017 and 2018 was 12.64 Mg ha^{-1}. For the year 2017, the minimum 129.49 Mg ha^{-1} AGB was assessed while the UAV-based AGB for the year 2018 was estimated 142.55 Mg ha^{-1}. On the other

hand, the maximum 349.27 Mg ha^{-1} AGB was estimated for the year 2017 whereas the UAV-based maximum 369.00 Mg ha^{-1} AGB was assessed for the year 2018. The plot-wise comparison of UAV-based AGB 2017 and UAV-based AGB 2018 is presented in Figure 13.

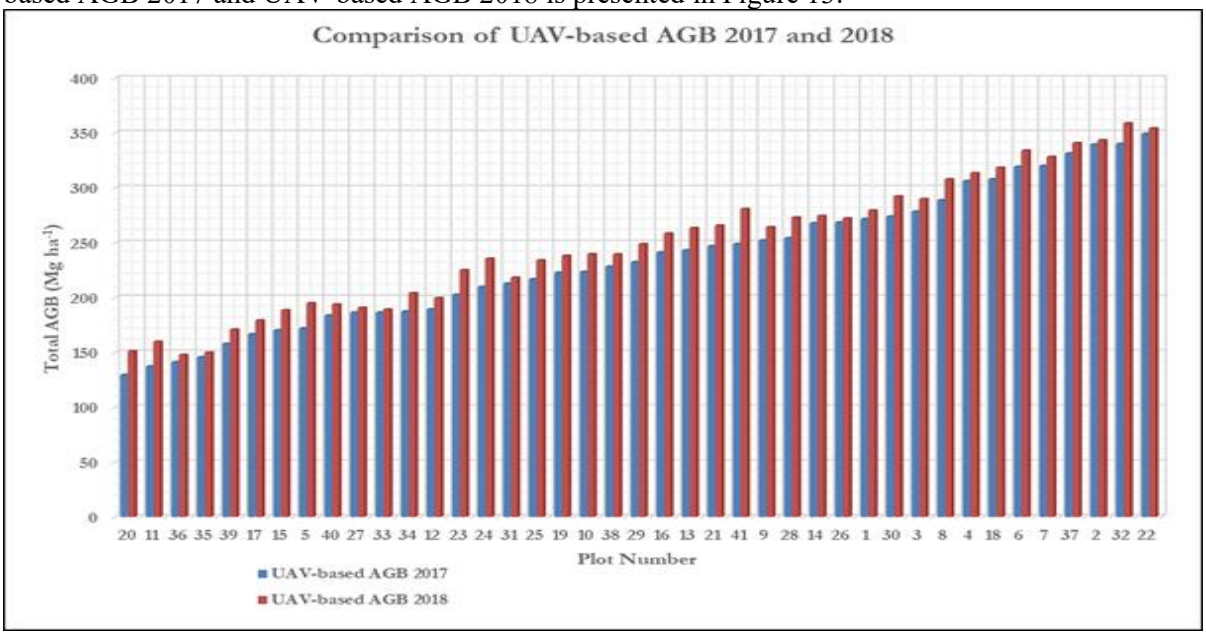

Figure 13. Comparison between UAV-based AGB 2017 and 2018.

3.7 Assessment of Carbon Sequestration

The UAV-based aboveground carbon for the year 2017 and 2018 was estimated and assessed for the 41 plots. The average UAV-based AGC for 2017 was estimated 117.68 Mg ha^{-1} while the mean UAV-based AGC for the year 2018 was assessed 124.00 Mg ha^{-1}. The difference between two means of UAV-based AGC for the year 2017 and 2018 was 6.32 Mg ha^{-1}. For the year 2017, the minimum 64.74 Mg ha^{-1} AGC was assessed while the UAV-based AGC for the year 2018 was estimated 71.28 Mg ha^{-1}. On the other hand, the maximum 174.64 Mg ha^{-1} AGC was estimated for the year 2017 whereas the UAV-based maximum 184.50 Mg ha^{-1} AGC was assessed for the year 2018. The total amount of sequestered carbon for one year was 6.32 Mg ha^{-1}. The plot-wise distribution of carbon stock is shown in Figure 14**.**

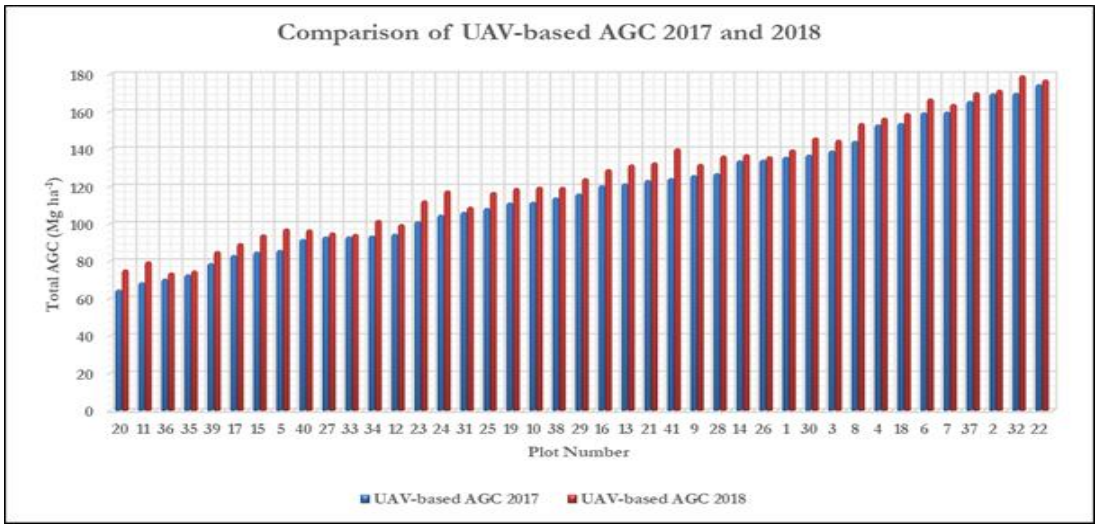

Figure 14. Carbon sequestration in the period 2017-2018

3.8 Assessment of Carbon Sequestration

The UAV-based aboveground carbon for the year 2017 and 2018 was estimated and assessed for the 41 plots. The total amount of sequestered carbon for one year was 6.32 Mg ha^{-1}. [22] applied a universal average rate of 6.24 Mg C/ha/yr in his study which was very much close to the result of this study. A study conducted by [23] found the amount of sequestered carbon for the species *Acacia mangium, Eucalyptus pelitta,* and *Gmelina arborea* were 5.9-9.9, 7.1-7.2, 8.3-12.3 Mg $ha^{-1}y^{-1}$. The result of this study was similar to and within the range of AGB of these three species. A study conducted on the tropical forest by [24] produced a table mentioning the amount of sequestering carbon assessed by the different researcher in different types of tropical forest (Table 3).

Table 3. Carbon sequestration in different tropical forests

Forest Type	Dry Matter	Carbon	Studied By	Source
	Mg/ha/year	Mg/ha/year		
Tropical rainforest	7.75- 10.19	3.88- 5.10	Bolin et al. (1986) (various sites)	Source: Adapted from Brown, (1992)
Seasonal tropical forest	5.50- 7.20	2.75- 3.60		
Rainforest (Manaus)	15.00	7.50	Cannell (1982)	
Rainforest (Ivory Coast)	12.73- 24.60	6.36- 12.30		
Amazonian rainforest (mean)	12.66	6.33	Jordan (1989)	
Slash and burn (after 3 years)	5.26	2.62		

From the table, it can be mentioned that the estimated amount of sequestered carbon in this study was very much close to the estimated amount of sequestered carbon in Amazonian rainforest and rainforest of Ivory Coast. The assessed sequestered carbon in this study was higher than the range of sequestered carbon estimated for tropical rainforest and seasonal tropical rainforest by others in various sites. This variation occurred due to different forest structure, different tree species and the size of the trees, etc.

4. Conclusions

In 2017, the average UAV-based AGB was assessed 235.37 Mg ha^{-1} while the mean UAV-based AGB was estimated at 248.01 Mg ha^{-1} for 2018. The difference between the two means of AGB was 12.64 Mg ha^{-1}. On the other hand, the average UAV-based carbon was estimated 117.69 Mg ha^{-1} for the year 2017 whereas, the average UAV-based carbon was estimated 124.00 Mg ha^{-1} for the year 2018.
The amount of sequestered carbon for one year was estimated at 6.32 Mg ha^{-1}. The total area of the KRUS educational forest is 238 hectares. Therefore, the annual amount of sequestered carbon was estimated 1504.16 Mg.

For the year 2017, the scatter plot demonstrated the relationship between UAV-based AGB and field-based AGB and the root mean square error (RMSE) was 42.35 Mg ha^{-1} which are equivalent to 18.27 % of the field-based AGB. For the year 2018, the root mean square error (RMSE) was 50.00 Mg ha^{-1} which are equivalent to 19.84 % of the field-based AGB. For both years, there was no significant difference between estimated AGB from UAV and field-based AGB, because the P-value was greater than 0.05 at $\alpha = 0.05$ and t-Statistics < t-Critical.
The effect of height error on biomass estimation was conducted based on the percentage of the root mean square error (RMSE). The percentage of RMSE was calculated at 8.94% for the UAV- derived tree height compared to the field-measured tree height. The mean difference of UAV-based AGB without inflated/deflated height and the UAV-based AGB with inflated/deflated height was 21.66 Mg ha^{-1}. The 8.73% biomass variation was found due to height error, and it was proved to be a significant effect on overall plot-based biomass assessment. The resultant estimated amount of carbon stock due to height error was greater than the amount of sequestered carbon for one year.

5. Acknowledgment
The Authors would like to highly acknowledge and appreciate the research permit issued by the Indonesian Ministry of Science and Technology and Higher Education. They would like to highly Acknowledge the support and contribution of Dr. Y. Budi Sulistioadi and the Faculty of Forestry University of Mulawarman, Samarinda, Indonesia for facilitating our research work, helping us with the logistic, collecting image and ground truth data in Kybun Raya UNMUL Samarinda Forest. We highly appreciate the support of Mr. Rafii Fauzan, Ms. Audina Rahmandana, Mr. Lutfi Hamdani, Ms. Shukiy Romatua Sigalingging, Mr. Gatot Puguh Bayu Aji and Mr. Yaadi for their continuous help during the collection of data in the month of October 2018. We acknowledged the UAV data collection by Dr. Y. Budi Sulistioadi in 2017 and 2018. Without the mentioned data and support, our research could not have been done.

6. References

[1] Dube, T. and O. Mutanga, *Evaluating the utility of the medium-spatial resolution Landsat 8 multispectral sensor in quantifying aboveground biomass in uMgeni catchment, South Africa.* ISPRS Journal of Photogrammetry and Remote Sensing, 2015. **101**: p. 36-46.

[2] Gibbs, H.K., et al., *Monitoring and estimating tropical forest carbon stocks: making REDD a reality.* Environmental Research Letters, 2007. **2**(4): p. 045023.

[3] Lu, D., et al., *Relationships between forest stand parameters and Landsat TM spectral responses in the Brazilian Amazon Basin.* Forest ecology and management, 2004. **198**(1-3): p. 149-167.

[4] Powell, S.L., et al., *Quantification of live aboveground forest biomass dynamics with Landsat time-series and field inventory data: A comparison of empirical modeling approaches.* Remote Sensing of Environment, 2010. **114**(5): p. 1053-1068.

[5] Kachamba, D., et al., *Biomass estimation using 3D data from unmanned aerial vehicle imagery in a tropical woodland.* Remote Sensing, 2016. **8**(11): p. 968.

[6] Koh, L.P. and S.A. Wich, *Dawn of drone ecology: low-cost autonomous aerial vehicles for conservation.* Tropical Conservation Science, 2012. **5**(2): p. 121-132.

[7] Villard, L., et al., *Forest biomass from radar remote sensing*, in *Land Surface Remote Sensing in Agriculture and Forest*. 2016, Elsevier. p. 363-425.

[8] Senthilnath, J., et al., *Application of UAV imaging platform for vegetation analysis based on spectral-spatial methods.* Computers and Electronics in Agriculture, 2017. **140**: p. 8-24.

[9] Brown, S., *Measuring carbon in forests: current status and future challenges.* Environmental pollution, 2002. **116**(3): p. 363-372.

[10] HASHEM, M.A., *ESTIMATION OF ABOVEGROUND BIOMASS/CARBON STOCK AND CARBON SEQUESTRATION USING UAV IMAGERY AT KEBUN RAYA UNMUL SAMARINDA EDUCATION FOREST, EAST KALIMANTAN, INDONESIA.* 2019.

[11] Guhardja, E., et al., *Rainforest ecosystems of East Kalimantan: El Niño, drought, fire and human impacts*. Vol. 140. 2012: Springer Science & Business Media.

[12] Ruiz, L., et al., *Analysis of the influence of plot size and LiDAR density on forest structure attribute estimates.* Forests, 2014. **5**(5): p. 936-951.

[13] Agüera-Vega, F., F. Carvajal-Ramírez, and P. Martínez-Carricondo, *Assessment of photogrammetric mapping accuracy based on variation ground control points number using unmanned aerial vehicle.* Measurement, 2017. **98**: p. 221-227.

[14] Dandois, J., M. Olano, and E. Ellis, *Optimal altitude, overlap, and weather conditions for computer vision UAV estimates of forest structure.* Remote Sensing, 2015. **7**(10): p. 13895-13920.

[15] Westoby, M.J., et al., *'Structure-from-Motion'photogrammetry: A low-cost, effective tool for geoscience applications.* Geomorphology, 2012. **179**: p. 300-314.

[16] Zarco-Tejada, P.J., et al., *Tree height quantification using very high resolution imagery acquired from an unmanned aerial vehicle (UAV) and automatic 3D photo-reconstruction methods.* European journal of agronomy, 2014. **55**: p. 89-99.
[17] Shewchuk, J., T.K. Dey, and S.-W. Cheng, *Delaunay mesh generation*. 2016: Chapman and Hall/CRC.
[18] Curtis, P.S., *Estimating aboveground carbon in live and standing dead trees*, in *Field Measurements for Forest Carbon Monitoring*. 2008, Springer. p. 39-44.
[19] Basuki, T., et al., *Allometric equations for estimating the above-ground biomass in tropical lowland Dipterocarp forests.* Forest ecology and management, 2009. **257**(8): p. 1684-1694.
[20] Chave, J., et al., *Improved allometric models to estimate the aboveground biomass of tropical trees.* Global change biology, 2014. **20**(10): p. 3177-3190.
[21] Drake, J.B., et al., *Estimation of tropical forest structural characteristics using large-footprint lidar.* Remote Sensing of Environment, 2002. **79**(2-3): p. 305-319.
[22] Sedjo, R.A., *Forests to offset the greenhouse effect.* Journal of Forestry;(USA), 1989. **87**(7).
[23] Diana, R., et al. *Carbon stocks of fast growing tree species and baselines after forest fire in east Kalimantan, Indonesia*. in *Proceedings Inernational Symposium on Forest Sequestration and Monitoring*. 2002.
[24] Brown, S., et al., *Management of forests for mitigation of greenhouse gas emissions*. 1995: Cambridge University Press.

Integrating terrestrial laser scanner and UAV data to estimate AGB/ carbon stock in KRUS tropical rain forest, East Kalimantan, Indonesia

W. B. Tesfay, Y A Hussin, L van Leeuwen
Department of Natural Resources, Faculty of Geo-information Science and Earth Observation (ITC), University of Twente, Hengelostraat 99, 7511 AE Enschede, The Netherlands, Tel: +31534874293
Fax: +31534874399
Corresponding author's email: y.a.hussin@utwente.nl
Y B Sulistioadi
Soil and Water Conservation Laboratory, Forestry Faculty, Center of Geospatial Information Infrastructure Development (CGIID), Institute for Research and Community Services (IRCS), Mulawarman University, Samarinda, Indonesia.
Corresponding author's email: bsulistioadi@gmail.com

Abstract. Remote sensing method is suggested by UNFCCC to be used for its REDD+ MRV mechanism for accurate assessment of AGB. However, estimation of AGB in a multi-layered tropical forest using one single remote sensing method, either aerial imagery or ground-based, is challenging and it can lead to underestimation. Because, both the aerial and ground-based remote sensing are associated with limitations to extract both the upper and lower canopy tree parameters (DBH, height) due to occlusion. However, by integrating the aerial and ground-based remote sensing methods, the accuracy of AGB estimation can be improved. In tropical forest tree height measurement using Airborne laser scanner is more accurate. However, it is costly, and it is not always available, compared with another remote sensing such as UAV. Hence, UAV technology can be used to acquire the upper canopy tree parameters at a reasonable cost and accuracy. In other cases TLS which is a ground-based remote sensing method it can provide the height of lower canopy trees, and DBH of all canopy trees accurately. Therefore, this study aims to test the potential of integrating UAV and TLS data to improve the accuracy of plot based AGB estimation of the multi-layered tropical rain forests.

1. Introduction

Remote sensing method is suggested by UNFCCC to be used for its REDD+ measuring, reporting, and verification (MRV) mechanism for AGB/carbon assessment in the member countries (REDD+, 2012). The Light Detection and Ranging (LiDAR), very high-resolution optical sensors, and Synthetic Aperture Radar (SAR) are among the commonly used remote sensing techniques [1]. These remote sensing techniques are used for large scale forest monitoring and estimation including tropical rain forests, but measurement of tree parameters in tropical forests have challenges due to the complex structure [2, 3]. The tropical rainforest has a dense and complex vertical structure, and it stores large amount of carbon stock. Even though, they have large amount of carbon stock estimation of carbon remains with uncertainties due to the density of the forest and other problems [3]. According to Larjavaara & Muller-Landau [4] tree height is one of the necessary forest parameters for biomass estimation, while in forests which has a dense, complex and multi-layered canopy, tree height measurement is difficult. In tropical forest data acquisition by aerial imagery can cover a large and inaccessible areas. However, it is not always effective because the lower canopy tree cannot be retrieved or assessed due to foliage and occlusion [5]. Nowadays, various type of research has been done to improve the uncertainties in forest biomass estimation by integrating different remote sensing techniques, for instance; Integrating TLS and ALS for tree height measurement of the lower and upper canopy respectively [6]. Thus, air-borne Lidar has a better accuracy in tree height measuring of the upper tropical forests. Althogh, this can pose a financial constraint and not always available [5]. Comparatively, using UAV and TLS have a potential to assess the upper and lower canopy tree parameters for the tropical rain forest with a reasonable cost and accuracy.

Unmanned Arial Vehicle (UAV) is an elating technology which has various advantages regarding cost-effectiveness, temporal and spatial resolution, and the ability of producing 3D dense point clouds for regular forest monitoring [7]. Thus, UAV data is appropriate to overcome the limitation of air born and satellite-based researches [8]. Previous studies show that CPA has a significant relation with DBH [9-11]. Undoubtedly, UAV images have a high spatial and spectral resolution these, segmentation of CPA using multi resolution algorithms can be done effectively and further it can be used as a proxy of DBH. TLS is a ground based remote sensing system in which the 3D point cloud can acquire tree parameters like DBH, height, number of trees and the position of trees accurately [12]. There are many ground-based hand-held instruments which can be used for tree height measurement. However, in forests which have closed canopy and complex structure tree height derived from hand-held laser instruments like laser height finder and hypsometers have certain level of errors [4].

In dense tropical forests (Figure 1) using TLS and UAV standalone have some limitations to extract accurate tree parameters. Because TLS method cannot access or its laser beam can not detect the top canopies of the tree due to occlusion, and on the other hand, the UAV point cloud also cannot access the lower stories due to the foliage occlusions, unlike the upper canopies. For this reason, using UAV as well as TLS as stand-alone or separately for estimation of aboveground biomass lead to underestimation [5].

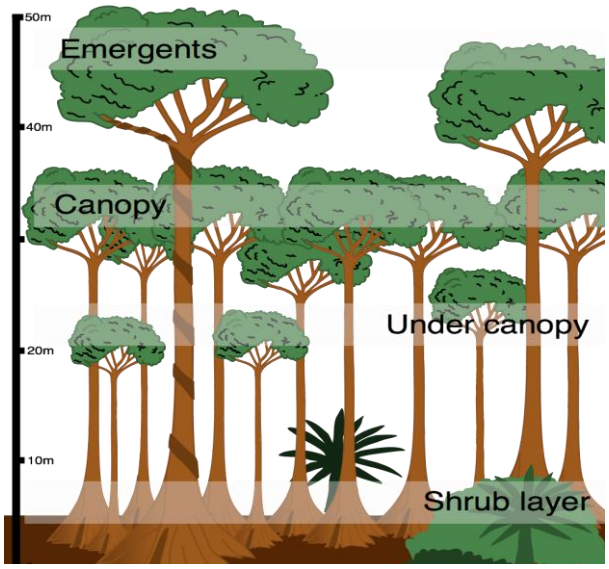

Figure 1. Illustration of tropical rainforest canopy strata.

Therefore, TLS can measure accurate tree height for the lower canopy and DBH for the upper and lower canopy of the tropical forests. Thus, it can surpass the limitation of aerial-based imagery to extract tree parameters of the under or lower canopy [13]. From UAV 3D photogrammetry or SfM tree parameters, i.e., height (CHM), and DBH can be estimated for the upper canopy trees [14]. Therefore, by complimenting TLS and UAV for tree parameter extraction of the lower and upper canopy respectively, it can improve the accuracy of AGB estimation in the tropical rainforest [5].

The allometric equation which includes both DBH and height measurements can improve the accuracy of AGB estimation [15]. Thus, plot-based estimation of AGB depends on accuracy of individual tree parameters (heights and DBH). In tropical forests, 2 -3% tree height error have an effect on the AGB estimation [16]. Accuracy of tree height estimation depends on the type of remote sensing technique used, and the type of the forest canopy structure [3]. As discussed above UAV and TLS can extract the

upper and lower canopy heights respectively. Unfortunately, there is no more studies on the integration of UAV and TLS to estimate AGB in the tropical forests.

Therefore, this study aims at integrating UAV and TLS derived forest parameters by using UAV derived minimum height, and TLS derived height as a threshold to integrate the upper and lower tree canopy to improve plot based AGB estimation in KRUS tropical forest. Having this done, in developing country REDD+ MRV mechanism could be adapted as one of the methods to be used for estimation of AGB/ carbon stock with a reasonable cost and accuracy.

2. Materials and Methods

2.1. Study Area

Kebun Raya Unmul Samarinda (KRUS) educational forest also known as Unmul Samarinda Botanical Garden is one of the tropical rain forests found in Eastern Kalimantan province, Indonesia. It is located approximately 10 kilometers to the north side of Samarinda city and covers an area of 300 hectares. The forest is used for different educational research purposes as a conservation forest by Mulawarman University of Indonesia, and in 2010 some part of the area (62 ha) is decided to be used as recreational area. In the past, the KRUS tropical forest was one of the areas affected by forest fire in East Kalimantan, and later the forest develop as secondary forests [17]. The geographical location of the KRUS tropical rain forest is between $0^0$25'10" N and 117 ^{0}14'14" E in the East Kalimantan province as shown in the Figure 2.

The KRUS conservation forest is characterized by an average annual temperature of 29.9 ^{0}C maximum and 21.4 ^{0}C minimum. The rain-fall ranges are between 2000 and 2500 mm/year, and the rain fall type is slightly seasonal in which the intensity of the rain fall is slightly lower from June to October. The soil type of the study area is Ultisoils [18]. The forest area has the same, undulating terrain surface.

The vegetation category of the forest was a Diprocarpace type of primary natural forest. Later as a result of fire disaster in 1983 the vegetation type replaced by a fast growing species and has developed as a secondary forest [19]. The forest is dominated by the species like Homalanthus, Trema, mollotus, and Macarange which are emerging by fast growing and succession after the forest was burned [17]. Nowadays, the forest is catagorized as conservation forest which includes secondary forest reserve and collection zone (natural and artificial forest) [19]. In general, it has a multi-layered canopy strata and has a high level of species diversity. The existence of multi-layered canopy structure and density of the forest compliance with the overall objective of this study to test the performance of the remote sensing methods to extract accurate tree parameters of the upper and lower canopies.

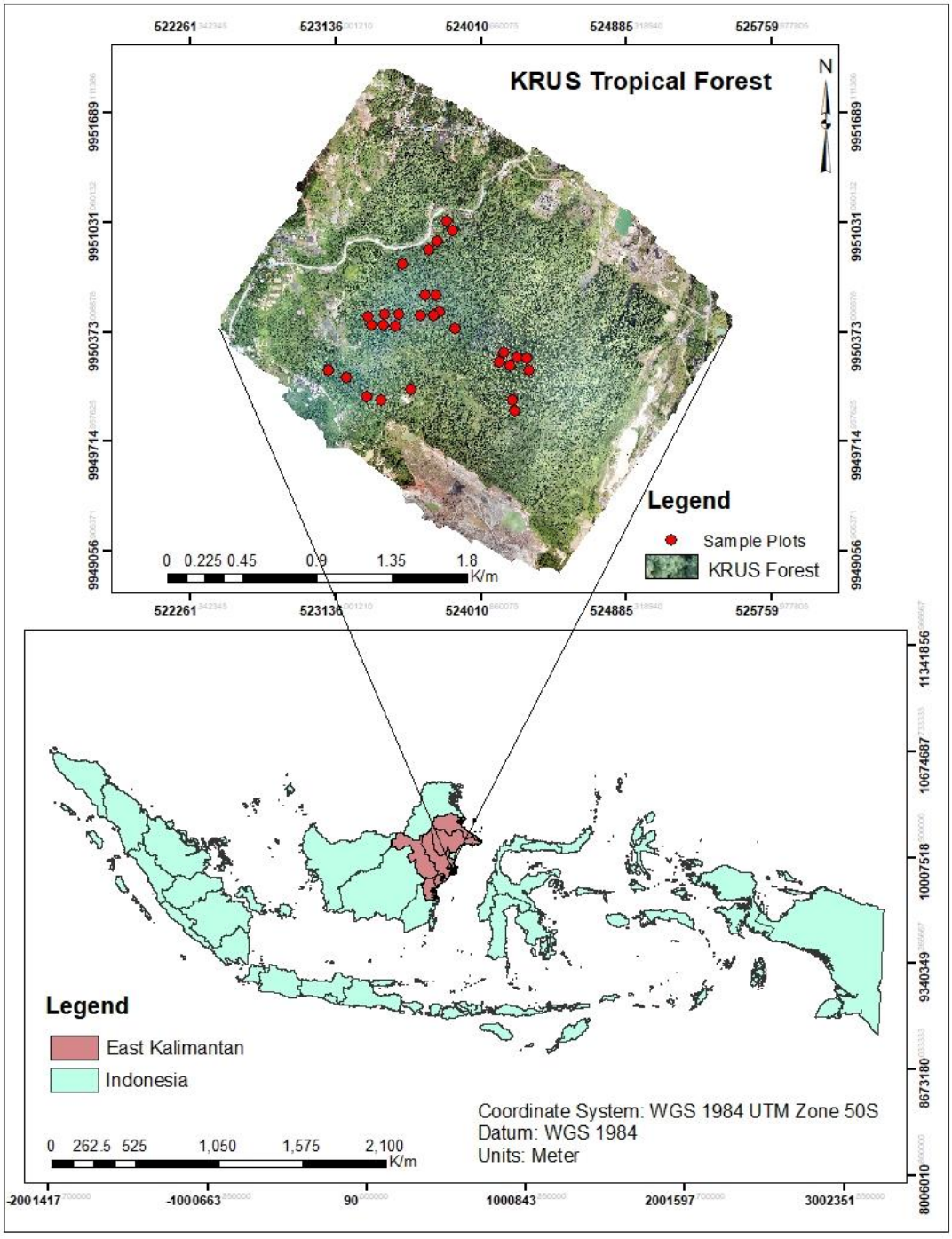

Figure 2. Study area of KRUS tropical forest location

2.2. Material

2.2.1. Field equipment and instruments

To collect the data different materials and equipment were used in the field. The details of the field instruments used are listed in Table 1.

Table 1. List of field instruments and equipment used in the research.

S/N	Instruments /equipment	Purpose /Specific function
1	UAV Phantom 4 DJI	Acquiring 2D sequence images
2	RIEGL VZ-400 - TLS	Tree acquisition (scanning)
3	Orthomosaic image of 2017	Sample plot designing
4	GPS (Garmin)	Positioning and navigation
5	Tablet/Mobile	Navigation and tree identification
6	Measuring tap (30m)	Plot layout and setting
7	Diameter tape (5m)	Tree DPH measurement
8	Leica DISTO D510	Tree height measurement
9	Suunto clinometer	Slope measurement
10	Tree tag	Tagging tree number
11	Datasheets	Recording data
12	Binder	Binding the data sheets

2.2.2. Tools and software

The collected remote sensing data were acquired using various tools, and for processing, extraction and analyzing different application packages were used. Detail of the tools and software were listed below in Table 2.

Table 2. List of software packages and tools used for the study.

S/N	Software	Purpose
1	RiSCAN PRO	TLS data processing
2	Pix4D	UAV data processing
3	ArcGIS 10.6	Data processing, extraction
4	CloudCompare	Analysing point clouds
5	ERDAS IMAGINE	Image processing
6	Mendeley Desktop	Citation and referencing
7	Lucid chart	Flowchart preparation
8	Microsoft Excel	Data analysis
9	Microsoft Word	Proposal and Thesis writing
10	Microsoft power point	Presentation of proposal and results
11	SPSS	Statistical analysis

2.3. Method

The method has four main parts to achieve the objectives of this study as shown in the flow chart in Figure 3.

Field biometric measurement and estimation of AGB

Biometric measurements of forest trees which includes DBH and height with its coordinates were measured for all individual trees at plot based. Based on the plot measurements AGB was estimated. Besides, field derived DBH were used to assess accuracy of TLS derived DBH.

UAV data acquisition and processing (upper canopy data extraction)

From the UAV 3D image-based modeling, the orthomosaic image and 3D point cloud were generated. These data were used for the segmentation of CPA and extraction of tree height. Trees height extracted from CHM was considered as an upper canopy, and its accuracy were assessed by field measured height. TLS scanning data and tree extraction (lower canopy data measurement)

The multi-scanned TLS data were registered and used to extract tree height for the lower canopy and DBH for both upper and lower canopies. Each tree derived from TLS were matched with its corresponding field recorded tree coordinate. The accuracy of TLS derived DBH (upper and lower canopy) were assessed using the field measured DBH.

Estimation of AGB from integrating UAV and TLS derived tree parameters and assessed its accuracy with field measured AGB.

In this study, two methods were used to integrate the data acquired by UAV and TLS to estimate the AGB. First, the data derived by UAV and TLS was integrated as upper and lower canopy using the following height thresholds;
A) UAV derived minimum height threshold; with in the plot, the minimum height (CHM) derived from UAV were used as threshold. Accordingly, all trees detected by UAV were consider as upper canopies while for the rest TLS data less than the threshold were considered as a lower canopy. Based on the mentioned criteria AGB was estimated.
B) Using TLS derived height (fully detected) threshold; within each plot, tree height range were defined based on trees which are fully detected by TLS and used as a threshold. Accordingly, TLS derived tree height less than or equal to the threshold were consider as lower canopy while the trees those its height were greater than the defined threshold were consider as upper canopies.
Then, both the estimated AGB were compared to assess the difference, and the accuracy was assessed compared with the field based AGB.

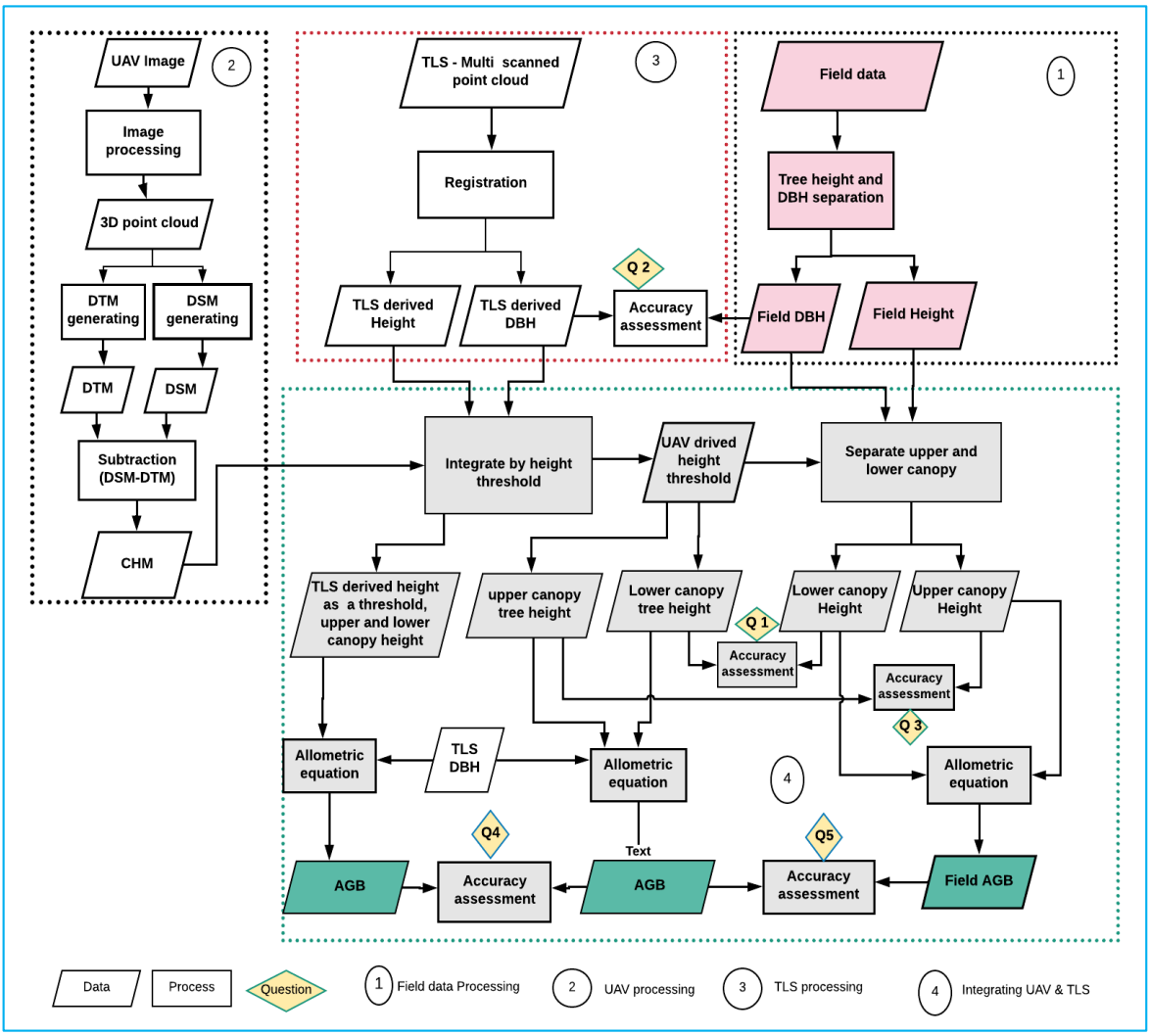

Figure 3. Shows flow chart of the research method.

2.3.1. Plot size

The sampling plots were designed as circular in shape with size of 500m^2 and radius of 12.62m. Besides, at sloping area, the radius of the plot were corrected based on the slope correction table. The circular plots were suitable for TLS scanning positions, and the number of trees stand on the edge are less as compared to the squire plots. Circular plots are preferable than rectangular sample plots because the method minimizes trees found (standing) on the corner edge. In adition, wider sample plot which is more than 500 – 600 m^2 increases the time and cost of data collection whereas its result have no significant effect on the accuracy of the data [20].

2.3.2. Sampling design

In this study, a purposive sampling method was adopted by considering the undergrowth vegetation, terrain type, time availability, and accessibility to the road. Thus, the actual selected sample plots were covered/represent the genuine characteristics of all the variation of the forest structure in the study area. It is a non-probability sampling method in which plots were selected by accessibility of the forest area. Moreover, the difficulty of holding and transporting of the TLS instrument with a very heavy weight of 28 KG was another reason why the purposive sampling was preferred. Based on this, data were collected from 30 circular plots, and the center of the plots were record by GPS on the data collection sheet.

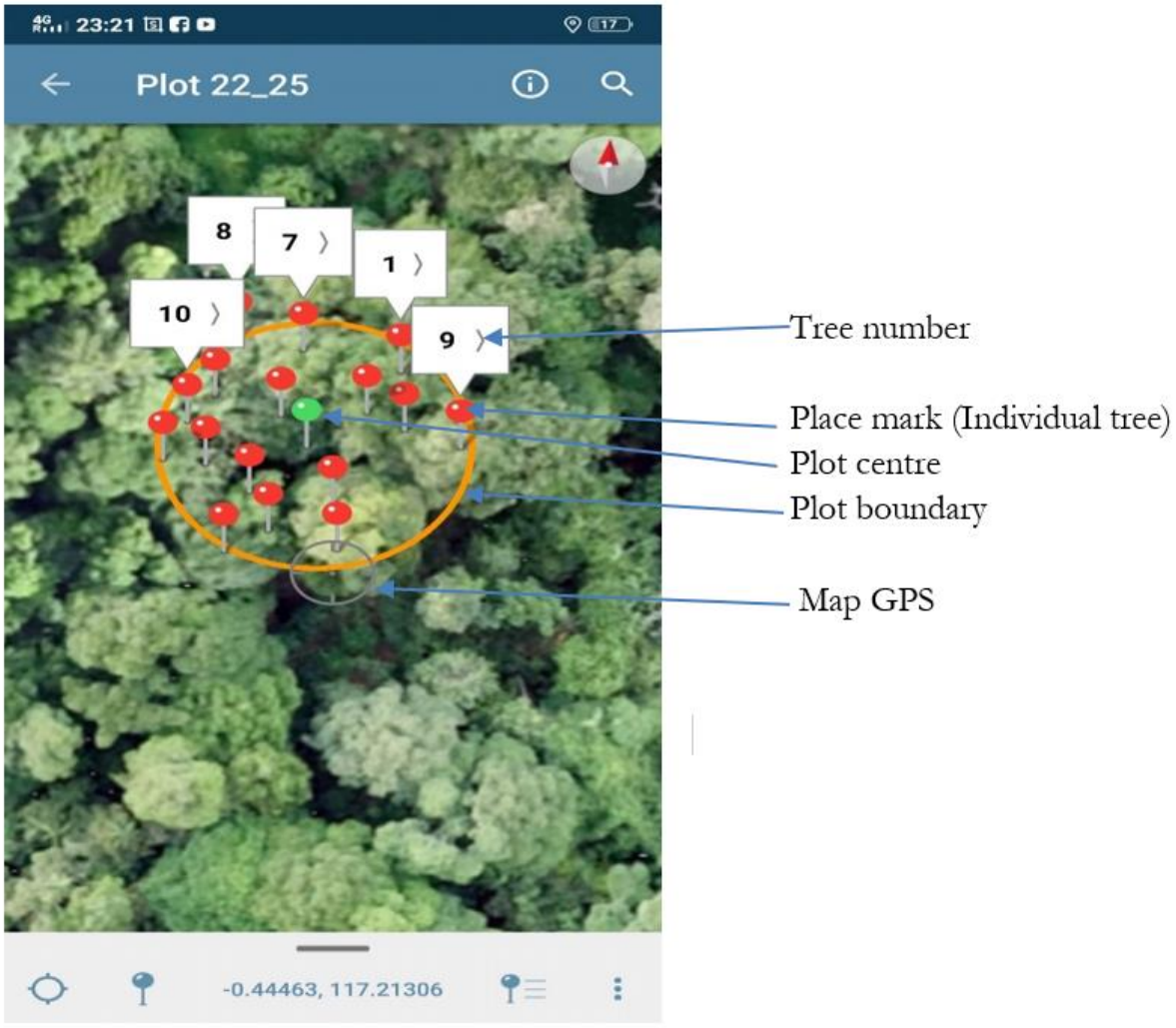

Figure 4. Illustration of individual upper canopy trees identification by Avenza Map (Plot 22).

2.3.3. UAV data acquisition
The Phantom 4 DJI multi-rotary UAV (Figure 5) was used to acquire a sequence of 2D over-lapping images because in tropical forests vertical flight is required to take-off and landing of the UAV inside the forest within the existing open area [5].

2.3.4. Ground control point
UAV image acquisition was considering the number and configuration of GCP. Based on the availability of existing open space of the forest, evenly distributed ground control points were used to ensure the quality of image matching and geo-referencing. The pre-identified open places were pre-marked using the GCP marked board, (Figure 5) and in each center of the marked board the coordinates (X,Y,Z) were recorded as GCP using Differential GPS (DGPS). Hence, these GCP were used for the spatial referencing (geo-referencing) of the 3D image-based modelling of the UAV data.

2.3.5. Flight planning

PIX 4D capture application was used for the mission planning (Figure 6, a), and the technical parameters settings such as overlapping, flight height and speed were defined in the setting button (Figure 6, c). The flight height (altitude) were defined based on the height of the trees and the terrain elevation level.

Figure 5. Phantom 4 DJI UAV and GCP 60x60cm Marker.

The highest terrain elevation points and height of the tree were taken as a reference to decide the flight height in each flight mission to reduce risk of collision among the emergent tree and UAV. Take-off and landing point were selected at places which have a little bit higher altitude and have more open space to avoid the connection loss with in the UAV and the remote-control device and also to avoid collision.

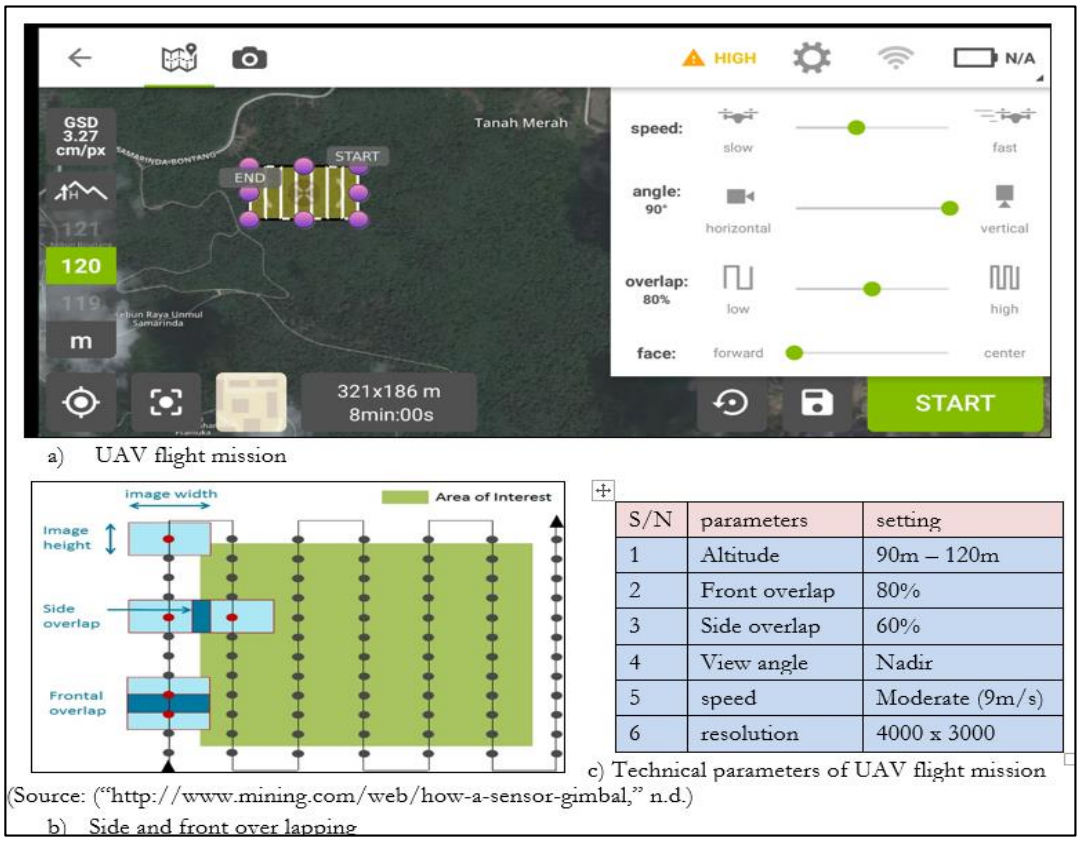

S/N	parameters	setting
1	Altitude	90m – 120m
2	Front overlap	80%
3	Side overlap	60%
4	View angle	Nadir
5	speed	Moderate (9m/s)
6	resolution	4000 x 3000

c) Technical parameters of UAV flight mission

(Source: ("http://www.mining.com/web/how-a-sensor-gimbal," n.d.)

Figure 6. UAV flight mission and technical parameter setups.

2.3.6. TLS data collection

For the TLS data acquisition, RIEGL VZ-400 TLS (Table 3) which has a capacity to emit and record a pulse up to 600m with a wavelength of near infrared 1550 nm was used [12]. the scanning approach can be single or multiple scans. Thus, to increase the density of the 3D point clouds a multiple scan with one central and three outer scans were applied for each sample plot. The technology has a GPS antenna and mounted digital camera. The digital camera attached with the device was used to acquire an RGB images with each corresponding scan positions.

Table 3. RIEGL YZ 400 TLS specification source: (RIEGL RIEGL VZ-400 VZ-400, 2017)

S/N	Specification	Level
1	Scan angle vertically and horizontal (Degree)	100, 360
2	Precision (mm)	3
3	Accuracy (mm)	5
4	Minimum range (m)	60
5	Maximum range (m)	1.5
6	Laser wavelength – Near-infrared (nm)	1550
7	Weight (kg)	9.6

2.3.7. Setting of the scane positions

The sample plots with a radius of 12.62 m were cleared from the foliage and undergrowth vegetation to reduce occlusion. For plots which have greater than 5% slope, their radius was corrected using the slope correction table. Then, the center of the plot was located carefully in a place where the TLS can clearly view the trees and to avoid occlusions created by tree trunks. The plot centre was used for the center scanning position, (Figure 7) and the other three scan points were located outside of the circular plot positioned around 1200 by undermining the tree trunk blocking effect. According to Liang et al. [21], trees trunk (stem) near to TLS can influence the scanning process of the point cloud by blocking the point cloud and creating shadow behind it.

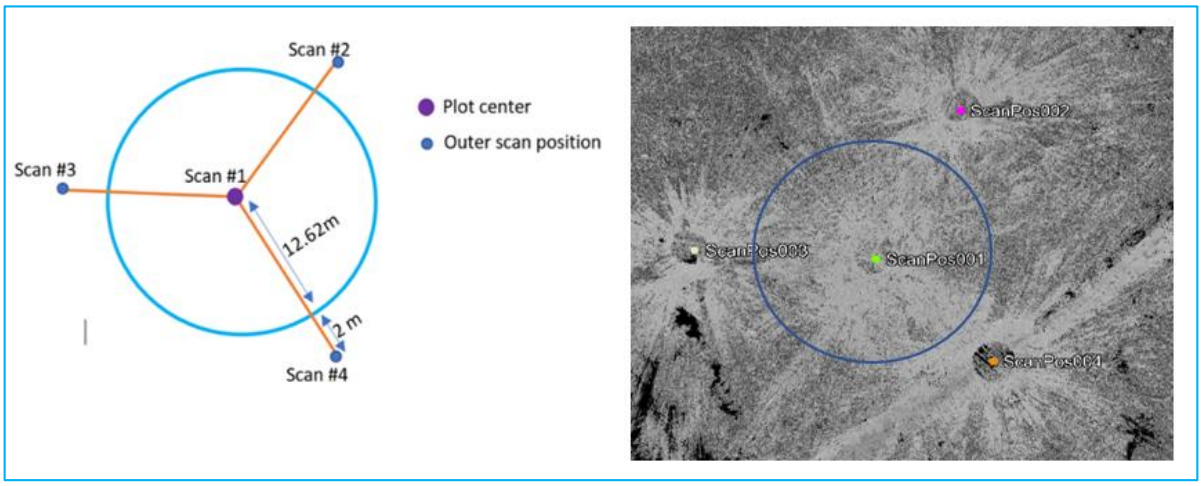

Figure 7. TLS multi-scanning position.

2.3.8. Setting of the reflectors and tree tags

After the plot preparation and positions of scanning were located, all trees found inside the circular plot which have ≥10 cm DBH (Figure 8b) were tagged on each tree stem by visible marked tree tags for tree identification purpose. Along with, greater than ten (10) circular and twelve (12) cylindrical retro-reflectors were used at different height and orientation (Figure 8a). The circular retro-reflectors are mounted on the tree stem facing (visible) to the central scan position in which at least one reflector was visible to the three outer scans. The cylindrical retro-reflectors are pointed on top of sticks and located in different height orientations, and positions within the circular plot in such a way that the reflectors were clearly visible to all the scan positions.

The cylindrical and circular retroreflectors were used for geo-referencing of the outer position scan, with the plot center position scanned point clouds [12]. For this reason, there must have at least one circular and four cylindrical retro-reflectors visible in the tie point. Therefore, to reduce error of registration 12 cylindrical and greater than 10 circular retro-reflectors were used in each plot.

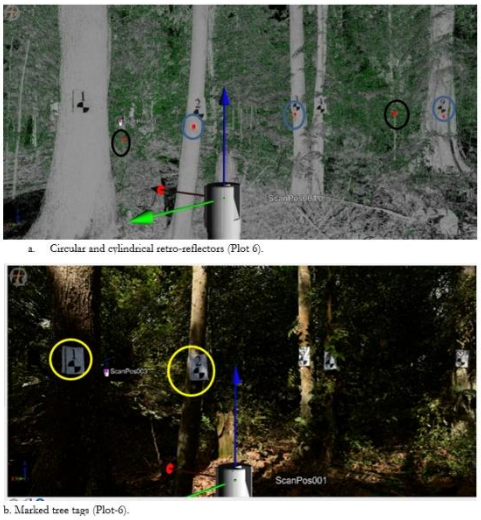

a. Circular and cylindrical retro-reflectors (Plot 6).

b. Marked tree tags (Plot-6).

Figure 8. Illustration of circular and cylindrical retro-reflectors (a) and mounted tree tags (b).

2.4. Field data collection

2.4.1. Biometric field data measurement and collection

The biometric field data collection was done with in October 2018, and it has included measurements of tree height and DBH. Diameter tape and Leica DISTO D510 were used to measure DBH and height respectively. From each sample plot ($500m^2$) the following data; Plot (Plot number, radius, slope, coordinate), and Individual tree parameters (Tree number, DBH, Height, coordinate) were recorded. Trees with DBH < 10cm were not considered because these trees have insignificance contribution to biomass. Tree DBH was measured at 1.3m sub-height of the stem from the base of the tree, while buttress trees were measured from the highest side of the ground base. In case of fork tree, if the fork height was below 1.3m, it was considered as more than one trees, and if the fork height was above 1.3m from the base of the tree, it was considered and measured as one tree.

2.4.2. Field level individual upper canopy tree identification

In multi-layered forests such as KRUS tropical forest, identification of the upper canopy from the lower canopy and matching of the upper canopy (CPA) with its respective DBH inside the forest was a challenging task. Thus, during the biometric data collection, the individual upper canopy tree crowns was identified using Avanza Map, Locus Map, and manual inspections. Before the data collection was started the orthomosaic image of 2017 KURUS forest was prepared as a Map in a PDF format and sqlitedb file by clipped from the orthomosaic image in to different large scales layers depending on the number of sample plots (1:700) for its visibility purpose. Then the sqlitedb file were uploaded to the Lucas Map on a Tablet (mobile), and the PDF format Map was uploaded to Avenza Map on a mobile. Both Maps have a navigation GPS and a pointer button which can be used to make a place mark on the clearly visible upper tree crowns on the orthomosaic image. Thus, using the navigating GPS on screen, and by manual observation on actual tree, a place mark was pinned on the upper tree crowns and tree number was written as the same number with the tree tag mounted in the steam.

Farther more, the Avenza Map enable to measure the radius of the plot and plotting the layout of the plot circle ($500m^2$) on the Map simultaneously with the biometric data recording time. For plotting the layout of the circle automatically first the centre of the plot was marked by navigation on the Map and manual inspected on the ground. Then, using the Avenza Map, the radius of the plot was measured starting from the centre plot then, the circle of the plot was generated automatically on the orthomosaic image. Hence, the generated plot circle helped as a reference to move and to identify the trees with-in the plot because the GPS of the Avenza Map shows whether the location (track) movement was inside the sample plot or outside the circle (Figure 4).

3. Results and Discussion

3.1. Integration of upper and lower canopies using height thresholds

The UAV derived, and TLS derived tree parameters were integrated using the height thresholds. Defining height threshold enables us to separate individual trees in to upper or lower canopy strata without double counting or missing of individual trees. In this study, two methods were applied to integrate the tree parameters derived using TLS and UAV remote sensing to upper, and lower canopies.

3.2. UAV derived minimum height –threshold

From the 699-field recorded individual tree, 436 tree crowns were recognized as upper canopies which are digitizing on the orthomosaic image. Later, the minimum height obtained in each plot was used as threshold to separate the upper canopies from the lower canopies (TLS data). The minimum, average and maximum height threshold recorded was 10.2, 14.4 and 18.1 respectively and the detail of the thresholds was listed in Table 4.

Table 4. Determined UAV-minimum height per plot.

Plot. No	1	2	3	4	5	6	7	8	9	10	11	12	13	14	15
Threshold	12.1	17.2	18.1	16.8	11.5	10.5	11.6	14.6	17.2	15.2	14.5	16.1	17.2	14.5	16
Plot. No	16	17	18	19	20	21	22	23	24	25	26	27	28	29	30
Threshol	15.9	13.7	12.9	15.8	10.2	14.2	14.2	13.8	16.1	11.3	16.2	13.6	15.3	12.3	13

The result showed, 436 (66.3%) were upper canopy, and 222 (33.7%) were lower canopies of the total (658) UAV and TLS extracted trees.

3.3. TLS derived height – threshold

The threshold was defined by manual observing on the extracted point clouds of individual tress on the RiSCAN PRO. Thus, trees which are fully detected by the point cloud of TLS were determined their height, and the measured height was considered as a threshold to separate the upper and lower canopies. Thus, using select by attribute on ArcGIS software individual trees were separated to upper and lower canopy based on the defined threshold. The minimum, average and maximum defined height thresholds were 12, 16.2 and 19 respectively and the details of the threshold in each plot are listed in Table 5.

Table 5. TLS derived tree height threshold per plot.

Plot. No	1	2	3	4	5	6	7	8	9	10	11	12	13	14	15
Threshold	17	14	18	19	15	19	16	16	18	18	16	14	17	16	16
Plot. No	16	17	18	19	20	21	22	23	24	25	26	27	28	29	30
Threshold	16	18	15	12	14	17	17	17	18	15	19	17	15	16	12

Based on the threshold, from the total tree extracted by the remote sensing method, 274 (41.6%) were under canopy, and 376 (57%) were lower canopy trees. Comparing with the result of UAV derived height threshold the number of the lower canopies were increased while the number of upper canopies were decreased as a result of threshold range change. From the result of trees which were categorized as upper canopies, 8 individual trees were not detected by UAV which means height from UAV-CHM cannot extracted. This was caused due to the defined TLS threshold in which few tree crowns were not visible to UAV but categorized as an upper canopy (Figure 9).

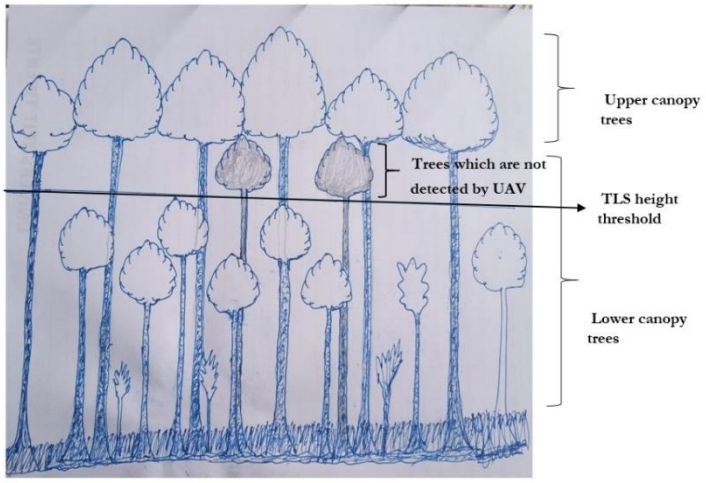

Figure 9. TLS derived height threshold to integrate upper and lower canopy.

3.4. Lower canopy tree height measurement and accuracy assessment

Individual trees crown which were not detected by UAV was categorized as a lower canopy based on the threshold defined. Of the 699 field recorded trees, 222 (33.7%) trees extracted from TLS were categorized as lower canopy and used to validate for the corresponding tree height measured by hand-held Leica DISTO D510. The accuracy of field measured lower canopy tree height was assessed using the linear regression considering TLS derived height as a reference. Thus, the linear regression result shows a coefficient of determination (R^2) of 0.8 as shown in Figure 10, and the RMSE was 1.0 m (8.37 %). The result shows field measurement height using Leica DISTO D510 was under estimated for the lower canopy tree height by mean of 0.47m.

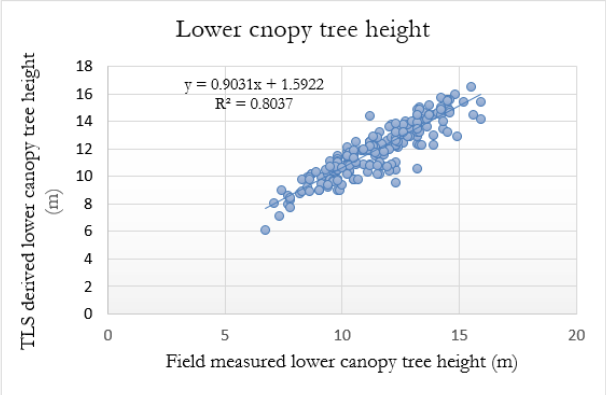

Figure 10. The relationship between field measured and TLS derived lower canopy height.

3.5. Upper canopy tree height accuracy assessment

In this study, the accuracy assessment of upper canopy tree height was conducted for trees extracted from UAV-CHM. Based on the defined threshold trees which have height greater than the threshold height was considered as an upper-canopies. Of the 699-field recorded trees, 436 trees were categorized as upper canopy trees and validated using the field based height measured by Leica DISTO D510. The linear regression between the field measured and UAV derived upper canopy height shows a coefficient of determination (R^2) of 0.768 (Figure 11) and a correlation (r) of 0.87. The result shows the UAV derived upper canopy height was over estimated as compared with the field measured height. Since the Leica DISTO D510 pulse measurement is influenced by the dense undergrowth vegetation and foliage hence, the pulse may not reach the top of the upper canopy trees depending on the opens of the forest.

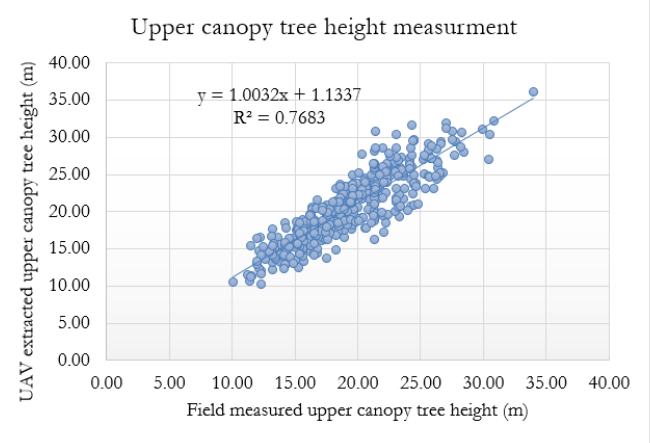

Figure 11. The relationship between field measured and UAV-CHM derived upper canopy trees.

3.6. Remote sensing based AGB estimation (using UAV and TLS)

The upper and lower canopy tree parameters derived from the remote sensing method was integrated using two methods i.e., the UAV defined height threshold and the TLS derived height thresholds. Afterward, AGB was estimated using the generic allometric equation developed by Chave et al., [15]. The AGB of upper canop trees was calculated using the input parameters derived from UAV (height) and TLS (DBH) including the average wood density (0.57). Besides, for 39 individual upper canopy trees in which their DBH was not found from TLS, a modelled DBH from CPA was used. In addition, for the lower canopy tree, TLS derived height and DBH with the average wood density were used.

TLS derived height threshold was used to integrate the upper and lower canopy of tree parameters derived by UAV and TLS as a second method. To define the range of height threshold a manual visualization on the tree extracted from TLS point cloud was used as a criterion in each plot. All the trees with in the plot which were extracted from the TLS point cloud were displayed on the screen RiSCAN PRO. Then, trees which are fully detected by the TLS point clouds were recognized, and the subsequent height threshold was defined by measuring their height (Figure 12).

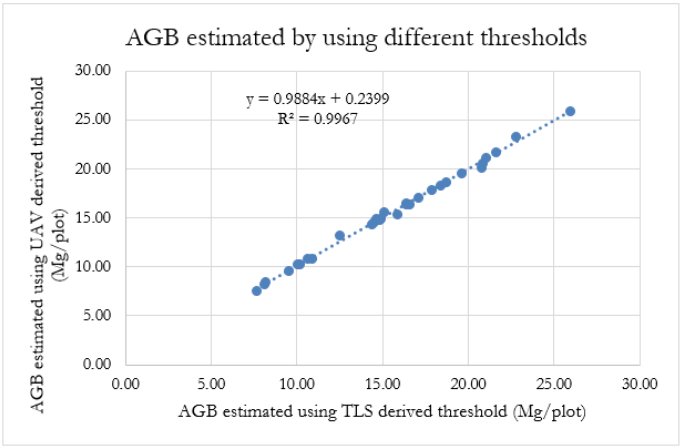

Figure 12. AGB estimated by using TLS and UAV derived threshold to integrate upper-lower canopies.

3.7. Relationship between field based estimated AGB and remote sensing AGB (UAV and TLS)

The result of field based and remote sensing method estimated AGB using the same allometric equation were compared. The average plot based estimated AGB using field based and remote sensing method was 15.44 and 15.59 Mg/plot respectively. The plot based estimated AGB using field based and remote

sensing method was presented using a bar graph in Figure 13. The relationship between the field based and remote sensing method AGB was assessed using the linear regression analysis to assess the accuracy and to validate the remote sensing method AGB. The output result shows a coefficient of determination (R^2) of 0.95 and the Pearson correlation was 0.97.

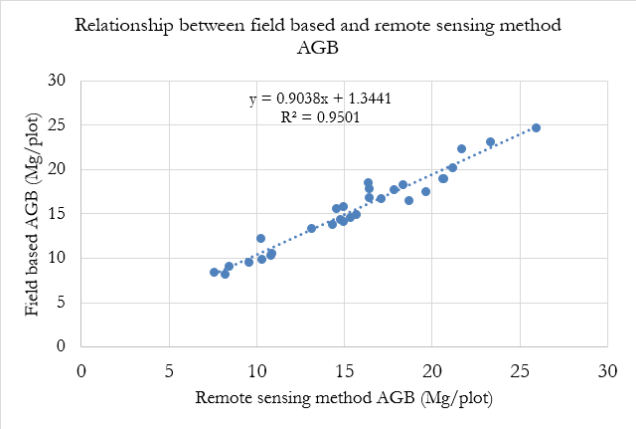

Figure 13. Scatter plot shows the relationship between field based and remote sense method estimated AGB.

3.8. Accuracy of AGB estimated by remote sensing method

In this study, the AGB was estimated using the same allometric equation which was mostly recommended for the tropical rain forests [15]. The tree parameters DBH and height, and wood density were input to the allometric equation used to calculate the AGB. For the wood density, the average 0.57g/cm^3 which is specified for the Asian forest was used [1]. In this study, two separate remote sensing method derived tree parameters were integrated to estimate the upper and lower canopies tree of the tropical forests. From the UAV-CHM tree height of the visible upper canopy was extracted and from the TLS 3D point cloud, the DBH of the upper and lower canopies trees and height of the lower canopy trees were extracted. For the upper canopy trees, there was an option to predict DBH from the CPA. However, the accuracy of result found from the field measured DBH, and TLS derived DBH shows R^2 of 0.99 which was more accurate than using CPA as a proxy to DBH. Therefore, the DBH derived from TLS point cloud was used for the upper canopy and lower canopies trees.

The total estimated AGB was the summation of the lower and upper canopies integrated using the UAV derived height threshold. Thus, the remote sensing method (UAV and TLS) estimated AGB was compared against the field based estimated AGB. The statistical regression analysis shows that a coefficient of determination R^2 of 0.95 and the RMSE was 1.07Mg which is 6.%. A t-test was conducted to check if there is a significance difference between the field based and remote sensing method estimated AGB. The result of t-test indicates that there is no significance difference between the estimated AGB at higher than 95- % of confidence level ($P > 0.05$).

The obtained result of this study was compared with other studies of Ayer Hitam tropical forest Malaysia. For instance, the study by Lawas [22], was a combination of TLS and ALS and has found R^2 of 0.98. In addition, a study by Mtui [23] was integrated TLS for the lower canopy trees and CHM (From UAV and ALS) for the upper canopy trees, and he achieved R^2 of 0.98. These findings have slightly higher accuracy than this study. The reason could be due to the type of remote sensing data used. This is because in this study the integration of remote sensing was among UAV and TLS while in the above-mentioned studies, the integration was between ALS and TLS to extract the upper and lower canopy tree parameters. Thus, the integration of ALS and TLS shows a slightly higher accuracy than the integration of UAV and TLS, because of the height measurement of ALS is more accurate comparable

with other remote sensing measurements in a dense forest. Moreover, CHM of UAV from which the trees height was derived is an inferential or an estimation method. While the ALS CHM is considered as a measured tree height, which is very accurate compared to UAV SfM method. Previous study shows ALS height measurement have comparatively better accuracy for tree height measurement [5]. However, with the same study in tropical forest Malaysia, by Bazezew [24] he has achieved R^2 of 0.96 using integration of ALS and TLS. Thus, his results were closer with the result of this study.
The average estimated AGB using the field based and remote sensing method of this study was 15.44066 and 15.59640 Mg plot^{-1} respectively. Thus, the obtained result has a high correlation with (r) of 0.97 because of the integration of the remote sensing technique to extract the tree parameter of the lower and upper canopies. Although, the remote sense method AGB shows a small difference with 0.15 Mg. The reason can be due to the error encountered in Leica DISTO D510 height measurement because the result of lower canopy accuracy assessment was an indicator that the Leica DISTO D510 was under estimated for the lower canopy trees when it compared with TLS height. Moreover, the mean of the plot based estimated AGB using field based and remote sensing method was 15.44 and 15.59Mg plot^{-1} which is equivalent to 308ton ha^{-1} and 311ton ha^{-1} respectively. The obtained result was comparable with the study by Stas, [25] in Moluccas, Indonesia which found 349.9 ton ha^{-1} in primary forests. Besides, the obtained result has little differences because this study is conducted in secondary forests. Previously, the secondary forest of East Kalimantan was affected by illegal logging and fires, thus the level of AGB is depending on the intensity of disturbance. Moreover, the obtained result of this study has agreement with study by Toma et al., [26] in East Kalimantan, Indonesia which founds 280, 315 Mgha-^{1} for the heavily and moderate disturbed secondary forests.

4. Conclusions

The accuracy of field measured tree height using Leica DISTO D510 was compared with TLS derived lower canopy tree height. The result shows R^2 of 0.80 and the RMSE was 1m (8%). The statistical analysis reveals that there is a significance difference between the height measurement of the lower canopies ($P<0.05$). The accuracy of TLS derived lower, and upper canopies DBH was assessed with the field measured DBH. Hence, the result reveals that R^2 of 0.99 and the RMSE was 1.59cm (5%). It has a high correlation with (r) of 0.99, and the t-statistics reveals that there is no significance difference between the measured DBH.

The accuracy of upper canopy tree height derived from UAV-CHM was assessed with the field measured height using Leica DISTO D510. Hence, the result was found R^2 of 0.76 and the RMSE was 2.53 m which is (13%). Thus, the statistical analysis reveals that there is a significance difference between the upper canopy tree height measurement.

The tree parameters extracted using the two-remote sensing (UAV and TLS) was integrated using UAV derived, and TLS derived height threshold for the upper and lower canopies. Thus, the AGB estimated using TLS threshold was compared with the AGB estimated using UAV derived height threshold in plot based. accordingly, the mean of AGB estimated using TLS threshold, and UAV derived threshold was 15.53 and 15.59 Mg plot^{-1} respectively. Hence, the result reveals R^2 of 0.99 and the RMSE was 0.27 Mg in which the TLS derived height threshold was underestimated by 0.059 Mg. The statistical analysis shows that there is no significance difference between the estimated AGB using the two thresholds to integrate the upper and lower canopies.

The accuracy of remote sensing method estimated AGB was compared and validated using the field based estimated AGB on plot based. The remote sense method and the field based estimated AGB has a mean of 15.59 and 15.44 Mg plot^{-1} which is equivalent to 311.93 and, 308.81ton ha^{-1} respectively. And sum of the 30 plots was 467.89204 Mg and 463.21992 Mg respectively. The t-test analysis reveals that there is no significance difference between the remote sensing based and field based estimated AGB.

5. Acknowledgment
The Authors would like to highly acknowledge and appreciate the research permit issued by the Indonesian Ministry of Science and Technology and Higher Education. They would like to highly Acknowledge the support and contribution of Dr. Y. Budi Sulistioadi and the Faculty of Forestry University of Mulawarman, Samarinda, Indonesia for facilitating our research work, helping us with the logistic, collecting image and ground truth data in Kybun Raya UNMUL Samarinda Forest. We highly appreciate the support of Mr. Rafii Fauzan, Ms. Audina Rahmandana, Mr. Lutfi Hamdani, Ms. Shukiy Romatua Sigalingging, Mr. Gatot Puguh Bayu Aji and Mr. Yaadi for their continuous help during the collection of data in the month of October 2018. We acknowledged the UAV data collection by Dr. Y. Budi Sulistioadi in 2017 and 2018. Without the mentioned data and support, our research could not have been done.

6. References

[1] CARBON, M.F., *COOKBOOK.* 2012.
[2] Lu, D., *Aboveground biomass estimation using Landsat TM data in the Brazilian Amazon.* International Journal of Remote Sensing, 2005. **26**(12): p. 2509-2525.
[3] Hunter, M., et al., *Tree height and tropical forest biomass estimation.* Biogeosciences, 2013. **10**(12): p. 8385-8399.
[4] Larjavaara, M. and H.C. Muller-Landau, *Measuring tree height: a quantitative comparison of two common field methods in a moist tropical forest.* Methods in Ecology and Evolution, 2013. **4**(9): p. 793-801.
[5] Aicardi, I., et al., *Integration between TLS and UAV photogrammetry techniques for forestry applications.* iForest-Biogeosciences and Forestry, 2016. **10**(1): p. 41.
[6] Fritz, A., H. Weinacker, and B. Koch, *A method for linking TLS-and ALS-derived trees.* Proceedings of SilviLaser 2011, 2011.
[7] Turner, D., A. Lucieer, and C. Watson, *An automated technique for generating georectified mosaics from ultra-high resolution unmanned aerial vehicle (UAV) imagery, based on structure from motion (SfM) point clouds.* Remote sensing, 2012. **4**(5): p. 1392-1410.
[8] Anderson, K. and K.J. Gaston, *Lightweight unmanned aerial vehicles will revolutionize spatial ecology.* Frontiers in Ecology and the Environment, 2013. **11**(3): p. 138-146.
[9] Hirata, Y., Y. Tsubota, and A. Sakai, *Allometric models of DBH and crown area derived from QuickBird panchromatic data in Cryptomeria japonica and Chamaecyparis obtusa stands.* International Journal of Remote Sensing, 2009. **30**(19): p. 5071-5088.
[10] Hemery, G., P. Savill, and S. Pryor, *Applications of the crown diameter–stem diameter relationship for different species of broadleaved trees.* Forest ecology and management, 2005. **215**(1-3): p. 285-294.
[11] Song, C., et al., *Estimating average tree crown size using spatial information from Ikonos and QuickBird images: Across-sensor and across-site comparisons.* Remote sensing of environment, 2010. **114**(5): p. 1099-1107.
[12] Bienert, A., et al., *Application of terrestrial laser scanners for the determination of forest inventory parameters.* International Archives of Photogrammetry, Remote Sensing and Spatial Information Sciences, 2006. **36**(5).
[13] Srinivasan, S., et al., *Terrestrial laser scanning as an effective tool to retrieve tree level height, crown width, and stem diameter.* Remote Sensing, 2015. **7**(2): p. 1877-1896.
[14] Næsset, E., et al., *Laser scanning of forest resources: the Nordic experience.* Scandinavian Journal of Forest Research, 2004. **19**(6): p. 482-499.
[15] Chave, J., et al., *Improved allometric models to estimate the aboveground biomass of tropical trees.* Global change biology, 2014. **20**(10): p. 3177-3190.
[16] Molto, Q., V. Rossi, and L. Blanc, *Error propagation in biomass estimation in tropical forests.* Methods in Ecology and Evolution, 2013. **4**(2): p. 175-183.

[17] Diana, R., et al. *Carbon stocks of fast growing tree species and baselines after forest fire in east Kalimantan, Indonesia*. in *Proceedings Inernational Symposium on Forest Sequestration and Monitoring*. 2002.

[18] Ohta, S. and S. Effendi, *Ultisols of "lowland Dipterocarp forest" in East Kalimantan, Indonesia: II. Status of carbon, nitrogen, and phosphorus.* Soil science and plant nutrition, 1992. **38**(2): p. 207-216.

[19] Sus Trimurti, L., *Differences Of Basidiomycotina Types In Natural Forest Arboretum Gardens Unmul Samarinda.* International Journal of Scientific & Technology Research, 2018. **7**(1).

[20] Ruiz, L., et al., *Analysis of the influence of plot size and LiDAR density on forest structure attribute estimates.* Forests, 2014. **5**(5): p. 936-951.

[21] Liang, X., et al., *Automatic stem mapping using single-scan terrestrial laser scanning.* IEEE Transactions on Geoscience and Remote Sensing, 2011. **50**(2): p. 661-670.

[22] MTUI, Y.P., *Tropical rainforest above Ground Biomass and Carbon Stock Estimation for Upper and Lower canopies Using Terrestrial Laser Scanner and Canopy Height Model from Unmanned Aerial Vehicle (UAV) Imagery in Ayer-Hitam, Malaysia*. 2017, University of Twente Faculty of Geo-Information and Earth Observation (ITC ….

[23] Lawas, C., *Complementary Use of Airborne LiDAR and Terrestrial Laser Scanner to Assess Aboveground Biomass/Carbon in Ayer Hitam Tropical Rain Forest Reserve*. 2016, MSc thesis, University of Twente Faculity of Geo-information and Earth ….

[24] Bazezew, M.N., *Integrating airborne lidar and terrestrial laser scanner forest parameters for accurate estimation of above-ground biomass/carbon in Ayer Hitam tropical forest reserve, Malaysia*. 2017, M. Sc. thesis, University of Twente, Faculty of Geo-Information Science and ….

[25] Stas, S.M., *Above-ground biomass and carbon stocks in a secondary forest in comparison with adjacent primary forest on limestone in Seram, the Moluccas, Indonesia*. Vol. 145. 2014: CIFOR.

[26] Toma, T., A. Ishida, and P. Matius, *Long-term monitoring of post-fire aboveground biomass recovery in a lowland dipterocarp forest in East Kalimantan, Indonesia.* Nutrient Cycling in Agroecosystems, 2005. **71**(1): p. 63-72.

Estimating aboveground biomass/carbon stock and carbon sequestration using UAV (unmanned aerial vehicle) images in the mangrove forests Mahakam Delta, East Kalimantan, Indonesia

E Kustiyanto[1], Y A Hussin[1*], I van Duren[1] , Y B Sulistioadi[2]

[1] Department of Natural Resources, Faculty of Geo-information Science and Earth Observation (ITC), University of Twente, Hengelostraat 99, 7511 AE Enschede, The Netherlands, Tel: +31534874293 Fax: +31534874399

[2]Soil and Water Conservation Laboratory, Forestry Faculty, Center of Geospatial Information Infrastructure Development (CGIID), Institute for Research and Community Services (IRCS), Mulawarman University, Samarinda, Indonesia

e-mail: y.a.hussin@utwente.nl, bsulistioadi@gmail.com

Abstract. Mangrove forest which provides ecosystem services plays a pivotal rule to storage a large amount of carbon than any other tropical forest. However, the existing mangrove forests are threatened by deforestation and forest degradation. Mahakam Delta mangrove forest, East Kalimantan, Indonesia is one of the most extensive mangrove forests in Southeast Asia which has lost a massive part of its area due to conversion into aquaculture, agriculture, mining, oil exploration and settlement. UNFCCC thought REDD+ program and its MRV mechanism is doing its best to reduce greenhouse gases emission, which is addressed to IPCC for using earth observation data to mitigate climate change. UAV is one of promising advanced technology of remote sensing which has many benefits such as, very-height spatial resolution data, cost-effectiveness, reliable data quality, and multi-temporal. UAV images can be used for forest monitoring and management. This research aimed to assess aboveground biomass (AGB)/carbon stock using UAV images of 2017 and 2018 as well as calculate carbon sequestration over a one-year period in a part of mangrove forest in Mahakam Delta, East Kalimantan, Indonesia. The results from UAV images of the period October 2017 to December 2018, sequestered carbon was 6 Mg/ha/year which was reasonably accurate.

1. Introduction

Mangroves have an important role to cope with climate change and have ecosystem services such as carbon storage. In fact, mangroves are one of the most prominent carbon sink ecosystems, which store carbon approximately 1,023 ton/ha, including both above and below ground biomass [1]. Reported that above ground biomass of mangroves reaches 436.4-ton carbon/ha are varying depending on age, species and location. It is almost double compared to a tropical forest, estimated 228.7 Mg [2]. However, estimating biomass/carbon stock in a unique mangroves ecosystem is challenging due to the structure of trees, habitat, location and accessibility.

UNFCCC has the initiative REDD+ program and its mechanism MVR to monitoring, verifying and reporting carbon emission base on ecosystem service to obtain global benefits using remote sensing data and field-base measurement [3]. Monitoring could be applied to get information related to the natural dynamic of forest and the changes in the forest area due to natural disturbance and human encroachment. On the other hands, monitoring has to deal with multi-temporal or spatio-temporal data to achieve information in term of dynamic changes. One of the applications on monitoring, verification and reporting in term of REDD+ is using remote sensing data to estimate carbon stock in mangroves forest. The monitoring of mangrove requires accurate data to extract information to help to manage, such an important natural resource. Remote sensing is essential as data source and technique to derive biometric

mangrove trees parameters (e.g. DBH and height) to be used for biomass/carbon stock assessment and other management purpose. The integration of remotely sensed data with ground truth would help to assess the mangrove its biomass, biophysical conditions and sustainable forest management.

There are several studies which have conducted in the mangroves area to assess biomass/carbon stock using different remote sensing data with some benefits and drawback. The majority of them is by using satellite data both active and passive sensor, as well as terrestrial and airborne LiDAR [4-6]. Those data have limitations, for instances, optical remote sensing has medium to coarse spatial resolution, and its energy cannot penetrate cloud and other atmospheric disturbance. Radar has a drawback such as coarse spatial resolution, error variation related to topographic, and other difficulties in complex canopy structure. While Lidar required field data calibration, expensive, time-consuming, and cannot penetrate leaves. Based on all issues mentioned, there are a lot of uncertainties using these sensors.

In contrast, there are few studies done in mangroves for forest inventory or biomass/carbon stock assessment using UAV [7-9]. Surprisingly, those studies acknowledged that using UAV is a low-cost, rapid processing, time-effectiveness, reasonable accuracy and multi-temporal acquisition data, which is promising for monitoring application. UAV can capture a relatively large area with very high spatial resolution. It also flies with low altitude less than 100 m above the ground to minimise cloud and atmospheric disturbances as well as to get a higher quality of ground sample distance. Moreover, it can acquire data more rapid and frequent.

Furthermore, UAV captures areas of interest using different sensor and camera to obtain a specific characteristic of the object sensed. RGB sensor is generally assembled on UAV, while others sensor, such as (e.g. Sequoia and FireflEYE) can be installed for a specific application such as forest, agriculture and urban area since they have infrared and red-edge spectral bands. Here, one of the applications of the multispectral sensor of Sequoia camera which has five bands namely green, red, red-edged, near infra-red and RGB, is to distinguish trees species by digital image classification.

The accuracy assessment of remotely sensed data can be done using ground truth data as a reference to validate the derived data from UAV. Structure from motion (SfM) is applied to reconstruct 3D space image from 2D scene base on consecutive overlapped images to generates data such as points cloud, digital surface model (DSM), digital retain model (DTM), orthophoto, mosaic and finally canopy height model (CHM) which is the tree height in the case of inland and mangrove forest [10]. In this case, ground truth data of tree height is employed to assess the accuracy of crown height measurement (CHM) derived from DSM and DTM data. Whereas, crown projection area (CPA) which is obtained from UAV mosaic images, can be segmented automatically using the OBIA technique [11], assessed by manual on-screen digitation. CPA can also be used to model DBH since there is a relationship between these two parameters. Consequently, above ground biomass (AGB) and carbon stock can be assessed using the estimated height and modelled DBH with reasonable accuracy.

Therefore, this research will assess the application of UAV images to estimate above ground biomass/carbon stock and carbon sequestration in the mangrove area, where these areas comprise natural and planted mangrove ecosystem. The derived data (predicted DBH and trees height derived from CHM) from UAV images then will be evaluated with ground truth data for accuracy assessment. The main issues in this research are mangrove area which sequesters more carbon compared to another forest ecosystem. Thus, using two different years of UAV images data, monitoring carbon sequestration is possible. Meanwhile, the UAV data gives very high spatial resolution, cost-effectiveness, time-efficient and multi-temporal acquisition data serving the purpose REDD+ MRV approaches. Looking at the scientific published literatures, there is hardly any publication on the use of UAV images for assessing carbon sequestration in the mangrove forest. We believe that this research is an innovative one.

2. Materials and Methods

2.1 Study Area

Study area is located in Tani Baru Village, Anggana District, Kutai Kartanegara Region, East Kalimantan Province, Indonesia, which is situated on latitude 0°32'20.95"S and longitude 117°34'8.19"E. It is a conservation area of mangrove forest, where some of the areas were replanted after were converted into shrimp ponds. The study area is remnant mangroves forest which consists of old (natural) and planted mangroves. The study area location can be seen in Figure 1.

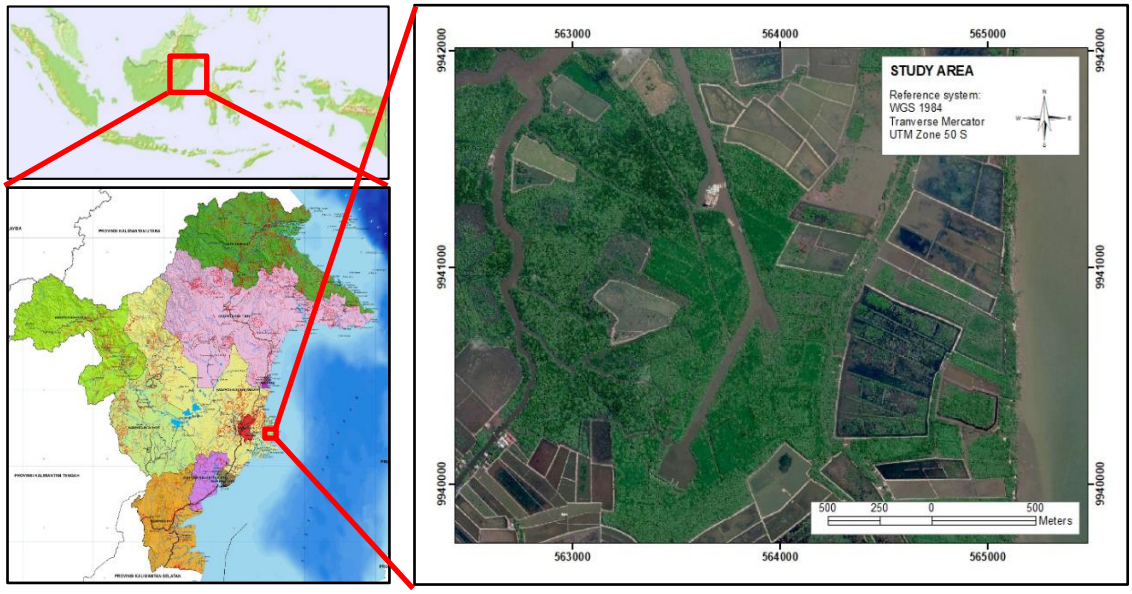

Figure 1. Location of the study area.

The study area is located in the equator zone; thus, the climate is humid, and rainfall happens during the year. The average temperature of the study area is approximately in the range of 23 - 32 °C, while the average rainfall in the dry season (July-September) is 35–40 cm/month and in the wet season (October – June) is 67–70 cm/month. The annual precipitation in the study area is more than 2500mm.

[12] Divides vegetation zone based on the distance from the sea into Pedada, Bakau, Transition, Nypa and Nibung. Padada is situated close to the delta front and dominated by *Sonneratia alba* and *Avicennia spp,* while Bakau zone is dominated by *Rhizophora spp.* The transition zones are with many species such as *Avicennia spp., Sonneratia caseolaris, Rhizophora spp, Bruguiera spp., Xylocarpus granatum* and nipa. Meanwhile, Nipa and Nibung zone are located in the central and upper area of Mahakam Delta. The study area is part of Tani Baru Village which covers an area of 71 km². Tani Baru is located in Anggana District which has 43,990 inhabitants in 2017 consist of 23,341 male and 20.469 female. While the growth rate in Anggana District is 3.96 % and population density is 24 per square km in 2017 [13]. The majority of inhabitants is Bajau and Bugisness, where the fisherman is the main source of livelihood.

2.2 Materials

During the research work of this thesis, materials were used, namely data, equipment and software, which used for fieldwork planning, data acquisition, data pre-processing, data processing and analysis, data and result presentation as well as thesis writing. These materials are described in the following subsections.

2.3 Data

The list of data and sources of the data used in this research consists of two types, primary and secondary data. Primary data were collected during fieldwork, while secondary data were obtained from other

sources, such as institution, internet, and literature review. Collected data in fieldwork comprises ground truth data (biometric) of DBH, tree height and species, while coordinate of sample plot and tree were retrieve by GPS handheld. Moreover, GPC were collected using GNSS RTK, and UAV image 2018 were collected using DJI Phantom 4.

On the other hand, secondary data of Google Earth image were employed to recognise the study area to determine the sample plot and UAV flight plan. TLS and UAV image 2017 were used to retrieve trees parameters such as tree height, CPA, crown diameter and canopy cover. In term of literature review, it was done to search for the mean annual increment of the mangrove growth rate of DBH and height as well as woody density for tree-specific mangrove species, namely *Avicennia spp, Rhizophora spp,* and *Xylocarpus granatum*. While other literature review performed to find an allometric equation for mangrove to calculate biomass and conversion factor to calculate carbon stock. Data, the source of data and type of data are illustrated in Table 1.

Table 1. Data and source of data used in this research.

Data	Sources of data	Type of data
Sample plot plan, flight plan	Google Earth image	Secondary
DBH, tree height, species	Ground truth	Primary
Tree height of TLS	Terrestrial laser scanner (TLS)	Secondary
Coordinate of sample plot and tree	Global satellite system (GPS) handheld	Primary
Ground control points (GCPs)	Global navigation satellite system real-time kinematic (GNSS RTK)	Primary
UAV image 2017	University of Mulawarman	Secondary
UAV image 2018	Unmanned aerial vehicle (UAV)	Primary
Growth rate of mangrove	Literature review	Secondary
Wood density	Word Agroforestry	Secondary
Allometric equation	Literature review	Secondary
Conversion factor	Literature review	Secondary

2.4 Software

There are several software packages that were used to pre-process, process, analyze and interpret data in this research during planning, fieldwork data collection, pre-processing, processing, analysis, and writing report. Here, Google Earth Pro was used to download fine resolution image of the study area in order to make flight planning and sample plot design. PIX4D Capture, PIX4D Ctr+DJI and PIX4D Mapper were used to make a flight plan, capture image using DJI Phantom 4 and image processing through Structure from Motion (SfM). Coordinate data of sample plot and trees that collected using GPS were processed via Garmin Map Source.

Arc GIS was used for the segmentation of crown canopy, resampling image of DTM, generating CHM and map layout. While Microsoft Excel and R-Studio were used to calculate and analyse statistical data, as well as making tables and diagrams. In term of the research thesis, Microsoft Word and Mendeley were used during thesis writing and retrieving citation. Moreover, Microsoft PowerPoint was used during presentations. Table 2 shows the list of software used in this research.

Table Error! No text of specified style in document.**.** Software used in this research.

Software	Purpose
Pix4D Capture	UAV flight planning
Pix4D Ctrl+DJI	UAV drone imagery captured
Pix4D Mapper	UAV image processing
Google Earth Pro	Download image, plotting coordinate
Garmin Map Source	GPS handheld data retrieving
ArcGIS	Manual on-screen segmentation of CPA, resampling image, generating CHM, layout
R-studio	Statistical data analysis
Microsoft Excel	Calculation, statistic data, table and diagram
Microsoft Word	Writing report
Microsoft PowerPoint	Presentation
Mendeley	Citation and reference

2.5 Equipment

Implementation of fieldwork required equipment to collect ground truth or measure trees parameters, e.g., DBH, trees height, setting sample plots. In the same time, they were used for GCP(s) and UAV imaging campaign. Compass was used for navigation. For tree height measurement two instruments were used: Leica DISTO D510 laser ranger and TLS RIEGL VZ 400. Diameter Tape 5 m were used to measure DBH of the individual tree inside the sample plot, while 30m measuring tape was used to measure the radius of the plot from the centre of the circular 500m2 plot, i.e.,12.6m.

Tree tags were used for numbering the trees in order to easily identify them during the data collection inside the sample plot. Handheld Garmin GPS E-Trax 30x was used to mark the coordinates of the plot centre and tree coordinates. Moreover, the digital camera was used to capture images of the plot in order to reconstruct the trees setup inside the plot and capture images for documentation. Table sheets were used to record fieldwork measurements of DBH and tree height, while some other stationaries were also used during fieldwork. TLS RIEGL VZ 400 was used to collect three-dimension point clouds to derived tree parameters. For UAV image rectification, ground control point was used inside the study area. Before UAV image acquisition and GCP measurement, tie mark was placed on the ground which was used as GCP location, then the X, Y, Z coordinates of the centre of tie marks were measured using GNSS RTK Leica GS 18 T. In terms of UAV image acquisition of 2018, DJI Phantom 4 was used to capture the images of the study area. The equipment is shown in Table 3**Table 2**.

Table 2. Fieldwork equipment used in this research.

Equipment	Purpose
Compass	Navigation
Leica DISTO D510 laser ranger	Tree height measurement
Diameter tape 5 m	DBH measurement
Tape 30 m	Diameter sample plot
Tree tag	Numbering trees
Garmin GPS E-Trax 30x	Navigation, marking coordinates
Digital camera	Capturing pictures
Table sheet	Recoding tree height, DBH, coordinate, trees species

TLS RIEGL VZ 400	Tree height measurement derived from laser point cloud data
GNSS RTK Leica GS 18 T	Measuring the GCPs
DJI Phantom 4	Collecting UAV imagery data
Ties mark paper	GCP ties mark

2.6 Research method

Figure 2 shows the research methods flowchart.

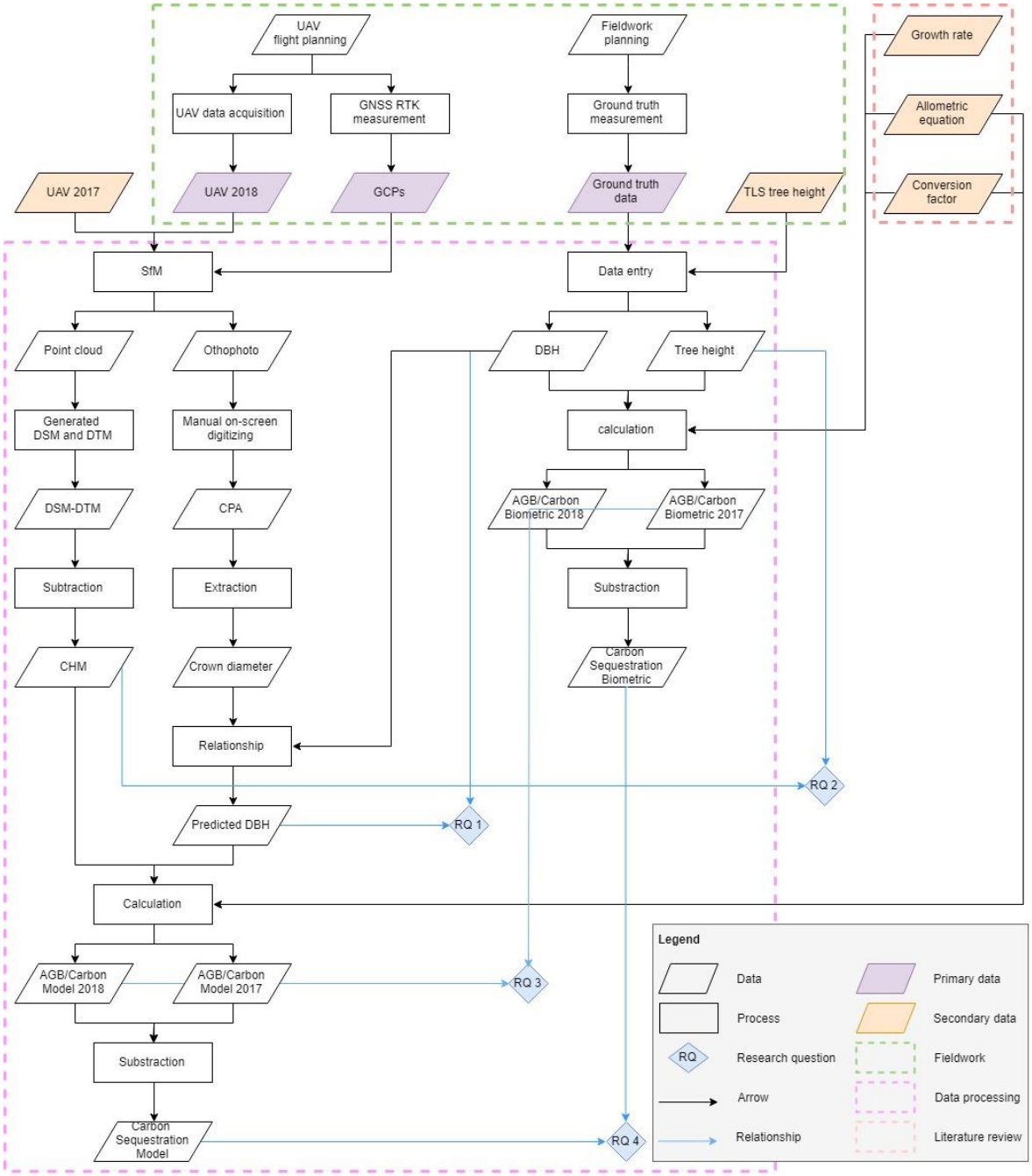

Figure 2. Flowchart of research method.

2.7 UAV image data acquisition

UAV images 2017 and 2018 were collected by a special team from the Faculty of Forestry, University of Mulawarman. These images were collected on 25 October 2017 and 18 December 2018. It was by chance that the University of Mulawarman had done the imaging survey in 2017 for PT Pertamina Oil company of Indonesia and we have used these images to assess carbon sequestration.

In 2017, DJI Phantom 4 camera model 3610 was employed using 375 m altitude above ground and 9 mm of focal length to collect 54 images. While in 2018, DJI Phantom 4 FC330 using 4 mm of focal length was used to collect 369 images from an altitude of 165 m above the ground floor. Table shows UAV data collection parameters of 2017 and 2018.

Table 4. UAV data collection of 2017 and 2018.

Information	UAV 2017	UAV 2018
Date	25 October 2017	18 December 2018
Time	15.30	12.30
Pixel	4864 x 3648	4000 x 3000
Camera model	DJI FC3610	DJI FC330
Focal length (mm)	9	4
Altitude (m)	375	165
Number of images	54	369
Forward overlap	80%	70%
Side overlap	70%	60%

PIX4D Capture was used to make UAV mission planning, which comprised parameters such as flight speed, angle, forward and side overlap, flight height, number of flight lines etc. The number of captured images was determined by area captured, flight height, focal length and forward and side overlap. Figure 3 shows some of the steps in collecting UAV images using DJI Phantom 4. Before UAV images were acquired, Ground Control Points GCPs (Figure 4) were collected using GNSS RTK Leica GS 18 T which consisted of base and rover receiver, while tie marks were placed in GCP point locations in the field.

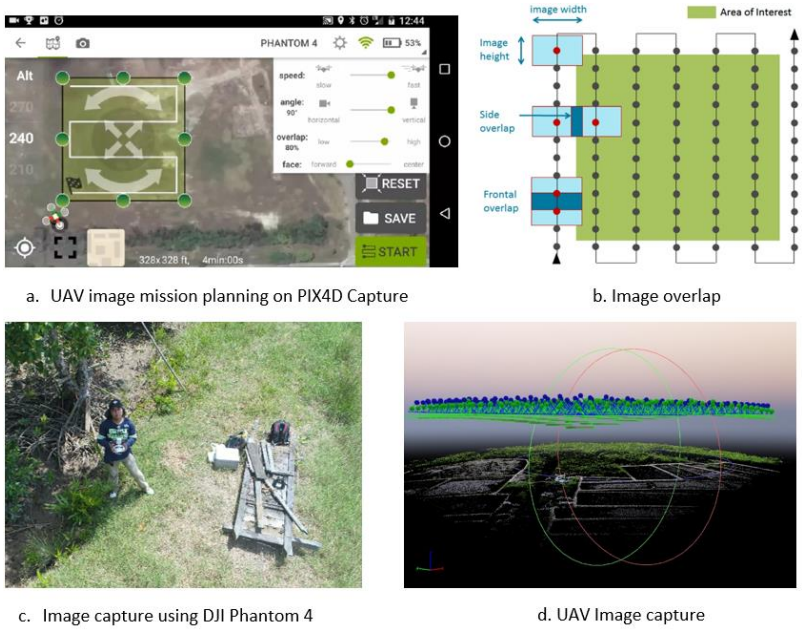

Figure 3. Some steps in collecting UAV images using DJI Phantom 4.

2.7.1 Biomass and Carbon Stock Assessment Using UAV Images

To assess above ground biomass (AGB) and carbon stock, Diameter at Breast Height DBH and tree heights were input into allometric equation to get the AGB. However, since DBH can't be seen from UAV images Crown Projected Area (CPA) was used to model DBH. CPA is the crown area seen from the UAV images. While tree height was extracted from subtracting the Digital Terrain Model (DTM) from Digital Surface Model (DSM) after constructing the point clouds as an output of the Mosaicking of the UAV images using Structure from Motion (SfM) technique using Pix4D software.

Manual digitising of CPA in each recorded individual tree was done on the ortho-mosaic image of UAV 2017 and 2018 using ArcGIS. The issue of identifying and matching every single tree in each plot, which was measured in the field in both ortho-mosaics of UAV images was very crucial. This was because we needed to match between the DBH measured in the field and the CPA and crown diameter (CD) on the image. Manual on-screen digitization of CPA was done by delineating the crown area of each individual tree. After that, we calculated its area to represent CPA and then CPA was used to generate CD.

Extracting individual tree height derived from Canopy Height Model CHM was done using CPA area using the Spatial Analyst Tool in ArcGIS software. In this case, CHM was overlaid and masked by the shapefile of CPA. Furthermore, the zonal statistic was run to calculate the maximum value in the CHM, which is the highest point in the canopy. Afterwards, the CPA of the individual tree is converted into a point feature. Then, the maximum value of CHM within CPA for every individual tree was used to retrieve tree height derived from UAV CHM.

Aboveground biomass is estimated using an allometric equation which is a mathematic equation to calculate biomass using DBH, tree height and woody density [14]. This research has used DBH, trees height and wood density as explanatory variables in the allometric equation to calculate biomass. Aboveground biomass model was calculated and reconstructed based on selected trees and assessed its accuracy using aboveground biomass/carbon stock biometric. The allometric equation which was used to calculate biomass is based on [14].

$$AGB = 0.0509 * WD * DBH^{2} * H \quad (1)$$

Where, AGB= above ground biomass (kg/tree), WD= wood density DBH= diameter breast height (cm), and H= trees height (meter)

While the calculation of carbon stock based on spatial extrapolation of remote sensing data and temporal analyse of fieldwork carbon stock measurement. Carbon stock was estimated using the above ground biomass (ABG) and the conversion factor (CF). Conversion factor that was used to calculate carbon stock both on biometric and model data was in the amount of 0.5 [15, 16]

$$C = ABG * CF \quad (2)$$

Where, C=carbon stock, ABG= above ground biomass, CF= conversion factor (0.5)

2.7.2 Ground truth data

Field data collection (DBH and tree height) which were recorder first manually in the field from every individual tree within the sampling plot and then transferred to Microsoft Excel in a digital format. These truth measured DBH and tree height were used to measure AGB/ carbon stock in the field to assess the accuracy of the estimated AGB/ carbon stock using UAV images. Microsoft Excel, R-Studio were used to record, calculate, store, present, analyse, interpret and save the data in different types and format. DBH and trees height data were analysed using a statistical method to obtain statistical parameter such as sum, mean, standard deviation, variance, maximum and minimum.

Defining sampling plot design, plot shape, and plot size are important steps to be taken before data collection. A circular shape plot with radii 12.62m was chosen to minimise borderline and perimeter of plot shape, to make the boundary of the plot easy to established and seen, to make the simple correction and to represent 500m² coverage area [17]. Purposive sampling was used in this research due to several

consideration and difficulties when working in mangrove forest such as time, cost, accessibility, efficiency and plot size.

Consequently, 30 sampling plots were used in this research distributed in the study area and equally spread in both old mangroves trees and planted mangrove to represent all variations in the study site. Biophysical parameters of the mangrove trees were collected such as DBH, trees height, coordinates of trees and trees species by using Leica DISTO Laser Ranger, diameter tape 5 m and handheld GPS.

Figure 4. Ground Control Points (GCP) used in the study area before UAV.

a. 130 cm above ground b. 30 cm above the highest aerial root

Figure 5. Measuring DBH using diameter type.

3. Results and Discussions

3.1 The relationship between DBH and CPA and trees height and UAV CHM of 2017 and 2018

301 trees were selected randomly to assess the relationship between DBH and CPA on one hand and the relationship between the ground trees height and CHM or UAV trees height in both years of 2017 and 2018.

The correlation and regression of DBH and CPA 2018 showed 0.87 in R-square, while the relationship between two variables consisted of intercept and slope, namely -1.6148 and 0.5795x. Figure 6 shows the relationship between DBH and CPA in 2018.

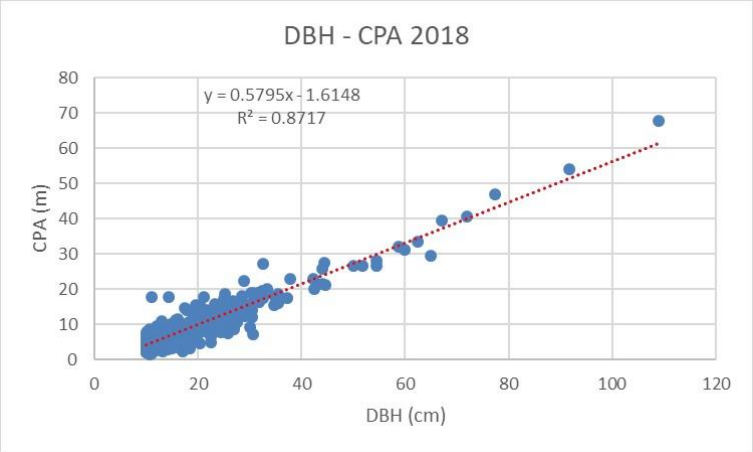

Figure 6. Relationship of DBH and CPA of 2018.

The relationship between DBH and CPA in 2017 using the elected trees was assessed. The R-square was almost the same as R-square of DBH and CPA 2018. R2 of 2017 data was 0.874. While its intercept was -1.4016 and 0.5251x was its slope (Figure 7).

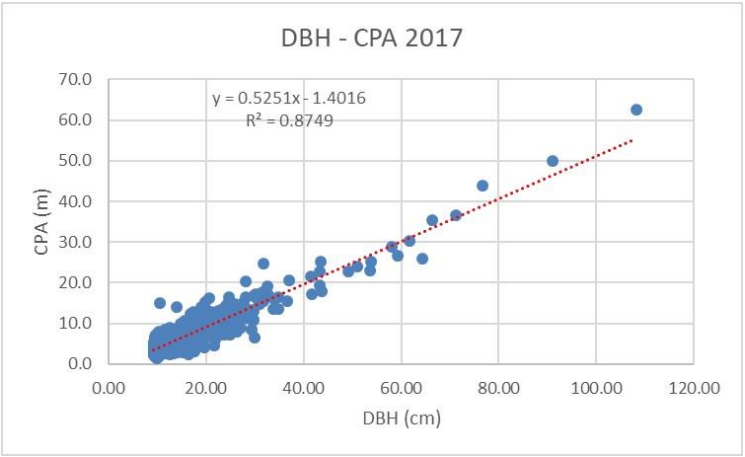

Figure 7. Relationship of DBH and CPA of 2017.

The relationship between tree height and CHM 2018 for selected trees showed a high correlation. The figures showed 0.85 of R-square, 0.5367 of intercept and 0.9556x of the slope. The relationship between tree height and CHM 2018 is presented in Figure 8.

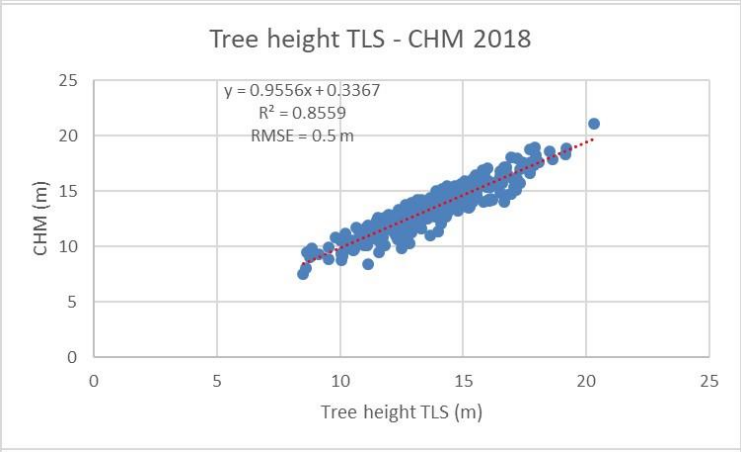

Figure 8. Relationship between tree height and CHM of 2018.

Compared to the relationship of tree height TLS and CHM 2018, the relationship between tree height TLS and CHM in 2017 was lower. It just performed 0.81 of R-square compared to 0.85. The intercept and slope are -0.5874 and 0.9427x respectively (Figure 9).

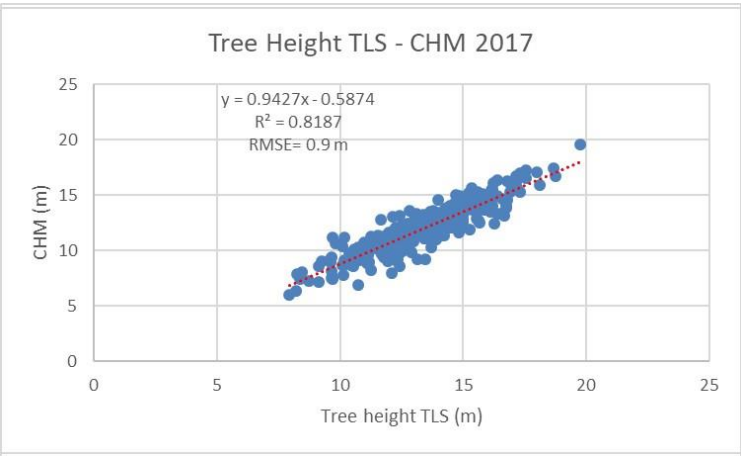

Figure 9. Relationship between tree height and CHM of 2017.

3.2 Comparison biometric and modelled of carbon stock 2018

There were four plots that stored more carbon stock than 100 Mg/ha in the biometric data in 2018 which comprise of plot 5, 17, 23 and 27. Only five plots of the carbon stock model 2018 data exceeded the storage of 75Mg/ha. Most of both biometric and model of carbon stock data sequestered carbon stock in the range of 25 to 75Mg/ha in 2018.

Table 5. Statistics summary of carbon stock.

Statistics	Carbon Stock Biometric (Mg/ha)			Carbon Stock Model (Mg/ha)		
	2018	2017	Sequestration	2018	2017	Sequestration
Total	1711.4	1565.6	145.8	1687.3	1523.7	163.6
Average	57.0	52.2	4.9	56.2	50.8	5.5
St. Dev	29.2	27.8	1.5	25.2	24.2	1.2
Max	146.6	137.0	9.7	137.2	129.3	7.8
Min	16.6	14.3	2.0	24.3	21.1	2.6

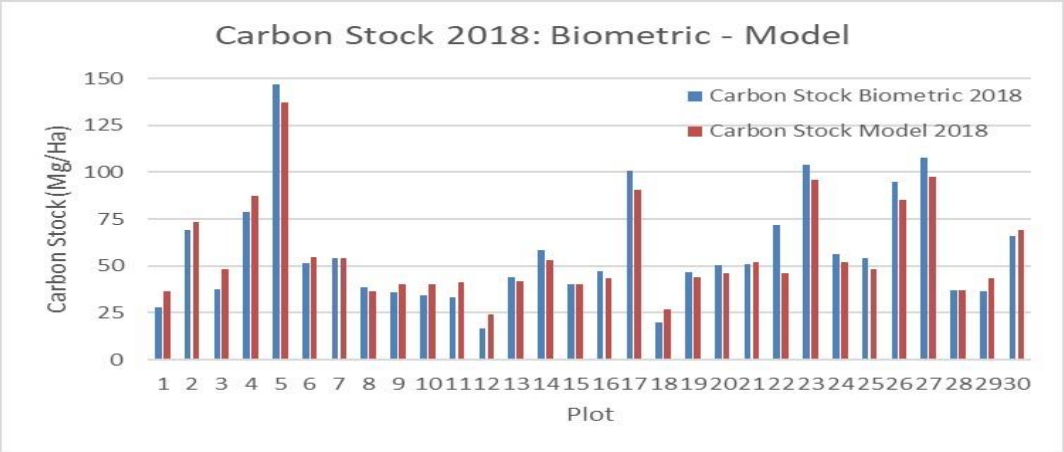

Figure 10. Comparison biometric and modelled of carbon stock in 2018.

Correlation between carbon stock 2018 biometric and model shows a significant relationship. The R-square was 0.93, while the RMS error was 7.8 Mg/ha. Furthermore, intercept and slope of that relationship were 8.6212 and 0.8348x. Figure 11 depicts the relationship between biometric and model carbon stock in 2018.

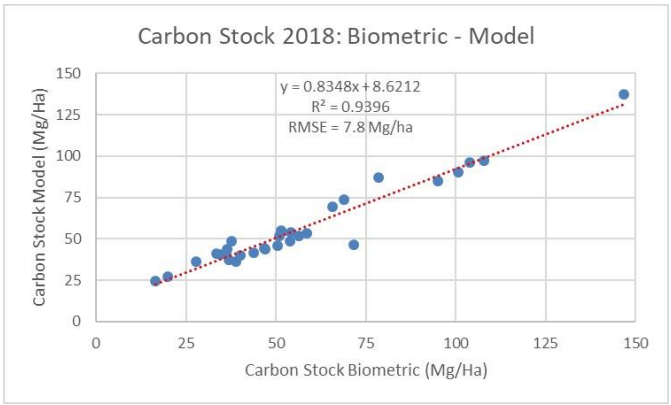

Figure 11. Relationship between biometric and modelled of carbon stock in 2018.

3.2.1 Comparison biometric and modelled of carbon stock 2017

Based on Figure , there was a difference between biometric and modelled carbon stock 2017, which was similar to carbon stock 2018 in plot 5, 17, 22, 26 and 27. While plot 6, 7, 21 and 38 were very close in the amount of carbon stock in 2017 both for biometric and model data. Overall, biometric data show more sequestration of carbon stock than the model in 2017, except in plots 1, 2, 3, 4, 9, 10, 11, 12, 18 and 29.

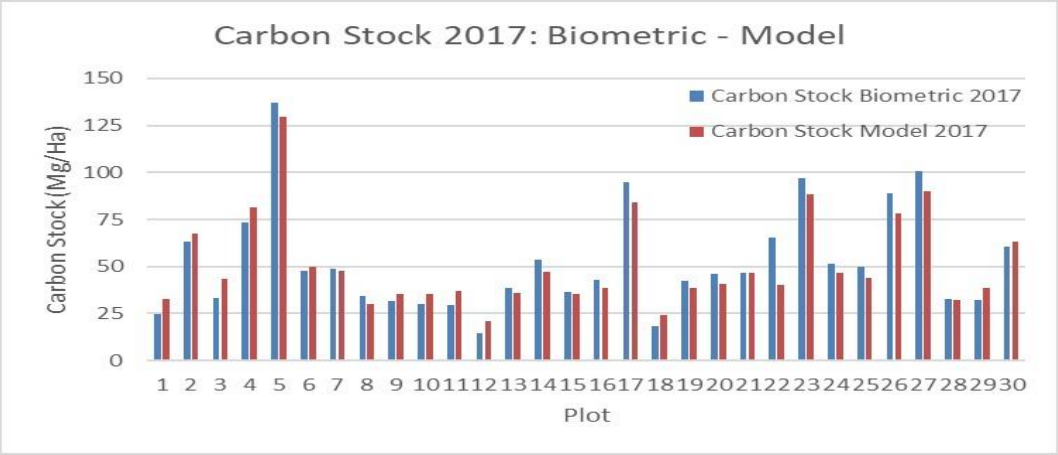

Figure 12. Comparison biometric and modelled of carbon stock in 2017.

R-square and RMS error of the relationship between carbon stock biometric and carbon stock modelled in 2017 were 0.93 and 7.71 respectively. While the intercept and slope are 6.9529 and 0.84x. Figure presents the relationship between carbon stock biometric and modelled in 2017.

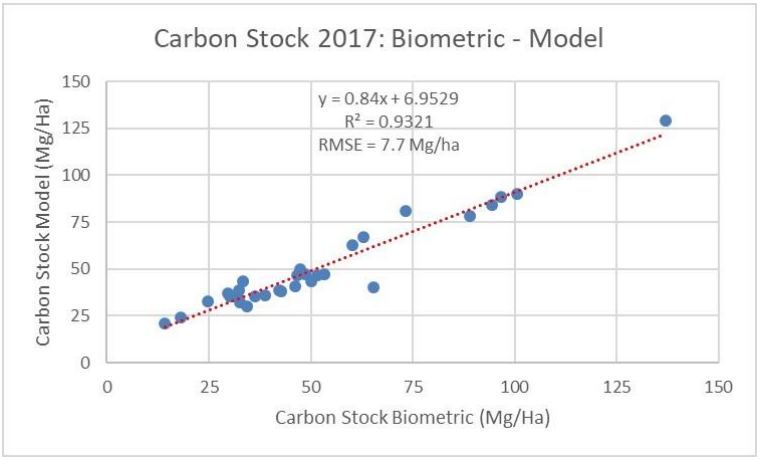

Figure 13. Relationship between biometric and modelled of carbon stock in 2017.

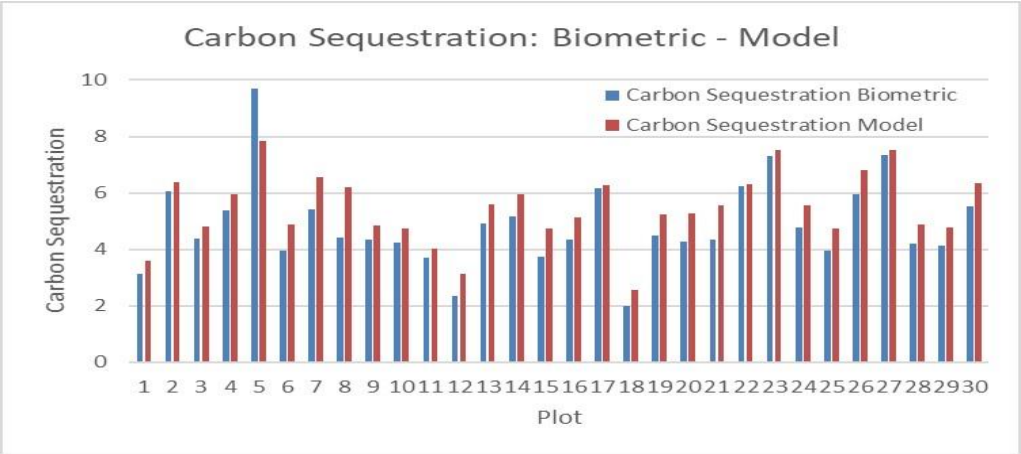

Figure 14. Comparison biometric and modelled of carbon sequestration.

3.2.2 Comparison biometric and modelled of carbon sequestration

In terms of carbon sequestration, the overall carbon stock model shows more carbon sequestered than the biometric. None of the model plots sequestered more than 10 Mg/ha/year, while in the biometric data of plot 5 carbon sequestration exceeded 8 Mg/ha/year. The majority of biometric and model data sequester carbon in the range 2 Mg/ha to 8 Mg/ha a year (Figure 14).

Figure 15 shows a significant relationship between carbon sequestration in biometric and modelled data. The R-square was 0.87, and the RMS error was 0.8 Mg/ha. Moreover, this relationship had an intercept and slope which of 1.7956 and 0.7526x, respectively.

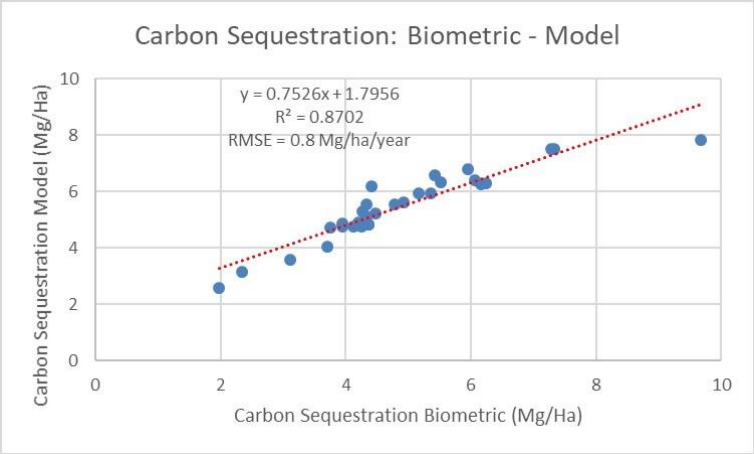

Figure 15. Relationship between biometric and modelled of carbon sequestration

3.3 AGB/Carbon stock estimation

The average aboveground biomass model in 2018 and 2017 was 112.5Mg/ha and 101.6 Mg/ha while the average aboveground biomass biometric (i.e., estimated from measurements in the field or the reference ground truth) was 114.1 Mg/ha in 2018 and 104.4 Mg/ha in 2017. This result is nearly similar to [18], in which they calculate land-use carbon footprint and carbon dynamic in mangroves-converted aquaculture in Mahakam Delta, Indonesia. The dominant mangrove species were *Avicennia alba, Bruguiera sexangula*, and *Rhizophora apiculata* which had a diameter in the range 5 – 10 cm. The average aboveground biomass of mangroves was 118 Mg/ha. Comparison between aboveground biomass biometric and the modelled AGB in 2018 and 2017 show that there are variabilities of above ground biomass in both data. Above ground biomass of biometric data is higher than the model in plots which have a high amount of biomass, namely plot 5, 17, 13, 26 and 27. It happens because the majority

of large DBH when predicted by DBH model, were underestimated. It also influenced by trees height derived from CHM, since the average of trees height derived CHM is lower than the average of trees height derived from TLS.

An example of high biomass plots is shown in **Error! Reference source not found.**. This plot shows the biomass of 293 Mg/ha. This plot shows big trees in size and high-density mangrove trees. While Plot 22 is was the only plot where the difference between the modelled AGB and the biometric AGB is high. The AGB biometric in 2018 and 2017 were 143 Mg/ha and 130 Mg/ha. While the modelled AGB in 2018 and 2017 were 92.7Mg/ha and 80.1Mg/ha. We believe that the source of error in assessing the AGB in this plot was because of error in the assessment of CPA and height of the trees in this plot both in 2018 and 2017. Although the difference between the AGB of two years was reasonable (e.g. 13 and 12 Mg/ha in the biometric and the modelled AGB), but still the AGB was not assessed accurately. The plot has 16 Avicennia trees and 14 of Rhizophora which show small CPA but the reasonable size of stem. Consequently, the modelling of AGB shows an error. Moreover, the majority of trees AGB in plots 1, 3, 4, 5, 11, 12, 18, 29 were overpredicted because trees height derived from CHM were higher than trees height derived from TLS and predicted DBH were also overpredicted.

Error in aboveground biomass estimation can be influenced by many factors such as an inappropriate allometric equation, inaccurate measurement of variable, instrument and calibration error while this research used a general allometric equation of mangroves, which contains diameter breast height, tree height and wood density. Moreover, the likely source of errors for collecting ground truth data in the field (i.e. measuring DBH, tree height, location and species) to calculate aboveground biomass to are human error and instrument error. As a result of the lack of information related to mangrove species, identification of mangroves was classified into tree species which did not represent the real specific species of mangroves. In some case, the recorded location of trees using GPS handheld were shifting, since GPS did not receive appropriate signals when measuring location due to occlusion of high density canopy cover of mangrove forest.

3.4 Carbon sequestration estimation

The average carbon sequestration of the model was 5.5 Mg/ha/year, while the average carbon sequestration of biometric was 4.9 Mg/ha/year. There was a difference of approximately 11% between model and biometric. This result is close to 4.71 Mg/ha/year of annual increment of carbon sequestration based on DBH in Sundarbans, Bangladesh [19]. [20] Assessed globally the overall carbon sequestration which is 13.5 Mg/ha/year of carbon sequestration of mangrove forest, which comprised above ground and below ground biomass. Knowing that mangrove forest trees sequester carbon 2-3 times of the trees in the tropical in-land forest [20], our modelled carbon sequestration is one-third of the total AGB plus belowground biomass.

Above ground carbon stock is generally calculated as 0.5 the amount of AGB biomass. In the study area, carbon sequestration model is higher around 0.6 Mg/ha than carbon sequestration biometric. All of the plots except plot 5, the carbon sequestration modelled were higher than the biometric. In plot 5, the majority of predicted DBH were underestimated, and there was a small difference between CHM 2018 and CHM 2017. Therefore, modelled AGB and consequently, carbon shows less carbon sequestration than in the biometric data. Carbon sequestration modelled in Plot 7 and eight were more than the biometric data since the difference in trees height of CHM 2018 and 2017 were around 1.5 m. The average annual increment of tree height in biometric was 43 cm only. Therefore, in those plots, tree height shows it affects three to four times in the allometric equation. Consequently, the modelled biomass and carbon stock were higher than the biometric data.

The advantages of UAV to capture a consecutive overlapping image with fine resolution has the opportunity to retrieve the structure of an object in single-level. UAV can use regularly capture the same

area to monitor forest system. This is evidence that UAV can be employed to estimate biomass/carbon stock and carbon sequestration in the mangrove forest.

This research work was done in response to the call of the REDD+ MRV program for new applications of remotely sensed data to assess biomass/ carbon stock and carbon sequestration. The world needs new methods and techniques using remotely sensed data to be presented as an example for a practical, less expensive, reasonably accurate and operational methods to assess carbon sequestration in tropical in-land forests and mangrove forests. Looking at the previous and current literatures, there is no literature on the use of UAV data to assess AGB/carbon stock and carbon sequestration. We believe that this research work is a reasonable, innovative example of the applications of multitemporal UAV images and SfM to assess AGB/ carbon stock and carbon sequestration.

4. Conclusions

There was a significant relationship between crown diameter derived from CPA of UAV images and DBH of ground truth data in 2018 and 2017. The R^2 and RMS error of 2018 were 0.80 and 1.5 cm, while in 2017 the R^2 was 0.81 and the RMS error was 1.4 cm.

There was a significant relationship between trees height derived from CHM of UAV images and field tree height both in 2018 and 2017. The relationship between trees height derived from CHM of UAV images and field trees height in 2018 shows an R^2 and RMS error of 0.85 and 0.5 m respectively. Whereas, the relationship between trees height derived from CHM of UAV images and field trees height in 2017 showed an R^2 of 0.81 and RMS error of 0.9 m.

The average AGB/carbon stock modelled from UAV images in 2017 and 2018 were 101 Mg/ha and 112 Mg/ha, while the average of AGB/carbon stock of the biometric data (ground truth) was 104 Mg/ha and 114 Mg/ha in 2017 and 2018 respectively. There was a significant relationship between AGB/carbon stock modelled from UAV images and biometric data in 2017 and 2018. The relationship between AGB/carbon stock modelled from UAV images and biometric data in 2017 was significant with an R^2 of 0.93 and an RMS error of 15 Mg/ha. While in 2018, the R^2 and RMS error of the significant relationship AGB/carbon stock between modelled from UAV images and biometric data were 0.93 and 15 Mg/ha.

Carbon sequestration modelled from UAV images of 2017 and 2018 was 6 Mg/ha/year compared to 5 Mg/ha/year of the biometric carbon sequestration of the years 2017 and 2018. There was a significant relationship between carbon sequestration modelled from UAV images of the years 2017 and 2018 and carbon sequestration of the biometric data which showed an of R^2 and RMS error of 0.87 and 1 Mg/ha/year, respectively.

5. Acknowledgment

The Authors would like to highly acknowledge and appreciate the research permit issued by the Indonesian Ministry of Science and Technology and Higher Education. They would like to highly Acknowledge the support and contribution of Dr. Y. Budi Sulistioadi and the Faculty of Forestry University of Mulawarman, Samarinda, Indonesia for facilitating our research work, helping us with the logistic, collecting image and ground truth data in Tani Baru mangrove forest. We highly appreciate the support of the team of Mita Priskawanti and Muhammad Lutfi Hamdani for their continuous help during October 2018. We acknowledged the UAV data collection by Dr. Y. Budi Sulistioadi in 2017 and 2018. Without the data and support, our research could not have been done.

6. References

[1] Komiyama, A., J.E. Ong, and S. Poungparn, *Allometry, biomass, and productivity of mangrove forests: A review.* Aquatic Botany, 2008. **89**(2): p. 128-137.

[2] Baccini, A., et al., *Estimated carbon dioxide emissions from tropical deforestation improved by carbon-density maps.* Nature climate change, 2012. **2**(3): p. 182.
[3] Stickler, C.M., et al., *The potential ecological costs and cobenefits of REDD: a critical review and case study from the Amazon region.* Global Change Biology, 2009. **15**(12): p. 2803-2824.
[4] Boudreau, J., et al., *Regional aboveground forest biomass using airborne and spaceborne LiDAR in Québec.* Remote Sensing of Environment, 2008. **112**(10): p. 3876-3890.
[5] Dube, T. and O. Mutanga, *Evaluating the utility of the medium-spatial resolution Landsat 8 multispectral sensor in quantifying aboveground biomass in uMgeni catchment, South Africa.* ISPRS Journal of Photogrammetry and Remote Sensing, 2015. **101**: p. 36-46.
[6] Le Toan, T., et al., *Relating radar remote sensing of biomass to modelling of forest carbon budgets.* Climatic Change, 2004. **67**(2-3): p. 379-402.
[7] Otero, V., et al., *Managing mangrove forests from the sky: Forest inventory using field data and Unmanned Aerial Vehicle (UAV) imagery in the Matang Mangrove Forest Reserve, peninsular Malaysia.* Forest ecology and management, 2018. **411**: p. 35-45.
[8] Tian, J., et al., *Comparison of UAV and WorldView-2 imagery for mapping leaf area index of mangrove forest.* International journal of applied earth observation and geoinformation, 2017. **61**: p. 22-31.
[9] Zahawi, R.A., et al., *Using lightweight unmanned aerial vehicles to monitor tropical forest recovery.* Biological Conservation, 2015. **186**: p. 287-295.
[10] Remondino, F., et al., *State of the art in high density image matching.* The photogrammetric record, 2014. **29**(146): p. 144-166.
[11] Blaschke, T., *Object based image analysis for remote sensing.* ISPRS journal of photogrammetry and remote sensing, 2010. **65**(1): p. 2-16.
[12] Sidik, A.S., *THE CHANGES OF MANGROVE ECOSYSTEM IN MAHAKAM DELTA, INDONESIA: A COMPLEX SOCIALENVIRONMENTAL PATTERN OF LINKAGES IN RESOURCES UTILIZATION.* Borneo Research Journal, 2010. **4**: p. 27-46.
[13] Kartanegara, B.K.K., *Kutai Kartanegara Dalam Angka 2010*. 2016: BadanPusatStatistik. Com.
[14] Chave, J., et al., *Improved allometric models to estimate the aboveground biomass of tropical trees.* Global change biology, 2014. **20**(10): p. 3177-3190.
[15] Brown, S., *Measuring carbon in forests: current status and future challenges.* Environmental pollution, 2002. **116**(3): p. 363-372.
[16] IPCC, *IPCC Guidelines for National Greenhouse Gas Inventories Volume 4: Agriculture, Forest and Other Land Use*. 2006, 2006 IPCC Guidelines for National Greenhouse Gas Inventories. p. 4.1-4.83.
[17] Hussin, Y.A., I.C. van Duren, and Y.B. Sulistioadi, *EKO KUSTIYANTO February 2019.* 2019.
[18] Arifanti, V.B., et al., *Carbon dynamics and land use carbon footprints in mangrove-converted aquaculture: The case of the Mahakam Delta, Indonesia.* Forest ecology and management, 2019. **432**: p. 17-29.
[19] Ray, R., et al., *Carbon sequestration and annual increase of carbon stock in a mangrove forest.* Atmospheric Environment, 2011. **45**(28): p. 5016-5024.
[20] Alongi, D.M., *Carbon sequestration in mangrove forests.* Carbon management, 2012. **3**(3): p. 313-322.

HOSTED BY:

SUPPORTED BY:

GOLD SPONSOR

SILVER SPONSOR

penerbit itenas
Jl. PKH. Mustapha No.23, Bandung 40124
Telp. +62 22 7272215, Fax.: +62 22 7202892
e-mail: penerbit@itenas.ac.id